



Development of a receptor targeted nanotherapy using a pro-apoptotic peptide

Nicole Remaliah Samantha Sibuyi



A thesis submitted in partial fulfilment of the requirements for the degree of Doctor Philosophiae in the Department of Biotechnology, University of the Western Cape.

2015

Supervisors: Prof M Meyer

Co-Supervisor: Dr AM Madiehe

Abstract

Development of a receptor targeted nanotherapy using a pro-apoptotic peptide

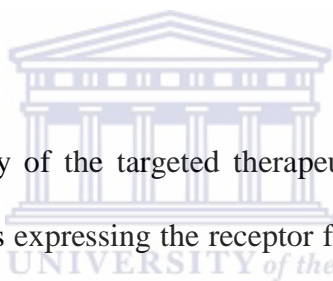
NRS Sibuyi

PhD Thesis, Department of Biotechnology, Faculty of Natural Science, University of the Western Cape, South Africa

The prevalence of obesity amongst South Africans is alarming, with more than 29% of men and 56% of women considered to be obese. Angiogenesis, a process for development of new blood vessels play a major role in growth and survival of the adipose tissues. Pharmacological inhibitors of angiogenesis are therefore a sensible strategy to reduce excess body weight. Current anti-obesity drugs have limitations because of their lack of selectivity and specificity, which lead to undesirable side effects and reduced drug efficacy. Future anti-obesity therapeutic strategies should be target-specific, with minimal toxicity towards healthy tissues will be more appropriate for obesity treatment. Targeted nano-therapeutic agents are currently being developed to overcome the drawbacks associated with conventional drug therapies. The nano-based delivery vehicles that specifically target diseased cells are appealing as they could reduce drug toxicity towards healthy tissues and be more effective at lower dosages.

The main aim of this study was to develop a receptor-mediated nanotherapy that specifically targets the white adipose tissue vasculature and trigger the death of these cells through apoptosis. The 14 nm gold nanoparticles (AuNPs) were synthesized using the Turkevich method following reduction of gold aurate by sodium citrate salt. Different

chemistries were used to functionalise the AuNPs for biological application by conjugating with either vascular targeting peptide or pro-apoptotic peptide on their surface or both. The nanomaterials were characterised by UV-Vis, Zeta potential and transmission electron microscopy (TEM). The sensitivity and specificity of various AuNP conjugates were tested *in vitro* on colon and breast cancer cell lines. A human (Caco-2) cell line that expresses the receptor for the adipose homing peptide was chosen as an *in vitro* model system. Cellular toxicity and uptake of the nanoparticles was evaluated using the WST-1 assay, Inductively Coupled Plasma-Optical Emission Spectra (ICP-OES) and TEM. The induction of apoptosis following exposure to the nanoparticles was examined by Western blot and flow cytometric analysis.



The anti-proliferative activity of the targeted therapeutic nanoparticles on the cells was more pronounced on the cells expressing the receptor for the adipose homing peptide. The uptake of unfunctionalised AuNPs was higher compared to functionalised nanoparticles, but this did not impair cell viability. The activity of the therapeutic peptide was retained and enhanced following conjugation to AuNPs as shown by Western blot and flow cytometric analysis. The nanotherapy under study demonstrated receptor mediated targeting, and enhanced activity on the cells expressing the receptor. However, the therapeutic and efficacy of the targeted nanotherapy still need to be tested in animal models of obesity to confirm the treatment specificity.

Keywords

Obesity

Adipose Tissue

Vascular targeting

Angiogenesis

Nanotechnology

Nanomedicine



Declaration

I declare that *Development of a receptor targeted nanotherapy using a pro-apoptotic peptide* is my own work, that it has not been submitted for any degree or examination in any other university, and that all the sources I have used or quoted have been indicated and acknowledged by complete references.



Nicole Remaliah Samantha Sibuyi

Date: July 2015

Signed.....

Acknowledgements

All honour and glory to *Almighty God and my beloved father*, I never would have made it without your support. It was never easy but through your grace here we are at the end of the chapter. You were my strength when I felt weak to continue and encouraged me when I wanted to turn my back and moved away from it all. You provided me with the right people who stood by my side and walk through this journey with me. Thank you for trusting me with this gift, I will cherish it forevermore!

I would like to express my sincere gratitude to all the people and institutions that have made this project possible.

I will be forever grateful to be granted an amazing opportunity to work under the supervision of the brilliant minds: **Prof Mervin Meyer, Dr Abram Madiehe and Dr Amanda Skepu**. I have learnt a lot from you and have become a better researcher through your mentorship. Thank very much for your patience and support, it has got me through some difficult phases of this work.

This work would not have been possible without collaborating with Mintek, Advanced Materials Division. Special thanks to **Dr Maya Makatini and Dr Frankline Keter** for synthesizing the peptides and AuNP conjugates used in this study.

Dr Bernhard Fromme, Dr Danni Ramduth and Miss Sarika Vandayar from BD Biosciences (SA), you really are God sent. Thank you very much for all the help with the flow cytometer, taking your time to thoroughly train me at short notice. Words are honestly not enough to express my gratitude, I'll forever be grateful for your selfless sacrifice. May God richly bless you and continue to work wonders through you.

Mnr Andrew Tomboer and Mrs Bridget Daniels, your assistance and support throughout the years is highly appreciated. You made the running of the project less strenuous.

I'm grateful to have friends who kept me sane when my academic life seems to be closing in on me. Your support and constant encouragements cheered me up and kept my feet steady on the wagon. Many thanks dearest friends you made the journey endurable: *Mrs Linah and Dr Peter Malatji, Ms Wisani Khoza, Mr Brian Sehume, Ps Sello Ramogayana, Dr Maropeng Ngobeni, Cmde Cornelius Silaule, Mr Sydwell Shikweni, Dr Hasani Chauke and Miss Rabelani Mutondwa*

My reliable librarian **Dr Keleabetswe Mpye**, thank you for making sure no paper was beyond my reach. I'm sincerely grateful for the support and constant encouragement during the course of the study.

Dr Kwazikwakhe Gabuza, if you can did it....I can did it too.....lolest! You are a rarest gem my friend, thank you for showing me that family isn't always about blood bonds. Your support and encouragement throughout the years kept me going, I doubt I would have made it this far without you. My brother from another mother, you stuck with me for life!

I would like to extend my heartfelt gratitude to all my former and present colleagues in the **Apoptosis, NIC Biolabels groups** and Biotechnology Department, Lab life would have been absolutely booooring without you fellow lab rats. *Dr Andrew Faro, Dr Jyoti Sharma, Mr Habeeb Bankole, Dr Ntevheleni Thovhogi and Dr Takalani Mulaudzi*, your support and encouragement is highly appreciated.

Mr Peter Ristow and Dr Franscois Taute, baie dankie vir julle hulp met die AuNP-GSH-NTA synthesis.

Dr Mustafa Drah, my dearest friend working with you has been an honour. An exhilarating experience that made sure each day brought new lessons! I will miss you when you go back to Libya.

Mr Mulisa Muthelo for making me realize the value of Science and always keeping me on my toes in the lab. You've been an inspiration, thank you.

I'm grateful to **DST/Mintek Nanotechnology Innovation Centre** for funding this project.

Saving the best for last: **MY FAMILY, MY LIFE, MY ALL!** BLOOD bonds are by far the strongest and unbreakable and have realized the value of having family support through this trying period. You guys are my world, the best treasure any human being can ask for. You are my pride and joy, the very best part of me! I'm practically nothing without you by my side. You've been patient and supportive throughout my studies, with you by my side I know I can laugh at the face of whatever the world throws at me. You all are my anchor, my strength, with you lot...I can fly higher than an eagle. *I love you to the moon and back, forevermore!*

My heartfelt gratitude goes to my sister in law, **Mrs Meriam Sibuyi** whose prayers and support kept me going.

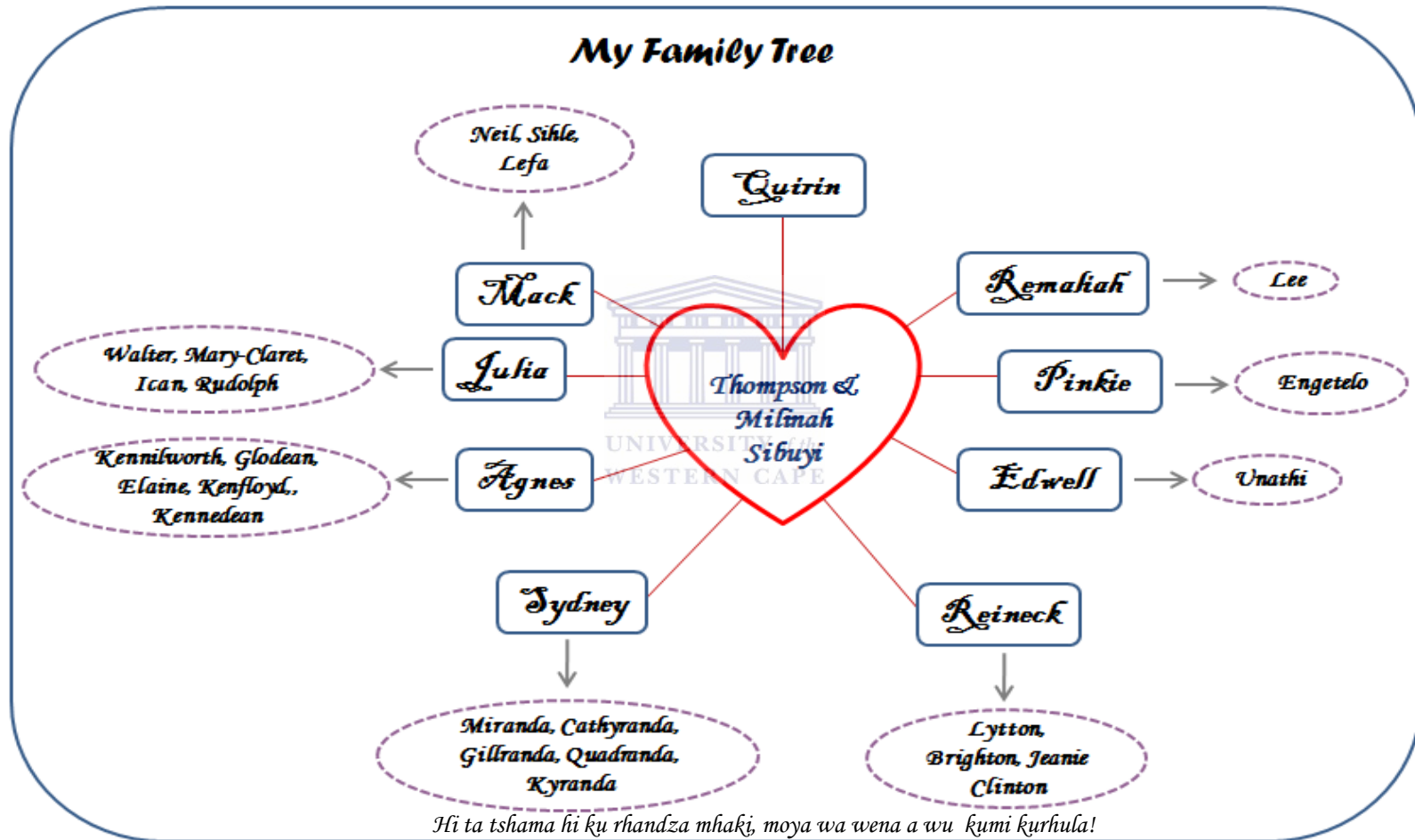
Miranda and **Cathyranda Sibuyi**, you girls rock and thank you so very much for keeping the family together while I was chasing the silver lining.

Lee Khoza how you have grown my angel, sadly I've missed it all! I'm glad you walked this part of my journey with me. Thank you for always being there and never complained about my absence. Hopefully, now we can finally catch up on the lost time. I love you my flower!

Engetelo Silaule, thank you my boy for the shows you always put up! Somehow they always took my mind off my troubles, thank you for being there!

Dedication

FOR MY LOVING FAMILY



To God be the honour and glory!

Table of Contents

Abstract.....	i
Keywords.....	iii
Declaration.....	iv
Acknowledgements.....	v
Dedication.....	viii
List of Abbreviations.....	xv
List of Figures.....	xxi
List of Tables.....	xxiv

Chapter 1: Literature Review

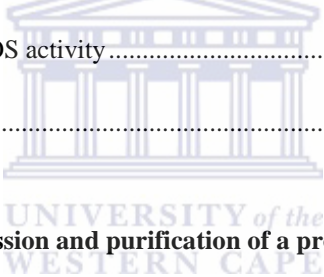
Introduction.....	1
1.1 Obesity.....	2
1.1.1 Aetiology of obesity.....	4
1.1.2 Management of obesity.....	7
1.1.3 Adipose tissue.....	8
1.1.3.1 Physiological functions of white adipose tissue.....	10
1.1.3.2 White adipose tissue as an endocrine organ.....	13
1.1.3.3 Effect of obesity on white adipose tissues.....	15
1.2 Cell targeting as a strategy for obesity reversal.....	17
1.2.1 Cell penetrating peptides.....	18
1.2.2 Mechanisms of uptake.....	19
1.2.3 Targeting peptides.....	21
1.2.3.1 Vascular targeting peptide: Adipose homing domain.....	22
1.2.3.2 Prohibitin.....	25

1.3 Vascular targeting	27
1.3.1 Angiogenesis.....	28
1.3.1.1 The process of angiogenesis	29
1.3.2 Clinical significance of angiogenesis.....	33
1.3.3 Angiogenesis in obesity	35
1.3.3.1 Adipose tissue vasculature	37
1.4 Apoptosis	41
1.4.1 Apoptosis pathways	42
1.4.2 Apoptosis in obesity.....	45
1.5 Nanotechnology	49
1.5.1 Nanomaterials	50
1.5.2 Nanomaterials used for drug delivery	51
1.5.2.1 Gold nanoparticles	52
1.5.3 Biological and medical application of nanotechnology	54
1.5.3.1 Drug delivery using nanoparticles	55
1.5.4 Challenges and advantages of nanotechnology.....	57
1.5.5 Potential application of nanotechnology in obesity	59
1.6 Aim(s) of the study	62
1.6.1 Objectives of the Study	62

Chapter 2: Materials and Methods

2.1 Reagents and their suppliers	63
2.2 Preparation of solutions and reagents	64
2.2.1 Cloning, protein expression and purification	64
2.2.2 SDS-PAGE analysis	67
2.2.3 Western Blot Analysis	68

2.3 Research Methodology	70
2.3.1 Recombinant DNA technology	70
2.3.1.1 mTK and TK ₃ constructs	70
2.3.1.2 Preparation of chemically competent cells	70
2.3.1.3 Transformation of mTK and TK ₃ into cloning cells	71
2.3.1.4 Colony PCR to Analyse <i>E. coli</i> Transformants.....	73
2.3.1.5 Preparation of mTK and TK ₃ plasmid DNA	75
2.3.1.6 DNA sequencing.....	76
2.3.1.7 Transformation of mTK and TK ₃ into expression cells	76
2.3.1.8 mTK and TK ₃ recombinant protein expression screening and solubility test	76
2.3.1.9 Analysis of protein expression by SDS-PAGE	77
2.3.1.10 Large Scale expression of the Recombinant Proteins	78
2.3.1.11 Affinity purification of recombinant proteins	79
2.3.1.12 Western blotting.....	80
2.3.2 Cell culture.....	81
2.3.2.1 Cell Splitting and Trypsinization	82
2.3.2.2 Cell count/ viability: Trypan Blue Exclusion Assay	82
2.3.3 Evaluation of PHB expression in various cell lines	83
2.3.3.1 Western blot analysis of PHB expression	83
a) Protein Extraction	83
b) Protein Quantification	83
c) SDS-PAGE and Western blot analysis	84
2.3.3.2 Immunocytochemistry: localization of PHB.....	84
2.3.4 The effect of mTK and TK ₃ recombinant proteins by MTT assay.....	85
2.3.5 The design and development of the nanotherapy.....	86
2.3.5.1 Fabrication of the gold nanoparticles.....	86

2.3.5.2	Characterization of functionalised gold nanoparticles	86
2.3.5.3	Quantification of AuNPs by ICP-OES.....	87
2.3.6	<i>In vitro</i> nanoparticle uptake and localization studies	88
2.3.6.1	Effect of the nanotherapy on cell proliferation: the WST-1 assay	88
2.3.6.2	Cellular Uptake and localization of the AuNPs	89
a)	Quantification of AuNP uptake by ICP-OES analysis.....	89
b)	Cell specimen preparation for TEM	90
2.3.6.3	Mode of cell death induced by AuNP conjugates	90
a)	Analysis of apoptosis cell death induced by AuNP conjugates	91
b)	Western blotting analysis of Caspase 3 activation.....	92
c)	Analysis Caspase 9 activation by Flow Cytometry	92
d)	Mitochondrial Dysfunction: ROS activity.....	93
2.3.7	Statistical Analysis.....	93
		
Chapter 3: Recombinant expression and purification of a pro-apoptotic protein		
3.1	Introduction.....	94
3.2	Results.....	96
3.2.1	Colony PCR: Screening for mTK and TK ₃ positive clones	96
3.2.2	Sequence analysis of positive clones	97
3.2.3	Recombinant protein expression and purification.....	100
3.2.3.1	Protein expression screen for mTK and TK ₃	100
3.2.3.2	Solubility screening of the recombinant proteins.....	103
3.2.3.3	Affinity purification of the recombinant proteins	105
3.2.3.4	Western blot analysis of Histidine-fusion proteins	108
3.2.4	Analysis of the effects of recombinant proteins on Caco-2 cell line.....	110
3.2.4.1	Evaluating PHB expression in various cell lines	110

3.2.4.2 Cytotoxicity effects of the recombinant proteins	111
a) The effect of the recombinant proteins on cell morphology	113
3.3 Discussion.....	114

Chapter 4: The development of PHB-targeted nanotherapy for target specific induction of apoptosis

4.1 Introduction.....	117
4.2 Results.....	119
4.2.1 Conjugation of the recombinant proteins to AuNPs	119
4.2.1.1 Synthesis and characterization of NTA-gold nanoparticles	120
4.2.2 Development of targeted nanotherapy using $D(KLAKLAK)_2$ peptide	122
4.2.2.1 Design of the AuNP conjugates	122
4.2.2.2 Synthesis and characterization of gold nanoparticles	124
4.2.3 Quantification of AuNPs and conjugates by ICP-OES	128
4.2.4 Therapeutic potential of targeted nanotherapy.....	130
4.2.4.1 Effect of AuNP conjugates on Caco-2 cell viability: WST-1 assay.....	131
4.2.4.2 Cellular uptake of AuNPs by Caco-2 cells as determined by ICP-OES	133
4.2.4.3 Intracellular localization of AuNPs by TEM	135
4.2.5 Investigation into the mode of cell death induced by AuNPs conjugates	137
4.2.5.1 Cellular morphological changes induced by AuNPs in Caco-2 cells.....	137
4.2.5.2 Detection of intracellular oxidative stress induced by AuNP conjugates	138
4.3 Discussion.....	140

Chapter 5: Conjugation of modified $D(KLAKLAK)$ to AuNPs for development of the ideal PHB-targeted nanotherapy

5.1 Introduction.....	144
5.2 Results.....	145

5.2.1 Analysis of TAT-D(KLAKLAK) ₂ biological activity on cancer cells.....	145
5.2.2 Development and analysis of anti-proliferative activity of the AuNP-conjugates	147
5.2.2.1 Design of the AuNP-conjugates.....	147
5.2.2.2 Characterization of AuNPs and conjugates.....	149
5.2.2.3 Nanoparticle quantification by ICP-OES.....	151
5.2.2.4 Therapeutic activity of the nanotherapy in cancer cells using the WST-1 assay	152
5.2.2.5 Cellular uptake of AuNPs by cancer cells as determined by ICP-OES	156
5.2.2.6 Intracellular localization of AuNPs by TEM	157
5.2.3 Cell death analysis: investigation of possible apoptotic cell death	159
5.2.3.1 Effect of AuNPs on cell morphology.....	159
5.2.3.2 Analysis of apoptotic effects induced by AuNP conjugates in Caco-2 cells.....	161
5.2.3.3 Analysis of caspase activity	163
a) Analysis of caspase 3 activation by Western blot.....	163
b) Analysis of Caspase 9 activation by flow cytometry.....	164
5.2.3.2 Detection of intracellular oxidative stress induced by AuNPs: ROS activity	166
5.3 Discussion.....	168
Chapter 6: General Discussion, concluding remarks and future perspectives	
6.1 General Discussion	172
6.2 Concluding remarks and future perspectives	176
References.....	179

List of Abbreviations

5-HT	5-hydroxytryptamine
AC	Adenylate cyclase
ACS	Acyl-CoA synthase
AIF	Apoptosis-inducing factor
AHP	Adipose homing peptide
Ang	Angiopoietin
ANT	Adenine nucleoside translocator
Antp	Antennapedia homeodomain
Apaf-1	Apoptotic protease activating factor-1
APS	Ammonium persulfate
AR	Adrenergic receptor
AT(s)	Adipose tissue(s)
ATM	Adipose tissue macrophages
AuNPs	Gold nanoparticles
BAT	Brown adipose tissue
Bax	Bcl-2 associated protein-X
BC	Before Christ
BM-MSCs	Bone marrow derived mesenchymal stem cells
CaCl ₂	Calcium chloride
Caspases	Cysteine aspartate-specific proteases
CDK	Cyclin-dependent kinase
CHO	Chinese hamster ovary cells
CM-H ₂ DCFDA	5-(and-6)-chloromethyl-2',7'-dichlorodihydrofluorescein diacetate acetyl ester

CPPs	Cell-penetrating peptides
CVD(s)	Cardiovascular disease(s)
DAG	Diacylglycerols
DAPI	4', 6'-Diamino-2-phenylindole
DEVD	Caspase 3 cleavage site
DISC	Death-inducing signal complex
DMEM	Dulbecco's Modified Eagle's Medium
DMF	Dimethylformamide
DMSO	Dimethyl sulfoxide
DNA	Deoxyribonucleic acid
dNTPs	Deoxyribonucleotide triphosphates
DTT	Dithiothreitol
<i>E. coli</i>	<i>Escherichia coli</i>
EC(s)	Endothelial cell(s)
ECM	Extracellular matrix
EDTA	Ethylene diamine tetra acetic acid
EE	Energy expenditure
EI	Energy intake
EPR	Enhanced permeability and retention
EtBr	Ethidium bromide
FADD	Fas-associated protein with death domain
FBG	Fasting blood glucose
FBS	Foetal bovine serum
FDA	Food and Drug Administration
FFAs	Free fatty acids

FGF	Fibroblast growth factor
GF(s)	Growth factor(s)
HGF	Hepatocyte growth factor
HIV	Human immunodeficiency virus
HRP	Horseradish peroxidase
HSL	Hormone-sensitive lipase
ICs	Inflammatory cells
ICP-OES	Inductively coupled plasma optical emission spectrometer
IMM	Inner mitochondrial membrane
IPTG	Isopropyl-L-thio- β -D-galactopyranoside
IR	Insulin receptor
kb	Kilo base
KCl	Potassium chloride
kDa	kilodalton
KH ₂ PO ₄	Potassium dihydrogen phosphate
KOAc	Potassium acetate
LB	Luria bertani
LETO	Long-Evans Tokushima Otsuka
LPL	Lipoprotein lipase
LSPR	Localized surface plasmon resonance
MC	Melanocortin
MgCl ₂	Magnesium chloride
MMP	Matrix metalloproteinase
MnCl ₂	Manganese (II) chloride
MRI	Magnetic resonance imaging

mTK	TAT-DLSLARLATARLAI
MTT	3-(4,5-dimethylthiazol-2-yl)-2,5-diphenyltetrazolium bromide
Na ₂ HPO ₄	Disodium hydrogen phosphate
NaCl	Sodium chloride
Na-Mops	3-(N-morpholino) propanesulfonic acid sodium salt
Ni-NTA	Nickel-nitrilotriacetic acid
nm	Nanometer
nM	Nanomolar
NP(s)	Nanoparticle(s)
OD	Optical density
OLETF	Otsuka Long–Evans Tokushima fatty
OMM	Outer mitochondrial membrane
PA	Plasminogen activator
PBS	Phosphate buffered saline
PCR	Polymerase chain reaction
PEG	Polyethylene glycol
PFA	Paraformaldehyde
PHB	Prohibitin
PI3K	Phosphatidylinositol 3-kinase
PKA	Protein kinase A
PMSF	Phenylmethylsulfonyl fluoride
PS	Phosphatidylserine
PTD(s)	Protein transduction domain(s)
PTP	Permeability transition pore
PVDF	Polyvinylidene difluoride

QDs	Quantum dots
RDT	Recombinant DNA technology
ROS	Reactive oxygen species
RT	Room temperature
SA	South Africa
SDS	Sodium dodecyl sulphate
SDS-PAGE	Sodium dodecyl sulphate-polyacrylamide gel electrophoresis
SPR	Surface plasmon resonance
t.i.d	Ter in die
T2D	Type 2 diabetes mellitus
TAE	Tris-acetate EDTA (buffer)
TAG(s)	Triacylglycerol(s)
TEM	Transmission electron microscopy
TEMED	<i>N, N, N', N'</i> -tetra methylethylenediamine
TF(s)	Transcription factor(s)
Tfb	Transformation buffer
TK ₃	TAT-D(KLAKLAK) ₂ -DEVD-D(KLAKLAK) ₂ -DEVD-D(KLAKLAK) ₂
tPA	Tissue-type plasminogen activator
TRADD	TNF receptor-1 associated death domain protein
Tris	(Hydroxymethyl) aminomethane
uPA	Urokinase-type plasminogen activator
UV	Ultra-violet
V	Volts
VDAC	Voltage-dependent anion channel

VEGF	Vascular endothelial growth factor
VSMC(s)	Vascular smooth muscle cell(s)
WAT(s)	White adipose tissue(s)
WHO	World Health Organization
WST-1	Water-soluble tetrazolium-1



List of Figures

Figure 1.1: Lipid metabolism in adipocytes.....	11
Figure 1.2: Obesity-induced changes in adipokine secretion.....	16
Figure 1.3: Cellular delivery of target validation tools by protein transduction domains	20
Figure 1.4: Internalization of nanoparticles via receptor-mediated endocytosis.....	23
Figure 1.5: The subcellular localization and potential mechanisms involved in PHB action	26
Figure 1.6: The process of angiogenesis.....	30
Figure 1.7: Functions of adipose tissue vasculature.....	39
Figure 1.8: Models for the cytosolic escape of mitochondrial proteins in response to apoptotic stimuli. .	44
Figure 1.9: Proposed model for the role of adipocyte apoptosis in complications of obesity.....	46
Figure 1.10: Basic structure of inorganic nanoparticles.....	51
Figure 2.1: A circular map of pET-22b(+) plasmid DNA.....	72
Figure 3.1: Amplification of mTK positive clones by colony PCR.....	96
Figure 3.2: Amplification of TK ₃ positive clones by colony PCR.....	97
Figure 3.3: Analysis of TK ₃ DNA sequence.....	99
Figure 3.4: Alignment of TK ₃ amino acid sequence	100
Figure 3.5: Expression screen for recombinant mTK protein.....	101
Figure 3.6: Expression screen for recombinant TK ₃ protein.....	102
Figure 3.7: Evaluation of recombinant mTK protein solubility	104
Figure 3.8: Evaluation of recombinant TK ₃ protein solubility.....	104
Figure 3.9: Large scale protein expression and affinity purification of mTK protein.....	107
Figure 3.10: Large scale protein expression and affinity purification of TK ₃ protein.....	107
Figure 3.11: Western blot analysis of the recombinant mTK His-fusion proteins.....	109
Figure 3.12: Western blot analyses of the recombinant TK ₃ His-fusion proteins.	109

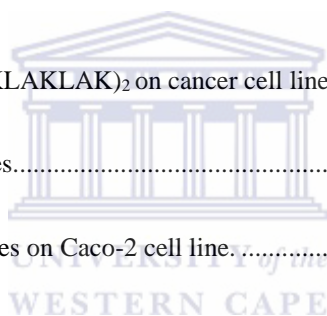
Figure 3.13: Analysis of PHB expression in cell culture	110
Figure 3.14: Immunocytochemistry analysis of PHB expression and localization	111
Figure 3.15: Effects of mTK and TK3 recombinant proteins on CaCo-2 cells.....	112
Figure 3.16: Light microscopy images of Caco-2 cells treated with recombinant mTK and TK ₃	113
Figure 4.1: Possible mechanisms by which nanomaterials interact with biological tissue	119
Figure 4.2: Schematic diagram of the PHB-targeted nanotherapy.....	120
Figure 4.3: Optical properties of AuNP and AuNP-GSH-NTA determined by UV-vis spectroscopy. ...	121
Figure 4.4: Schematic diagram of the AuNP design.....	122
Figure 4. 5: UV-Vis spectrophotometer absorption spectrum of AuNPs conjugates.....	125
Figure 4.6: Representative TEM micrographs of the AuNP conjugates	126
Figure 4.7: ζ -potential of the AuNPs determined using Malvern Zetasizer	127
Figure 4.8: Quantification of AuNPs by ICP-OES	129
Figure 4.9: Viability and proliferation of Caco-2 cells after 24 h exposure to various AuNPs	132
Figure 4.10: Quantification of internalized AuNPs in Caco-2 cells by ICP-OES.....	134
Figure 4.11: Localization of AuNPs in Caco-2 cells analysed by TEM.	136
Figure 4.12: Cell morphology after the Caco-2 cells were exposed to various AuNP conjugates.....	138
Figure 4.13: ROS activity in response to AuNPs treatment.....	140
Figure 5.1: Anti-proliferative activity of TAT- _D (KLAKLAK) ₂ -DEVD-SH on colon and breast cancer cells.....	146
Figure 5.2: Schematic diagram of the AuNP design.....	148
Figure 5.3: Representative TEM micrographs of the AuNP conjugates	150
Figure 5.4: Zeta potential of the AuNP conjugates determined using Malvern Zetasizer	151
Figure 5.5: Quantification of AuNP conjugates by ICP-OES.....	152
Figure 5.6: Effect of various AuNP conjugates on Caco-2 cells, HT 29 and MCF-7 cells.....	154

Figure 5.7: Selectivity of AG _D K compared with other AuNP conjugates on Caco-2, MCF-7 and HT-29 cells treated with 8 nM AuNP conjugates.....	155
Figure 5.8: Quantification of internalized AuNPs in cancer cell lines by ICP-OES.....	156
Figure 5.9: Localization of AuNPs in Caco-2 cells by TEM.....	158
Figure 5.10: Cell morphology of Caco-2, MCF-7 and HT-29 cells after exposure to various AuNPs.	160
Figure 5.11: Analysis of apoptotic cells by APOPercentage TM assay.....	162
Figure 5.12: Western blot analysis of caspase 3 activation in Caco-2 cells.....	164
Figure 5.13: Evaluation of caspase 9 activity by flow cytometry in Caco-2 cells	165
Figure 5.14: ROS levels in Caco-2 cells in response to AuNPs treatment.....	167



List of Tables

Table 1.1: Types of commonly used cell penetrating peptides	19
Table 2.1: List of reagents and suppliers	63
Table 2.2: Preparation of resolving and stacking gels	68
Table 2.3: Preparation of PCR reaction cocktail per reaction.....	74
Table 2. 4: Cell lines used for screening of PHB expression.....	81
Table 2.5: Preparations of the standards and sample for protein estimation.....	84
Table 4.1: The IC ₅₀ values of various AuNP conjugates after their exposure to Caco-2 cells.....	133
Table 5.1: IC ₅₀ values for TAT-(KLAKLAK) ₂ on cancer cell lines.....	146
Table 5.2: AuNP optical properties.....	149
Table 5.3: IC ₅₀ of AuNP conjugates on Caco-2 cell line.....	155



Chapter 1: Literature Review

Introduction

Pharmaceutical drugs used for treatment of chronic diseases such as obesity and cancer, suffer from lack of specificity which reduces the sensitivity and efficacy of the prescribed drugs. Due to side effects these drugs cannot be used indefinitely, discontinuation is often followed by disease relapse. Alternative strategies that can treat chronic diseases are of utmost significance in health economics, life expectancy and reduction of mortality. As such, treatment strategies that can reduce the burden of chronic diseases are urgently required. For this purpose, precision or targeted therapy is receiving a considerable amount of attention as a potential therapy that can alleviate chronic diseases. Ability to ferry therapeutic materials directly to desired targets (pathological cells) with no effect to healthy tissues could overcome certain drawbacks associated with current treatment regimen. Disease-associated antigens can be exploited to develop targeted nanotherapy by using nanoparticles as stealth drug carriers. In this manner, toxicity could be limited to target cells, reducing side effects and preventing immune response. This will significantly enhance the half-life of the therapy, mask the therapy from attack by phagocytes and reduce early drug clearance from the blood system.

The future of nanomedicine is projected towards detection and eradication of diseased cells through targeted nanotherapy. For targeted therapy to be effective, disease specific targets have to be identified. The targeting peptide used in this study targets a cell surface

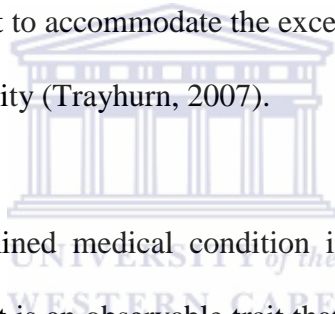
receptor in the white adipose tissue (WAT) vasculature of obese subjects. The feasibility of the vascular targeted nanotherapy in obese subjects is reviewed in this chapter.

1.1 OBESITY

Obesity is a complex, multifaceted medical condition that is prevalent in both developing and industrialized countries (Trayhurn, 2007). It is a global epidemic and health problem that does not discriminate between adults, children and adolescents. Worldwide, women are found to be more obese than men, while there are a higher proportion of overweight men than overweight women (WHO, 2010). The same trend in obesity statistics was observed in both African and white populations in South Africa (Puone *et al.*, 2002, Van der Merwe and Pepper, 2006).

Obesity is a major risk factor for development of serious chronic diseases, such as cardiovascular diseases (CVDs) including hypertension, stroke, coronary heart diseases (Carl *et al.*, 2009; Narkiewicz, 2006), type 2 diabetes mellitus (T2D) (Eckel *et al.*, 2011) and various forms of cancer, such as breast cancer, colon and prostate cancer (Bray, 2002). Obesity as a medical condition endangers millions of lives through its association with the chronic diseases mentioned above. These chronic diseases are further associated with adverse health events, increased medical care costs that further decrease life expectancy leading to premature death. It was projected that 60% of deaths worldwide by 2025 will be caused by obesity-associated chronic diseases. This evidence suggests that the prevention and control of obesity needs to be taken very seriously in both industrialized and developing countries (World Health Organization, 2000).

Obesity is a metabolic condition that results from energy imbalance in genetically susceptible individuals. The genetic basis of obesity was proven through animal studies, and strongly correlates to human trials, as discussed in section 1.1.1 (Arner, 2000; O’rahilly *et al.*, 2003; Sorensen and Echwald, 2001). Thus, obesity results from positive energy imbalance where energy intake (EI) chronically exceeds energy expenditure (EE) in terms of basal metabolic rate, thermogenesis or physical activity. The excess energy or fat is normally stored as triacylglycerols (TAGs) in the specialized storage organ, the adipocytes in the WATs. Excessive and chronic fat accumulation in the adipocytes consequently causes metabolic alterations within the WATs. The WAT mass expands beyond its physiological limit to accommodate the excess energy leading to increased total body fat mass leading to obesity (Trayhurn, 2007).



Obesity is the most undermined medical condition in both developed and developing countries throughout world. It is an observable trait that is used to be regarded as a sign of wealth and health status mostly in African countries where diseases such as HIV/Aids exist (Arojo and Osungbade, 2013; Renzaho, 2004). Sadly, there is still doubt by healthcare professionals and the public to regard obesity as a disease. As such, it is difficult to get a proper prescription to help in its management. Chronic accumulation of the excess fat in different fat depots has been associated with progression to chronic diseases that has detrimental health effects and non-fatal conditions (gout, sleep apnoea, respiratory conditions, gastro-oesophageal reflux disease, osteoarthritis and infertility) when not taken care of (Ofei, 2005).

1.1.1 Aetiology of obesity

The causes of obesity are classified into genetic and environmental factors. Most of these discoveries are owed to animal models of obesity (Dubnov *et al.*, 2003; Kennedy *et al.*, 2010). There is also strong evidence from human trials pointing to genes as role players in obesity, however, the overwhelming evidence shows that increasing prevalence of obesity is triggered by environmental factors. Environmental factor, such as sedentary lifestyle encourages consumption of high caloric diets and discourages physical activity leading to weight gain. Therefore, the interaction between genetic and environmental factors is a major determinant for the development of obesity (Dubnov *et al.*, 2003; Hill and Peters, 1998).

Genetic factors

The development of obesity has a potential genetic component as proven through animal models of obesity, however, the mechanism thereof is still not known. Various genes play a major role in body functioning, not limited to appetite, metabolism and deposition of fat in the body. For instance several genes such as *fat*, *obese (ob)*, *diabetes (db)*, *tubby (tub)* and *agouti yellow (A^y)* that predispose animals to obesity have been identified and their actions studied (Chen and Garg, 1999; Kennedy *et al.*, 2010). Mutations of these genes lead to development of obesity following different mechanisms of action. The *ob* gene encode for leptin (a satiety signalling protein predominantly secreted by adipocytes), *db* gene encode for the leptin receptor (Ob-R) (Zhang *et al.*, 1994). Leptin effects are mediated by binding to the Ob-R in the hypothalamus through the Jak/STAT pathway (Hegyí *et al.*, 2004). Leptin receptor mutations in mice resulted in severe obesity and T2D (Fei *et al.*, 1997). Conversely, leptin deficiency in mice and humans causes obesity and

may also cause diabetes syndromes such as hyperinsulinaemia. Administration of leptin in *ob/ob* mice inhibits food intake and reduces body weight *via* activation of specific brain receptors (Montague, 2003).

The *fat* gene encodes for carboxypeptidase E or prohormone convertase 1, the enzyme responsible for conversion of pro-hormones into active and functional hormones. *Fat* defects predispose mice to a range of abnormalities: progressive adult onset obesity and obesity-induced disorders such as hyperinsulinaemia and infertility (Naggert *et al.*, 1997). The *A^y* gene defect is associated with maturity onset obesity, pigmentation defects, insulin resistance and development of tumours in mice (Kennedy *et al.*, 2010). The yellow coat colour observed in mice is due to defects in melanocortin (MC)-1 receptor to synthesize eumelanin in the hair follicle, this is involved in counteracting the actions of MC4 receptors expressed in the hypothalamus resulting in development of obesity (Naggert *et al.*, 1997). These monogenic forms of obesity in rodents have shed some light into human obesity. Most of the genes responsible for development of obesity in rodents correspond to juvenile-onset morbid obesity in humans (Arner, 2000; O'Rahilly *et al.*, 2003).

Genetic influences are difficult to elucidate and identification of the genes is not easily achieved in familial studies. Moreover, the influence that genotype might have on the aetiology of obesity is generally attenuated by non-genetic factors including high caloric diets (Afridi and Khan, 2004). The tendency to gain weight is hereditary; however, family members share not only genes but also diet and lifestyle habits that may contribute to obesity. Separating these lifestyle factors from genetic factors is often difficult, especially with evidence pointing to heredity as a strong determinant of obesity (Afridi and Khan, 2004). Genetic studies of monozygotic (identical) and dizygotic (non-identical) twins

proved beyond doubt that obesity development is influenced by genetic factors, which account for as much as 50 to 80% of variance in monozygotic twins (Mitchell *et al.*, 2007; Sorensen and Echwald, 2001). Moreover, studies of adopted twins showed no relationship between the body weight of those children and their adoptive parents, but a close correlation with their biological parents (Sorensen and Echwald, 2001).

Environmental factors

Although genetic factors certainly play an important role in the susceptibility for obesity, the real culprit is the environment that promotes a sedentary lifestyle and long-term energy imbalance due to excessive caloric intake relative to energy expenditure (Fruhbeck *et al.*, 2001). Thus, the development of obesity is dependent on the disequilibrium between energy intake and energy expenditure (Brandt *et al.*, 2006; Racette *et al.*, 2003).

The human body is designed in a way that will help it maintain and regulate the metabolic processes and maintain the healthy body weight in return. Under physiological conditions, energy intake and expenditure is highly regulated and kept in balance at all times. However, when subjected to the environment that allows excessive food intake and discourages physical activity it is very challenging to avoid weight gain. Consumption of high energy diet should be followed by physical activity to expend the excess energy in order to protect the body against weight gain. In an environment where fast foods are readily available it is very difficult to maintain healthy dietary habits, and makes it difficult for healthcare givers to help obese patients lose and maintain a healthy weight. Hence more effort is directed towards prevention of weight gain by educating and alerting people through educational trainings starting from Primary schools (Hill and Peters, 1998).

1.1.2 Management of obesity

Different clinical and non-clinical strategies have been tried over the years with exciting but unsustainable results. Clinically, obesity management is preferably directed to individuals that are at a greater risk of developing medical complications associated with obesity (Guri *et al.*, 2006). Managing healthy body weight can reduce or treat the medical consequences of obesity. The clinical approach to management of obesity involves three stages of interventions: lifestyle modification, pharmacotherapy and surgery. Pharmacotherapy as discussed below is most preferred over the other two management strategies as it is easily accessible and promises immediate weight loss (Bray, 2000).

1.1.2.1 Pharmacotherapy

Pharmacotherapy is the second phase of clinical management of obesity after lifestyle modification. It is an option for patients with a body mass index of $\geq 30 \text{ kg/m}^2$ with at least one of the obesity health hazards (Bray, 2000). The therapy is prescribed for patients who have gone through lifestyle modification with no success for the first six months. It was initially an option for obese adults (≤ 65 years), however children and adolescents are now allowed to use anti-obesity drugs (Bray, 2000; Hainer *et al.*, 2008).

Pharmacotherapy still remains an area of ongoing research with only three groups of drugs approved by Food and Drug Administration (FDA): (1) those that reduce food intake, (2) increase thermogenesis, and (3) alter the body's energy metabolism (Bray, 2000; Lee and Aronne, 2007). Monoamines act on noradrenergic, serotonin, dopamine and histamine receptors to reduce food intake. The noradrenergic drugs such as phentermine, mazindol,

and phendimetrazine, are approved only for short-term use (Bray, 2000; Lee and Aronne, 2007). The only thermogenic drug combination that has shown efficiency in weight reduction is ephedrine and caffeine. Although the two did not receive FDA approval as anti-obesity drugs (Bray, 2000; Coffey *et al.*, 2004), their combination can be used as supplements to help reduce body weight without prescription (Cheung *et al.*, 2013; Coffey *et al.*, 2004).

There were only two FDA approved long-term anti-obesity drugs: orlistat and sibutramine. However, sibutramine has been withdrawn due to its adverse cardiovascular health effects (Williams, 2010). Orlistat is used to inhibit the actions of gastric and pancreatic lipase in the small intestine thereby reducing the dietary fat intake and inhibits fat absorption by 30% (Carriere *et al.*, 2001; Hollander *et al.*, 1998; Sternby *et al.*, 2002). The efficacy and safety of orlistat is short lived, its use is limited to 2 years as it can be accompanied by adverse health effects. The effects include oily spotting, fatty stool, flatus and discharge, increased defecation and faecal incontinence. Fat soluble drugs (vitamins A, D, E, and K) when taken together with orlistat lose their effect, 5-15% of long term users need vitamin supplements (Hauner, 2001).

1.1.3 Adipose tissue

Adipose tissue (AT) simply referred to as 'fat', is a loose connective tissue comprised of various cells held together by a matrix of collagen fibres. The main cellular components in the ATs are mature, lipid-filled fat cells (adipocytes) which make up a two third of the entire tissue, preadipocytes and endothelial cells (ECs). Additional components include fibroblasts, mesenchymal stem cells, nerve fibres, monocytes, macrophages, pericytes and

immune cells. The AT is distributed throughout the body and shows plasticity throughout life (Hauner, 2004). The ATs in mammals are classified into two types: the WAT and brown AT (BAT). The two types (WAT and BAT) share many metabolic characteristics despite their distinct functions. The WAT mainly stores excess energy for subsequent needs whereas the BAT serves as an energy dissipating organ (Gustafson *et al*, 2007).

Adipocytes are the main components in the ATs and play a crucial role in its development and function. Adipocytes size varies depending on the size of individuals, lean humans have an average cell diameter of approximately 70 μm whereas in obese subjects it can expand up to 120 μm (Hauner, 2004). The adipocytes are made of 60-85% of lipid, 5-30% water and 2-3% protein. The lipid droplets in the adipocytes can be unilocular (WATs) or multilocular (BATs). In WATs the lipid droplet contains 90-99% TAGs and does not contain any organelles. The cell nucleus is pushed against the plasma membrane by the lipid droplet to the side (Hausman *et al.*, 2001).

The WATs are located primarily in three major anatomical areas: subcutaneous (inguinal, dorsosubcutaneous and interscapular fat depots), dermal (a relatively continuous sheath of lipid) and intraperitoneal (mesenteric, omental, perirenal, retroperitoneal, epididymal) fat depots (Hausman *et al.*, 2001). The major WATs in human are subcutaneous and visceral or intraperitoneal (omental and mesenteric) depots. The visceral depot has been on the forefront as the most metabolically active tissue that transports WAT secreted molecules to the portal venous system. However, the amount of subcutaneous WAT depot is 3-4 fold bigger than the visceral depot. These two depots can interact in a coordinate and compensatory manner and both are responsible for obesity and obesity-induced diseases (Gustafson *et al*, 2007). Hence the study will focus mainly on the functions of WAT and

its effect on the development of obesity and the obesity induced diseases. The WATs are especially interesting in this study as they are major organs affected during development of obesity. A better understanding of the tissue development and their physiological roles may help in identifying new, safer and better therapeutic approaches for obesity.

1.1.3.1 Physiological functions of white adipose tissue

White adipose tissues provide insulation, mechanical support to the body and also serve as the storage organ. The primary function of WATs is to store energy in the form of TAGs during periods of energy excess, and to release energy during fasting or starvation as free fatty acids (FFAs) and glycerol as shown in Figure 1.1 (Lucas *et al*, 2009). During chronic positive energy balance, the excess calories are converted into TAGs mainly under the control of insulin. The TAGs are rapidly mobilized through the actions of catecholamines and other lipolytic hormones (Hauner, 2004).

Fat or lipid metabolism is an important factor in the functioning of WAT as depicted in Figure 1.1. Lipid metabolism is a highly regulated process in a normal or healthy individual that determines the fate of excess fat in the adipocytes through lipogenesis and lipolysis. The two processes are mediated by several key enzymes found in the adipocytes, for instance: the lipases are required for TAGs break down into glycerol and FFAs that can then be transported to the liver, muscle and BAT where they are used in fatty acid oxidation (Sethi and Vidal-Puig, 2007). The storage of excess fat as TAGs in WATs in humans and animals is crucial for the normal functioning of the entire body. In order to keep up with the metabolic processes, consumption of more calories than is required is a must (The Endocrine Society, 2005). The excess fat is regulated through two opposing

processes that are equally important for survival: lipogenesis and lipolysis. The two processes are highly dependent on energy status within the WATs and secreted hormonal signals. For example decrease in systemic glucose and insulin and increase in counter-regulatory hormones (epinephrine, growth hormone and glucocorticoids) will inhibit lipogenesis and stimulate lipolysis. Adipocytes are well equipped with the machinery to respond to both hormonal and sympathetic (adrenergic) stimulation for both cellular and biochemical mechanisms (Ahima and Flier, 2000; Sethi and Vidal-Puig, 2007).

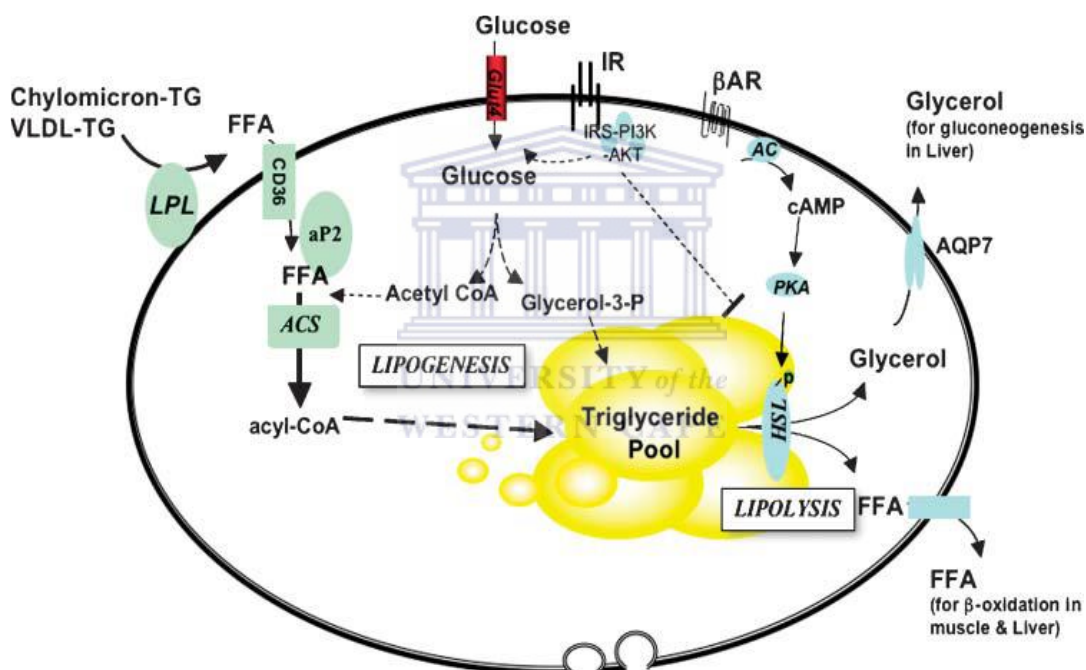


Figure 1.1: Lipid metabolism in adipocytes. Adipocytes are equipped with the biochemical machinery to function effectively as the body’s fuel store. To do this, it must mediate lipogenesis and lipolysis. It is also sensitive to changing nutritional cues. For example, it is insulin-sensitive [insulin stimulates glucose uptake and lipogenesis and inhibits lipolysis] and subject to adrenergic regulation [stimulates lipolysis and adaptive thermogenesis (BAT)]. AC, adenylate cyclase; ACS, acyl-CoA synthase; AKT, AKR mouse thymoma viral proto-oncogene; AR, adrenergic receptor; HSL; IR, insulin receptor; PI3K, phosphatidylinositol 3-kinase; PKA, protein kinase A (Sethi and Vidal-Puig, 2007). *Figure reprinted with permission from American Society for Biochemistry and Molecular Biology.*

Lipogenesis or lipid synthesis is defined as a process in which carbohydrates, glucose or other energy sources from the diet are converted into TAGs for storage in WATs.

Lipogenesis occurs in liver and WAT in rodents, whereas in humans it occurs mostly in liver and to a lesser extent in WAT. Lipid synthesis is activated during postprandial state and food consumption and inhibited during starvation or fasting conditions. FFAs are hydrolysed from the diet through the actions of lipoprotein lipase (LPL) found in the adipocytes. FFAs are transported into adipocytes via fatty acid transporter and are converted into TAGs following multiple enzymatic steps. The rate limiting enzyme being acyl-CoA synthetase. Glycolysis is another cellular route for oxidation of excess glucose in the adipocyte to acetyl-CoA. Glucose is translocated via glucose transporters 1 and 4 into the adipocytes where it is converted into acetyl-CoA through acetyl-CoA carboxylase and fatty acid synthase. Acetyl-CoA is then converted into acyl-CoA. Acyl-CoA is esterified in the endoplasmic reticulum to TAG and transported into the lipid droplet within the adipocyte (Ahima and Flier, 2000; Vázquez-Vela *et al.*, 2008; Warne, 2003).

The increased amount of TAGs is reduced by lipolysis during fasting, starvation or during energy expenditure (exercise). Lipolysis is the breakdown of stored TAGs into FFAs and glycerols during energy deprivation (The Endocrine Society, 2005). This process is also regulated by hormonal signals such as glucagon and catecholamines, their increased levels in blood stimulate lipolysis in the adipocytes by activating protein kinase A and several lipases (Langin, 2006; Vázquez-Vela *et al.*, 2008). The G-protein-coupled receptors become activated, increasing cAMP levels. The increased cAMP levels lead to phosphorylation of perilipin (phospho-protein located in the membrane of the lipid droplet inside the adipocytes and inhibits lipolysis) and hormone-sensitive lipase (HSL). HSL translocate from the cytoplasm into the lipid droplet and initiates hydrolysis of TAG into FFA and glycerol. The reaction starts by hydrolysis of TAGs by adipose triglyceride lipase

to diacylglycerol (DAG) moiety and FFA. The DAG moiety is hydrolyzed by HSL and 2-monoacylglycerol lipase to release another FFAs and monoglyceride molecules. The monoglycerides are transported to nonadipose tissues for gluconeogenesis (synthesis of glucose from glycerol) and the FFAs are available for β -oxidation in the liver and muscle (Ahima and Flier, 2000; Warne, 2003).

These processes play an important role within the body, as the other organs are dependent on them for energy. Therefore, the major role of WATs and their functioning are crucial for the whole body functioning as they provide other tissues with energy when required. Failure or disturbances in these processes lead to undesired consequences. For instance, dysfunctions in lipolysis lead to increased fat mass that will result in obesity. Thus, lipid metabolism balance has to be maintained at all times to stay healthy (Langin, 2006).

1.1.3.2 White adipose tissue as an endocrine organ

White adipose tissues have been perceived as a passive organ responsible for energy storage and providing insulation to the body. However, the discovery of leptin in 1994, a satiety factor produced predominantly by WAT proved that WATs are capable of other functions (Ronti *et al.*, 2006). Since then, many secretory products of WATs have been discovered through independent studies. The WAT products include cytokines, growth factors (GFs), acylation stimulating protein, plasminogen activator inhibitor-1 and LPL (Goossens, 2008). This led to WAT regarded as highly active and an endocrine organ secreting several adipokines that regulate body functioning. The adipokines and other WAT secreted factors are responsible for the body's metabolism and energy homeostasis

by influencing a variety of biological and physiological processes (Hajer *et al.*, 2008; Krug and Ehrhart-Bornstein, 2005; Sethi and Vidal-Puig, 2007).

The endocrine function of WAT is best explained through their secreted adipokines. Circulating adipokine levels appear to correlate closely with adiposity in animals and humans, increasing levels have been observed in obese and insulin resistant states (Otero *et al.*, 2005; Zieba *et al.*, 2005). Various adipokines are involved in different roles within the body. The first to be discovered and most studied adipokine in obesity research is leptin, a satiety signal that regulates appetite and body weight in both humans and rodents (Koerner *et al.*, 2005; Zhang *et al.*, 1994). Leptin acts on the central circuits in the hypothalamus in order to reduce food intake and increase energy expenditure. Leptin controls the body fat stores, appetite and maintenance of body weight through coordinated regulation of metabolism, the autonomic nervous system, and body energy balance (Otero *et al.*, 2005; Zieba *et al.*, 2005). Adiponectin is involved in insulin action, resistin regulates glucose metabolism while chemerin regulates angiogenesis. Other functions include regulation of energy balance, vascular remodelling, regulation of blood pressure and blood coagulation (Hajer *et al.*, 2008; Krug and Ehrhart-Bornstein, 2005; Sethi and Vidal-Puig, 2007).

The endocrine functioning of WATs is attributed to the presence of different cell types as mentioned in 1.1.3. These additional cell types play important roles in regulating WAT function and are involved in WAT secretory function. The secreted molecules are mostly responsible for communication between AT and different organs within the body. Dysregulation in adipokines' secretion is associated with the development of obesity and

obesity-induced diseases such as insulin resistance, T2D and CVD (Hauner, 2004; Sethi and Vidal-Puig, 2007).

1.1.3.3 Effect of obesity on white adipose tissues

Weight gain during adulthood is characterized by adipocyte hypertrophy, a process by which adipocytes increase in size to accommodate the excess lipid. In an evolutionary context, the ability to store excess energy in WATs is essential for survival, because energy could be drawn from this storage depot in times of famine. Paradoxically, this survival characteristic is disadvantageous when food is continuously abundant and palatable (Racette *et al.*, 2003). Another disadvantage is that adipocytes can only increase to a certain limit and can never expand beyond this critical size. The maximum volume of each adipocyte is genetically determined and varies among different fat depot. Once the available adipocytes are saturated, the hypertrophic adipocytes produce and release proliferative paracrine factors to trigger preadipocyte proliferation and differentiation to new adipocytes, thus increasing their cell number (Cinti, 2005). Males have 9-18% fat mass and 14-28% in females in relation to bodyweight, and can increase to 22% in males and 32% in females (Hausman *et al.*, 2001).

Increased WAT mass alters glucose metabolism and insulin sensitivity in muscles and liver due to impaired secretion of insulin by β -cells leading to systemic insulin resistance as depicted in Figure 1.2. Insulin resistance can be attributed to increased lipolysis and secretion of FFAs and glycerol (Galic *et al.*, 2009; Vázquez-Vela *et al.*, 2008). The increased flux of FFAs impairs insulin secretion and induces insulin resistance in muscle and the liver by interfering with glucose transport and insulin-mediated glucose uptake,

exerting negative influences on cardiovascular health (Lau *et al.*, 2005). Adipocytes are at the centre of obesity development, cellular and molecular dysfunctions occur in WAT as a consequence of excess TAGs stored in adipocytes and spread throughout the rest of the organs via the adipokines secreted by the WAT cells, leading to the events mentioned above (Greenberg and Obin, 2006).

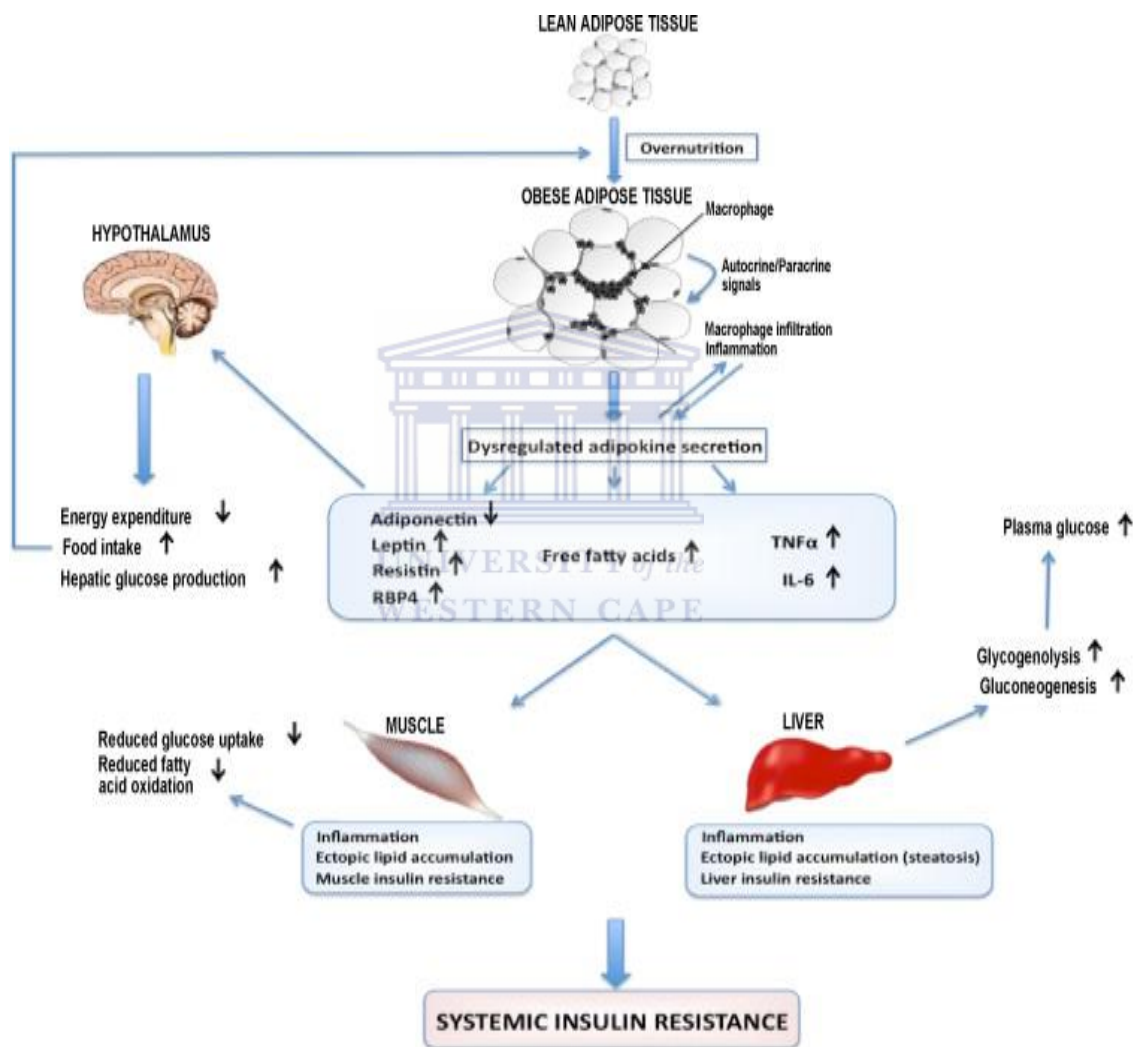


Figure 1.2: Obesity-induced changes in adipokine secretion and the development of insulin resistance. Expansion of AT in obesity leads to increased macrophage infiltration and inflammation with enhanced production of pro-inflammatory cytokines such as TNF- α and IL-6. This is accompanied by an increased release of FFAs and dysregulated secretion of leptin, adiponectin, resistin and retinol binding protein-4. Together, these adipocyte- and macrophage-derived substances can act in a paracrine or autocrine fashion to further exacerbate AT inflammation. On the systemic level, altered adipokine secretion can lead to increased food intake and reduced energy expenditure through actions in the hypothalamus and to decrease muscle and liver insulin sensitivity through enhanced ectopic lipid deposition and inflammation (Galic *et al.*, 2009). *Figure reprinted with permission from Elsevier.*

The stored TAGs cannot be hydrolyzed and metabolized due to deficiency of perilipin. Perilipins are considered gatekeepers for lipases, which are involved in the hydrolysis of TAG to facilitate the release of FFAs. Under normal conditions the dephosphorylated perilipins are bound to the surface of TAGs droplets to prevent hydrolysis of TAGs by lipases during obesity. In starvation, perilipins are activated by protein kinase A and the phosphorylated perilipins move from the surface allowing lipases access to TAGs and FFAs. However, their expression in obese individuals is downregulated, which is associated with their reduced basal rate of lipolysis (Galic *et al.*, 2009; Guo *et al.*, 2009).

1.2 CELL TARGETING AS A STRATEGY FOR OBESITY REVERSAL

Cell targeting also known as targeted therapy refers to the use of ligands that interact with disease-associated biomarkers to deliver therapeutic agents that will inhibit certain cellular actions leading to cell death and treatment of the disease (Ofei, 2005). Since targeting moieties are specific for the diseased cells or tissues (e.g. WATs in obesity), targeted therapies will have little or no effect on the surrounding normal cells or tissues. Cell targeting as a strategy for obesity reversal is reviewed below. A receptor targeted nanotherapy that could be used as anti-obesity therapy will be developed in this study. The targeted nanotherapy will result in elimination of hypertrophic adipocytes by targeting a WAT vascular marker. Obesity is a major risk factor for the development of serious chronic diseases as discussed in section 1.1. Its treatment and management may lead to an early intervention for prevention of these maladies and their consequences (Ofei, 2005).

Nanotechnology will be useful in minimizing the treatment dosage and help the treatment to circulate longer within a biological system. The targeting molecules will aid to transverse their cargo through the lipid bilayer into the cells for the treatment to be effective. Direct delivery of ligand-directed nanoparticles (treatment) to the relevant site will increase its efficacy. On binding to the target cells, the treatment will result in killing the cells in a controlled manner (apoptosis). The importance of *nanotechnology*, *vascular targeting (angiogenesis)* and *apoptosis* in development of receptor targeted therapy is discussed in the following section.

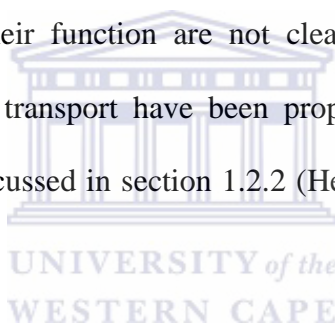
1.2.1 Cell penetrating peptides

Cell penetrating peptides (CPPs) are amino acids short sequences (<30 amino acids) which can translocate across the cell membrane in an energy, receptor and temperature-independent manner (El-Andaloussi *et al.*, 2007; Palm-Apergi *et al.*, 2012). They are cationic and hydrophilic peptides consisting of basic amino acids, arginine (R) and lysine (K) that allows them to pass through cell membrane with ease (Herce and Garcia, 2007; Palm-Apergi *et al.*, 2012; Sandoval *et al.*, 2007). Biologically useful CPPs, such as transactivator of transcription (TAT) from HIV-1, the herpes simplex virus VP22 protein, penetratin from the *Drosophila Antennapedia* homeodomain, and transportan have been identified (Herce and Garcia, 2007; Sandoval *et al.*, 2007). The main and commonly used CPPs are shown in Table 1.1. The first CPP to be discovered was TAT with the 11 amino acid sequence responsible for its translocation into cells (Frankel and Pabo, 1988). All the available CPPs have similar translocatory properties that are attributed to the polyarginines and polylysines in their sequences as highlighted in Table 1.1 (Leifert *et al.*, 2002).

Table 1.1: Types of commonly used cell penetrating peptides

Cell Penetrating Peptides	PTD Sequence
HIV-1 TAT	YGRKKRRQRRR
Drosophila Antennapedia homeodomain (penetratin)	RQIKIWFQNRRMKWKK
Herpes simplex virus VP22 protein	DAATATRGRSAASRPTERPRAPA -RSASRPRRPVE
Transportan	GWTLNSAGYLLGKINLKALAAL- AKKIL

In medical research, the CPPs are used to translocate cargoes such as nucleic acids, enzymes, proteins and drug-loaded liposomes through biological membranes (Herce and Garcia, 2007; Leifert *et al.*, 2002; Ziegler and Seelig, 2004). The exact mechanisms by which the CPPs perform their function are not clearly understood. However, several mechanisms of intracellular transport have been proposed for these peptides and vary among different CPPs as discussed in section 1.2.2 (Herce and Garcia, 2007; Sandoval *et al.*, 2007).



1.2.2 Mechanisms of uptake

Every living cell within the body is composed of a plasma membrane that serves as a boundary between the intracellular and extracellular environment. The plasma membrane controls what goes in and out of the cell. Smaller and polar molecules can readily diffuse in and out of the cell while larger molecules require transporter proteins that will alter the structure of the cell to transport them inside the cell. Due to selective permeability of cell membrane, several CPPs are often used to help molecules pass through into the cell in order to perform their functions. Translocation of the CPPs and their cargoes through cell

membranes can be achieved through different mechanisms indicated in Figure 1.3 (Green *et al.*, 2003; Trehin and Merkle, 2004).

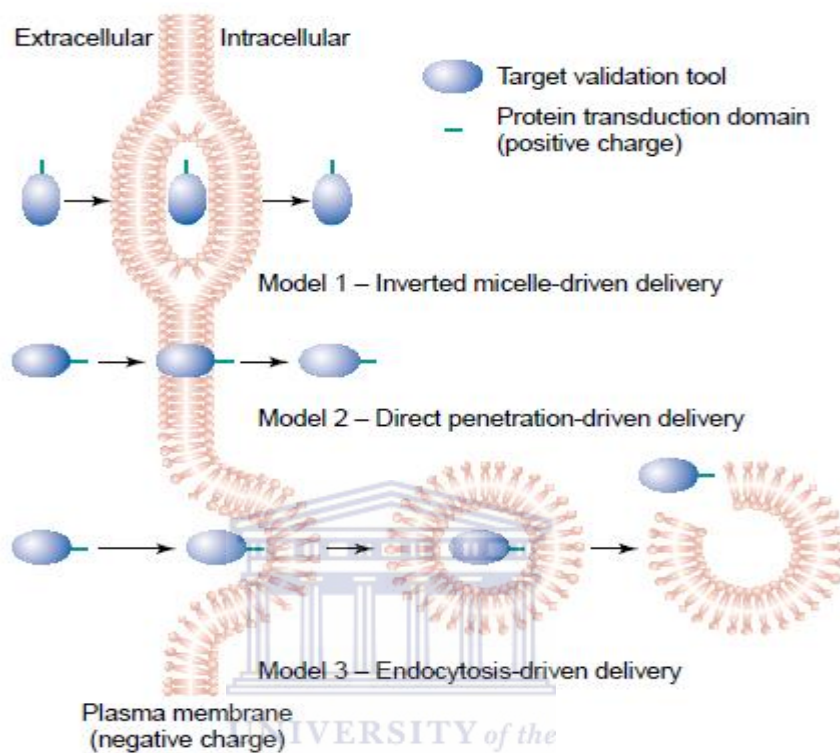


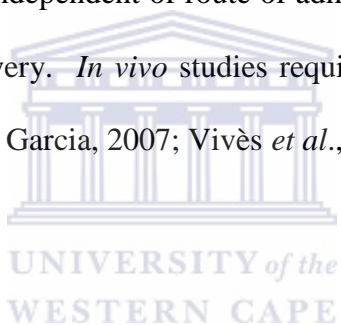
Figure 1.3: Cellular delivery of target validation tools by protein transduction domains. Initial binding of the PTD (green)-linked target validation tools (blue; including peptides, proteins and antisense) is mediated via an electrostatic interaction between the positively charged PTD and the negatively charged plasma membrane. Subsequent uptake was speculated to occur via a rapid, ATP- and receptor-dependent mechanism through formation of either an inverted micelle (Model 1) or direct insertion through the membrane (Model 2). However, recent studies suggest that PTD-conjugates are taken up by endocytosis from which small quantities of the conjugates are released via an unknown mechanism (Model 3) (Green *et al.*, 2003). *Figure reprinted with permission from Elsevier*

The three proposed mechanisms include the formation of micelles with the plasma membrane, direct penetration through the membrane that results in pore formation, and through engulfment of the molecule (phagocytosis). Some of these mechanisms require energy and are not necessarily receptor dependent or cell specific (Green *et al.*, 2003; Trehin and Merkle, 2004). The Antennapedia homeodomain-derived antennapedia (Antp) CPP for instance, transports their cargos through endocytosis. The interaction between the

CPP and the cell membrane results in formation of micelles that are then transferred into the cytoplasm and releases its cargo. Translocation of Antp across the membrane is due to the presence of R and K in its amino acid sequence and energy independent (Console *et al.*, 2003; Sebbage, 2009).

Due to the non-toxic nature of CPPs, they have been extensively used to deliver cargoes such as peptides and nucleic acids for therapeutic purposes (Heitz *et al.*, 2009). Cellular uptake and toxicity have been shown to be cargo dependent. However, CPPs are only effective for *in vitro* studies (Lindgren *et al.*, 2000; Sandoval *et al.*, 2007), their ability to translocate every given cell independent of route of administration, makes it impossible to use in animals for drug delivery. *In vivo* studies require specificity, the kind offered by targeting peptides (Herce and Garcia, 2007; Vivès *et al.*, 2008).

1.2.3 Targeting peptides



Targeting peptides are moieties or ligands that bind to specific cell receptors with higher sensitivity and affinity. They can be useful in targeting disease-specific markers that are upregulated or exclusively expressed in diseased cells in relation to normal tissues and often used as targets for diagnostic and therapeutic purposes. The targeting peptides are also able to bind to specified receptors and translocate their cargoes into the cell. Unlike CPPs they bind to specific cell-surface receptors to exert their functions (Leifert *et al.*, 2002). The targeting peptides are used in drug delivery as they allow more specificity and sensitivity of the drug, even at minute dosage it's possible to accumulate at specified site. Targeting peptides offers a promising opportunity for development of targeted therapy for chronic diseases, not limited to obesity (Kolonin *et al.*, 2004) and cancer (Li and Cho,

2012). Various targeting moieties are used to deliver molecules to specified areas such as carbohydrates, short peptides, aptamers and antibodies. For therapeutic purposes these moieties are usually targeted to extracellular domains of cell membrane receptors (Li and Cho, 2012).

1.2.3.1 Vascular targeting peptide: Adipose homing domain

Some important targets for therapeutic intervention in obesity have been discovered. Of interest to this research is the peptide known to associate with the cell surface receptor over expressed by endothelial cells (ECs) in the WAT vasculature of obese mice. Adipose Homing peptide (AHP) was coined to refer to this peptide. The peptide was discovered through phage display (screening method to determine interactions between receptors and ligands) by Kolonin and colleagues in *ob/ob* mice. The peptide has a nine amino acid sequence (CKGGRAKDC) and will be referred to as AHP now henceforth. The domain binds specifically to a cell membrane associated protein in the WAT vasculature, prohibitin (PHB). The protein (PHB, as discussed in section 1.2.3.2) was found to be abundant in the vascular ECs of the WAT of obese mice and human subjects (Kolonin *et al.*, 2004).

In the study done in 2004 by Kolonin and colleagues, a pro-apoptotic peptide $D(KLAKLAK)_2$ was coupled to AHP and systemically injected to obese mice. The AHP-conjugate was localized and internalized by the blood vessels of subcutaneous and peripheral white fat, but not other organs. This led to vascular EC death by apoptosis, resorption of fat in the WAT, normalization of metabolic processes and weight loss. Due to the specificity of the targeting ligand, no systemic or bystander effects was observed.

The desired effect of treatment was dependent on the internalization of treatment through the interaction between the PHB and the AHP-complex (Kolonin *et al.*, 2004). Internalization usually occurs via receptor-mediated endocytosis. The example of the folate receptor as shown in Figure 1.4 will be used to demonstrate the receptor-mediated mechanism of action (Cho *et al.*, 2008).

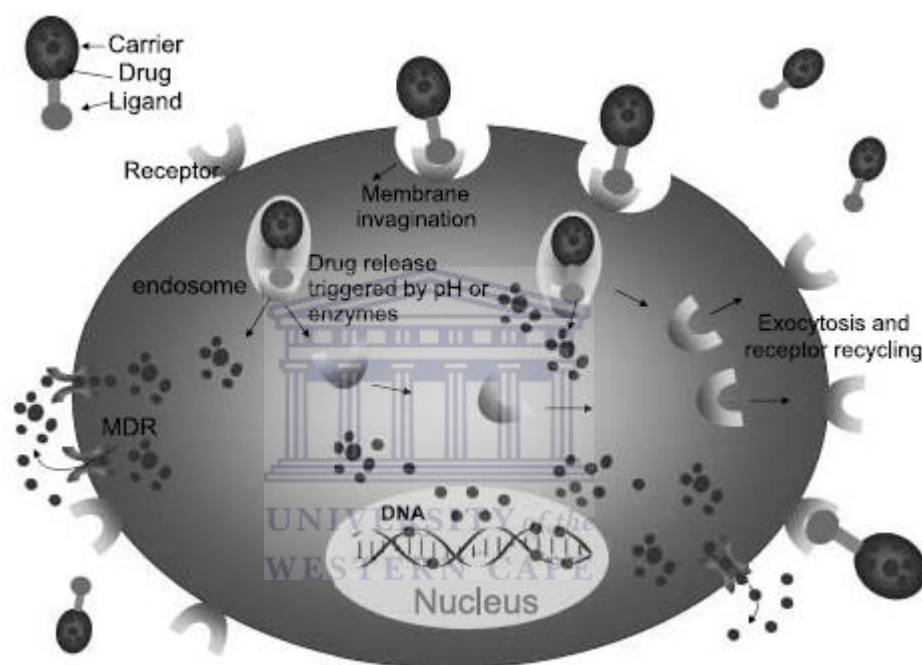


Figure 1.4: Internalization of nanoparticles via receptor-mediated endocytosis. Tumour-specific ligands or antibodies on the nanoparticles bind to cell-surface receptors, which trigger internalization of the nanoparticles into the cell through endosome. As a pH value in the interior of the endosome becomes acidic, the drug is released from the nanoparticles and goes into the cytoplasm. Drug-loaded nanoparticles bypass the P-glycoprotein efflux pump not being recognized when the drug enters cells, leading to high intracellular concentration (Cho *et al.*, 2008). *Figure reprinted with permission from American Association for Cancer Research.*

A folate-targeted conjugate binds to a folate receptor on the cell surface, the invaginating plasma membrane envelopes the complex of the receptor and ligand to form an endosome. Newly formed endosomes are transported inside the cell. The drug is then released from the conjugate and enters the cytoplasm. Released drugs are then trafficked by their target

organelle, the fate of the cell depends on the drug action. Meanwhile, the folate receptor is released from the conjugate and returns to the cell membrane to start a second round of transport by binding with new folate-targeted conjugates (Cho *et al.*, 2008).

AHP is presumably internalized in a similar manner. On binding to the PHB receptor, the AHP-conjugate gets internalized. The AHP-conjugate is released inside the cell and PHB receptor is then recycled and available for the next cycle if the cell is still alive (Kolonin *et al.*, 2004). The AHP serves as an ideal targeting ligand for development of anti-obesity therapy or drugs. Most anti-obesity drugs that are withdrawn from the market due to their toxicity towards normal tissues could benefit from this strategy. For therapeutic purposes, the targeting peptides must also meet certain requirements, first and foremost they should be target specific. PHB is highly expressed by the vascular ECs in the WAT of obese subjects as a cell surface protein not exposed in any other organs, as observed by Kolonin *et al.*, 2004. This is very important as it can increase the treatment's effectiveness without affecting other tissues. Another important requirement, the treatment has to be able to reach the desired target without losing their activity and also manage to escape phagocytic cells after passing through the circulatory system. These can potentially improve effectiveness of treatment by concentrating the drug at the diseased tissue and reduces systemic and bystander toxicity (Cho *et al.*, 2008).

This strategy suggests that membrane associated protein (PHB) in the vascular endothelium could serve as a useful target for the delivery of therapeutic compounds to enhance fat resorption in obese subjects (Hossen *et al.*, 2010; Thovhogi *et al.*, 2015). The data obtained through two independent studies proves that the vascular PHB can serve as a

biomarker for obesity treatment. The AHP-pro-apoptotic peptide conjugate through its interaction with the PHB was able to translocate the cell membrane, disrupt the mitochondrial functions causing cell death. Therefore, PHB targeting by its associate ligand (AHP) coupled to therapeutics is an appealing strategy for obesity treatment and prevention of its related diseases (Hossen *et al.*, 2010; Kolonin *et al.*, 2004).

1.2.3.2 Prohibitin

Prohibitin is of interest in this study as it is highly expressed by ECs in the WAT vasculature of obese rats and human subjects and will be used as target for obesity therapy intervention. It was found to be expressed as the cell surface receptor by vascular ECs of obese mice and human (Kolonin *et al.*, 2004).

Prohibitin is a highly conserved protein among different animal species and has a molecular weight of 30–32 kDa. The mouse and rat PHB amino acid sequences are identical, and differ from the human sequence by a single amino acid. Prohibitin, as shown in Figure 1.5, localizes in many cellular compartments such as the cell membrane, mitochondria, nucleus and other intracellular organelles (Mishra *et al.*, 2005). Regardless of its location, PHB might have distinct but overlapping functions in all the organs. In the plasma membrane, PHB functions as a chaperone for newly imported proteins and exerts its cellular function by binding to other biomolecules. The mitochondria-localized PHBs plays a role in cellular homeostasis and mitochondrial biogenesis by interacting with complex I and subunits of cytochrome *c* oxidase of the respiratory chain. Loss of mitochondria PHB impairs the mitochondrial respiratory chain function resulting in

oxidative stress and alters the mitochondrial morphology and membrane potential in most cells (Merkwirth and Langer, 2009; Artal-Sanz and Tavernarakis, 2009).

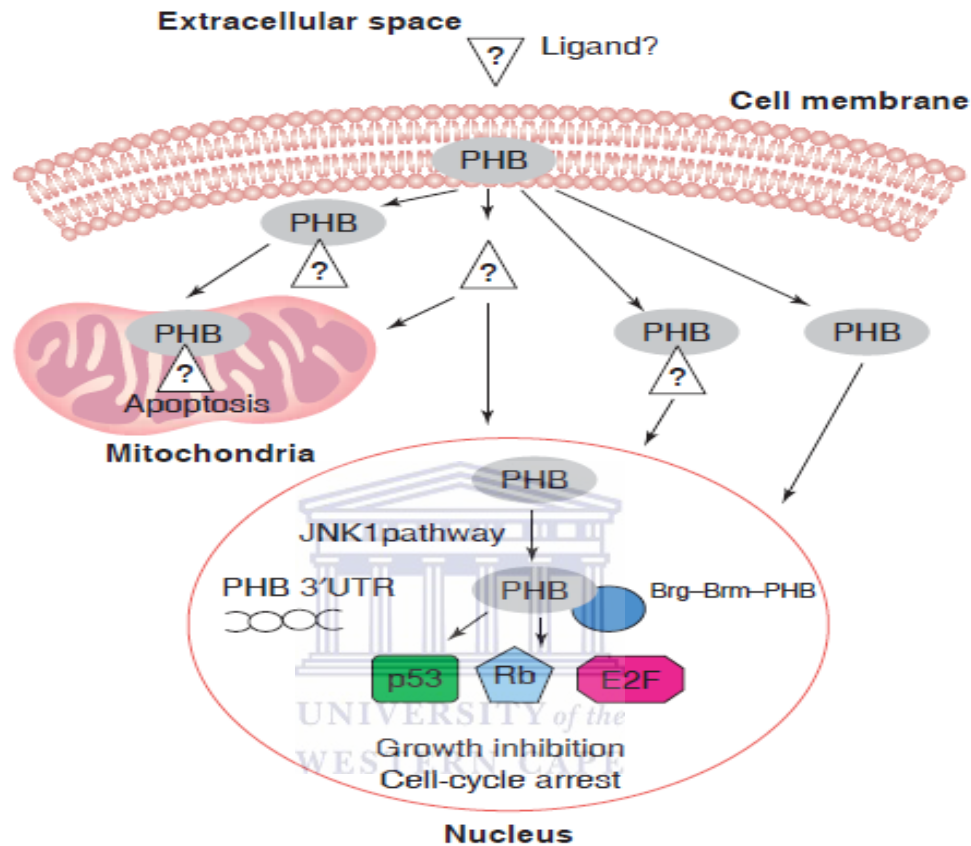


Figure 1.5: The subcellular localization of prohibitin and potential mechanisms involved in PHB action. PHB is present on the cell membrane where it can interact with peptides and possibly endogenous ligand or ligands. Such ligands could be potentially translocated to the mitochondria and disrupt mitochondrial function, resulting in apoptosis. Membrane-bound PHB might be involved in modulating the expression of cytokines, such as IL-6, by MAP kinase and other signalling pathways. PHB might also be translocated from the cell membrane to the nuclear compartment. In the nuclear compartment, PHB might function as a modulator of transcription. The phosphorylation of PHB, possibly by the JNK1 pathway, might be necessary for the anti-proliferative effects of PHB. The latter involves the interaction with Brg1–Brm, inhibition of the E2F pathway and both p53- and pRB-dependent and p53- and pRB-independent mechanisms (Mishra *et al.*, 2005). *Figure reprinted with permission from Elsevier.*

When translocated to the nucleus, PHB modulates transcriptional activity. Phosphorylation of PHB through the JNK1 signalling pathway is thought to play a part in transcription and exerts its anti-proliferative effects and other biological functions. PHB interacts with

ATPase components, Brg1 and Brm and repress the E2F transcriptional activity through remodelling of local chromatin (Mishra *et al.*, 2005).

The role of PHB in adipocyte differentiation is elusive. Interestingly, overexpression of MicroRNA-27 in human adipose-derived stem cells led to downregulation of its expression and adipocyte differentiation (Kang *et al.*, 2013). This further confirms that AT growth can be regulated by targeting PHB in the EC surface of WAT vasculature serve as a target for therapeutic intervention in obesity. As a cell surface protein it can easily interact with antibodies, peptides and ligands that bind to it and translocate their cargoes into the cells to disrupt their biological functions (Mishra *et al.*, 2005; Kolonin *et al.*, 2004). The cargoes can be therapeutic peptides or diagnostic agents, used to detect the presence of certain disease markers or induce cell death in order to reverse the disease effects on target tissues (Mishra *et al.*, 2005). Physiologically, PHB is a multifunctional protein that plays crucial roles as a tumour suppressor gene, a chaperone protein that stabilizes mitochondrial proteins and as a regulator of cell cycle (Gamble *et al.*, 2004; Mishra *et al.*, 2005). However, our interest in PHB originates from being a cell surface receptor that can be used as a vascular target for obesity treatment (Kolonin *et al.*, 2004).

1.3 VASCULAR TARGETING

Vascular targeting has been used in recent years for treatment of chronic diseases, different forms of cancer and arthritis. Vascular targeting through angiogenesis offers an attractive strategy for disease treatment with minimal toxicity and resistance. Cells involved in angiogenesis tend to overexpress cell membrane receptors during development of a disease state. Targeting these cells disturbs the growth and functioning of the diseased cells or

tissues as they rely on them for oxygen and nutrient supply. The vascular ECs are at the centre of vascular targeting as they are the cells that are responsible for most tissue haemostasis by supplying all necessary components for cell growth. They are easily accessible, one EC is responsible for more than one adipocyte and disrupting their function indirectly disturbs the survival and growth of the unwanted cells (Ruoslahti, 2000).

1.3.1 Angiogenesis

Angiogenesis was first introduced by John Hunter in 1787 and gained popularity in 1971 in cancer research through Judah Folkman's hypothesis that tumour growth is dependent on angiogenesis. The term angiogenesis or neovascularisation refers to the growth of new blood vessels from pre-existing capillaries (Gupta and Zhang, 2005). Angiogenesis is a physiological process that plays an important role in distribution of oxygen and nutrients to different cells and organs throughout the body, as well as removal of waste products. Angiogenesis is a sequential process that occurs throughout life with minimal occurrence in healthy adults. Angiogenesis starts early in life from development of embryos, continues through menstrual cycles in women and also takes part in wound healing and repair (Griffioen and Molema, 2000; Liekens *et al.*, 2001).

Angiogenesis is a tightly regulated process and dysfunction in the growth of blood vessels contributes to the pathogenesis of numerous disorders. Angiogenesis dysfunction has been implicated in a number of serious chronic diseases such as obesity, diabetic retinopathy, cancer, rheumatoid arthritis, AIDS and autoimmune disease. These are some of the conditions in which angiogenesis is switched on when they develop (Colville-Nash and Scott, 1992). In conditions where angiogenic switch is insufficient; blood vessel

revascularization, healing and regeneration is prevented (Carmeliet, 2005; Liekens *et al.*, 2001).

1.3.1.1 The process of angiogenesis

Life form begins with the development of vascular systems that leads to formation of essential tissues or organs. This is a highly regulated and sequential process that maintains blood flow throughout the tissues and organs within the body. Blood vessels regeneration in response to wound healing or cellular growth involves several steps and complex interaction between vascular cells (ECs, pericytes, smooth muscle cells, etc) and the corresponding extracellular environment. The process of angiogenesis is stimulated when the damaged or diseased tissues require nutrients and oxygen (Nishida *et al.*, 2006). The interaction between ECs with the extracellular matrix (ECM) is very crucial for induction of angiogenesis. The whole process is coordinated by integrins and a number of growth factors (GFs). The integrins are responsible for specific cell–ECM interactions for EC adhesion and migration to growing tissues or organs (Eliceiri and Cheresh, 2001).

Angiogenesis is regulated by both modulator (vascular endothelial growth factor (VEGF), integrins, matrix metalloproteinase (MMPs) and inhibitor (Angiostatin, Endostatin) molecules. Under physiological conditions, the activity of these molecules is kept on a balance. Shift in the balance between the modulators and inhibitors of angiogenesis will determine whether to switch on or off. For instance, up-regulation of angiogenic or activator molecules favours angiogenesis, the opposite discourages its occurrence (Nishida *et al.*, 2006).

Angiogenesis is a complex process that follows a series of steps in diseased or growing tissues as illustrated in Figure 1.6 (Pandya *et al.*, 2006).

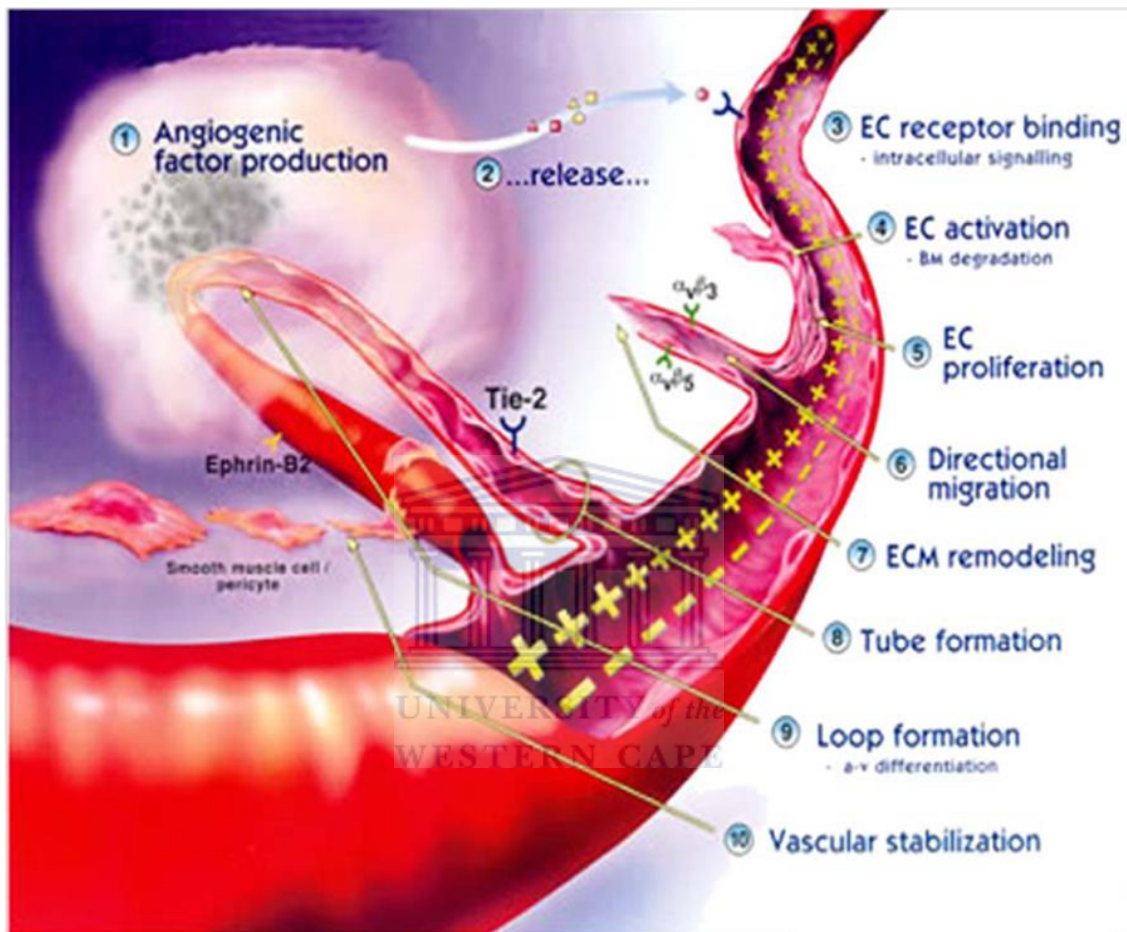


Figure 1.6: The process of angiogenesis. (1) Tumours produce and release angiogenic GFs that diffuse into the nearby tissues. (2) The angiogenic GFs bind to specific receptors located on the ECs of nearby pre-existing blood vessels. (3) Once GFs bind to their receptors, the ECs become activated. Signals are sent from the cell's surface to the nucleus. The EC's machinery begins to produce new molecules including enzymes. (4) Enzymes dissolve tiny holes in the sheath-like covering (basement membrane) surrounding all existing blood vessels. (5) The ECs begin to divide (proliferate), and they migrate out through the dissolved holes of the existing vessel towards the diseased tissue (tumour). (6) Specialized molecules called adhesion molecules, or integrins ($\alpha_v \beta_3$, $\alpha_v \beta_5$) serve as grappling hooks to help pull the sprouting new blood vessel sprout forward. (7) Additional enzymes (MMP) are produced to dissolve the tissue in front of the sprouting vessel tip in order to accommodate it. As the vessel extends, the tissue is remoulded around the vessel. (8) Sprouting ECs roll up to form a blood vessel tube. (9) Individual blood vessel tubes connect to form blood vessel loops that can circulate blood. (10) Finally, newly formed blood vessel tubes are stabilized by specialized muscle cells (smooth muscle cells, pericytes) that provide structural support. Blood flow then begins (Pandya *et al.*, 2006). *Figure reprinted with permission from Elsevier.*

Development of diseases such as cancer and adiposity (obesity) characterized by increased size or number of cells beyond their critical size limit are said to be dependent on this process (Cao, 2010). The proliferating cells produce and release angiogenic GFs (such as fibroblast growth factor (FGF), angiopoietin-1 (Ang-1), VEGF) that diffuse into the nearby tissues in order to interact with the existing vascular bed. The GFs bind to specific receptors on the ECs of pre-existing blood vessels within the affected tissue or organ. The ECs are then stimulated to send signals from the cell's surface to the nucleus that will lead to production of angiogenic factors including proteolytic enzymes such as MMPs. The proteolytic enzymes punch holes in the basement membrane surrounding the existing blood vessels. The ECs branch out from the holes in the pre-existing blood vessels by sprouting and migrating towards their target cells (diseased tissue) in order to extend the vasculature (Tassi and Wellstein, 2006; Ucuizian and Greisler, 2007).

The entire process in diseased and physiological states is dependent on proliferation and migration of ECs to growing cells (Gupta and Zhang, 2005). The proliferation and migration of ECs followed by its invasion to growing or diseased organs is dependent on the activities of the plasminogen activator (PA) system and the MMPs. The urokinase-type plasminogen activator (uPA) and tissue-type plasminogen activator (tPA) are serine proteases that are responsible for conversion of plasminogen into plasmin within the vascular network. Plasmin is required for degradation of ECM components such as fibrin, fibronectin, laminin, the protein core of proteoglycans and is suspected to activate MMP-1, 3 and 9 (Liekens *et al.*, 2001).

The tPA mainly controls the fibrinolytic activity in blood whereas uPA is responsible for activation of plasminogen in tissues. The pro-uPA binds to the uPA receptor, plasmin and

several molecules (Factor XIIIa, or cathepsin B) responsible for activation of pro-uPA. Activation of uPA enhances its activity on the cell surface and stimulates signal transduction through the uPA receptor, leading to cell migration and invasion (Liekens *et al.*, 2001).

The coordination between adhesion molecules () and GFs are also equally important. The GFs are required to interact with its surrounding ECM for the cells to proliferate and migrate to the diseased cells. This process helps these cells escape cell death via apoptosis or starvation (Gupta and Zhang, 2005). The vascular ECs takes time to divide (about every 1000 days), integrins (avb3, avb5) directs the whole process. The sprouting ECs move towards the diseased cells, the new forming vessel extends and surrounds the cells. The new vessels are stabilized by smooth muscle cells and pericytes in the vascular bed. The blood now begins to flow to the cells and supply all the necessary ingredients for their survival (Eliceiri and Cheresh, 2001; Ucuzian and Greisler, 2007).

Cells all over the body grow to a certain diameter. Beyond this limit, it becomes difficult to grow because blood supply is insufficient to reach the hypertrophic or over-sized cells. When blood supply is limited, the supply of nutrients and oxygen, and removal of waste from the growing cells become problematic. Under these conditions, the cells secrete angiogenic stimulators that will switch on the angiogenic process and new blood vessels are formed. This process supports growth of the diseased cells and in return causes over expression of certain angiogenesis associated proteins (e.g. VEGF receptor-II) that are distinct from quiescent ECs in healthy adult tissues. The differential expressed disease markers are potential targets for therapeutic interventions, targeting the vasculature could be effective for treating diseases as the cells are dependent on angiogenesis for growth.

Insufficient food and oxygen supply will slow down the growth of diseased cells or kill them in the process as these cells are dependent on newly formed blood vessels, a process that is highly regulated by proliferation of ECs. Vascular targeting is an appealing strategy as the toxic effects of treatment will be restricted to the targeted cells, thereby increasing the therapy efficacy and reduce undesirable effects (Okaji *et al.*, 2006; Tassi and Wellstein, 2006).

1.3.2 Clinical significance of angiogenesis

Angiogenesis as a potential therapy for cancer was discovered in the early 1970s. However, research in angiogenesis began in the 1990s after the discovery of the first compounds with specific angiostatic effects. These discoveries proved that cancer growth can be prevented by inhibition of angiogenesis (Ingber *et al.*, 1990; O'Reilly *et al.*, 1994). Various diseases including cancer and obesity are highly dependent on the formation of new vasculature for their progression (Cao, 2010; Hausman and Richardson, 2004). Therefore, the diseased areas will be highly vascularised in order to support the continually growing tissues, following the formation of blood vessels triggered by ECs migration and proliferation, as explained in section 1.3.1.1. The excessive blood vessel growth renders these areas vulnerable at the level of their blood supply. Thus, angiogenesis inhibition serves as a better therapeutic option for these diseases. The angiogenic process is mostly vulnerable at the proliferation stage of ECs, as their growth during disease development is often followed by over secretion of pro-angiogenic factors which might be useful as targets for therapeutic intervention (Griffioen and Molema, 2000).

Angiogenesis inhibitors have gained popularity in cancer research and shown great potential in its treatment in preclinical and clinical studies (Griffioen and Molema, 2000; Tassi and Wellstein, 2006). The anti-angiogenic inhibitors are mostly targeted at arresting vascular EC's growth in the diseased areas, this prevents the diseased cell' growth and metastasis. It is believed that one EC is responsible for several cells, therefore delaying or prevention of their proliferation will starve the diseased cells/ tissue leading to cell death. Moreover, occurrence of physiological angiogenesis is minimal in adults and side effects associated with long-term treatment effects will be reduced (Tassi and Wellstein, 2006). Another crucial fact about ECs is that they are always in contact with the blood vessels and the surrounding tissues, this makes them easily assessable by systemically administered treatment (Okaji *et al.*, 2006).

Anti-angiogenic agents such as monoclonal antibodies and synthetic molecules in animal models has generated useful information about their mechanisms of action and the desirable effects, and some of them are recently used in clinical trials (Carmeliet, 2005). The first FDA clinically approved and mostly studied anti-angiogenic agent is Bevacizumab (its trade name is Avastin). Bevacizumab is a humanized mouse monoclonal antibody that binds to VEGF-A receptor in the blood vessels. In the United State Bevacizumab is approved for treatment of metastatic cancers (colorectal, lung, and kidney cancer) and eye disease. Bevacizumab is undergoing phase III of clinical studies in patients with metastatic colorectal cancer. Most of the anti-angiogenic agents studied inhibits EC growth by binding to VEGF receptors, prevents vessel growth, but also induces regression of existing vessels by increasing EC death. VEGF inhibitors being studied include a VEGF trap (Regeneron) and antibodies against VEGFR-1 (Imclone) or

VEGFR-2 and placenta GF (a VEGF homologue). Targeting VEGF receptors is a safer option as it is highly expressed in disease state than in healthy tissues. Although VEGF inhibitors have exciting outcomes in pre- and clinical studies, it is cytotoxic to some extent in some malignant cells. These inhibitors are also associated with immune response that suppresses the proangiogenic activity of haematopoietic cells (Carmeliet, 2005).

Furthermore, the monoclonal antibodies used are produced in mice and when used in human subjects can elicit an immune response. To avoid this action, they will have to be humanized before clinical applications (Carmeliet, 2005). These antibodies have a short half-life and higher dosage for extended period will be required to obtain a desired effect. The shortfalls can be overcome by development of cell specific anti-angiogenic treatment. Vascular ECs produce receptors that are cell and disease specific, as such can be used as biomarkers. Research is being conducted in pre-clinical animal models using the targeted-therapy mainly in cancer research (Carmeliet, 2005; Okaji *et al.*, 2006).

1.3.3 Angiogenesis in obesity

Angiogenesis is an important factor in the expansion of WATs. Adipose tissue growth and expansion through hypertrophy or hyperplasia is highly dependent on the plasticity of the vasculature (Cao, 2010). During development of obesity, hypertrophy and hyperplasia are excessive and require the extension of blood vessels to reach the newly formed and the overgrown adipocytes. This extensive blood vessel network maintains the WAT's physiological role by secreting GFs, hormones, cytokines and angiogenic factors required for tissue remodelling. For this purposes angiogenesis is an attractive target for therapeutic intervention for reversal of obesity, as these vessels are readily accessible for targeted

therapy particularly when administered systemically. There are several studies demonstrating the efficiency of antiangiogenic therapy in animal models of obesity (Cao, 2010, Kolonin *et al.*, 2004, Barnhart *et al.*, 2011).

Angiogenesis in WATs is dependent on the balance between pro-angiogenic and anti-angiogenic factors. Increase in proangiogenic factors, mainly VEGF-A and hepatocyte growth factor (HGF) in WATs initiates the angiogenesis process (Christiaens and Lijnen, 2010). Adipocytes growth in WATs is highly dependent on angiogenesis, thus, inhibition of this process through proangiogenic factors can be helpful in regulating WAT mass and prevent weight gain (Hajer *et al.*, 2008). This was proven with both *in vitro* and *in vivo* models of obesity (Bråkenhielm *et al.*, 2004). Antibodies or ligands that target angiogenic GFs in WAT vasculature have been shown to inhibit angiogenesis by blocking activities of receptors such as VEGFR-2 to prevent WAT growth in a genetic and diet-induced animal models of obesity (Christiaens and Lijnen, 2010; Tam *et al.*, 2009).

Angiogenesis inhibitors with anti-obesity effects were discovered through *in vitro* studies. The widely studied include TNP 470, angiostatin, endostatin and leptin; all discovered to reduce body mass in obese subjects. Inhibition of angiogenesis in WATs by the use of these inhibitors proves that these tissues are vulnerable at their vasculature, and angiogenesis serve as a desirable target for therapy intervention. Different inhibitors have different targets, working towards the same goal (Bråkenhielm *et al.*, 2004; Rupnick *et al.*, 2002). TNP 470 for instance, targets Methionine aminopeptidase-2 in the ECs (Bråkenhielm *et al.*, 2004). TNP 470 analogs (CDK 732) also showed similar effects. CDK 732 acts by decreasing food intake, the size of adipocytes, fat mass, and body weight in selected rodent models of obesity (C57BL/6J ob/ob mice, Otsuka Long–Evans

Tokushima fatty (OLETF) rats, Sprague-Dawley rats, Long-Evans Tokushima Otsuka (LETO) rats). The efficacy of CDK 732 was found to be higher than TNP 470 in both *in vitro* and animal studies (Kim *et al.*, 2007).

Angiogenesis can also be disrupted at a gene level by knocking down genes that promote blood vessel growth. WATs secretes a number of proangiogenic factors including HGF, VEGF-B, VEGF-C, placental GF, FGF-2, Ang-1, Ang-2, tumour necrosis factor (TNF) and MMPs (Christiaens and Lijnen, 2010). One of the major genes responsible for angiogenesis in WAT is HGF, it is exclusively secreted by WAT and has angiogenic and mitogenic effects. Their levels are increased in serum of obese subjects than healthy subjects. The HGF effects on WAT angiogenesis was determined *in vitro* (3T3-F442A preadipocytes) and *in vivo* (BALB/c athymic nude mice) studies. The HGF gene was silenced in 3T3-F442A preadipocytes through siRNA technology and injected in BALB/c athymic nude mice. Differentiation of the preadipocytes into adipocytes and formation of functional fat pads in the mice occurred at a slower rate compared to the normal controls. The ability of developing fat pads to recruit ECs for neovascularization in the treated mice was impaired (Bell *et al.*, 2008).

1.3.3.1 Adipose tissue vasculature

The development and maturation of adipocytes (adipogenesis) and various cells in the ATs is dependent on angiogenesis, for this purpose the ATs are highly vascularised. The AT vascularity is very crucial for the functioning of AT as an endocrine organ (Cao, 2010; Hausman and Richardson, 2004). Adipocytes in WAT are in contact with one or more

capillaries, thus their growth is always associated with the neovascularisation and remodelling of the vascular network. Neovascularization promotes the hyperplastic adipocyte through pre-adipocyte differentiation and remodelling and also accommodates the hypertrophic adipocytes (Christiaens and Lijnen, 2010; Lijnen, 2008).

The vasculature plays a key role in the development of obesity as expansion of AT is supported by angiogenesis. Angiogenic factors promote differentiation of pre-adipocytes to adipocytes through several mechanisms as illustrated in Figure 1.7 (Cao, 2010). The growing AT cells requires nutrients and oxygen for tissue growth, and to maintain their physiological functions and for their maintenance. Blood supply is very crucial for the body's functions: tissue homeostatic and the metabolic activities. Adipocytes also require blood supply for their metabolic or endocrine functioning that occurs in the thin rim of cytoplasm surrounding the lipid droplet. For this reason, each adipocyte in ATs is constantly in contact with blood capillaries. The amount of blood flow to these adipocytes is dependent upon the body weight and nutritional state, with blood flow increasing during fasting. Blood flow to AT seems minimal to other organs, 3–7% of cardiac output is required to supply 0.2–0.6L of blood per minute in normal human adipose organ and increases to 15–30% in morbid obesity. This causes a lot of strain to the heart and can cause hypertension and congestive heart failure in obese subjects, however weight loss can reverse these hemodynamic factors (Hausman *et al.*, 2001).

Blood vessels are enriched with the GFs and cytokines that are important in growth and survival of adipocytes and maintenance of their physiological functions. Stem cells derived from bone marrow and other tissues destined to be AT cells are transported through blood vessels. The most important function of the WAT vascular cells is their

ability to secrete cell surface receptors which can be useful targets for disease treatment. The ECs are the major key factors in execution of angiogenesis, they secrete GFs, cytokines and act as a mediator between vascular cells and the ECM (Cao, 2010).

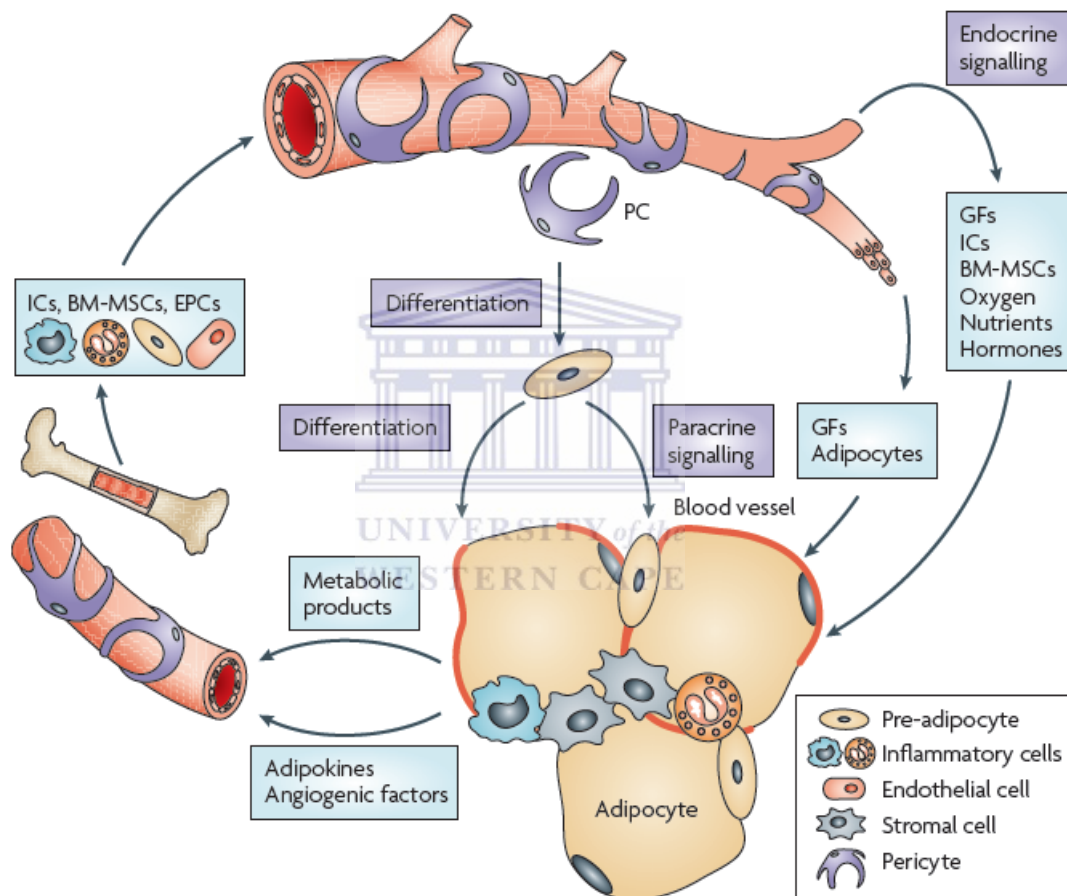


Figure 1. 7: Functions of adipose tissue vasculature. Outgrowth of blood vessels in adipose tissue provides oxygen, nutrients, GFs, hormones, inflammatory cells (ICs) and bone marrow derived mesenchymal stem cells (BM-MSCs) for maintaining homeostatic functions of adipocytes and expanding adipose tissue. Adipose tissue vasculature also removes metabolic products from the adipocytes. In the circulation, bone marrow-derived ICs, BM-MSCs and endothelial progenitor cells actively participate in adipogenesis and angiogenesis. Endothelial cells in angiogenic vessels produce growth factors and adipokines to maintain homeostatic functions and expand AT. Perivascular cells such as pericytes can differentiate into WAT preadipocytes that become adipocytes. Adipocytes also produce angiogenic factors and adipokines that induce angiogenesis (Cao, 2010). *Figure reprinted with permission from Nature Publishing Group.*

The ECs once activated during pathological angiogenesis, overexpress surface receptors that can serve as targets for drug discovery (Cao, 2010; Sengenès *et al.*, 2007). This led to discovery of PHB, overexpressed by EC in WAT vasculature of obese *ob/ob* mice. Targeting PHB with pro-apoptotic peptide led to reversal of obesity, proving that the concept is feasible (Kolonin *et al.*, 2004).

Vascular growth and remodelling in WATs is responsible for several functions such as cellular growth and tissue homeostasis and communication with the surrounding organs. WATs as a fat storage organ grows, expands and shrinks throughout life, these functions are regulated through their angiogenic capability (Cao, 2010; Kolonin *et al.*, 2004). Thus, hypervascularization of WAT occurs during obesity development. Increase in WAT mass affect various cells in the WATs through their secreted adipokines. Adipocytes interact with ECs leading to production of proangiogenic factors and cytokines during their (adipocytes) developmental stages. Vascular dysfunctions in the WATs can lead to dysfunction between the interplay between ECs and adipocytes. Alteration in EC's function in obese individuals has a negative impact in surrounding tissues and organs by affecting their roles in lipid metabolism, tissue homeostasis leading to the development of disorders such as CVD, insulin resistance, T2D and cancer (Cao, 2010). Thus, disturbance of endothelium function in WAT's vasculature of obese rats and eventually human beings is an appealing approach for the prevention and treatment of obesity and obesity-induced diseases. This is likely to force the hypertrophic adipocytes to metabolize the excess fat, thereby reducing the WAT mass leading to body weight loss that can be maintained for a longer period. In this study, a pro-apoptotic peptide will be attached to the ligand that binds to PHB to induce EC death by apoptosis.

1.4 APOPTOSIS

Apoptosis is a physiological cell death process, a suicide death that a cell undergoes in response to internal or external stimuli to remove damaged and infected cells from the body. The stimuli can be anything that can induce DNA damage in the nucleus, such as radiation or toxicants. Apoptosis is a sequential signalling pathway that involves protein-cleaving proteases known as cysteinyl-aspartate-specific proteases, caspases. Caspases plays a critical role in the execution phase of apoptosis. The formation of proteolytic caspase cascade activates or deactivates substrates, amplifying and integrating pro-apoptotic signals as detailed in section 1.4.1 (Derakhshan, 2007; Gullicksen *et al.*, 2003).

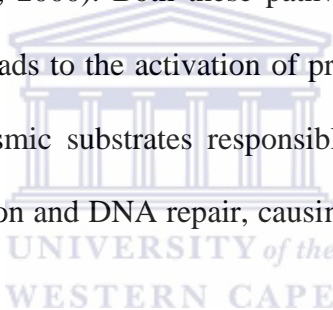
Morphologically, apoptosis is characterized by loss of cellular contact with the surrounding cells, cytoplasmic contraction and chromatin condensation. Biochemically, several changes can be observed: this include genomic DNA fragmentation, externalization of phosphatidylserine (PS) component of the phospholipid bilayer, and formation of apoptotic bodies that are removed through endocytosis by macrophages before the cells lose their plasma membrane integrity (McConkey, 1998; Nelson-Dooley *et al.*, 2005).

Although a number of stimuli appear to trigger the process of apoptosis, there are two major signalling pathways: the death receptor pathway and the mitochondrial pathway (McConkey, 1998; Nelson-Dooley *et al.*, 2005). The stimuli in which the cell will trigger its self-destruction determine the mode of cell death. Extrinsic death signals such as Fas ligand and TNF- α induce cell death from the outside of the cell, whereas DNA damage,

oxidative stress, toxigens and deficiency of survival factors, are communicated through mitochondria to evoke intrinsic cell death (Asoh and Ohta, 2008).

1.4.1 Apoptosis pathways

Programmed cell death, as the name suggests is a naturally occurring process. Every cell within the body is equipped with all the necessary machinery to activate apoptosis when an irreparable DNA damage occurs. Apoptosis continually take place throughout the growing process, it can be initiated by intrinsic or extrinsic signal pathways and executed by caspases (Mallat and Tedgui, 2000). Both these pathways involve a series of molecular and biochemical steps that leads to the activation of pro-caspases. The activated caspases cleaves nuclear and cytoplasmic substrates responsible for the maintenance of nuclear integrity, cell cycle progression and DNA repair, causing cell death (Nelson-Dooley *et al.*, 2005).



Intrinsic pathway

The intrinsic or mitochondrial pathway is initiated when stress molecules (ROS, reactive nitrogen species), chemotherapeutic agents, UV radiation, withdrawal of survival factors and changes in hemodynamic parameters occurs within the cell (Nelson-Dooley *et al.*, 2005). As the name suggests, the mitochondrial pathway is dependent on the release of cytochrome c from the mitochondria induced by irreparable DNA damage. Failure to sense and repair damaged DNA at checkpoint stimulates this pathway. Depending on the extent of DNA damage, apoptosis can be an immediate or delayed reaction within the cell. Nuclear transcription factor, p53 is often involved in apoptosis. p53 upregulation activates

genes such as Bcl-2 associated protein-X (Bax), resulting in either a decrease in the inner mitochondrial transmembrane potential or opening of the voltage-dependent anion channel (VDAC). Cytochrome c is released from the mitochondria, apoptotic protease activating factor-1 (Apaf-1), procaspase 9 and either ATP or dATP forms a complex called apoptosome. Formation of the apoptosome activates caspase 3 leading to cell death (Kiechle and Zhang, 2002).

Intrinsic pathway is dependent on the permeability of mitochondrial membranes and release of cytochrome c as outlined in Figure 1.8. Briefly, the mitochondrial permeability transition pore (PTP) is the key regulator of intrinsic pathway. The PTP's crucial components in activation of apoptosis are VDAC-1 in the outer mitochondrial membrane (OMM) and adenine nucleoside translocator (ANT) in the inner mitochondrial membrane (IMM) (Nelson-Dooley *et al.*, 2005; Shore, 2009; Shoshan-Barmatz *et al.*, 2010).

Mitochondria are the power house of the cells, they contain all the necessary equipment for cell survival and death. Mitochondria are gatekeepers for apoptosis, under normal conditions they maintain a balance in production of ROS. Most of their functions are executed via ion channels, VDAC in apoptosis. Mitochondria are made up two distinct and important compartments: the matrix surrounded by the IMM, contains enzymes responsible for β -oxidation and citric acid cycle; the intermembrane space surrounded by the OMM contains several apoptosis-inducing factors (cytochrome c, procaspases and AIF). Thus apoptotic stimuli increase permeability of the OMM and/or IMM, and induce cytochrome c release (Nelson-Dooley *et al.*, 2005; Shoshan-Barmatz *et al.*, 2010). Release of cytochrome c seals the fate of the cell, which is death. This process can be counteracted

by anti-apoptotic proteins (Bcl-2 and Bcl-xL), their increased expression prevents cytochrome *c* release and promotes cell survival (Kutuk and Basaga, 2006).

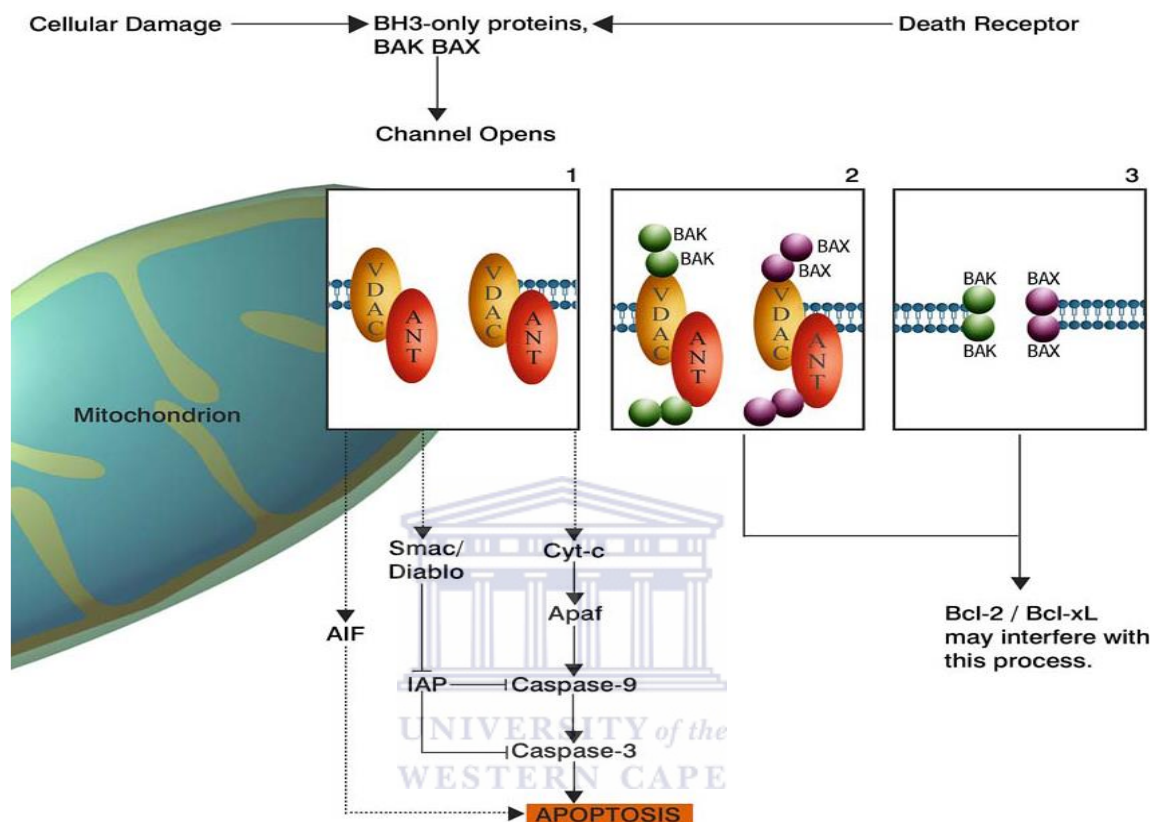


Figure 1.8: Three models for the cytosolic escape of mitochondrial proteins in response to apoptotic stimuli. Upon an apoptotic stimulus such as cellular stress (oxidative stress, UV irradiation, growth factor withdrawal) or activation of death receptors, a mitochondrial channel could be formed by: 1. Voltage-dependent anion channel (VDAC) and adenine nucleotide translocase (ANT), 2. VDAC-ANT-Bcl-2 proteins (Bax, Bak), 3. Only Bcl-2 proteins (Bax, Bak). Anti-apoptotic members of Bcl-2 protein family (Bcl-2, Bcl-xL) may interfere with the apoptotic process through the inhibition of cytosolic escape of mitochondrial proteins (Kutuk and Basaga, 2006). *Figure reprinted with permission from Springer.*

Extrinsic pathway

Extrinsic signals such as cytokines, hormones, oxidized lipids, chemotherapeutic, ionizing or viral agents are also capable of inducing apoptosis. Extrinsic pathway compared to Intrinsic is more acute and massive (Nelson-Dooley *et al.*, 2005). Cell death through this pathway involves recognition of cell membrane death receptors by the ligands from TNF

gene family, the most studied being Fas. Binding of a ligand to the death receptor recruits two signal transducing molecules: TNF receptor-1-associated death domain protein (TRADD) and Fas-associated protein with death domain (FADD). Either molecule binds procaspase-8 leading to formation of an intracellular complex known as death-inducing signal complex (DISC). The formation DISC results in proteolytic cleavage and activation of procaspase 8 to caspase 8 leading to DNA degradation by cleaving procaspase 3, or truncate Bid to tBid resulting in mitochondrial release of proapoptotic peptides through binding to Bak. Binding of tBid to Bak initiates similar steps as in intrinsic apoptotic pathway, the release of cytochrome c leading to formation of apoptosome followed by cell death (Nelson-Dooley *et al.*, 2005; Kiechle and Zhang, 2002).

The morphological and biochemical events in the two pathways can be detected through different assays and techniques: for instance translocation of PS can be detected by flow cytometry using annexin V which binds to externalized PS. This translocation is necessary for marking the apoptotic cells for their removal by macrophages. DNA fragmentation into 180–200 base-pair units initiated by caspase-3 activation can be determined by agarose gel electrophoresis. Morphological changes: cell shrinkage, chromatin condensation, membrane blebbing can be observed under light microscopy (Kiechle and Zhang, 2002; Sorisky *et al.*, 2000).

1.4.2 Apoptosis in obesity

Apoptosis is a process that has been known to occur during development of obesity in the ATs. Apoptosis in the hypertrophic adipocytes of obese rodents and humans was naturally triggered by either extrinsic or intrinsic pathway as shown in Figure 1.9 (Alkhoury *et al.*,

2009). Increase in AT mass during the development of obesity induces cell death by activating one of the apoptotic signalling pathways. The mode of cell death is dependent on the stimuli of DNA damage, death receptor or internal stimuli that results in mitochondrial dysfunction. Adipocyte apoptosis results in recruitment of AT macrophages (ATM) that localizes in dead adipocytes for their removal (Alkhoury *et al.*, 2009; Cinti *et al.*, 2005).

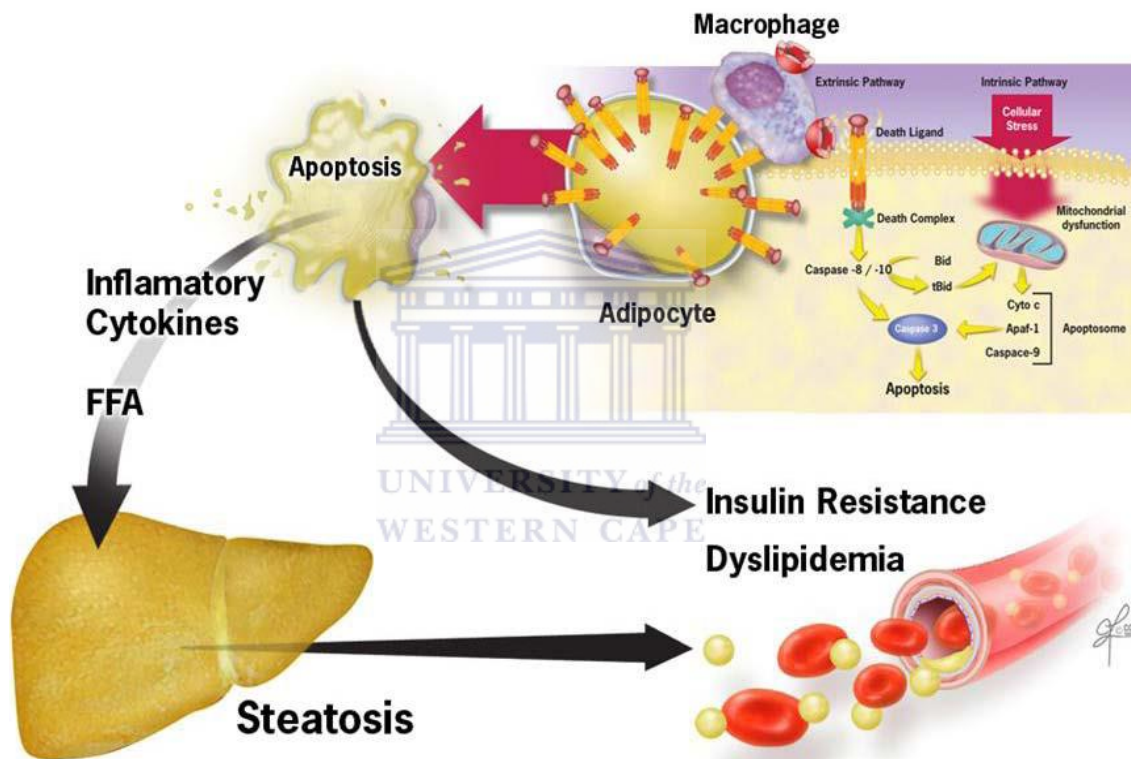


Figure 1.9: Proposed model for the role of adipocyte apoptosis in the metabolic complications of obesity. During the development of obesity, expansion of adipose tissue results in activation of apoptotic signalling including death receptor and mitochondrial pathways. These cytotoxic signalling pathways result in activation of effector caspases and adipocyte apoptosis. Pathologic increase in apoptosis results in ATM recruitment, with subsequent development of insulin resistance, hepatic steatosis, and dyslipidemia. Anti-apoptotic therapy target at inhibiting either the Fas- or mitochondrial-mediated pathways may be a new therapeutic strategy for treatment of obesity-associated metabolic complications (Alkhoury *et al.*, 2009). *Figure reprinted with permission from American Society for Biochemistry and Molecular Biology.*

Unfortunately, macrophage recruitment in diet-induced obese mice was associated with development of insulin resistance, fat accumulation in the liver (hepatic steatosis) and dyslipidemia. A study done by Alkhoury *et al.*, (2009), confirmed that adipocyte apoptosis

naturally occurs in obese mice and humans. This was proved by the high amount of pro-apoptotic protein (Bax) and the ratio of Bax: Bcl-xL detected in the epididymal fat from mice and human omental fat pads. And knocking out *Bid* gene in C57BL/6 mice reduced apoptosis and prevented macrophage infiltration of ATs and protected the mice from developing insulin resistance and hepatic steatosis (Alkhoury *et al.*, 2009; Cinti *et al.*, 2005).

Although the adipocytes were initially assumed to remain constant throughout life, independent studies have shown that new adipocytes can be generated by hyperplasia and old or damaged ones lost. Loss of the WAT mass due to apoptosis has been observed in various conditions associated with weight loss, such as in the HIV patients treated with protease inhibitors, rats with streptozotocin induced diabetes, in omental and subcutaneous ATs of humans with malignancy-associated weight loss (Prins *et al.*, 1994). The idea that apoptosis can be of value in obesity reversal was encouraged by surgical removal of fat in obese people such as liposuction, surgical removal of fat reduced body weight and improves metabolic activity. Weight loss achieved after liposuction can be maintained for at least a year in 80% of patients, this confirms that any strategy that can be able to eliminate adipocytes can be an effective way to reduce WAT mass and total body weight. A natural and non-invasive strategy could be a best option and elimination of adipocytes in the WAT could be a better strategy for obesity reversal (Nelson-Dooley *et al.*, 2005; Prins *et al.*, 1994). However lipectomy as seen in animal models of obesity is always followed by fat restoration within weeks accompanied by adverse metabolic effects (Mauer *et al.*, 2001) and a year in humans (Hernandez *et al.*, 2011). Fat redistribution to compensate the decrease in AT mass was observed also in non-surgical area, compensated for by

neurohormonal signals that increases appetite, food intake and irregular cytokine secretion (Mauer *et al.*, 2001; Hernandez *et al.*, 2011)

Apoptosis as strategy to treat obesity has been tested through *in vitro* and *in vivo* studies using leptin and TNF- α (Prins *et al.*, 1997). In both instances the ATs served as a target. Leptin was shown to have apoptotic effects in Sprague-Dawley rats through intra-cerebroventricular administration in rat brain and reduced fat mass by increasing lipolysis and stimulating adipocyte apoptosis (Gullicksen *et al.*, 2003; Qian *et al.*, 1998). The same leptin effects were observed in obese (C57Bl-*ob/ob*) female mice after transfection with differentiated 3T3-F442A that over-express leptin. The weight loss occurred within 48 hours of treatment, with this study apoptosis was observed in the microvasculature of WAT (Cohen *et al.*, 2001; Gullicksen *et al.*, 2003). TNF- α induced apoptosis in human AT explants and preadipocytes isolated from human AT (Sorisky *et al.*, 2000).

Apoptosis is a highly regulated process responsible for removal of damaged, toxic or diseased cells within the body, and thus should be expected to perform the same function during development of obesity. However, induction of apoptosis in the adipocytes might result in inflammation and other obesity-induced diseases as highlighted in the study done by Alkhouri *et al.*, (2009). Obesity is characterized by an increase in adipocytes number and size. Therefore, the AT mass can be regulated at adipocytes proliferation and differentiation from preadipocytes to reduce body weight (Sorisky *et al.*, 2000).

Most treatment strategies for obesity are aimed at reducing the cell size, however, the treatment that will reduce the cell size as well as number might work best. Induction of apoptosis in the WAT vasculature could be a nonsurgical approach for reducing total

WAT mass and provides long-term maintenance of the weight lost as observed in individuals that underwent liposuction and maintained weight loss for a year (Nelson-Dooley *et al.*, 2005). The problems that might result after the adipocyte has undergone apoptosis are discussed by Alkhouri *et al.*, (2009), stressing that accumulation of the fat in blood vessels and liver is detrimental to the body. Strategies that are able to help the adipocytes metabolize the excess energy could potentially suffice. Thus, induction of apoptosis in the cells (ECs) that promote adipocyte growth could increase lipolysis and starve the cells to death, and prevent development of secondary diseases mentioned above.

1.5 NANOTECHNOLOGY

The field of nanotechnology was first predicted in 1959 by Richard P Feynman (Nobel laureate in Physics, 1965) with his famous lecture entitled: “There’s plenty of Room at the Bottom”. The prefix ‘*nano*’ derives from Greek word for ‘dwarf’. Nanotechnology is a multi-disciplinary field derived from engineering, biology, physics and chemistry and deals with formation of particles that range in size from 1 to 100 nm. These particles are made in a nanometer scale for manipulation of physical, chemical or biologic processes, and therefore regarded as nanoparticles. One nanometer (nm) is equal to one billionth of a meter ($1 \text{ nm} = 10^{-9} \text{ m}$) (Pal and Nayak, 2010; Provenzale and Silva, 2009).

To understand these sizes in a biological context, an atom is 0.15 nm diameter, a double stranded DNA is 2 nm diameter, viruses range in size from 20 to 300 nm and cells are 1000 nm in diameter (Provenzale and Silva, 2009). The sizes of nanoparticles allow for their manipulation for biological processes, the functions that would have been otherwise impossible using larger particles including transporting materials across the blood-brain

barrier (Martinac and Metelko, 2006; Provenzale and Silva, 2009). Nanotechnology application in medicine has been growing, especially in the field of diagnostics and targeted delivery of treatment as discussed in 1.5.3. Nanotechnology can provide essential breakthroughs in the fight against different diseases by direct targeting of the problem areas with no harm to healthy tissues (Moghimi *et al.*, 2005; Yan *et al.*, 2012).

1.5.1 Nanomaterials

Nanomaterials also referred to as nanoparticles (NPs) first came to light almost 50 years ago. Nanomaterials are microscopic particles with at least one dimension that is < 100 nm (Provenzale and Silva, 2009). Nanomaterials are classified based on their composition. There are two major types of nanomaterials: particles that contain organic molecules as a major building material (biodegradable polymer, lipid materials such as liposomes) and those that use inorganic elements (metals) as a core such quantum dots (QDs) and as gold nanoparticles (AuNPs) which are discussed in section 1.5.2.1. The basic structure for most inorganic nanomaterials is shown in Figure 1.10, the metal core is coated by the shell that can be modified for biological or medical applications (Yezhelyev *et al.*, 2006).

In medicine they are developed as carriers or drug delivery agents for vaccines and therapeutic purposes. Liposomes were the first organic NPs used as drug delivery systems (Yezhelyev *et al.*, 2006). Liposomes are nanovectors made of lipids surrounding an aqueous core. The bilayered phospholipid particles were discovered over 40 years ago. Liposome structure mimics the lipid bilayer in biological systems, as such regarded biocompatible and ideal drug delivery agents. They are bio-degradable, a drug or therapeutic peptides can be incorporated inside a lipid layer. When internalized within the

cell, the lipid bilayer will be degraded releasing its contents or drugs to perform their functions (Kingsley et al., 2006; Sengupta *et al.*, 2005).

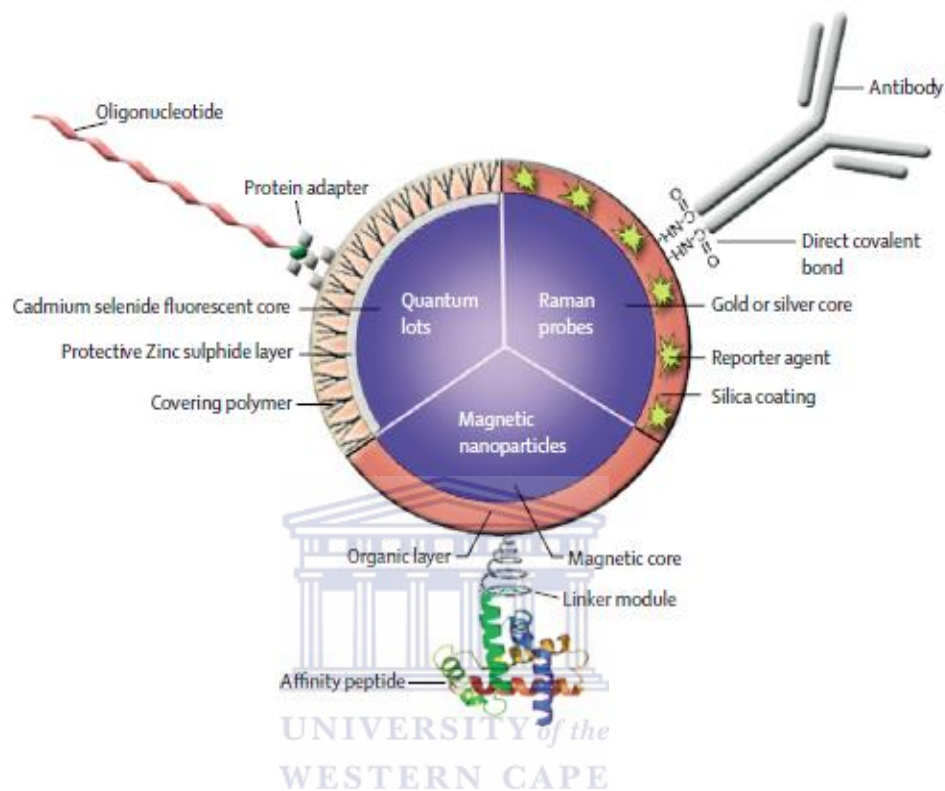


Figure 1.10: Basic structure of inorganic nanoparticles (Yezhelyev *et al.*, 2006). *Figure reprinted with permission from Elsevier.*

1.5.2 Nanomaterials used for drug delivery

Most commonly used nanomaterials in biological research are AuNPs, liposomes, dendrimers and QDs. These nanomaterials have interesting properties that were exploited in cancer research as either drug delivery agents or imaging agents (Thakor *et al.*, 2011). Gold nanoparticles are discussed below as they are used in this study as drug delivery agents.

1.5.2.1 Gold nanoparticles

Gold nanoparticles are stable, solid colloidal particles that range in size from 1 to 100 nm. The biological application of AuNPs is rooted in from their physico-chemical properties. The most important being their smaller size that allows modification of AuNPs to cross any biological barrier by attaching targeting and therapeutic peptides on their surface (Cho *et al.*, 2009). This property together with its unique optical properties is advantageous for use as diagnostic applications. Their synthesis is based on the method developed by Turkevich in 1985 through reduction of gold aurate by citrate (Kimling *et al.*, 2006). The AuNPs are stabilized by addition of proteins such as bovine serum albumin (BSA) on their surface, and can be used to attach targeting peptides and prevent their aggregation and precipitation that occurs at their isoelectric point (Liu and Franzen, 2008).

The biocompatibility of AuNPs is attributed to the long application of gold in human diseases. The therapeutic application of gold started centuries ago when gold compounds were used for medical purposes since 2500–2600 BC by Chinese and Indian people. For medical purposes, gold was used to treat conditions such as male impotence, epilepsy, syphilis, rheumatic diseases and tuberculosis. China was the first to discover the longevity effect of red colloidal gold. The application of red colloidal gold still continues in India for the same purposes (Ayurvedic medicine for rejuvenation and revitalization) as China by the elderly. Cinnabar-gold (Makaradhwaja) is used for fertility purposes in India. Gold has also been used to treat nervous disorder and epilepsy in Western countries and no toxicity was observed in both *in vitro* and *in vivo* studies (Bhattacharya *et al.*, 2007). Since then oral and injectable gold compounds continued to be used especially as treatment of

arthritis due to the bacteriostatic effects and also proved to have anti-cancer effects (Fraser, 1945; Rau and Rheumatol, 2005).

Since the approval of Cisplatin (platinum containing inorganic compound) in 1978 by FDA for cancer treatment, research for medical effects of inorganic metal has been rising. Since then Gold I and III compounds has been used to enhance activities of anti-tumour compounds (Bhattacharyya *et al.*, 2010). This led to hypothesis that gold at the nanoscale will also be not toxic and can be useful as a vehicle for drug delivery to diseased cells by targeting the overexpressed receptors such as the folate receptors in cancer (Bhattacharya *et al.*, 2007) and prohibitin in AT's vasculature (Kolonin *et al.*, 2004).

Gold has many applications in medicine and in nanotechnology it was found to have anti-angiogenic effect (Arvizo *et al.*, 2011) but is mostly used as a drug delivery agent. AuNPs are highly stable and have a distinct surface plasmon resonance (SPR) bands, thus provide easy characterization. They are highly biocompatible when conjugated to functional ligands for *in vivo* drug targeting (Sun *et al.*, 2008). There are currently two AuNP-formulations that have under gone human clinical trial in treatment of solid tumours. Aurimmune (CYT-6091) was the first citrate coated AuNPs to go through clinical trials which started in 2005 for delivery of anti-cancer therapy. CYT-6091 gold-based nanoparticles are made up of 27 nm AuNPs encapsulated with recombinant TNF- α and PEG. The clinical trial was conducted in late-stage pancreatic, breast, colon, melanoma, sarcoma and lung cancer patients. The CYT-6091 nanodrug achieved safe and targeted biologic response at the tumour site by using a dose lower than required for TNF- α alone (Libutti *et al.*, 2009; Libutti *et al.*, 2010). Phase II clinical trials of Aurimmune (CytImmune Sciences) are under investigation (ClinicalTrials.gov numbers,

NCT00356980 and NCT00436410). Aurolase nanoshells with a 15 nm gold shell are in the first human clinical trial for head and neck tumours as photothermal therapy (ClinicalTrials.gov number, NCT00848042).

1.5.3 Biological and medical application of nanotechnology

Application of nanotechnology in medical sciences referred to as nanomedicine by the National Institutes of Health, has been growing in recent years. Nanotechnology employs the use of nanomaterials such as AuNPs and QDs for treatment, diagnosis and imaging purposes. Bio-conjugated nanomaterials have been useful as drug delivery agents, clinical studies are being conducted in cancer research (Moghimi *et al.*, 2005; Yezhelyev *et al.*, 2006). Nanomedicine offers higher efficacy for treating diseased cells without causing any harm to normal cells or tissues, and the effects can be monitored noninvasively (Caruthers *et al.*, 2007; Moghimi *et al.*, 2005).

Bio-distribution of nanomaterials is depended on their physico-chemical properties, these include parameters such as size, charge and shape. These properties can be manipulated for biological use to help increase their circulation times within the body and therapeutic index. Nanomaterials less than 20 nm in size for instance, can pass through blood vessel walls, and allows for intravenous, intramuscular and subcutaneous applications. Targeted nanomaterials can minimize the irritant reactions at the injection site that occurs when using conventional treatments. Conventional treatment is limited by the bystander effects to normal tissues, short circulation time, insolubility and non-selectivity; limiting or reducing their therapeutic efficacy to desired cells. Bio-conjugated NPs can be developed with qualities that can help overcome these drawbacks for delivery of smaller doses of

drugs directly to the diseased tissues as discussed in 1.5.3.1 and be used to monitor their effect in biological system. Targeted NPs could mask the drug from proteolysis and prevent contact with healthy tissues increasing the dosage that reaches the diseased tissue (Praetorius and Mandal, 2007).

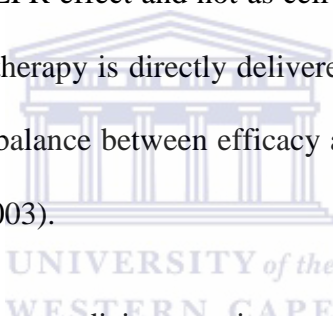
1.5.3.1 Drug delivery using nanoparticles

The most common and major application of NPs especially AuNPs, is in drug delivery. Nanomaterials as drug delivery agents are attractive in that they help in reduction of dosage of drugs and transportation of the insoluble treatment. They are also useful in protecting the drugs from proteolytic degradation as they travel through the circulatory system when attached to PEG or biological active molecules. These readily increase the efficacy of the targeted drugs by concentrating them in the diseased tissue with little or no effect to the normal tissues (Brigger *et al.*, 2002).

Nanoparticles as drug delivery agents are able to overcome most of the problems encountered when using conventional therapies such as drug resistance due to cellular barriers, distribution and early clearance from the biological system (Cho *et al.*, 2008; Ruoslahti *et al.*, 2010). Their use as vaccines and chemotherapy carriers for cancer treatment has been extensively studied. These treatments concentrate on diseased areas by taking advantage of the enhanced permeability and retention (EPR) effect on the vasculature of the diseased tissue when used without targeting molecules. In a pathological state, EPR is characterized by pathological and excessive angiogenesis and increased secretion of a various permeability mediators that can be target for disease intervention. These characteristics only occur in pathological states and not in normal tissues and

provide an opportunity for more selective targeting of NPs to diseased tissues (Kingsley et al., 2006).

The NPs as outlined in 1.5.3 have numerous advantages as drug delivery agents. They have a high payload capacity and are capable of carrying both hydrophilic and hydrophobic drugs into a cell. The treatment once inside a cell can be released in a controlled manner through active or passive targeting. Active targeting occurs in a manner discussed in 1.2.3.1. In some cases it might require external stimulus such as light in a photodynamic therapy or heat when using heat-labile liposomes to activate release of treatment. Passive targeting takes advantage of the EPR effect and is not as cell specific as active targeting. Active targeting makes sure that the therapy is directly delivered to the desired cell and minimizes systemic effects, achieving a balance between efficacy and toxicity (Provenzale and Silva, 2009; Lysik and Wu-Pong, 2003).



The earliest application of nanomedicine was in cancer research where liposomes were used to deliver chemotherapy payloads to the tumour tissues (Moghimi et al., 2005). Abraxane (NP albumin-bound paclitaxel) was the first chemotherapeutic NP to be approved by the FDA for treatment of metastatic breast cancer in the USA. Nanotreatment has greater efficacy with an improved safety profile than conventional paclitaxel (Caruthers *et al.*, 2007; Yezhelyev *et al.*, 2006). Doxorubicin is another drug used to treat cancer and is associated with cardiac toxic side effects. The nanodrug version of the same drug has now been approved by FDA for treatment of refractory ovarian cancer, breast cancer and Kaposi's sarcoma in the USA. Biodegradable liposome nanoparticles are used to deliver doxorubicin to the tumour site, help retain the drug efficacy and circulate longer than the normal drug (Sengupta and Sasisekharan, 2007; Yezhelyev *et al.*, 2006).

Selective cell targeting is a best strategy because the toxicity of the therapy will only be directed to diseased cells and spares the normal cells. Active targeting increases the therapeutic efficacy and reduces systemic toxic effects as observed with nanodoxorubicin and nanopaclitaxel. The interesting part is that the strategy can be applied in various diseases as long as biomarkers exclusively expressed during development of the disease are known or have been identified (Yezhelyev *et al.*, 2006). The nano-drug delivery system has been booming in active targeted therapy, the targeted NPs provide better efficacy and limited cytotoxicity. Targeted therapy targets disease-specific biomarkers and can therefore discriminate between normal and diseased cells or tissues (Breunig *et al.*, 2008; Kim and Nie, 2005; Pal and Nayak, 2010).

1.5.4 Challenges and advantages of nanotechnology

Nanotechnology application in biomedical research is still in its infancy, therefore still lacks assurance for *in vivo* usage. There is still reluctance to use nanotechnology-based products, especially the ones that are used in human (Cunningham, 2014). Changing the size of molecules is accompanied by altered physical and chemical properties that have consequences within the body, such as the change in clearance from the body from minutes to hours to days and maybe even years. These changes are likely to be associated with a lot of uncertainties, and therefore safety of the nanomaterials within the body still raises questions and should not be undermined (Caruthers *et al.*, 2007).

Gold has been used for decades for medical purposes and is thus regarded as nontoxic. However, the same may not be true for AuNPs. AuNPs have been observed to be toxic in

both cell culture and animals (Pompa *et al.*, 2011; Sabella *et al.*, 2011). Their toxicity has been associated with their physicochemical properties such as size and shape. Nanoparticles were often attacked by immune cells as they were considered foreign by the body (Cho *et al.*, 2009; Nel *et al.*, 2006).

The field of nanotechnology has been growing lately in theranostics despite the uncertainties that surround it. Nanotechnology together with molecular techniques, offer a great opportunity for development of treatment and diagnostic strategies for chronic diseases not limited to diabetes, cancer and obesity. Cancer and arthritis research has covered most of application with exciting outcomes. The characteristics of the nano-drugs or therapeutic agents such as solubility, circulating times, drug release over short or long durations and site-directed delivery can be controlled. Nanomaterials for drug delivery and molecular imaging have been developed that can overcome most of the challenges faced by current available tools. The NPs have increased surface area and very large payloads to accommodate attachment of targeting, therapeutic and imaging agents. Targeting permits quantification of the extent of disease and deliver therapeutic doses to the desired diseased tissue (Kim *et al.*, 2010). The efficacy of the targeted therapeutic NPs can be monitored by non-invasive imaging and quantified. The NPs can achieve therapeutic effect on the targeted tissues even at the lowest dose than the conventional dosage (Caruthers *et al.*, 2007). The use nanotechnology-based drug delivery strategies coupled with targeted therapy can significantly improve the safety profile of the drug by lowering dosage, reduce bystander side effects, increase drug half-life and maximize the efficacy of the drug at the desired site.

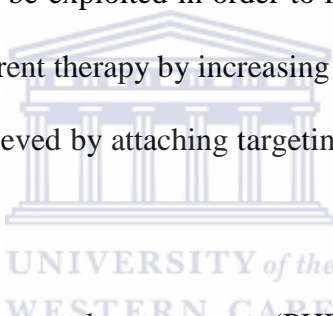
Despite the challenges associated with NPs, nanotechnology offers a great potential for treatment of obesity and its associated conditions. Ways of overcoming the short falls surrounding the use of NPs has been identified, such as the use of functionalized nanomaterials (Yan *et al.*, 2012). Targeted NPs are expected to be able to reach the desired diseased tissue, and in so doing overcome cellular barriers in the body without losing their efficacy while travelling through the blood circulation. Upon interacting with the diseased cells the nanotherapy should exert the drug action specifically on the target cells following a controlled release mechanism, and destroy these cells without any harm to normal cells. Nonspecific adsorption of NPs is normally overcome by addition of polymers such as PEG (Kelly and Kim, 2007; Provenzale and Silva, 2009; Yan *et al.*, 2012). This strategy will be able to improve chances of patient's survival by targeting and eliminating the diseased cells/ tissues with no bystander effect, therapeutic intervention for chronic diseases (obesity) can benefit a lot from both targeted therapy and nanotechnology.

1.5.5 Potential application of nanotechnology in obesity

After years of basic nanoscience research, followed by many on research and development, application of nanotechnology in medical science is delivering on its promises for a better nanomedicine. Nanomaterials customized for desired actions have been developed, capable of delivering, tracking of drugs to specified targets and evaluating drug response. Their size range and stability makes it possible for NPs to pass through the blood stream and circulate a bit longer than conventional therapy without altering their behaviour and biochemical properties. These properties allow time for the treatment to concentrate at the diseased area regardless of the route of administration. Use of targeting

moieties reduces systemic and bystander effects on the surrounding tissues (Praetorius and Mandal, 2007).

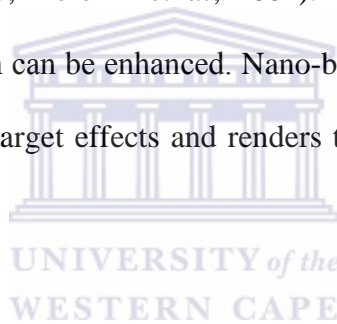
Nanoparticles have been extensively used for highly specific and efficient delivery of the treatment into target cells (Kim *et al.*, 2010; Praetorius and Mandal, 2007; Yan *et al.*, 2012). Nanoparticles can be designed for specific diseased tissues (in this case of obesity, WAT vascular ECs) through targeted therapy. Targeted therapy is mainly composed of a targeting molecule (e.g. aptamers, antibodies, ligands, dendrimers) specific for cellular receptors, drug load (therapeutic peptides) and/ or imaging agents (QDs). Surface modifications of the NPs can be exploited in order to resolve some of the noncompliance issues associated with the current therapy by increasing the biocompatibility. Specificity of the nanomaterials can be achieved by attaching targeting peptides (Praetorius and Mandal, 2007; Yan *et al.*, 2012).



The differentially expressed vascular receptors (PHB) on the endothelium are easily accessible for the binding of blood-borne compounds and can be used to indirectly target the diseased cells. PHB is upregulated in the vasculature of obese WAT compared to the normal blood vessels and therefore may serve as a target for obesity therapeutic intervention (Kolonin *et al.*, 2004). Vascular targeted nanotherapy can be beneficial for treatment of obesity. The WAT vascular marker (PHB) with its associated ligand (AHP) has already been identified (Kolonin *et al.*, 2004). Using AHP-nanodrug conjugate to target PHB receptors is expected to selectively induce cell death in the vascular ECs leading to fat resorption that will reduce WAT mass leading to total body weight loss. The PHB receptors are accessible to circulating AHP-conjugate in the blood (Arap *et al.*, 2002; Ruoslahti *et al.*, 2010), and home to specified vascular receptor in the WATs. Targeted

nanotherapy strategy is expected to enhance the drug toxic effects to only vasculature of diseased WATs. The drugs will be concentrated at a desired target sparing the healthy surrounding cells. This will definitely increase the treatment efficacy, reduce toxicity to healthy cells as opposed to non-targeted drugs that relies on passive targeting. By cutting off the adipocyte's blood supply, the adipocytes that are fed by the cut vasculature will be forced to metabolize excess fat and be destroyed (Arap *et al.*, 2002; Ruoslahti *et al.*, 2010).

The concept of targeted drug delivery is an attractive strategy for obesity reversal. Vascular targeted therapy has been tested and gave exciting outcomes in animal models of obesity (Hossen *et al.*, 2010; Kolonin *et al.*, 2004). Through nanotechnology, vascular targeted nanotherapy's action can be enhanced. Nano-based delivery systems will increase drug circulation, reduce off-target effects and renders the therapy effective even at lower dosages.



1.6 Aim(s) of the study

The aim of the study was to develop a nanotherapy that specifically targets a vascular network which supplies the pathologic adipose tissue with essential nutrients and trigger the death of these cells through apoptosis allowing greater efficacy at lower doses.

1.6.1 Objectives of the Study

- To express TK₃ pro-apoptotic and mTK recombinant proteins using recombinant DNA technology (RDT)
- To determine the effects of recombinant proteins in Caco-2 model cell line
- To develop nanotherapy by conjugating the recombinant proteins and WAT vascular targeting peptides to AuNPs
- To determine the effects of the PHB-targeted-nanotherapy, its cellular uptake, localization, specificity and the cytotoxicity effects on the model cell line.

Chapter 2: Materials and Methods

2.1 Reagents and their suppliers

All chemicals used in this study were purchased in their highest purity from the following suppliers listed in Table 2.1:

Table 2.1: List of reagents and suppliers

Suppliers	Reagents
BioLegend®	Purified rabbit anti-prohibitin antibody
Biorad	40% Acrylamide/ bis-acrylamide, Bradford dye reagent
Fermentas	<i>Nde</i> I, <i>Xho</i> I
Gibco	Dulbecco's Modified Eagle's Medium (DMEM), foetal bovine serum (FBS), penicillin, streptomycin, Trypan blue stain (0.4%)
Inqaba	T7 forward (F ⁺) and reverse (R ⁻) primers
Invitrogen	Competent cells (MC 1061, BL21 (DE3) PlyS, BL21-codon plus, <i>Rosetta</i> (DE3) and <i>ArcticExpress</i>)
Kimix	(Hydroxymethyl) aminomethan (Tris), Ethanol,
Life Technologies	2-mercaptoethanol
Lonza	Dulbecco's phosphate buffered saline (D-PBS)
Merck	Acetic acid, Bacteriological agar, Bromophenol blue, KCL, Methanol, NaCl, tryptone, Na ₂ HPO ₄ , KH ₂ PO ₄ , sucrose, Urea crystals, Yeast extract
Novagen	CytoBuster Protein Extraction Reagent
OncoImmunin, Inc	CaspaLux 9-M ₁ D ₂ substrate
Promega	dNTPs, MgCl ₂ , Green Go Taq Flexi buffer, Go Taq pol
Roche	2-(4-Iodophenyl)-3-(4-nitrophenyl)-5-(2,4-disulfophenyl)-2H-tetrazolium (WST-1), bovine serum albumin (BSA)

Santa Cruz Biotechnology	His-probe (H-3) mouse monoclonal antibody, Caspase-3 rabbit polyclonal antibody, Caspase -9 mouse polyclonal antibody, Actin-HRP mouse monoclonal IgG ₁
Sigma-Aldrich	2',7'-dichlorofluorescein diacetate (DCFH-DA), 3-(4,5-dimethyl-2-thiazolyl)-2,5-diphenyl-2 <i>H</i> -tetrazolium bromide (MTT), Ampicillin sodium salt (ampicillin), Bradford dye reagent concentrate, coomassie brilliant blue R-250, Flouroshield™ with Dapi (Dapi), glutaraldehyde, glycine, G418 disulfate Salt, hydrogen tetrachloroaurate (HAuCl ₄), kanamycin sulphate (Kanamycin), lauryl sulfate (SDS), HIS-Select® Nickel Affinity Gel, TEMED, trisodium citrate,
Thermo Scientific	SuperSignal® West Pico Chemiluminescent Substrate
WhiteScientific	Agarose molecular grade



2.2 Preparation of solutions and reagents

2.2.1 Cloning, protein expression and purification

IPTG: 1M IPTG was dissolved in distilled water (dH₂O), filter sterilized and stored at -20°C in 2 ml aliquots

Ampicillin antibiotic: 100 mg/ml Ampicillin was prepared in dH₂O, filter sterilised. Aliquots of 2ml were stored at -20°C

Kanamycin and G418 antibiotics: 50 mg/ml of both antibiotics was prepared in dH₂O, filter sterilised. Aliquots of 2 ml per antibiotic were stored at -20°C

Luria Bertani (LB) Broth (1Liter): 10 g of tryptone

5 g of NaCl

5 g of yeast extract

TYM Broth (500 ml): 2% tryptone

0.5% Yeast extract

0.1 M NaCl

10 mM MgCl₂

LB Agar (per litre): 10 g tryptone

5 g yeast extract

5 g NaCl

15 g bacteriological agar

The ingredients for TYM, LB broth and agar were dissolved in dH₂O, the pH was adjusted to 7.0 with NaOH. The final volume was adjusted to 1 litre with dH₂O. The solutions were autoclaved. The LB and TYM broths were stored at room temperature (RT) without antibiotics.

The LB agar was cooled to $\leq 55^{\circ}\text{C}$ and appropriate concentration of antibiotics was added. Then poured into Petri dishes ~25 ml/100-mm plate, the plates were allowed to set at RT. The plates were covered with foil and stored at 4°C lid side down.

Transformation (Tfb) 1 buffer: 30 mM KOAc

50 mM MnCl₂

100 mM KCl

10 mM CaCl₂

15% glycerol

Tfb 2 buffer: 10 mM NaMops

75 mM CaCl₂

10 mM KCl

15% Glycerol

The Tfb buffer ingredients were dissolved in half of the required volume of dH₂O the adjusted to required volume with dH₂O. The buffers were filter sterilized and stored at 4°C

0.5 M EDTA (pH 8.0): 18.6 g disodium EDTA was dissolved in 80 ml of dH₂O, the pH was adjusted to 8.0 with NaOH. The final volume was adjusted to 100 ml, the buffer was sterilized by autoclaving and stored at RT.

Tris-EDTA (TE) Buffer: 10 mM Tris (pH 7.5)

1 mM EDTA (pH 8.0)

The buffer was adjusted to required volume with dH₂O.

50 X TAE DNA Electrophoresis Buffer: 242 g Tris base

57.1 ml acetic acid

100 ml 0.5 M EDTA (pH 8.0)

The Tris base was dissolved in ~600 ml dH₂O, the glacial acetic acid was added followed by the EDTA buffer. The volume was brought to a litre with dH₂O.

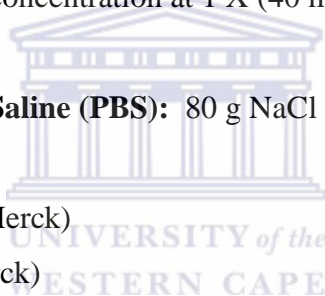
Note: Final working buffer concentration at 1 X (40 mM Tris-acetate; 1 mM EDTA)

10 X Phosphate Buffered Saline (PBS): 80 g NaCl

2.0 g KCl (Merck)

14.4 g Na₂HPO₄ (Merck)

2.4 g KH₂PO₄ (Merck)



The ingredients were dissolved in ~800ml distilled H₂O, adjusted pH to 7.4. Then final volume was adjusted to 1L with dH₂O. The buffer was sterilized by autoclaving and stored at RT.

1X PBS (makes 1 litre): 100 ml 10X PBS used to make up 1L with dH₂O, pH 7.2

Binding and equilibration buffer: 20 mM Tris-HCl (pH 8.0)

500 mM NaCl

5 mM imidazole (pH 7.9)

8 M urea

1 mM phenylmethylsulfonyl fluoride

0.5 mM DTT

Wash Buffers: 20 mM Tris-HCl (pH 8.0)

500 mM NaCl

0, 30, 50, 100 mM imidazole (pH 7.9)

8 M urea

1 mM phenylmethylsulfonyl fluoride

0.5 mM DTT

Elution buffer: 20 mM Tris-HCl

500 mM NaCl

300 mM imidazole (pH 7.9)

8 M urea

The buffers were made up to required volume with dH₂O

2.2.2 SDS-PAGE analysis



Protein quantification: One mg/ml stock solution of bovine serum albumin (BSA) was prepared in dH₂O and stored at 4°C.

SDS-PAGE:

2X Laemmli sample buffer: 4% SDS

1% 2-Mercaptoethanol

0.01% Bromophenol blue

15% Glycerol

0.125 M Tris-HCl, pH 6.8

SDS-PAGE Gels:

1.5 M Tris pH 8.8: Dissolve 90.86 g Tris in 400 ml distilled water (dH₂O), used HCl/NaOH to adjust pH to 8.8 and filled up to 500 ml. Stored at 4°C.

0.5 M Tris pH 6.8: For 200 ml, mixed 66.6 ml of 1.5 M Tris pH 8.8 to 150 ml with dH₂O, adjusted pH to 6.8 with HCl/ NaOH then filled up to 200ml.

10% SDS: Dissolved 10 g of SDS in dH₂O to make up 100 ml solution and stored at room temperature.

10% APS: Dissolved 1 g APS in 10 ml dH₂O and stored aliquots of 2 ml at -20°C.

Table 2.2: Preparation of resolving and stacking gels

COMPONENTS	Resolving Gels (ml)		Stacking Gel (ml)
	<i>12% Acrylamide Acrylamide</i>	<i>15%</i>	<i>(5% Acrylamide)</i>
dH ₂ O	4.3	3.55	3.6
40% Acrylamide/bis-acrylamide	3	3.75	0.625
0.5 M Tris pH 6.8	0	0	0.630
1.5 M Tris pH 8.8	2.5	2.5	0
10% SDS	0.1	0.1	0.05
10% APS	0.1	0.1	0.05
TEMED	0.004	0.004	0.005

10X SDS electrophoresis running buffer: 10 g SDS

30.3 g Tris

144.1 g Glycine (make to 1L with dH₂O)

Coomassie stain: 0.1% Coomassie brilliant blue R-250

40% Methanol

10% Acetic acid in dH₂O

Destaining solution: 40% Methanol

10% Acetic acid in dH₂O

2.2.3 Western Blot Analysis

10X TBST/ Wash buffer: 250 mM Tris

1400 mM NaCl

30 mM KCl

0.5% Tween-20

The ingredients were dissolved in dH₂O, adjusted pH to 7.4 then filled up to required volume with dH₂O.

10X Blotting / Transfer buffer: 0.025 M Tris – 30.28 g

0.192 M Glycine – 144 g

0.1% SDS – 1 g (optional)

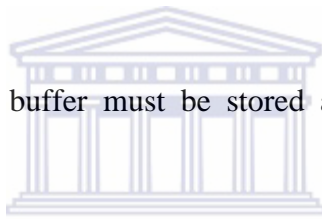
Make up to a litre with dH₂O, made in advance and refrigerated.

1X Blotting: 100 ml 10X blotting buffer

200 ml Methanol – make up to a litre with dH₂O.

Blocking buffer: 5% Carnation non-fat dry milk in TBST. The same buffer was used for preparation of the primary and the secondary antibodies as the **Antibody binding buffer**.

(*Caution:* The 1X blotting buffer must be stored at 4°C before the electrophoretic transfer).



Stripping Buffer: 0.2 M NaOH prepared in dH₂O

the
WESTERN CAPE

Paraformaldehyde (PFA) fixation solution: 4% PFA was dissolved in 1X PBS (*NOTE:* PFA must be heated to >65°C to dissolve), 1-2 drops 10 M NaOH was added while mixing.

2.3 Research Methodology

2.3.1 Recombinant DNA technology

2.3.1.1 mTK and TK₃ constructs

mTK and TK₃ constructs were a previous gift from Kwon *et al.*, 2008. TK₃ was constructed by inserting a PTD sequence expressing a HIV-1-TAT (TAT) domain (amino acids 49-57: RKKRRQRRR) fused with three tandem repeats of pro-apoptotic oligonucleotides that codes for _D(KLAKLAK)₂-DEVD-GG in a pET30a(+) vector. mTK was generated by inserting a double-stranded oligonucleotide encoding DLSLARLATARLAI in place of _D(KLAKLAK)₂ (Kwon *et al.*, 2008).

2.3.1.2 Preparation of chemically competent cells

The glycerol stocks containing *Escherichia coli* MC 1061, BL21 (DE3) PlysS, BL21-codon plus, *Rosetta* (DE3) and *ArcticExpress* competent cells were streaked out on a Luria agar plate without antibiotics. The plates were incubated at 37°C overnight in a Heraeus B5042 incubator (ThermoScientific), with the lid side down. A single colony per plate was inoculated into a 20 ml TYM broth and incubated overnight at 37°C in a shaker incubator (Multitron II Shaker Incubator, Infors HT). The overnight culture was diluted 1:10 to 100 ml with fresh TYM broth in a 2L flask and incubated at 37°C until it reached an optical density at 550 nm (OD_{550nm}) of 0.2. A fresh TYM broth (400 ml) was added to the flask and incubated until the OD_{550nm} reached 0.5.

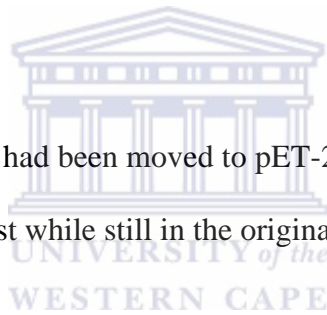
The cells were cooled by gently swirling in ice water and then transferred to polypropylene tubes and centrifuged with Sorvall RC6 plus centrifuge (Thermoscientific) at 6000 rpm for 10 minutes. The media was discarded and the pellets

resuspended in 100 ml of transformation buffer (Tb) 1 and incubated on ice for 30 minutes. The cells were spun at 3000 rpm for 8 minutes at 4°C. The supernatant was discarded and the cell pellets were gently resuspended in 30 ml of Tb 2. The aliquots of 0.2 ml were transferred into microcentrifuge tubes that were pre-cooled on ice. The competent cells were snap-frozen in liquid nitrogen and stored at -80°C.

2.3.1.3 Transformation of mTK and TK₃ into cloning cells

Upon arrival the plasmid DNA spotted in the filter papers was reconstituted in 1X TE buffer. The DNA was quantified by NanoDrop® ND-1000 Spectrophotometer (ThermoScientific) and 10 ng of mTK and TK₃ was used to transform the *E.coli* MC1061 competent cells.

Note: at this stage the mTK had been moved to pET-22b(+) vector after few attempts to express the protein of interest while still in the original vector (pET-30a(+)).



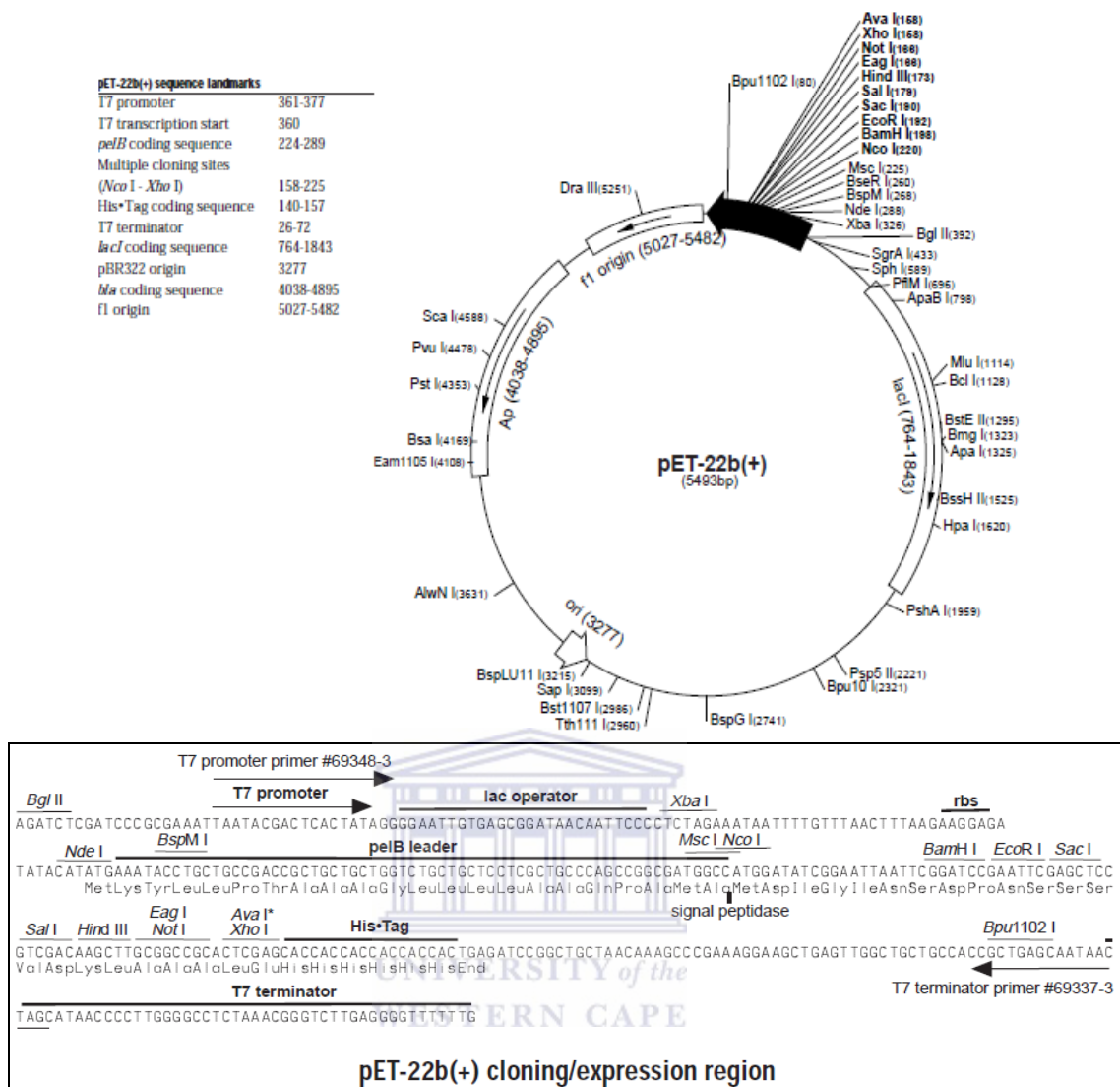


Figure 2.1: A circular map of pET-22b(+) prokaryotic expression plasmid DNA (vector) and the multiple cloning site used to insert foreign DNA for expression of recombinant proteins. The proteins are expressed as is-fusion protein with the His tag (6XHis) at the C-terminal used for affinity purification of the proteins. The vector has a β -lactamase gene for Ampicillin resistance that is used to screen for pET-22b(+) constructs. Ori denotes the origin of replication.

The MC 1061 competent cells were retrieved from -80°C and thawed on ice. The cells were kept on ice for ± 10 minutes, swirling gently every 2 minutes and gently mixed by tapping the tube. For each plasmid transformation, 100 μl of competent cells were transferred into a prechilled 1.5 ml eppendorf tube. The plasmid DNA containing either TK₃ or mTK genes was added at a final concentration of 10 ng, to each tube of cells and swirled gently. For the transformation reaction controls, an aliquot of 100 μl of

competent cells with 10 ng of the pUC18 control plasmid and cells without plasmid DNA were prepared. All the reactions were incubated on ice for 30 minutes, then heat-shocked by placing each transformation reaction on a heating block (HB/01 digital heating block, OMEG Scientific) set at 37°C for 30 seconds. The reactions were returned to ice for further 2 minutes. Then 0.9 ml of LB medium without antibiotic was added to each transformation reaction and incubated at 37°C for 1 hour with shaking at 250 rpm in Multitron II Shaker Incubator.

Using a sterile spreader, 100 µl of the cells transformed with the experimental DNA and cells only were spread onto LB agar plates that contained the appropriate antibiotic for selection of test plasmids. Kanamycin antibiotic at 40 µg/ml was used for TK₃ and mTK and ampicillin antibiotic for pUC18 (100 µg/ml). The plates were incubated at 37°C overnight with the lid side upside down. The transformants appeared as colonies following overnight incubation and the transformation efficiency was calculated following the example, i.e.: 10 ng DNA used for transformation, 20 µl of transformation was plated and gave 120 colonies: 120×12.5 (plating factor) = 1500 colonies/10 ng DNA = 150000 colonies/µg DNA = 1.5×10^5 /µg DNA = Transformation efficiency.

2.3.1.4 Colony PCR to analyse *E. coli* transformants

Ten bacterial colonies per plate for mTK and twenty for TK₃ were picked with a pipette tip and swirled into 10 µl of nuclease free water (nH₂O) in an autoclaved 0.2 ml PCR microcentrifuge tube, the cells were mixed by pipetting up and down 4 or 5 times. One micro litre of the colony sample was transferred into a pre-labelled PCR tube and used as template. The genes of interest were amplified by vector specific primers. The primer DNA sequences are as follows: T7 forward primer 5'-TAATACGACTCACTATAGGG-3' and the T7 reverse primer 5'-GCTAGTTATTGCTCAGCGG-3'.

The PCR cocktail sample was prepared as indicated in Table 2.3. The negative control (1 μl of nH_2O) and positive control (1 μl of DNA from pET 30a(+) construct) were included.

Table 2.3: Preparation of PCR reaction cocktail per reaction.

Reagents	Initial concentration	Final concentration
dNTPs	10 μM	0.2 μM
T7 Forward primer	10 μM	0.4 μM
T7 Reverse primer	10 μM	0.4 μM
MgCl_2	25 mM	0.5 mM
Green Go Taq Flexi buffer	5 X	1X
Go Taq pol	5U/ μl	0.05 U/ μl

The PCR reaction cocktail was prepared in a 1.5 ml eppendorf tube pre-chilled on ice to give the desired number of reactions (9 μl of PCR reaction cocktail mix per 1 reaction). Sterile nH_2O was used to make up the final volume. The cocktail mixture was mixed by vortexing briefly then 9 μl was aliquoted into pre-labelled 0.2 ml PCR tubes containing template DNA to make a final volume of 10 μl . The PCR reaction mixture was briefly mixed by vortex and amplified using GeneAmp[®] PCR system 2700 (Applied Biosystems). The PCR reaction was carried out following the reaction cycles below:

Cycling steps:

94°C - 2 minutes to completely denature the DNA and inactivate nucleases

94°C - 30 seconds (Denaturation step)

65°C - 30 seconds (Annealing step)

72°C – 1 minute (Initial extension step)

72°C - 5 minutes (Final extension step)

30 cycles

The samples were analysed on a 1% agarose gel containing ethidium bromide stain after amplification process, the gel images were captured by the UVP Bioimaging Systems.

2.3.1.5 Preparation of mTK and TK₃ plasmid DNA

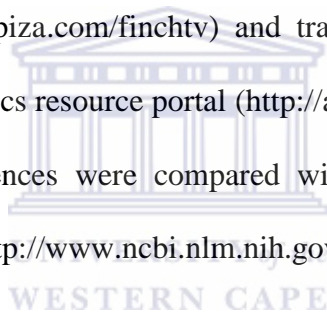
The clones that were positive for PCR were transferred into a 50 ml centrifuge tube containing 10 ml LB with appropriate antibiotics. The bacterial cells were grown overnight at 37°C while shaking. The glycerol stocks were prepared directly from overnight cultures, by adding an equal volume of overnight cultures and 80% sterile glycerol (500 µl each) and stored at -80°C. The remaining cultures were used to isolate plasmid DNA using Wizard® Plus SV Minipreps DNA Purification System (Promega), following the manufacturer's instructions.

Briefly, the cells were harvested by centrifugation at 6,000 rpm for 10 minutes. The supernatant was discarded and the pellet resuspended in 250 µl of cell resuspension solution and mixed by pipette. The cell suspension was transferred into a sterile 1.5ml microcentrifuge tube, 250 µl cell lysis solution was added to the cells. The cells were mixed by inverting the tube 4 times and incubated for 1-5 minutes. Alkaline protease solution (10 µl) was added to the cell suspension, mixed by inverting the tube 4 times and incubated at RT for 5 minutes. Neutralization solution at 350 µl was added, the cells were mixed and spun at 14,000 rpm for 10 minutes. The supernatant was carefully transferred to the spin column and spun at 14,000 rpm for 1 min at RT. The flow through was discarded and the spin column washed twice, first with 750 µl, then 250 µl of column wash solution diluted with 95% ethanol. The column was spun for 1 minute after the first wash and 2 minutes for the last wash, the flow through was discarded. The column was transferred to a sterile 1.5 ml microcentrifuge tube, the plasmid DNA was eluted by adding 100 µl of nH₂O to the column. The column was centrifuged at maximum speed for 1 minute, the DNA concentration was determined by NanoDrop®

ND-1000 Spectrophotometer. At this stage the DNA samples can be stored at -20°C until further analysis.

2.3.1.6 DNA sequencing

The positive mTK and TK₃ constructs were sequenced to verify that the coding sequence was in the correct reading frame and that no mutations had occurred. The glycerol stocks containing the constructs were streaked in agar plates containing appropriate antibiotics. The plates were incubated at 37°C overnight. The agar plates containing mTK and TK₃ clones were sent to InqabaBiotech (Pretoria, SA) for DNA sequencing using T7 vector specific primers. The resulting sequences were analysed by FinchTV (<http://www.geospiza.com/finchtv>) and translated to amino acid sequences using ExPASy Bioinformatics resource portal (<http://au.expasy.org/tools/dna.html>). The forward and reverse sequences were compared with each other using the Blast 2 sequence alignment tool (<http://www.ncbi.nlm.nih.gov/BLAST/bl2seq/wblast2.cgi>).



2.3.1.7 Transformation of mTK and TK₃ into expression cells

The *ArcticExpress* competent cells were transformed with 10 ng recombinant mTK and TK₃ plasmid DNA following the protocol described in section 2.1.1.3. The transformants were plated in LB agar plates containing 40µg/ml G418 and either 40 µg/ml kanamycin for TK₃ and 200 µg/ml ampicillin for mTK.

2.3.1.8 mTK and TK₃ recombinant protein expression screening and solubility test

The fusion proteins were expressed in *ArcticExpress* competent cells. Eighteen to twenty colonies were picked from the LB agar plates and inoculated in 10 ml of LB containing 40 µg/ml G418 and 40 µg/ml kanamycin (TK₃) or 200 µg/ml ampicillin

(mTK) antibiotics. The colonies were grown overnight at 37°C in a Multitron shaker incubator. Five hundred microliter of the overnight culture was used to prepare glycerol stocks and kept at -80°C for future use. The remaining overnight culture was diluted (1:10) with fresh LB media containing appropriate antibiotics. The cells were grown at 37°C until the OD_{550nm} reached 0.4-0.8. Protein expression was induced by addition of 1 mM isopropyl-L-thio-h-D-galactopyranoside (IPTG) and the culture was moved to the incubator set at 15°C for 48 hours.

To test solubility of the recombinant proteins, the bacterial cells were harvested by centrifugation at 3750 rpm for 10 minutes at 4°C in pre-weighed 15 ml conical tubes using Allegra X-15R Refrigerated Centrifuge (Beckman coulter). The supernatant was discarded and the cell pellet was resuspended in 500 µl BugBuster Reagent by gently vortexing or by pipetting up and down until the cell suspension is homogeneous. Following incubation at RT shaking for 10 minutes, the cell suspension was spun at 3750 rpm for 10 minutes at 4°C to separate the soluble proteins from the insoluble proteins. The supernatant was transferred into a clean tube as soluble sample and the pellet was resuspended with 500 µl of BugBuster Reagent as insoluble sample. The uninduced and induced samples were analysed by SDS-PAGE.

2.3.1.9 Analysis of protein expression by SDS-PAGE

Recombinant protein expression was analysed by SDS-PAGE on a 12-15% acrylamide gel using the Mini Protean III system (Bio-Rad) with 1 mm thickness gels. Twenty µl of the induced and un-induced samples were mixed with an equal amount of 2X Laemmli sample buffer in a microcentrifuge tubes. The samples were boiled at 95°C for 5 minutes in a block heater (Stuart Scientifica). The samples were left to cool at RT then pulse spun for 8 seconds at 14 000 rpm. After loading the samples on the gel, the

gel was run at 110 V through the stacking gel and at 120 V through the resolving gel. After electrophoresis the gels were stained with Coomassie staining solution for at least 15 to 30 minutes while shaking on an orbital shaker (Storvall Life Science Incorporated, USA). The gels were then destained and images captured with UVP Bioimaging system.

2.3.1.10 Large Scale expression of the Recombinant Proteins

Two samples that showed expression of mTK and TK₃ were inoculated into 200 ml LB broth containing appropriate antibiotics (40 µg/ml kanamycin and G418 for TK₃; 200 µg/ml ampicillin and 40 µg/ml G418 for mTK) using the glycerol stocks. The cultures were incubated at 37°C with shaking at 250 rpm overnight. The next morning, the cells were subcultured into a 2 litre fresh LB medium in a 5 litre flask with appropriate antibiotics and cultured following the steps in section 2.3.1.9. After the end of the induction period, the cells were harvested by centrifugation at 6,000 rpm for 15 minutes using a Sorvall RC6 plus centrifuge. The supernatant was discarded and the cell pellets were resuspended in 10 ml of 1X PBS. The cell suspension was sonicated on ice, 3 X 30 seconds. The samples were spun as before, the supernatants were transferred into a clean tube. The pellets containing the protein of interest (both mTK and TK₃ recombinant protein are insoluble) were resuspended in the binding buffer [20 mM Tris-HCl pH 8.0, 500 mM NaCl, 5 mM imidazole pH 7.9, 8 M urea, 1 mM phenylmethylsulfonyl fluoride, and 0.5 mM DTT] (adapted from Kwon *et al*, 2008), and the cell suspensions were clarified by centrifugation as before. The supernatant was collected into a clean tube and used for affinity purification.

2.3.1.11 Affinity purification of recombinant proteins

The recombinant proteins were purified under denaturing conditions using HIS-Select[®] Nickel Affinity Gel following the manufacturer's instructions. 1 ml HIS-Select Nickel Affinity Gel was transferred into a chromatography column (referred as Ni-NTA column), the column was washed with 2 volumes of dH₂O and equilibrated by 3 volumes of binding/ equilibration buffer (20 mM Tris, 500 mM NaCl, 5 mM Imidazole, 8 mM Urea and 0.5 mM DTT).

The supernatants of the insoluble fraction were subjected to purification on a Ni-NTA column under denatured conditions. The supernatants containing the insoluble proteins (mTK/ TK₃) obtained from 2.3.1.10 were loaded into the equilibrated Ni-NTA column and incubated at RT shaking for 30 minutes. The flow through was collected into a clean tube. The high background of contaminating bacterial proteins was removed/ washed by stepwise addition of increasing imidazole concentrations at pH 7.9 (0, 10, 30, 50, 100 mM) in a buffer containing 20 mM Tris-HCl pH 8.0, 500 mM urea, 0.5 mM DTT, 1 mM PMSF. The washing steps were repeated twice with 10 ml buffer. The target recombinant proteins were eluted using an elution buffer [20 mM Tris-HCl pH 8.0, 500 mM urea, 300 mM imidazole pH 7.9 and 8 M urea). The column was washed with 1 M imidazole to remove all that was bound to the column, the beads were stored in 30% ethanol with 1% sodium azide. The collected fractions were analysed by SDS-PAGE for the presence of the recombinant protein, and stained with Coomassie and destained as highlighted in section 2.3.1.9.

The fractions (2 X 10 ml) that contained the protein of interest were pooled, dialysed in 1X PBS and concentrated to 2 ml using a SnakeSkin Dialysis Tubing, 10 000 MWCO (22 mm X 35 feet dry diameter, ThermoScientific) 4 hours to overnight. Reverse

dialysis was carried out using sucrose. The recombinant proteins in elution buffer were added into the snakeskin tubing and placed into a clean container. Sucrose was then sprinkled on top of the tubing and allowed to stand until required volume was achieved at 4°C while shaking. The protein concentration was estimated by taking absorbance at 280 nm wavelength using NanoDrop® ND-1000 Spectrophotometer. The fusion proteins were stored at -20°C until required.

2.3.1.12 Western blotting

Twenty microliters of mTK and TK₃ recombinant protein together with the flow through and the washes, were resolved by 12% SDS-PAGE following the same conditions as described in section 2.2.1.9. The proteins were electroblotted onto polyvinyl difluoride (PVDF) using the wet transfer. Briefly, the filter paper and the fibre pads (the size of the gel) were soaked in cold 1X blotting buffer for 10 minutes prior to use. The PVDF membrane was activated by dipping into absolute methanol for 30 seconds and rinsed in 1X blotting buffer as soon as the gels are ready. The membrane sandwich was assembled according to the manufacturer's instructions using forceps to handle the membranes and filter papers. The sandwich was placed into the cassette and into the transfer tank. The tank was filled with 1X blotting buffer, and the cooling block was placed into the transfer apparatus. The tank was then placed on ice and the protein bands transferred at 110 V for 90 min. The prestained marker was used to ascertain the efficient transfer of proteins from the gel to the membrane. The membranes were rinsed with 1X tris-buffered saline tween-20 (TBST) and incubated with the blocking buffer (5% Carnation non-fat dry milk in 1X TBST) for 1 hour while shaking on an orbital shaker at RT. The blocking solution was discarded and the membranes washed with 1X TBST three times for 10 minutes each.

The membranes were probed with 1:5000 His-probe (H-3) mouse monoclonal HRP-conjugated antibody prepared in antibody binding buffer overnight at 4°C. The membranes were washed three times in 1X TBST for 10 minutes each. Then, 1 ml of SuperSignal® West Pico Chemiluminescent Substrate was added per blot, the reactive bands were captured and imaged using the UVP Bioimaging System.

2.3.2 Cell culture

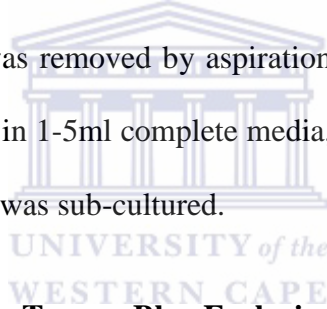
The cell lines used in this study were obtained from the American Type Culture Collection (Table 2.4). The cell lines were regularly cultured in T25 cm² culture flasks (Sigma) at 37°C in a 5% CO₂ humidified incubator in DMEM cell culture media. The media was supplemented with 10% heat-inactivated foetal bovine serum (FBS), 1% penicillin-streptomycin and 1% non-essential amino acid solution, this media mix will be referred as complete media from now henceforth. The media were changed and replaced with fresh complete media every three days. The procedures were performed in the Biological Safety Cabinet (Laminar flow) using aseptic techniques, all the regents to be used were sprayed with 70% ethanol before introducing them into Laminar flow.

Table 2.4: Cell lines used for screening of PHB expression.

Cell line	Acronym	Disease	Species
Colon cancer	Caco-2	Colorectal adenocarcinoma	<i>Homo sapiens</i>
Chinese Hamster Ovary cells	CHO-K1	Normal	<i>Cricetulus griseus</i> hamster
Cervical cancer	Hela	adenocarcinoma	<i>Homo sapiens</i>
Breast cancer	MCF 7	adenocarcinoma	<i>Homo sapiens</i>
Colon cancer	HT-29	Colorectal adenocarcinoma	<i>Homo sapiens</i>
Human Fibroblasts	KMST-6	Normal	<i>Homo sapiens</i>

2.3.2.1 Cell splitting and trypsinization

The cells were split when they reached $\geq 70\%$ confluency, the media was removed from flask using 10 ml serological pipette into a waste beaker. The cells were rinsed with 3 ml of D-PBS and discarded into a waste beaker, 3ml of 2X trypsin was added to the cells and incubated for 1-3 minutes at 37°C. The detachment of the cells from the flask was inspected with light microscope. As soon as the cells start to round up, the detachment was facilitated by gently tapping the flask on the surface to dislodge the cells. The reaction was terminated by adding 2 volumes of complete medium. The cells that were still attached to the flask were removed by pipetting. The cells were then transferred to the prelabeled 15 ml conical tubes and centrifuged at 3000 rpm for 5 minutes. The supernatant was removed by aspiration or pipetting into a waste beaker. The cells were resuspended in 1-5ml complete media, cell count was performed and the appropriate number of cells was sub-cultured.



2.3.2.2 Cell count/ viability: Trypan Blue Exclusion Assay

Cell viability was performed using trypan blue exclusion assay by the Countess® Automated Cell Counter (Life Technologies) following manufacturer's instructions. Briefly, 10 μ l aliquot of trypsinized cell suspension was mixed with 10 μ l of 0.4% trypan blue dye reagent. The cells were mixed by pipetting. 10 μ l of the cell-dye mixture was loaded into a Countess™ chamber slide (Life Technologies), followed by cell count, the data readout was given in total cells/ml, live cells/ml, dead cells/ml, and percent viability.

2.3.3 Evaluation of PHB expression in various cell lines

2.3.3.1 Western blot analysis of PHB expression

a) Protein Extraction

Several cancerous and non-cancerous cell lines from humans and one from a hamster as shown in Table 2.4, were cultured to screen for PHB expression. The cells were seeded at 5×10^5 cells/ml in a 6 well plate until they reached $\geq 80\%$ confluency. Protein was extracted from the cells using CytoBuster Protein Extraction Reagent following manufacturer's instructions. The culture medium was removed from the plate. The cells were washed with 2 ml 1X PBS. Upon removal of PBS, protein was extracted from the cells by adding 100 μ l of CytoBuster reagent and incubated at room temperature for 5 minutes. The cell debris was scraped from the 6 well plates using Nunc™ cell scrapers and transferred into a 1.5 ml eppendorf tube. The cells were spun at 14,000 rpm (4°C) for 5 minutes in an Eppendorf refrigerated microcentrifuge Model 5417R (Sigma-Aldrich). The soluble cytosolic fraction or supernatant containing the protein sample was collected into a clean tube. The protein sample was stored at -20°C until further analysis.

b) Protein Quantification

The protein concentration in cell lysates was estimated using the Bradford assay with bovine serum albumin (BSA) as a protein standard (Bradford, 1976). Different standard concentrations (0, 25, 125, 250, 500, 750 and 1000 $\mu\text{g/ml}$) were prepared from a 1 mg/ml BSA stock solution. The ingredients were mixed together with the Bradford dye reagent added last as illustrated in Table 2.5 in a 96 well plate. The samples were incubated for 30 minutes at RT. The absorbance was read at 595 nm using POLARstar

Omega plate reader (BMG Labtech). The absorbencies of both the standards and protein samples were recorded. The samples were prepared in triplicate.

Table 2.5: Preparations of the standards and sample for protein estimation.

	STANDARD PREPARATION					CELL SAMPLE
	Amount required (μ l)					
[BSA] (μg/ml)	25	125	500	750	1000	-
BSA standard	20	20	20	20	20	0
Cell sample	0	0	0	0	0	20
Bradford reagent	200	200	200	200	200	200

The absorbance values of the standards were used to plot a standard curve: absorbance versus [BSA]. The equation generated by the linear regression was used to calculate the concentration of the protein sample using the measured absorbance.

c) SDS-PAGE and Western blot analysis

The samples were retrieved from -20°C and thawed on ice. The samples were analysed by SDS-PAGE on a 12% acrylamide gel as in section 2.3.1.9. Sample containing 20 μ g of protein was loaded in the gel for western blot analysis following the steps in described in section 2.3.1.12. The membranes were probed with 1:5000 purified anti-prohibitin rabbit antibody, followed by 1: 10 000 anti-rabbit IgG-HRP secondary antibody prepared in antibody binding buffer.

2.3.3.2 Localization of PHB using immunocytochemistry

The cells that showed expression of PHB (Caco-2 and MCF 7 cells) were seeded in a 6 well plate with glass coverslip at a density of 1×10^4 cells/well. The cells were incubated for 24 hours at 37°C . The media was replaced with media containing 0.01 mM AHD-

FITC and incubated at 37°C for 3 hours. The culture medium was discarded, and the cells were washed twice with 1X PBS. The cells were fixed for 10 minutes with 4% (v/v) paraformaldehyde and washed twice with 1X PBS then permeabilized with 0.1 % Triton X-100 for 5 minutes. The cells were washed thrice and the coverslips were transferred to a microscope slide containing a mounting media and nuclear stain (Fluoroshield-DAPI). The cells were visualized under Axioplan-2 Imaging Fluorescent Microscope (Zeiss) using green and blue filters.

2.3.4 The effect of mTK and TK₃ recombinant proteins by MTT assay

The cellular viability was assessed by measuring the cell proliferation using a mitochondrial reduction activity or MTT assay. Briefly, 100 µl Caco-2 cells per well at 1x10⁵ cells/ml density were seeded in 96-well culture plates overnight. The medium was replaced with fresh medium containing TK₃ or mTK at different concentrations (0-8 µM). The cells were treated for 24 hours at 37°C, 10 µl of 0.5 mg/ml 3-(4,5-dimethylthiazol-2-yl)-2,5-diphenyltetrazolium bromide (MTT) solution was added to each well and incubated for 4 hours. The MTT solution was removed and the cells were then lysed with 100 µl DMSO to dissolve the insoluble formazan salt. The colour intensity was quantified by measuring the absorbance at 570 nm using a PolarSTAR Omega microplate reader (BMG Labtech), 650 nm was used as a reference wavelength. The cell viability was expressed as the percentage ratio of treated cells against untreated cells.

2.3.5 The design and development of the nanotherapy

2.3.5.1 Fabrication of the gold nanoparticles

The AuNPs were prepared following the classical method devised by Turkevich *et al.* (1951), using trisodium citrate as reducing agent in aqueous solution of hydrogen tetrachloroaurate (HAuCl₄). All glassware used for this process was cleaned in aqua regia (3 parts HCl, 1 part HNO₃), rinsed with distilled H₂O, and then oven dried. An aqueous solution of HAuCl₄ was brought to boiling in a volumetric flask and stirred continuously with a stirrer bar on a hot plate. An aliquot of a 38.8 mM trisodium citrate solution was added quickly at one time, resulting in a change in solution colour from pale yellow to colourless, very dark blue, purple, and finally wine red. After the colour change the solution was kept boiling for 30 minutes, the heat was switched off and allowed the solution to cool while stirring. The solution was subjected to high-speed centrifugation at 12,000 rpm for 15 minutes to isolate the particles. The pellet was washed in dH₂O after discarding the supernatant. The process was repeated three times to eliminate the free citrate. The resulting particles were coated with negatively charged citrate.

2.3.5.2 Characterization of functionalised gold nanoparticles

The 14 nm citrate stabilized AuNPs were functionalized for biological application by conjugating targeting and therapeutic peptides to them. The prohibitin targeting molecule (AHP) was conjugated to AuNPs through biotin-streptavidin chemistry, to enhance the cellular uptake of the nanotherapy and increase cellular retention of the therapeutic peptide for sustained antiproliferative activity. A free thiol group in the

Cysteine residue was introduced in the therapeutic peptide to facilitate its adsorption to the gold surface.

The resulting AuNPs including the citrate-coated NPs were characterized by UV-Vis absorption spectroscopy using JASCO V-570 spectrophotometer to study the peak absorption band. Transmission Electron Microscope (TEM) of the various AuNPs were collected on a Philips CM200 TEM (Mintek). The operating voltage range was 20–200 kV with a resolution of 2.4 Å. Zeta potential measurements were performed using a Malvern Zetasizer Nano ZS (Advanced Materials, Mintek) operating with a variable power (5–50mW) He-Ne laser at 633nm.

2.3.5.3 Quantification of AuNPs by ICP-OES

The NPs were diluted 1:10 in 1X PBS to a final volume of 500 µl and spun at 14,000 rpm for 5 minutes in a microcentrifuge. The pellet was lysed with 2 ml of aqua regia (3:1 HCl:HNO₃) solution. The samples were digested by incubation at 90°C for 2 hours, the samples were then diluted with 2% HCL to give a total sample volume of 10 ml. At this stage, the cell suspension could be stored at –20°C until analysis.

These samples were then analysed for total gold content by a Varian 710-ES ICP Optical Emission Spectrometer (Varian) at the Chemistry Department (University of the Western Cape). The measurement was repeated 3 times for each sample submitted, the values reported were based on a calibration curve using a gold ICP standard (Sigma-Aldrich). To determine the total amount of AuNPs per sample, the detected amount of each sample was multiplied by the dilution factor.

2.3.6 IN VITRO NANOPARTICLE UPTAKE AND LOCALIZATION STUDIES

The Caco-2 cells were grown to $\geq 70\%$ confluency before splitting and re-seeding at 20-30% confluency. The cells were grown under the conditions described in section 2.3.2.1 for 18-24 hours before the cells were treated. The cells were treated at 50 to 70% confluency for 24 hours.

2.3.6.1 Effect of the nanotherapy on cell proliferation: the WST-1 assay

The cytotoxicity of AuNPs on the Caco-2 cells was evaluated using water-soluble tetrazolium salts-1 (WST-1) cell proliferation reagent with the chemical formula: 2-(4-Iodophenyl)-3-(4-nitrophenyl)-5-(2,4-disulfophenyl)-2H-tetrazolium, monosodium salt. The assay was performed following manufacturer's instructions.

The Caco-2 cells were seeded at a density of 1×10^5 cells/well in a 96 well plate, 100 μ l per well. The cells were incubated for 24 hours at 37°C in a 5% CO₂ humidified incubator. After 24 hours, the media was removed from each well and replaced with 100 μ l of media with varying concentrations of the AuNP conjugates ranging from 0-8 nM. The AuNPs stock was prepared at 10 mM in complete media for treatment. The cells that were incubated with AuNPs-free medium were considered as control samples (untreated cells). One well consisted of 100 μ l media without cells and served as a blank. The cells were treated for 24 hours, then 10 μ l WST-1 cell proliferation reagent was added to all the wells. The cells were incubated at 37°C for 3 hours then covered in foil and shook for 1 min in an orbital shaker at RT.

The absorbance of the formazan product formed was measured at 440 nm wavelength (λ), with background subtracted at the λ of 630 nm using a PolarSTAR Omega plate reader. Each sample point was performed in triplicate. The percentage of cell viability

was calculated by comparing the absorbance of the test samples with the absorbance of the control (untreated) samples. The data reported represent the average means of triplicate measurement from two independent experiments. The average IC₅₀ values of NPs were estimated from a plot of the percentage of viable cells versus concentration.

2.3.6.2 Cellular uptake and localization of the AuNPs

The cellular uptake and localization of various AuNP conjugates was investigated using ICP-OES and TEM, respectively. The cells were seeded at a density of 1×10^5 cells/well on a 24-well cell culture plates for ICP-OES analysis, and 1×10^6 T25 cm² flask for TEM analysis. The cells were treated with non-toxic concentrations of the AuNPs at 4 nM and cultured for 24 hours.

a) Quantification of AuNP uptake by ICP-OES analysis

The amount of nanomaterials taken up by cells was quantified by ICP-OES. Cells were seeded on 24 well plates (Sigma). After reaching confluence the medium was replaced by the 1 ml of various nanoparticles suspension using their IC₅₀ concentrations, untreated control was included. After 24 hours, the floating cells were transferred into a 15 ml centrifuge tubes. The adherent cells on the wells were washed with PBS and detached by trypsin incubation and transferred into the corresponding 15ml centrifuge tube. The cells were spun at 3000 rpm for 3 minutes, the pellet was washed once with 2 ml 1X PBS. One millilitre of various AuNPs at the IC₅₀ concentration was spun down and used to determine the concentration used to treat the cells. To the cell lysate and crude AuNPs, 2 ml of aqua regia solution was added. The samples were digested and prepared for ICP-OES analysis following the steps described in section 2.3.4.3.

To determine the percentage of particles internalized by the cells, the total amount of gold nanoparticles administered was divided by the concentration detected by ICP-OES on the treated cells and multiplied 100%.

b) Cell specimen preparation for TEM

The Caco-2 cells were cultured in a T25 cm² flask at a density of 1x10⁶ cells /ml and cultured for 24 hours. The cells were exposed to various Au NPs treated with IC₅₀ concentrations for 24 hours. The supernatant with floating cells was transferred into 15 ml conical tubes and spun at 3000 rpm for 3 minutes. The adherent cells in the flask were washed with 2 ml 1X PBS twice, the supernatant was added to the floating cells. The floating cells were spun at 3000 rpm, the pellets were resuspended in 100 µl of 4% paraformaldehyde fixative (in 0.1M phosphate buffer, pH 7.2) and transferred back into the flasks. The volume of the 4% paraformaldehyde was adjusted to a final volume of 2 ml. The flasks were allowed to shake at 4°C for 5 – 15 minutes. The cells were removed from the flask by a cell scraper and transferred into a 2 ml eppendorf tube using a pre-cut tip. The cell suspension was centrifuged at 3000 rpm for 5 minutes. The pellet samples (cell pellets) were stored in approximately 100 µl of 2.5% glutaraldehyde at 4°C until further analysis. The samples were analysed by Jeol JEM-1011 electron microscope at the Tygerberg Hospital, NHLS pathology Unit.

2.3.6.3 Mode of cell death induced by AuNP conjugates

Several biochemical and cytometry assays were conducted to determine whether incorporating therapeutic peptide D(KLAKLAK)₂ to the AuNPs would alter peptide activity.

a) Analysis of apoptosis cell death induced by AuNP conjugates

The percentage of cells undergoing apoptosis were detected and quantified by using the APOPercentage™ apoptosis assay (Biocolor, UK). The cells were seeded in a 12-well culture plates at a density of 2×10^5 cells/ml and incubated for 24 hours at 37°C. The culture media was then removed and replaced with media containing IC_{50} of the AuNPs. The cells were then incubated for 24 hours at 37°C. Untreated and cells treated with apoptosis inducing agents were included as controls.

After incubation, all the media from each well containing floating cells, was transferred to 15 ml conical tubes using a sterile pipette. The wells were washed with 1 ml DPBS and transferred into the corresponding 15 ml conical tubes containing floating cells. The cells were detached using 2X trypsin and transferred to their corresponding 15 ml conical tubes. Cells were harvested by centrifugation at 3000 rpm for 5 minutes at RT. The supernatant was discarded, the pellet was gently re-suspended in 250 μ l of a 1:160 diluted APOPercentage™ dye diluted in complete DMEM media. The cells were incubated for further 30 minutes at 37°C, 4 ml of 1X PBS was then added to each tube and centrifuged at 3000 rpm for 5 minutes at RT. The supernatant was discarded and the cell pellets were re-suspended in 300 μ l of 1X PBS. Cell staining was measured by Attune Acoustic flow cytometer (Applied Biosystems, Germany) or Accuri flow cytometer (BD Biosciences). Acquisition was done in log mode and a maximum of 10 000 to 30 000 events per sample were acquired and analysed using Attune software (Applied Biosystems, German) and Flowjo software.

b) Western blotting analysis of Caspase 3 activation

Caco-2 cells were seeded at 5×10^5 cells/ml in a 6 well plate then treated with various AuNP conjugates for 24 hours. The cells were trypsinized and harvested from each sample by centrifugation. Protein was extracted from the cells using CytoBuster Protein Extraction Reagent following manufacturer's instructions. Protein was quantified by Bradford assay as described previously. Caspase 3 expression levels were examined using SDS-PAGE and Western blotting, as described in section 2.3.1.12. Equal amounts of protein (10 μ g) from each sample were separated by 12% SDS-PAGE and transferred to PVDF membrane. The membrane was probed with 1:1000 caspase 3 rabbit polyclonal primary antibody overnight at 4°C. After washing with TBST, the membrane was incubated with goat anti-rabbit HRP-conjugated secondary antibody that was diluted 1:10 00 in TBST for 1 hour at room temperature. Actin-HRP mouse monoclonal IgG₁ at 1:5000 dilutions was used as a loading control. The reactive bands or chemiluminescent signals were captured and imaged using the UVP Bioimaging System.

c) Analysis Caspase 9 activation by Flow Cytometry

Caspase 9 activity was assessed using CaspaLux 9-M₁D₂ substrate (OncoImmunin, Inc), according to manufacturer's instructions. Briefly, 2×10^5 cells/well of Caco-2 cells were grown in a 12-well plate, the cells treated with various AuNP conjugates at IC₅₀ for 24 hours. The cells treated with 50 μ M cisplatin were used as positive control. The cells were detached using trypsin after 24 hours treatment, washed with 1X PBS and transferred into 2 ml eppendorf tubes. The cells were harvested by centrifugation at 3000 rpm for 5 minutes and 50 μ l of 10 μ M CaspaLux 9-M₁D₂ substrate solution was added to the cell pellet, mixed by pipetting and incubated at 37°C for 60 minutes. The cells were washed once by adding 1 ml of 1X PBS and centrifuged as before. The cell

pellets were resuspended in 300 μ l fresh PBS. Caspase 9 activity was determined and analysed by Accuri flow cytometer within 60 to 90 minutes.

d) Mitochondrial dysfunction: ROS activity

The intracellular ROS generation in cells exposed to the AuNP conjugates was investigated using the 5-(and-6)-chloromethyl-2',7'-dichlorodihydrofluorescein diacetate acetyl ester (CM-H₂DCFDA) fluorescence probe (Life Technologies). The Caco-2 cells were seeded in a 12 well plate at 2×10^5 cells/ml density and cultured at 37°C overnight. The cells were treated with AuNPs at IC₅₀ for 24 hours. Cells treated with 50 μ M cisplatin were used as an apoptosis inducer control, H₂O₂ as a positive control induction of ROS. Cells were detached using trypsin, washed twice with 2 ml of 1X PBS and resuspended in 350 μ l of 7.5 μ M DCFH-DA prepared in PBS. The cells were incubated at 37°C incubator for 30 minutes. Then 4ml of PBS was added to the sample and centrifuged as before. The pellets were resuspended in 350 μ l 1X PBS. The mean fluorescence intensity in the cells was determined by Attune or Accuri flow cytometers.

2.3.7 Statistical analysis

Statistical and multiple-comparison analyses were performed within each group. Data were expressed as the mean \pm standard deviation of the three replicates. Statistical analysis was conducted using the GraphPad Prism[®] 6 and two-tailed Student's *t*-test, differences among three or more groups were analysed by one or two-way analysis of variance (ANOVA). The differences with $P < 0.05$ were considered statistically significant. The IC₅₀ values were calculated using the GraphPad Prism[®] 6 by plotting the log concentration of the treatment versus percentage cell viability.

Chapter 3: Recombinant expression and purification of a pro-apoptotic protein

3.1 Introduction

The study aims to develop a targeted anti-angiogenic nanotherapy that can be selectively delivered to PHB-expressing ECs in the WAT vasculature of obese subjects and trigger cell death in the ECs through apoptosis. The PHB-targeted nanotherapy is composed of a recombinant pro-apoptotic protein (TK₃) that will serve as treatment. The pro-apoptotic protein (TK₃) and the mutated protein (mTK) used in this study were produced through RDT, the biological effects of the two recombinant proteins were investigated using Caco-2 cells as a model cell line for ECs in the WAT of obese subjects. The recombinant TK₃ protein is composed of a synthetic pro-apoptotic peptide, _D(KLAKLAK)₂ fused to a basic TAT (RKKRRQRRR) domain and caspase-3 cleavage site (DEVD), cloned into a pET 30a+ vector as described in section 2.3.1.1. mTK was used as a negative control, and was composed of TAT and a scrambled peptide (DLSLARLATALAI). The recombinant proteins were expressed with TAT as the protein transduction domain (PTD), which will facilitate cellular uptake of the recombinant proteins. The PTD has multiple arginine and lysine residue that facilitate internalization of TAT and its cargo through endocytosis (Frankel and Pabo, 1988).

The _D(KLAKLAK)₂ peptide is an amphipathic, α -helical peptide composed of 14 amino acids in a D-enantiomer to avoid its degradation by proteases in biological systems (Ellerby *et al.*, 1999). It has anti-bacterial activity and is capable of killing cells at a very low dosage. This polycationic peptide has antimicrobial activity that is triggered once the peptide penetrates the anionic bacterial membranes and disrupts the

mitochondrial function *in vitro* (Fantin *et al.*, 2005; Javadpour *et al.*, 1996). The $D(KLAKLAK)_2$ peptide is non-toxic to eukaryotic cells as it cannot disrupt the zwitterionic plasma membranes of the eukaryotic cells by itself (Ellerby *et al.*, 1999). However, the internalization of the peptide through PTD into mammalian cells was shown to disrupt the negatively charged mitochondrial membrane and induces cytochrome c release leading to cell death by apoptosis (Ellerby *et al.*, 1999; Fantin *et al.*, 2005).

The use of this peptide can be enhanced by developing targeting and internalization strategies into mammalian systems. TAT has been fused to $D(KLAKLAK)$ peptide to enhance its internalization by the cells. However, the activity of the TAT *in vivo* is compromised by its lack of specificity (Sandoval *et al.*, 2007; Vivès *et al.*, 2008). PTDs are readily taken up by cells following the mechanisms described in section 1.2.2. Targeting peptides, unlike PTDs, specifically home to target cells and can be used for intra- and extracellular targeting of therapeutic and diagnostic agents (Leifert *et al.*, 2002). Furthermore, the targeting peptides can enhance the therapeutic activity of its cargo and reduce toxic side effects at non-target sites through selective delivery. Targeting peptides are highly specific for certain biomarkers expressed by diseased cells and can be used to improve the efficacy of therapies. Attaching a targeting peptide to the $D(KLAKLAK)_2$ peptide has been successfully used to induce cell death of vascular ECs in the WAT of obese mice (Kolonin *et al.*, 2004) and HER-2 positive human breast cancer cells *in vitro* and mouse xenograft (Fantin *et al.*, 2005). The strategy was effective even in cancer cells that were known to be drug resistant (Fantin *et al.*, 2005). These studies demonstrated the potential application of the strategy in the treatment and eradication of chronic diseases.

3.2 Results

3.2.1 Colony PCR: Screening for mTK and TK₃ positive clones

E. coli MC 1061 competent cells were transformed with pET22(b)+-mTK and pET30(a)+-TK₃ plasmid DNA as described in Section 2.3.1.4. Eighteen to twenty colonies for each construct were selected through antibiotic resistance and screened for the transformation of mTK and TK₃ plasmids by colony PCR using T7 primers. A plasmid DNA amplifiable by the T7 primers was used as a positive control. The negative control with no DNA was included to check for non-specific amplification.

Figure 3.1 shows the amplified plasmid DNA containing the mTK gene. The amplified gene containing mTK in lane 1-18 was around 300 bp. The 18 ampicillin resistant genes tested positive with an amplicon at the expected size for the genes that had incorporated the mTK DNA. The positive control (+ve ctrl) showed an amplicon at 1kb.

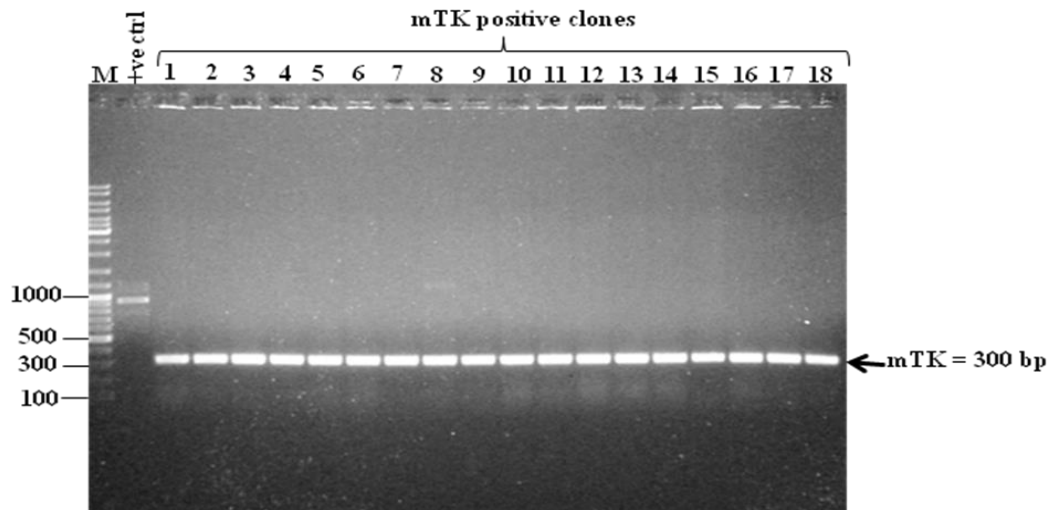


Figure 3.1: Amplification of mTK positive clones by colony PCR. Eighteen ampicillin-resistant colonies were selected to screen for recombinant mTK plasmids. The recombinant genes were amplified by PCR using T7 primers. Amplicons were analysed on a 1% agarose gel containing ethidium bromide stain. M=1 kb marker in bp, +ve ctrl = pET30(a+) construct used as a positive control, 1-18 = ampicillin-resistant clones, arrow points at 300 bp amplicon representing mTK.

The TK₃ positive clones were tested in a similar manner as mTK clones. Twenty kanamycin resistant colonies were amplified, all the clones that had taken up the gene are shown in Figure 3.2. This was confirmed by the amplicon size detected at 500 bp for TK₃ in lane 1-20. The agarose gel electrophoresis showed no bands in the negative control sample (nH₂O), confirming the specificity of the primers used. All the clones that tested positive were subcultured as described in methods for the extraction of plasmid DNA.

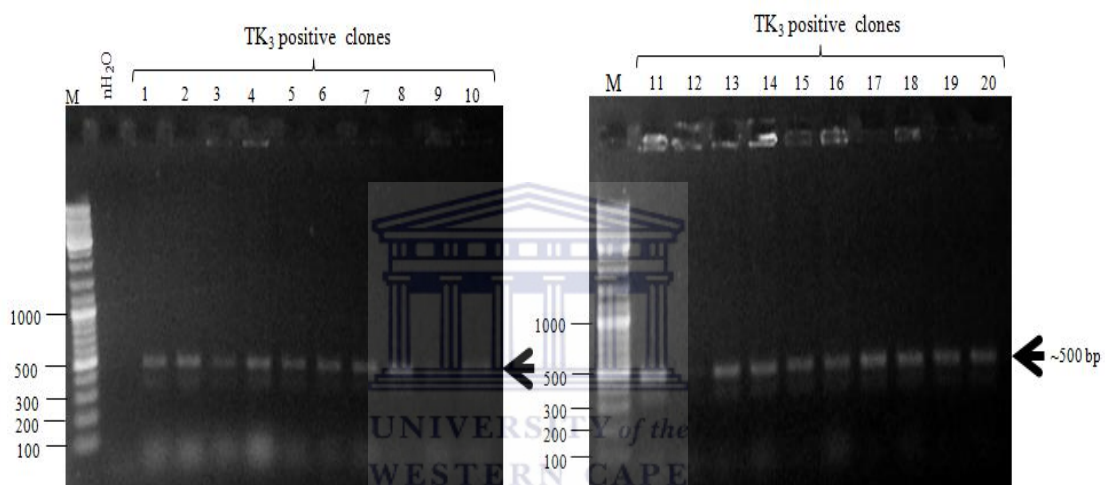


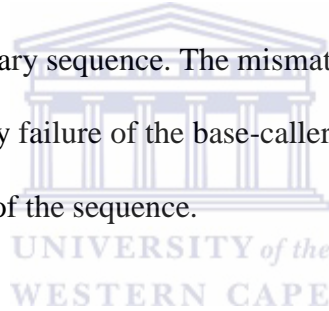
Figure 3.2: Amplification of TK₃ positive clones by colony PCR. Twenty kanamycin-resistant colonies were selected to screen for recombinant TK₃ plasmids. The recombinant genes were amplified by PCR using T7 primers. Amplicons were analysed on a 1% agarose gel containing ethidium bromide stain. M=1 kb marker in bp, nH₂O = nuclease free H₂O was used as a negative control, 1-20 = kanamycin-resistant clones, arrow points at 500 bp amplicon representing TK₃.

3.2.2 Sequence analysis of positive clones

The positive clones for TK₃ were sequenced to verify that the insert was present and that the coding sequence was in the correct reading frame and that no mutations had occurred during the cloning process. The T7 primers for the pET vector systems were used to amplify the inserted genes. The colonies on the agar plates were sequenced at

Inqaba Biotech (Pretoria), the resulting DNA sequence was analysed with FinchTV software and translated to amino acid sequence by using ExPASy software.

The DNA sequences in both forward (F⁺) and reverse (R⁻) primers confirmed the presence of the TK₃, composed of TAT, 3 repeating units of _D(KLAKLAK)₂ and the caspase-3 cleavage site (DEVD) as highlighted in Figure 3.3. The *Nde I* and *Xho I* restriction sites were used to clone the genes in the pET vectors at the N- and C-terminal, respectively. Although the sequence alignment showed mismatched bases at base pair 5 of the sequence generated with the forward primer and uncalled bases at base pair 373 and 376 sequence generated with the reverse primer, it can be concluded that the entire sequence of the construct has no mutations because the correct bases are included in the complementary sequence. The mismatched sequence can be attributed to sequence artefacts caused by failure of the base-caller to read the sequence accurately at the beginning or at the end of the sequence.



The DNA sequences in Figure 3.3 were translated using ExPASy software to check the amino acid sequence they code for. The translated sequences from both the forward (F⁺) and reverse (R⁻) primers, contained a PTD (TAT) at the N-terminal, followed by three tandem repeats of (KLAKLAK)₂- fused to the caspase-3 cleavage site (DEVDGGGS) and a (Histidine)₆ tag at the C-terminal as highlighted in Figure 3.4.

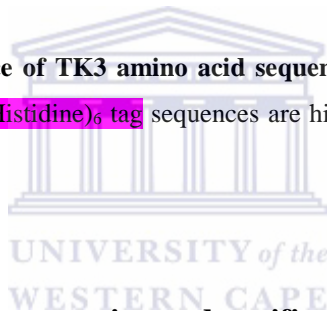
5' Frame 3'

```

1 EGDIIHMETRKKRRQRRRLQDIGSKLAKLAKKLAKLAKDEVDGGGS
46 KLAKLAKKLAKLAKDEVDGGGSKLAKLAKKLAKLAKDEVDGGGS
101 KLGPEQKLISEEDLNLEHHHHHH

```

Figure 3.4: Translated sequence of TK3 amino acid sequence. Start codon, TAT, caspase cleavage site, pro-apoptotic peptide and (Histidine)₆ tag sequences are highlighted. F⁺ = forward primer and R⁻ = reverse primer sequences.



3.2.3 Recombinant protein expression and purification

3.2.3.1 Protein expression screen for mTK and TK₃

Large scale plasmid DNA was prepared from clones containing the mTK and TK₃ plasmid DNA. This plasmid DNA was used to transform *ArcticExpress* competent cells. An expression screen for the presence of recombinant Histidine-tagged protein was performed in a small scale culture. Seven TK₃ and four mTK positive clones (which were selected based on the colony PCR screening) were subjected to IPTG induction to identify the clones that express the desired recombinant protein. The total bacterial lysates of the *E. coli* were resolved on a 15% SDS-PAGE as described in section 2.3.1.9, to analyse expression of the recombinant proteins among the bacterial

proteins. There was no detectable overexpression of any protein at the desired sizes for mTK or TK₃ as shown in Figures 3.5 and 3.6, respectively.

The expected size for the recombinant mTK protein was approximately 10 kDa. As shown in Figure 3.5, protein profiles of both uninduced and induced samples were similar and no distinguishable protein bands were observed at the molecular weight below 15 kDa. Similar trend in TK₃ expression profiles as mTK were observed. The expected size for the recombinant TK₃ protein was 18 kDa, no detectable protein expression levels were observed for TK₃ following SDS-PAGE analysis as shown in Figure 3.6.

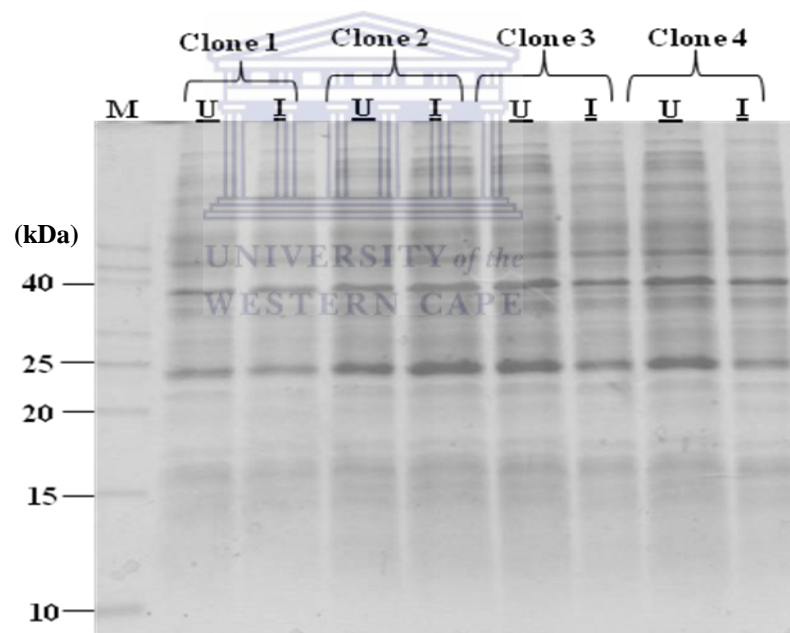


Figure 3.5: Expression screen for recombinant mTK protein. The fusion proteins were expressed in the *ArcticExpress* competent cells, protein expression was induced in the presence of 1 mM IPTG for 48 hours at 15°C. The 10 ml culture of induced (I) and uninduced (U) bacterial suspensions were harvested by centrifugation and was resuspended in 2ml 1X PBS. The protein expression was analysed by SDS-PAGE. M- protein ladder in kDa.

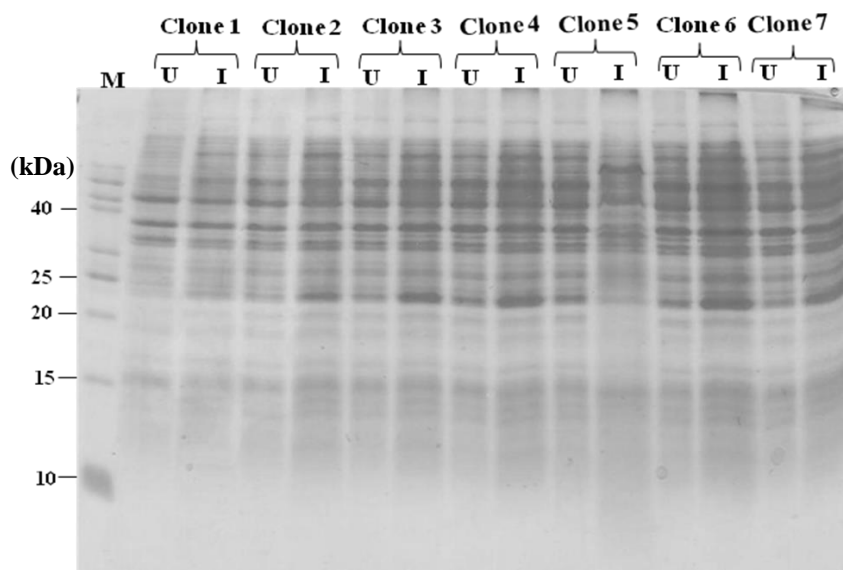


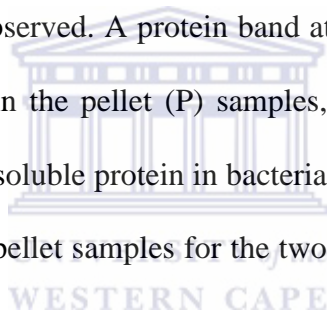
Figure 3.6: Expression screen for recombinant TK₃ protein. The fusion proteins were expressed in the *ArcticExpress* competent cells, protein expression was induced in the presence of 1 mM IPTG for 48 hours at 15°C. The 10 ml culture of induced (I) and uninduced (U) bacterial suspensions were harvested by centrifugation and was resuspended in 2ml 1X PBS. The protein expression was analysed by SDS-PAGE. M- protein ladder in kDa.

At first glance, it appeared as if the proteins of interest were not expressed at all since there was no over expression or presence of additional protein bands at the expected sizes, when compared to the unstimulated (uninduced) samples. The same expression patterns for the small scale test expression of the two constructs (mTK and TK₃) in both induced and uninduced samples were observed. Kwon *et al* (2008) demonstrated that these two proteins are expressed in inclusion bodies when expressed in *E. coli*. It is therefore possible that the conditions of protein isolations used in this experiment were not suitable to release the entrapped proteins of interest from the inclusion bodies. Therefore, alternative protein extraction method using the BugBuster reagent was used to help extract the recombinant proteins.

3.2.3.2 Solubility screening of the recombinant proteins

Four clones for each of the two proteins were selected for scale-up (50 ml) for protein expression screen. The bacterial cells were harvested and resuspended in BugBuster reagent to examine the expression and relative distribution of the soluble and insoluble proteins. Proteins present in the supernatant represent soluble proteins, while proteins in the pellet represent insoluble proteins. The expression level was relatively low and the protein bands detected on Coomassie-stained SDS-PAGE are shown in Figure 3.7 for mTK and 3.8 for TK₃ expression.

Different protein profiles between the supernatant (soluble proteins) and the pellet (insoluble proteins) were observed. A protein band at the expected size of recombinant protein was detected only in the pellet (P) samples, this indicated that the protein of interest was expressed as insoluble protein in bacterial inclusion bodies. The differential expression observed in the pellet samples for the two constructs is marked by circles in Figure 3.7 and Figure 3.8.



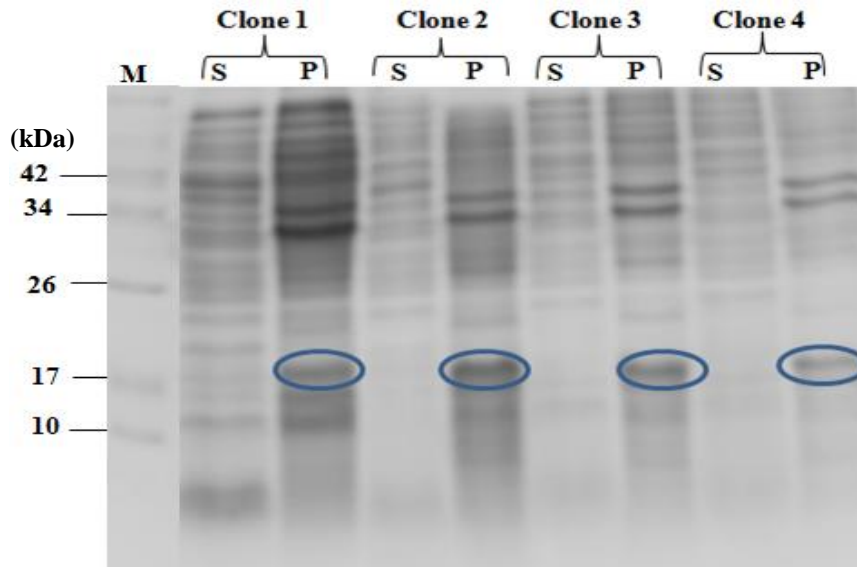


Figure 3.7: Evaluation of recombinant mTK protein solubility. The fusion proteins were expressed in the *ArticExpress* express competent cells. The recombinant proteins were induced in the presence of 1 mM IPTG for 48 hours at 15°C. The cells were lysed in 500µl BugBuster reagent. The supernatant (S) was collected into a clean tube. The pellet (P) samples was resuspended in 500µl 1X PBS. Blue circles represent the overexpressed mTK protein.

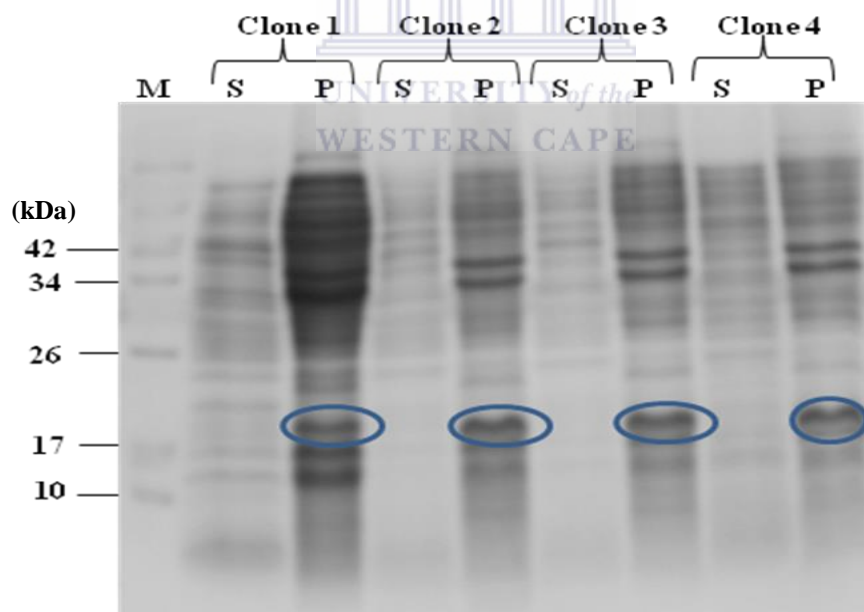


Figure 3.8: Evaluation of recombinant TK₃ protein solubility. The fusion proteins were expressed in the *ArticExpress* competent cells. The recombinant proteins were induced with 1 mM IPTG for 48 hours at 15°C. The cells were lysed in 500µl BugBuster reagent. The supernatant (S) was collected into a clean tube. The pellet (P) samples was resuspended in 500µl 1X PBS. Blue circles represent the overexpressed TK₃ protein.

Recombinant expression of the two proteins was confirmed following affinity chromatography to check for the ability of His-tag fusion protein to bind the Ni-NTA agarose beads in section 3.2.3.3 and Western blot analysis using a monoclonal anti-His antibody as described in section 3.2.3.4.

3.2.3.3 Affinity purification of the recombinant proteins

The recombinant proteins from mTK and TK₃ were purified under denaturing conditions as described in section 2.3.1.11, the proteins were expressed with a (His)₆-tag at the N-terminus to enable affinity purification using Ni-NTA-agarose. The (His)₆-tag in the recombinant protein allows affinity binding to Ni²⁺ in the Ni-NTA matrix in the column. The recombinant proteins when loaded on a Ni-NTA column, two Histidine residues will bind with one Ni²⁺ ion and trap the tagged protein. The untagged protein in the column will be washed out. The tagged protein is eluted by adding high concentrations of imidazole which competes with His for the Ni²⁺ binding, and displaces it and release the recombinant protein from nickel resin.

The bacterial lysates were subjected to binding buffer to disrupt the inclusion bodies and isolate the recombinant mTK and TK₃ proteins. The solubilised protein fractions were purified on the His-select Nickel affinity gel as described in section 2.3.1.11. After washing the column with 10 ml of gradient imidazole concentrations (0-100 mM) twice, the proteins were eluted by addition of 300 mM imidazole. The presence of recombinant protein in the eluted fractions and protein purity was examined on a 15 % SDS-PAGE from the collected fractions.

Affinity purification of recombinant mTK and TK₃ proteins is shown in Figures 3.9 and 3.10, respectively. The total bacterial lysate, flow through and the samples from all the washes were analysed to determine the presence of His-fusion proteins.

As shown in Figure 3.9, a single band at 18 kDa was observed in mTK samples starting from 30-300 mM imidazole concentrations. SDS-PAGE analysis of TK₃ in Figure 3.10 showed no bands at 20 -100 mM imidazole washes, the recombinant protein eluted at 300 mM imidazole elution buffer. The two TK₃ fractions from 300 mM were pooled, imidazole was replaced by PBS through buffer exchange and the protein was concentrated as described in section 2.3.1.11. The concentrated samples were stored at -20 °C until further analysis.



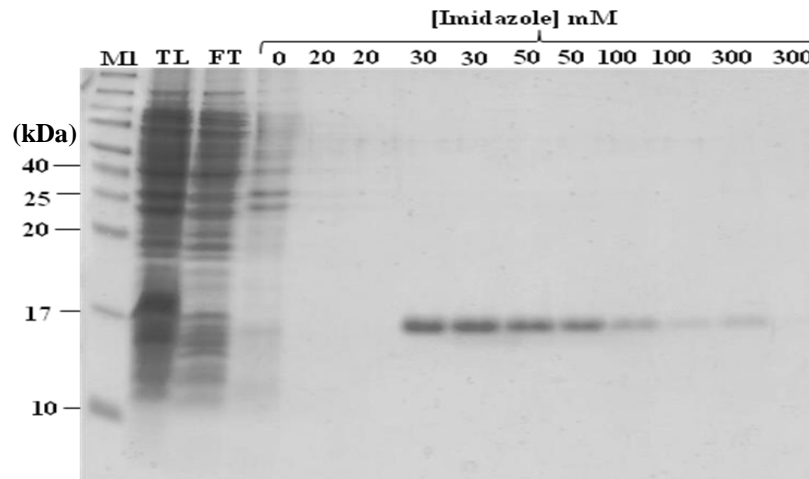


Figure 3.9: Large scale protein expression and affinity purification of mTK. The pellet or insoluble fraction containing the fusion protein was resuspended in binding buffer, clarified by centrifugation and purified on a Ni-NTA column under denaturing conditions. The high background of contaminating bacterial proteins was removed by washing with the stepwise addition of increasing imidazole concentrations. The target proteins were eluted with 300 mM imidazole elution buffer and analysed on a 15% SDS-PAGE and visualized by Coomassie staining. M - protein marker in kDa, TL – total lysate, FT– flow through.



Figure 3.10: Large scale protein expression and affinity purification of TK₃. The pellet or insoluble fraction containing the fusion protein was resuspended in binding buffer, clarified by centrifugation and purified on a Ni-NTA column under denaturing conditions. The high background of contaminating bacterial proteins was removed by washing with the stepwise addition of increasing imidazole concentrations. The target proteins were eluted with 300 mM imidazole elution buffer and analysed on a 15% SDS-PAGE and visualized by Coomassie staining. M - protein marker in kDa, TL – total lysate, FT– flow through.

3.2.3.4 Western blot analysis of Histidine-fusion proteins

Since the recombinant proteins did not have specific antibodies, an antibody against the (Histidine)₆ tag was used to determine expression of (Histidine)₆-fusion proteins. The flow through and washes following affinity purification of the recombinant proteins were subjected SDS-PAGE and the proteins were transferred to PVDF membrane for Western blot analysis. The sizes of the recombinant proteins were 18 kDa on the Coomassie stained gels after affinity purification in Figure 3.9 and 3.10.

The chemiluminescent molecular weight marker did not show bands below 40 kDa, however only the samples that contained a histidine-fusion proteins at 18 kDa were detected on the blots as show in Figures 3.11 and 3.12. The immuno detected bands confirmed the expression of recombinant His-TK₃ protein eluted at 300 mM imidazole, while mTK eluted at 30-300 mM, Figure 3.11 and Figure 3.12, respectively. The seven mTK fractions from 30-300 mM were pooled, imidazole was replaced by PBS through buffer exchange and concentrated as described in section 2.3.1.11. The concentrated samples were stored at -20 °C until further analysis.

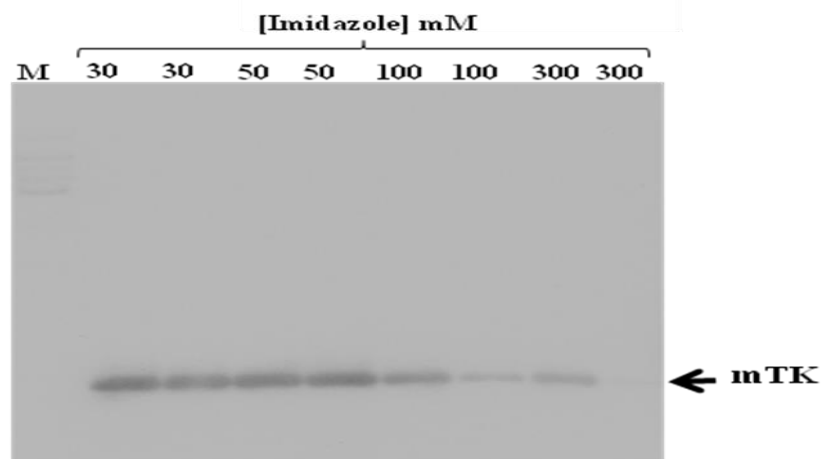


Figure 3.11: Western blot analysis of the recombinant His-fusion proteins. The protein samples subjected for Ni-NTA purification were separated by 12% SDS-PAGE. The proteins were then transferred onto PVDF membrane and probed with His-probe monoclonal HRP conjugated antibody. Protein bands were visualized using enhanced chemiluminescence as described by the supplier. M-chemiluminescent molecular weight marker in kDa.

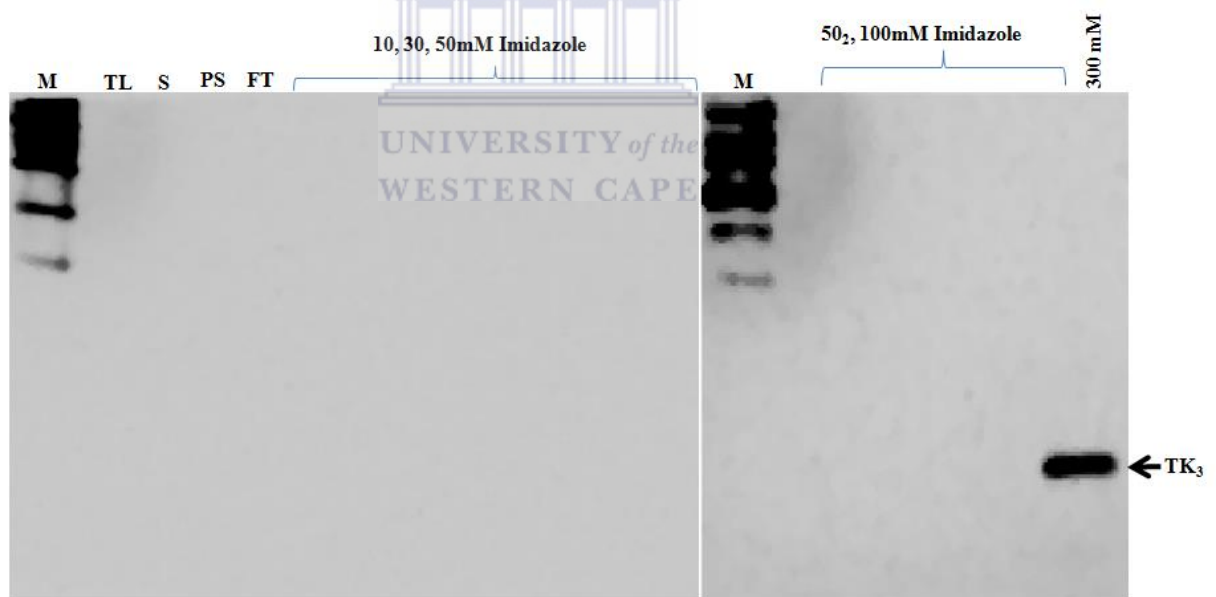


Figure 3.12: Western blot analyses of the recombinant TK₃ His-fusion proteins. The protein samples subjected for Ni-NTA purification were separated by 12% SDS-PAGE. The proteins were then transferred onto PVDF membrane and probed with His-probe monoclonal HRP conjugated antibody. Protein bands were visualized using enhanced chemiluminescence as described by the supplier. M-chemiluminescent molecular weight marker in kDa, TL –total lysate, S –supernatant, PS – supernatant from insoluble fraction, FT – flow through.

3.2.4 Analysis of the effects of recombinant proteins on Caco-2 cell line

3.2.4.1 Evaluating PHB expression in various cell lines

The ultimate application of the recombinant proteins was in development of a receptor targeted nanotherapy that will selectively bind to PHB protein, which is specifically expressed by vascular ECs in the WAT of obese subjects. Thus, for *in vitro* studies a cell line that express PHB protein on the surface of the cell was sought by Western blot and immunocytochemistry as described in section 2.3.3.

Several cancerous and non-cancerous cell lines shown in Table 2.4 (section 2.3.2) were cultured to at least 70% confluency. Total protein was extracted from the cell lines using Cytobuster protein extraction reagent as described in section 2.3.3.1. The expression of PHB in the cell extracts was immuno detected using an antibody against PHB. As shown in Figure 3.13, only the colon (Caco-2) and breast (MCF-7) cancer cell lines showed binding to anti-PHB. Immunoreaction served as an indication of protein expression. The protein has a molecular weight of ~30 kDa.

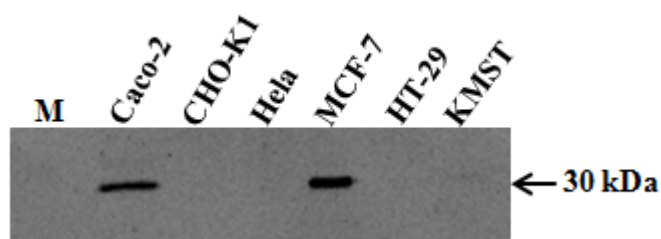


Figure 3.13: Analysis of PHB expression in cell lines. Protein samples from cancerous and non-cancerous cell lines were separated on 12% SDS-PAGE and immunoblotted on PVDF membrane using an antibody against PHB. M- chemiluminescent molecular weight marker in kDa.

Immunocytochemistry was used to investigate localization of the PHB protein in Caco-2 and MCF-7 cancer cell lines to confirm the subcellular expression of the protein. The two cell lines were incubated with PHB targeting peptide (AHP) which was attached to a fluorescein isothiocyanate (FITC) for 1-3 hours as described in 2.3.3.2 to determine

the cellular uptake of AHP-FITC and localization of PHB on the cell lines. The interest was on the cell line that expresses PHB as a cell surface or membrane receptor, which will be used as a model cell line for *in vitro* studies and to determine the effect of the targeted nanotherapy. Uptake of AHP-FITC was observed only in Caco-2 cells as shown in Figure 3.14, signifying that MCF-7 most probably express PHB in the cytoplasm and Caco-2 on the cell surface. The Caco-2 was chosen as an *in vitro* model cell line to represent ECs that express PHB on the cell's surface.

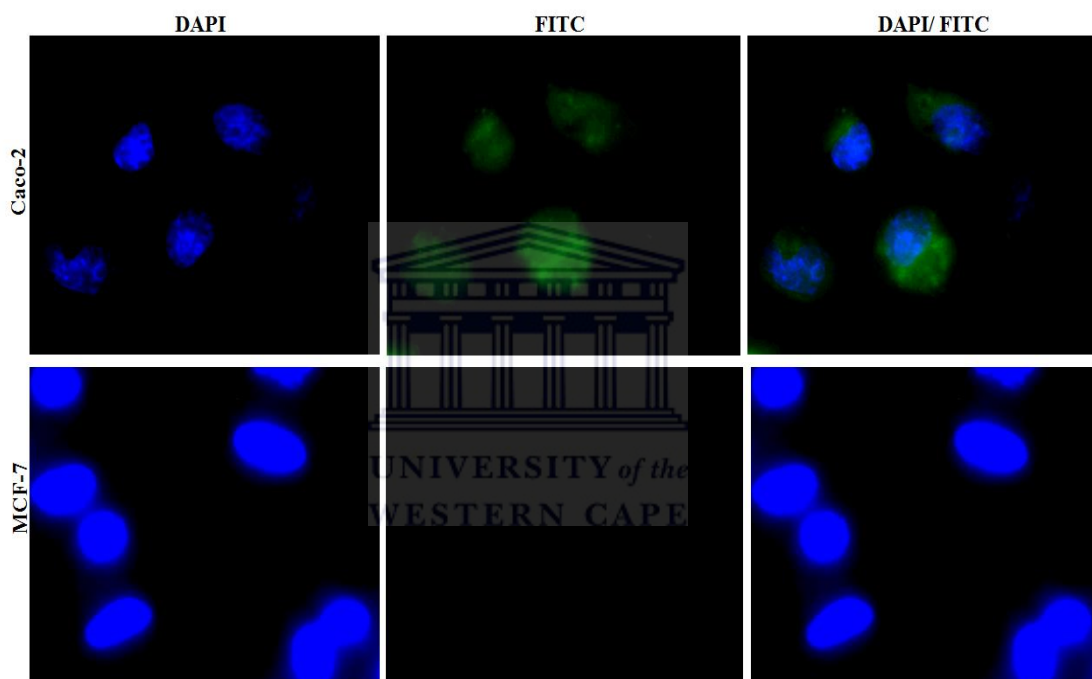


Figure 3.14: Immunocytochemistry analysis of PHB expression and localization in Caco-2 and MCF-7 cell lines. The two cell lines were incubated with 0.01 mM AHP-FITC for 3 hours and analysed for uptake using fluorescent microscopy. DAPI (blue) stains the cell nuclei, FITC (green stain) positive cells indicates the localization of AHP-FITC and therefore also PHB.

3.2.4.2 Cytotoxicity effects of the recombinant proteins

The anti-proliferative activity of the recombinant proteins (mTK and TK₃) was evaluated spectrophotometrically by measuring the degree of mitochondrial reduction of the tetrazolium salt, MTT. The assay is based upon the enzymatic conversion of

MTT substrate to a formazan product by viable cells at the assay end point. The number of viable cells was proportional to the extent of formazan production.

The Caco-2 cells were treated with either mTK or TK₃ in triplicate for 24 hours and the viability of the cells were assessed by the MTT assay. The results as shown in Figure 3.15 showed that mTK was not toxic to the cells at all the tested doses (0.25 – 8 μM). The mitochondrial function of the cells treated with TK₃ has decreased, an indication of cell growth inhibition or cell death. The recombinant TK₃ protein proved to be significantly cytotoxic from 4-8 μM when compared to untreated cells and cells treated with recombinant mTK protein. The IC₅₀ concentration of TK₃ was 5 μM.

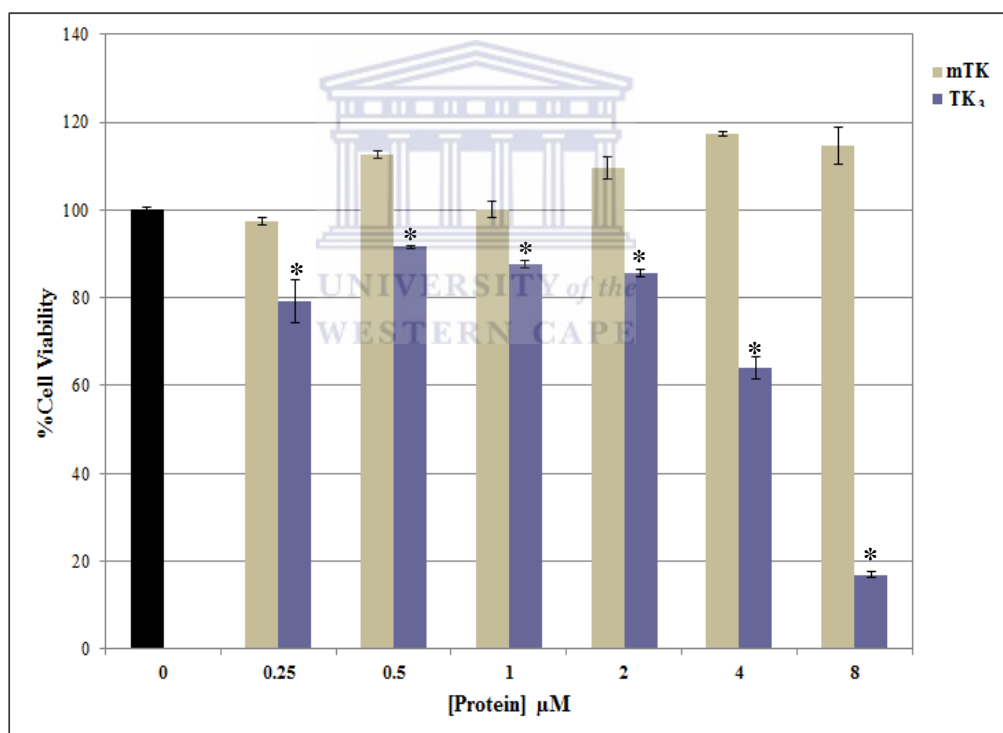


Figure 3.15: Effects of increasing concentrations of mTK and TK₃ recombinant proteins on viability of CaCo-2 cells. Cell viability was analysed using the MTT assay. Cells were treated with increasing concentrations of mTK and TK₃ for 24 hours. Results represent the average of two independent experiments performed in triplicate. A two-tailed, unpaired t-test was used to analyse significance. *p<0.05, significant difference compared to untreated sample.

The difference in cell death induced by TK₃ was statistical significant at all concentrations tested when compared to the negative controls (untreated and cells treated with mTK).

a) The effect of the recombinant proteins on cell morphology

The cells were treated with the IC₅₀ concentration (5 μM) of the recombinant protein to confirm the MTT assay results (Figure 3.15) and determine the effect of the recombinant proteins on the cellular morphology. The viability of the mTK treated cells was unaffected when compared to the untreated cells and the ones exposed to TK₃ when viewed under the light microscope. The elongated morphology of the cells under the light microscope was the same for the negative controls, i.e. the cells treated with mTK protein and untreated cells, as shown in the images in Figure 3.16. However the cells treated with recombinant TK₃ had reduced cell density compared to the untreated and cells treated with mTK. The TK₃ treated cells had detached from each other and started shrinking, which are features associated with the cells undergoing apoptosis.

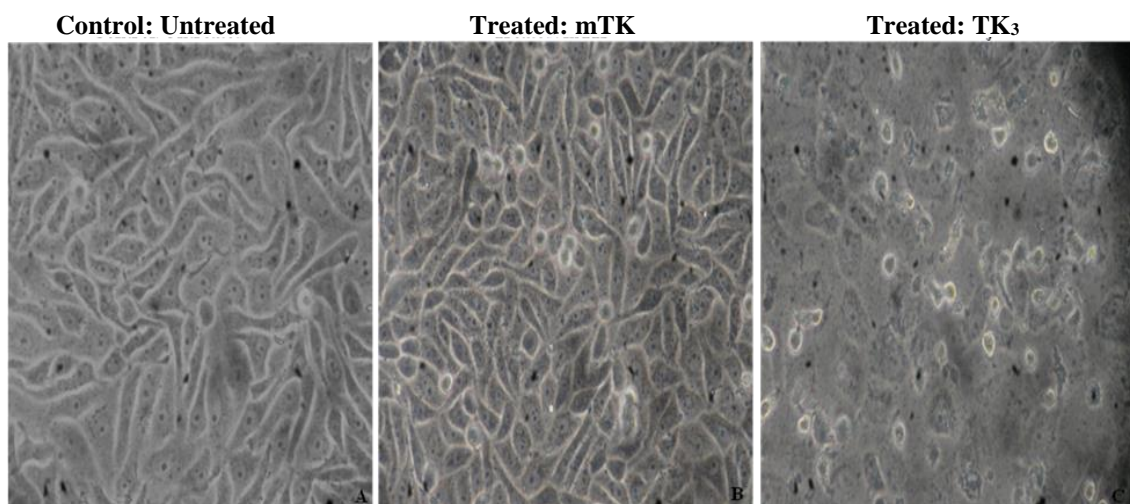
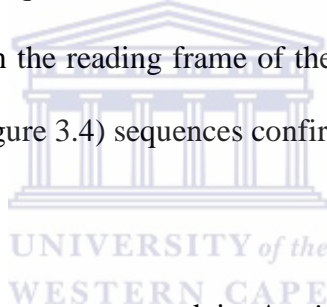


Figure 3.16: Light microscopy images of cells treated with recombinant mTK and TK₃. Caco-2 cells were treated with the recombinant proteins, cell morphology was studied under the light microscopy at 20X magnification.

3.3 Discussion

The goal for this chapter was to express the pro-apoptotic protein (TK₃) using RDT mass production, the recombinant protein was to serve as therapy in the development of PHB-targeted nanotherapy. RDT was used instead of chemical synthesis, since this method would produce higher yield of the recombinant proteins at lower costs (Kyle, 2009). The recombinant plasmids containing mTK and TK₃ encoding DNA sequences were used to transform MC 1061 competent cells. Positive clones containing the mTK and TK₃ genes were screened by colony PCR. An amplicon at 300bp for mTK and 500bp for TK₃ (Figures 3.1 and 3.2, respectively) indicated the presence of the genes. The colonies were further sequenced to confirm the gene orientation and to check for any mutations or changes in the reading frame of the coding sequence. Both the gene (Figure 3.3) and protein (Figure 3.4) sequences confirmed the presence of the two genes in the correct reading frame.



The recombinant proteins were expressed in *ArcticExpress*TM(DE3) competent cells trapped in inclusion bodies as insoluble proteins, refer to Figures 3.7 and 3.8. Kwon *et al.*, (2008) described a similar finding. The recombinant proteins were purified under denaturing conditions through affinity purification. The recombinant Histidine-fusion protein (~18 kDa) corresponding to the expected sizes of mTK (Figure 3.9) and TK₃ (Figure 3.10) were eluted from the Ni-NTA beads. Western blot analyses of the purified recombinant protein samples (Figure 3.11 and 3.12) results indicated that the recombinant Histidine-tagged proteins were present and indicated the expression of both mTK and TK₃ proteins. All the parameters mentioned did not have any relation to the protein identity or its sequence, however the sizes confirmed the presence of both mTK and TK₃ genes and their expression.

Although the fusion proteins were expressed, there were challenges that were encountered through the expression process. The major challenge was the cytotoxicity nature of the pro-apoptotic protein to *E. coli* cells as confirmed by reduced biomass harvested after protein expression. Several chemically competent expression bacterial strains, different IPTG concentrations and temperatures were tested and gave similar results. The bacterial strains used were BL 21(DE3) pLysS, BL21-*CodonPlus* (DE3)-RIL, *Rosetta*TM(DE3) pLysS and the *ArcticExpress*TM(DE3) competent cells. Secondly, since the protein was insoluble, it proved to be very difficult to identify the proteins of interest using SDS-PAGE analysis at the small scale as shown in Figure 3.5 and 3.6. The recombinant proteins were active in their denatured form and proved to be stable and functional in this form when stored at -20°C. And there was no need for refolding the recombinant proteins to its native form.

The recombinant Histidine-tagged proteins did not lose their activity when used to treat the Caco-2 cells. The Caco-2 cell line was used as the model cell line because the cells express the PHB protein (Lenaerts *et al.*, 2007) on their cell surface, the protein that was shown to be overexpressed in the obese state and serve as a receptor for the targeting molecule (Kolonin *et al.*, 2004) used in the study. The cells expressing the PHB protein were sought by subjecting several non-cancerous and cancerous cell lines to Western blot analysis (Figure 3.13). Human colon carcinoma (Caco-2) and breast cancer (MCF-7) cell lines showed PHB expression and further analysed by immunocytochemistry to determine PHB localization. Only the Caco-2 cells showed the uptake and internalization of the AHP-FITC (Figure 3.14), and were chosen as a model cell line for *in vitro* studies. The Caco-2 cell line is derived from a human colon adenocarcinoma, and differentiate spontaneously *in vitro* under standard culture conditions (Pinto *et al.*, 1983).

The activity of the cells in response to the recombinant proteins was studied *in vitro* on the Caco-2 cell line. The control protein (mTK) was not toxic at all concentrations tested when compared to the untreated samples and TK₃ as shown in Figure 3.15. TK₃ behaved in an expected manner, by inducing cell death in all the concentrations used (Figure 3.15). At 8 μ M the protein had killed >80% of cells. Kwon *et al.*, (2008) showed a similar response when the two recombinant proteins were used to treat CHO, MCF-7 and B16F10. TK₃ killed the cells in a dose-dependent concentration while mTK showed no effect on cell proliferation at all concentrations tested (Kwon *et al.*, 2008).

In summary, the recombinant mTK and TK₃ proteins were expressed in *E.coli ArcticExpress*TM(DE3) competent cells and purified as described in this chapter. The recombinant proteins showed desired response in Caco-2 model cell line as shown in Figure 3.15. The next step required was to use these two proteins in the development of targeted nanotherapy and determine whether the protein still retained its pro-apoptotic activity when conjugated to AuNPs, and also determine whether the recombinant protein's therapeutic effect could be channelled to specific targets by attaching a targeting peptide.

Chapter 4: The development of PHB-targeted nanotherapy for target specific induction of apoptosis

4.1 Introduction

PHB-targeted nanotherapy was developed by conjugating the recombinant proapoptotic protein expressed and purified in Chapter 3 and a PHB-targeting peptide (AHP) to AuNPs. The resulting PHB-targeted nanotherapy was expected to induce apoptosis when internalized by the ECs in the WAT vasculature of obese subjects. By so doing, the adipocytes will be forced to metabolise the excess calories and starve to death, followed by reduction of AT mass and total body weight in an obese animal model. The AuNPs served as delivery agents and several negative controls were included to prove that the antiproliferative effect on the cells was due to the therapeutic peptide not the AuNPs. The effects of the AuNP conjugates were tested on PHB-expressing cell line (Caco-2).

Although the gold core is considered to be non-toxic, independent studies have demonstrated the toxicity of the AuNPs through *in vitro* and *in vivo* studies (Cho *et al.*, 2009; Freese *et al.*, 2012; Sabella *et al.*, 2011), and that the toxicity can be easily channelled to specific cells by modifying the AuNP surface with biomolecules and facilitate their uptake and targeted delivery (Kumar *et al.*, 2012). The use of AuNPs as drug delivery agents has shown great potential in cancer clinical studies (Libutti *et al.*, 2010). Pre-clinical studies have also demonstrated that the AuNP bio-conjugates are more efficient than the biomolecules on their own (Sperling *et al.*, 2008). Although these nanomaterials have beneficial aspects, literature shows conflicting data regarding the toxicity of AuNPs raising serious issues regarding its possible risks for human

health and the environment (Caruthers *et al.*, 2007). The bulk gold material is bio-inert (Brown *et al.*, 2008; Murphy *et al.*, 2008), however, alteration of their physico-chemical properties for biological application has been associated with undesirable results that raise adverse effects on biological systems (Caruthers *et al.*, 2007; Cunningham, 2014).

The NPs are of similar size to typical cellular components, and may easily bypass natural mechanical barriers. The resulting effects might not be inherently benign and they might affect biological behaviours at the cellular, subcellular, and protein levels (Service, 2004; Donaldson *et al.*, 2004; Oberdorster *et al.*, 2005; Royal Society, 2004). These NPs can penetrate both the cell and nuclear membranes and accumulate in tissues, interfering with cellular functions leading to genotoxicity, possibly cell death through their interaction with cellular organelles (Gibson *et al.*, 2011; Li *et al.*, 2003). Therefore, NP interaction with cellular components might affect biological mechanisms possibly leading to adverse tissue reaction as highlighted in Figure 4.1. The NPs are usually charged and can easily adsorb serum proteins leading to cyto- or genotoxicity (Nel *et al.*, 2009). The possible lethal effects of AuNPs on cells cannot be ignored. The fate and effect of AuNPs upon their entrance into the living cells is still questionable (Sperling *et al.*, 2008) and requires investigations that can ascertain their safety and biocompatibility. This chapter aims to explore the effect of the untargeted and targeted AuNPs on Caco-2 cancer cells using cell biological and biochemical assays.

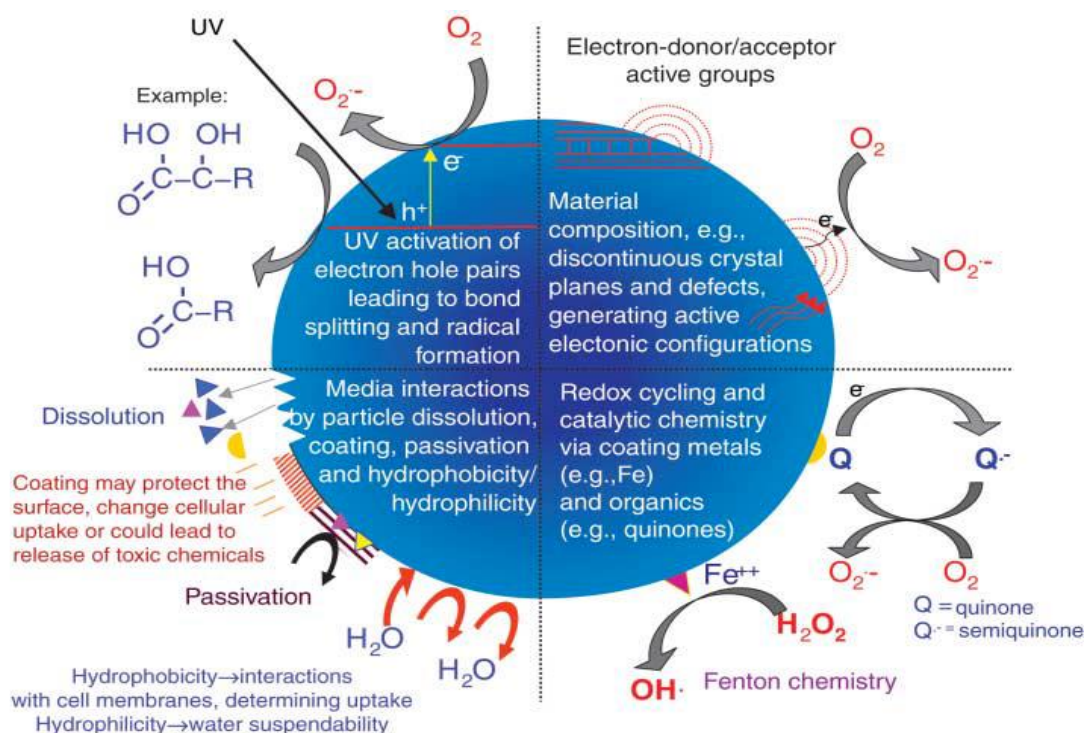


Figure 4.1: Possible mechanisms by which nanomaterials interact with biological tissue. Examples illustrate the importance of material composition, electronic structure, bonded surface species (e.g., metal-containing), surface coatings (active or passive), and solubility, including the contribution of surface species and coatings and interactions with other environmental factors (e.g., UV activation) (Nel *et al.*, 2009). Figure reprinted with permission from Elsevier AAAS.

UNIVERSITY of the
WESTERN CAPE

4.2 Results

4.2.1 Conjugation of the recombinant proteins to AuNPs

The mTK and TK₃ recombinant proteins were expressed as Histidine-tagged proteins as described in section 3.2.3.2 and 3.2.3.3. The (Histidine)₆-tag at the C-terminus was retained for attaching the recombinant proteins to nitrilotriacetic acid (NTA) modified AuNPs. The design of the AHP-targeted nanotherapy is shown in Figure 4.2.

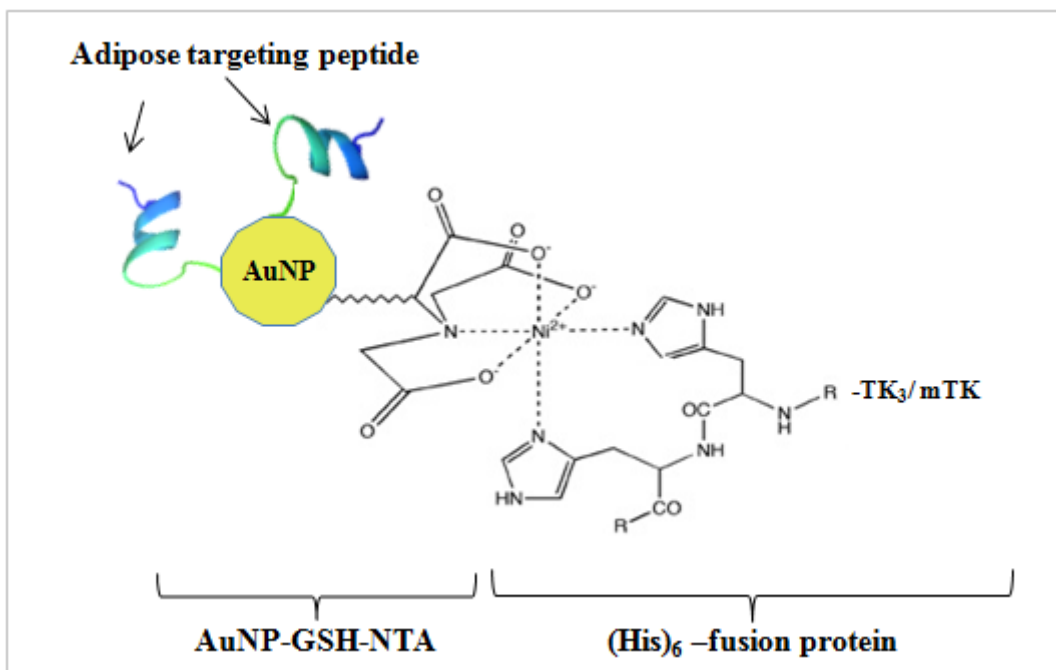


Figure 4.2: Schematic diagram of the PHB-targeted nanotherapy. The recombinant proteins and the AHP targeting peptide were conjugated to AuNP-GSH-NTA.

4.2.1.1 Synthesis and characterization of NTA-gold nanoparticles

The AuNPs were synthesized following reduction of gold aurate and modified by the addition of NTA using glutathione (GSH) as a linker (Taute *et al.*, 2014). Figure 4.3 shows the optical properties of AuNP-GSH-NTA compared to citrate AuNPs as characterised by UV-Vis spectroscopy. The maximum absorption spectrum for AuNPs and AuNP-GSH-NTA observed was 523 nm with an absorbance of 0.97 and 0.95, respectively.

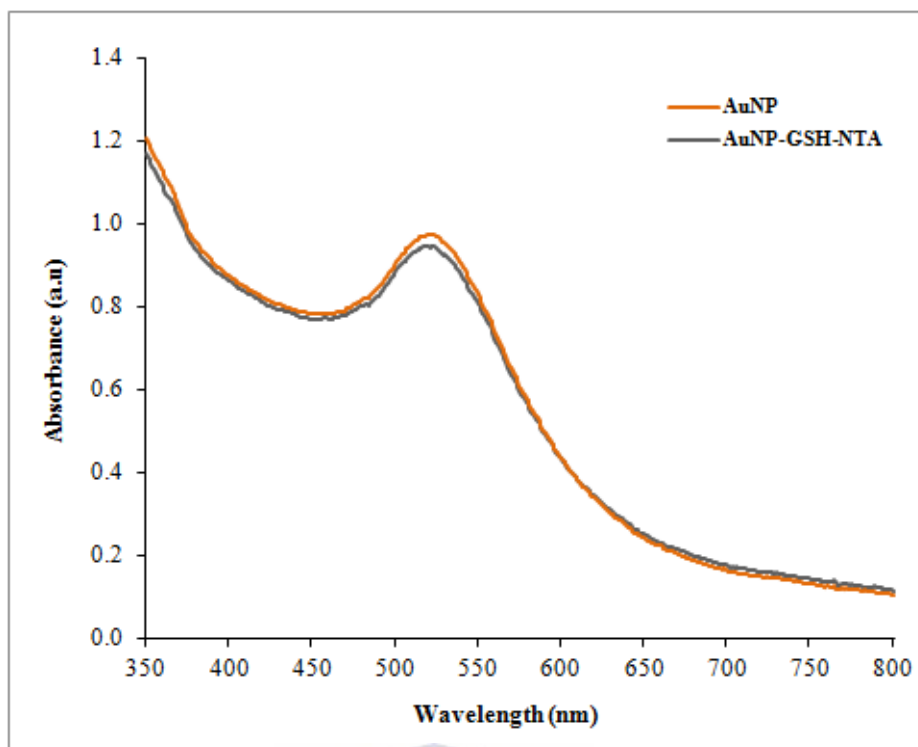


Figure 4.3: Optical properties of AuNP and AuNP-GSH-NTA determined by UV-vis spectroscopy.

The size and concentration of the AuNPs was determined from the UV-vis data as described by Haiss *et al.*, (2007). The AuNP concentration was calculated based on the formula:

$$C = A_{450} / \epsilon_{450}$$

where: C = concentration, A_{450} = absorbance at 450nm, ϵ_{450} = molar extinction coefficient at 450nm. The concentration of the AuNP-GSH-NTA was 1.36×10^{-7} M and their diameter was ~5nm.

Different concentration of NiSO_4 (0-1 mM) was used to activate the AuNP-GSH-NTA before the recombinant proteins were attached. NiSO_4 concentration of 0.3 mM was found to be the most effective. The AuNP-GSH-NTA were activated with 0.3 mM NiSO_4 and functionalized with increasing concentration of mTK and TK₃ recombinant

proteins. The flocculation behaviours of the modified AuNPs were investigated by colorimetric and optical changes of the NPs after addition of 10% NaCl using a UV–vis spectrophotometer. The flocculation rate of the modified AuNPs was depended on the concentration of the protein added, the AuNPs flocculated at all concentration tested.

4.2.2 Development of targeted nanotherapy using $D(KLAKLAK)_2$ peptide

4.2.2.1 Design of the AuNP conjugates

When conjugation of recombinant proteins to AuNPs-GSH-NTA failed, custom-designed $D(KLAKLAK)_2$ -SH peptide was synthesized by AnaSpec and used to construct the PHB-targeted nanotherapy as discussed below. The design of the AuNP conjugates is shown in Figure 4.4.

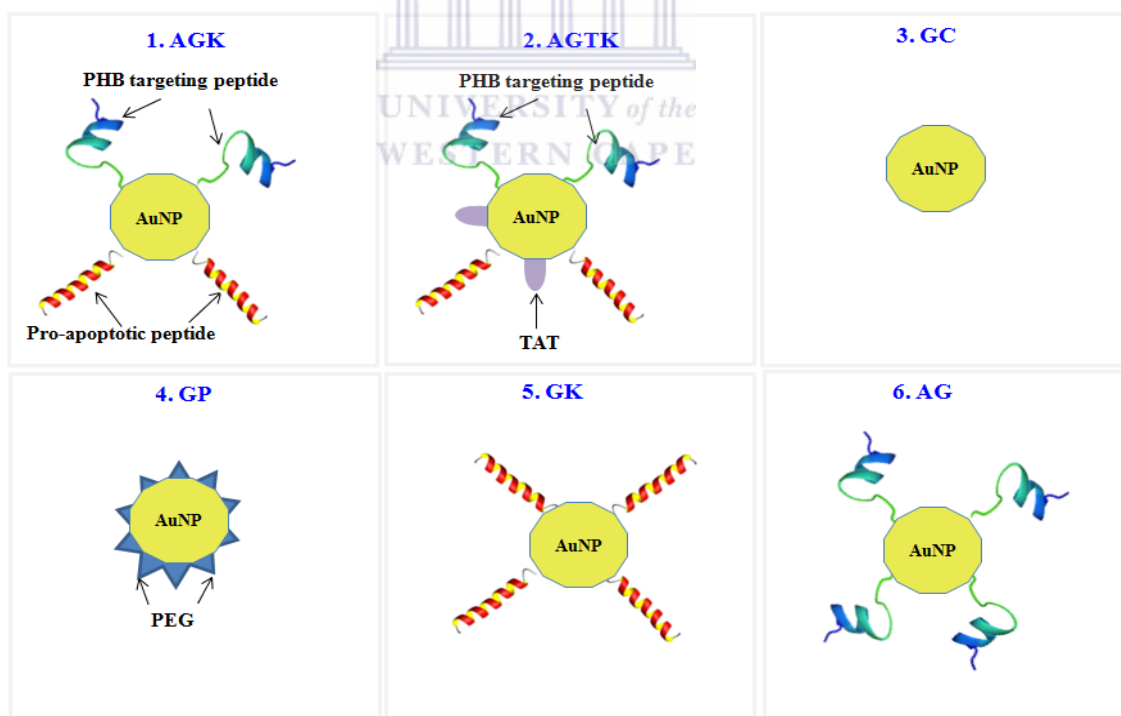


Figure 4.4: Schematic diagram of the AuNP design. AGK = has both targeting and therapeutic peptides, AGTK = has TAT, targeting and therapeutic peptides. GC = citrate coated AuNPs, GP = PEGylated AuNPs, GK = AuNPs with therapeutic peptide, and AG = targeted pegylated AuNPs.

The various AuNP conjugates used in this study are listed in Table 4.1 with their acronyms. These acronyms will be used to refer to the AuNPs. Naked metal NPs tend to be unstable in organic solvents, to prevent aggregation in solution PEG (HS-PEG-OH) was used as a stabilizer and emulsifying agent for all AuNP conjugates. Encapsulation of the metal core with PEG creates a dielectric shell around the metal core, this provides means of protection for the AuNPs from the surrounding environment or opsonisation when used in biological system. The functionalities on the shell were manipulated by adding targeting and therapeutic peptides for biomedical applications.

Table 4.1: Preparation of various AuNPs for biological application and their acronyms.

Final AuNP conjugate	Acronyms	Ratios				
		PEG-OH	PEG-STREP	Biotin-AHD	TAT	KLAKLAK
Citrate AuNPs	GC	0	0	0	0	0
AuNP-PEG	GP	11	0	0	0	0
AHP-AuNP-PEG	AG	10	0.5	0.5	0	0
AuNP-KLAKLAK) ₂	GK	10	0.5	0	0	0.5
AHP-AuNP-(KLAKLAK) ₂	AGK	9.5	0.5	0.5	0	0.5
AHP-AuNP-TAT-(KLAKLAK) ₂	AGTK	9	0.5	0.5	0.5	0.5

The biotinylated prohibitin-targeting peptide (AHP-Biotin) was attached to AuNPs using streptavidin. The targeting peptide will increase the specificity and sensitivity of the attached pro-apoptotic [D(KLAKLAK)₂-SH] peptide. The pro-apoptotic peptide was incorporated to the AuNPs through the thiol group and served as a therapeutic peptide. TAT was added to AGTK particles to determine if an extra PTD can enhance the AuNP uptake and therapeutic potential as compared to AGK.

4.2.2.2 Synthesis and characterization of gold nanoparticles

The AuNPs were synthesized following the sodium citrate reduction method established by Turkevich as described in section 2.3.5.1. Different molecules were coupled to the citrate-AuNPs through different chemistries to develop biologically active or functionalized AuNPs. The citrate-coated AuNPs and AuNP-peptide conjugates were sterilized by filtration and the optical properties of those AuNPs were characterized by UV-Visible spectroscopy. The size distribution, shape and quality of the NPs was studied by TEM and electrical conductivity examined by Zeta (ζ -) potential.

Absorption spectrum of gold colloids has been used to indicate immobilization of other molecules on the surface of the gold colloids based on their λ_{max} or localized surface plasmon resonance (LSPR). Gold nanoparticles exhibit a strong absorption band in the visible region that can be used to determine whether modification of the NP surface has been successful (Ghosh *et al* 2004; Philip, 2008). The colloidal LSPR is dependent on several factors such as the size, solvent and surface modification and is useful in distinguishing AuNP conjugates as well as to monitor adsorption or conjugation of biomolecules on the surface of the AuNPs.

The effect of modifying the surface of citrate coated AuNPs (GC) on the LSRP is shown on Figure 4.5. The interaction of the metal particles with the stabilizing agents or biomolecules induced the LSPR changes reflected in the absorption spectral features of AuNP conjugates. The UV-Vis absorption properties of the colloidal nanoparticles were compared to the other AuNP conjugates in Figure 4.5. The change in optical properties of the AuNP-peptide conjugates suggested the formation and adsorption of biomolecules on the surface of GC. The UV-Vis spectrum of GC with a defined plasmon resonance peak at 519 nm was observed. There was a red shift and either

increase or decrease in the peak intensities after the addition of AHP and D(KLAKLAK)₂ peptides on GC as an indication of a change in the dielectric constant of the AuNP surface. Compared to GC, the peak intensity for AGK increased and maximum absorption wavelength shifted from 519 nm to 524 nm. The degree of red shift for AGTK was the same as AGK. Reduced peak intensity for AG and GK and increased absorption maxima from 519 nm to 525 nm was observed. For GP, the λ_{max} was 519 nm with a slight increase in peak intensity. The shift in the absorption peak was attributed to the presence of other molecules on the surface of the citrate AuNPs.

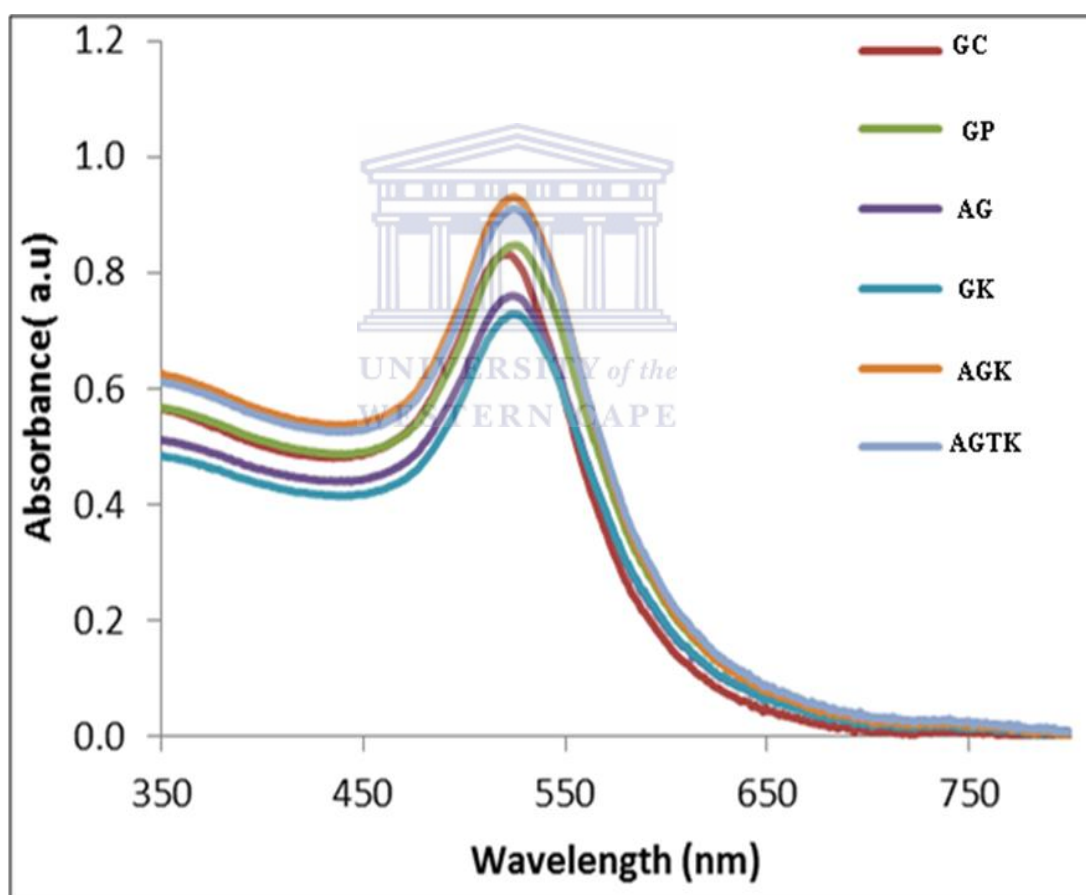


Figure 4.5: UV-Vis spectrophotometer absorption spectrum of citrate capped AuNPs and their respective AuNP-peptide conjugates. GC = citrate coated AuNPs, GP = PEGylated AuNPs, AG = targeted GP, GK = AuNPs with therapeutic peptide, AGK = has both targeting and therapeutic peptides, AGTK = has TAT, targeting and therapeutic peptides.

The size distribution, quality and morphology (shape) of the AuNPs was characterized by TEM analysis. Representative TEM micrographs of the different AuNPs are shown in Figure 4.6. The TEM micrographs of all the AuNPs showed particles with uniform spherical shapes that had an average diameter of 14 nm (± 2 nm). The AuNPs dispersion showed no signs of aggregation. GC particles appeared to be more separated as compared to the other AuNPs that seem to associate closely with each other.

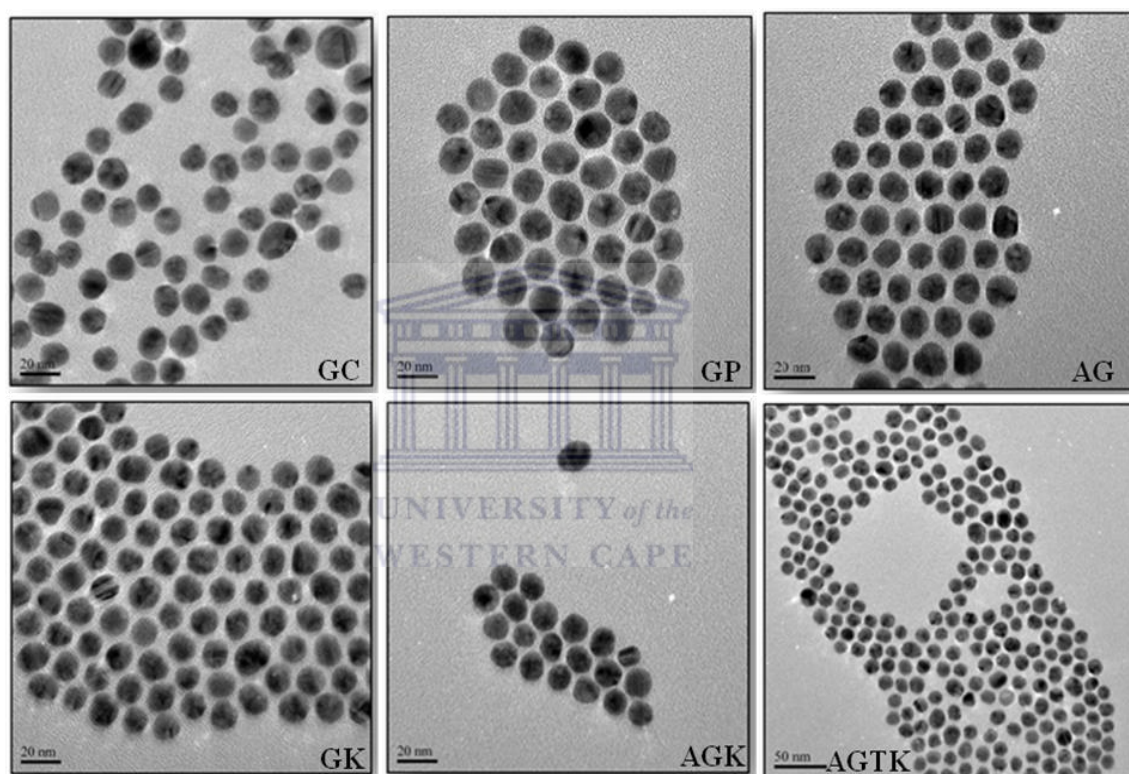


Figure 4.6: Representative TEM micrographs of the AuNP conjugates. GC = citrate coated AuNPs, GP = PEGylated AuNPs, AG = targeted GP, GK = AuNPs with therapeutic peptide, AGK = has both targeting and therapeutic peptides, AGTK = has PTD, targeting and therapeutic peptides. Scale bars in the micrographs are used to represent magnification of AuNPs.

The ζ -potential or the surface charge of the AuNP conjugates as a measure of their charge and stability was measured using a Malvern Zetasizer Nano ZS. The ζ -potential determines the behaviour of the colloids in solution, range between +100 mV to -100 mV can be used to determine the colloidal stability (Clogston and Patri, 2011; Leroy *et al.*, 2011). NPs with a ζ -potential between -10 and +10 mV are considered to be

neutral, while particles with ζ -potential greater than +30 mV are said to be strongly cationic and strongly anionic if the ζ -potential is less than -30 mV (Clogston and Patri, 2011). These values can also determine how readily the NPs will aggregate in solution. NPs with ζ -Potential values greater than +25 mV or less than -25 mV are highly stable and will resist aggregation. While NPs with lower ζ -potential values closer to zero can easily coagulate or flocculate when dispersed in solution (Clogston and Patri, 2011).

In Figure 4.7, the ζ -potential of GC was found to be -42.5 mV. The value increased after bio-conjugation of targeting and therapeutic peptides. Of all the AuNPs synthesized, GP had the highest ζ -potential at -2 mV followed by AG (-11 mV), AGTK (-11.7 mV), AGK (-12.4 mV) and GK (-16.9 mV). The changes are attributable to molecules attached to the AuNP surface and their charges. The change in ζ -potential suggests modification of the AuNP surfaces and values can also be used to predict how these AuNPs are going to behave when used in biological system.

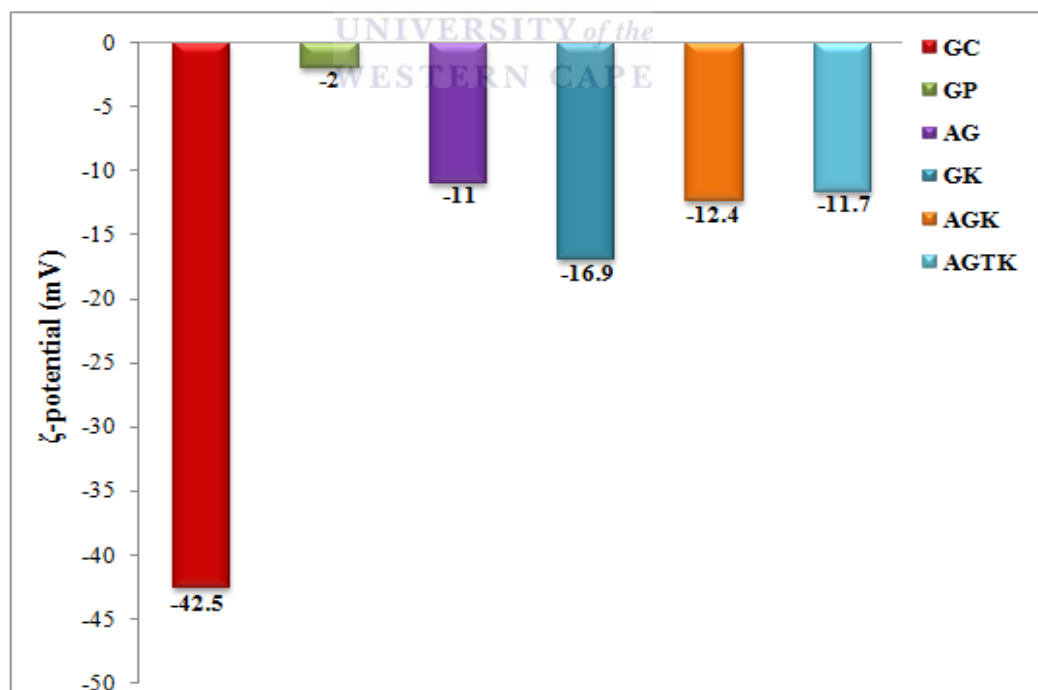


Figure 4.7: ζ -potential of the AuNPs determined using Malvern Zetasizer as a measure of AuNP stability and charge. GC = citrate coated NPs, GP = PEGylated NPs, AG = targeted GP, GK = AuNPs with therapeutic peptide, AGK = has both targeting and therapeutic peptides, AGTK = has PTD, targeting and therapeutic peptides.

The molecules attached on the AuNPs reduced their ζ -potential when compared to the citrate coated AuNPs (GC) which are strongly anionic. GP has highest ζ -potential compared to the other AuNPs, the value has significantly been reduced from -42.5 mV for GC, and this is attributed to the PEG polymer attached to GP. PEG polymer is hydrophilic (Veronese and Pasut, 2005) and have been used to passivate the GP particles and made them to have a neutral charge. The other AuNPs with targeting and pro-apoptotic peptides became moderately negatively charged compared to GC and GP. This is due to the change in PEG ratio and addition of the pro-apoptotic peptide. This can be attributed to the large number of positively charged lysine residues in the peptide.

4.2.3 Quantification of AuNPs and conjugates by ICP-OES

The concentrations of the AuNP conjugates were determined using UV-Vis data through the equation described by Haiss *et al.*, (2007). The stock concentration for all AuNP conjugates was 20 nM. ICP-OES was used to verify if these AuNPs contained the same number of Au metal at the same concentration. Equal amount of the AuNPs (as described in section 2.3.5.3) was digested with aqua-regia and Au metal quantified by ICP-OES.

ICP-OES is an analytical technique used to detect trace element in suspensions from concentration as low as 1 part per trillion. The elements are first ionized by acid bath in oxidizing acids (HCl and HNO₃). The metal concentration is determined by running the samples with a known concentration of the target analyte, in this case TraceSELECT[®] gold was used as a standard.

Figure 4.8 indicates the number of detectable Au atoms in the AuNP conjugates. The highest amount of Au metal was detected on citrate coated AuNPs (GC) at 10.42 ppm,

followed by pegylated AuNPs (GP) at 5.77 ppm when compared to the other AuNP-conjugated with either targeting (A) and/ or therapeutic (K) peptides that was lower than 3.15 ppm.

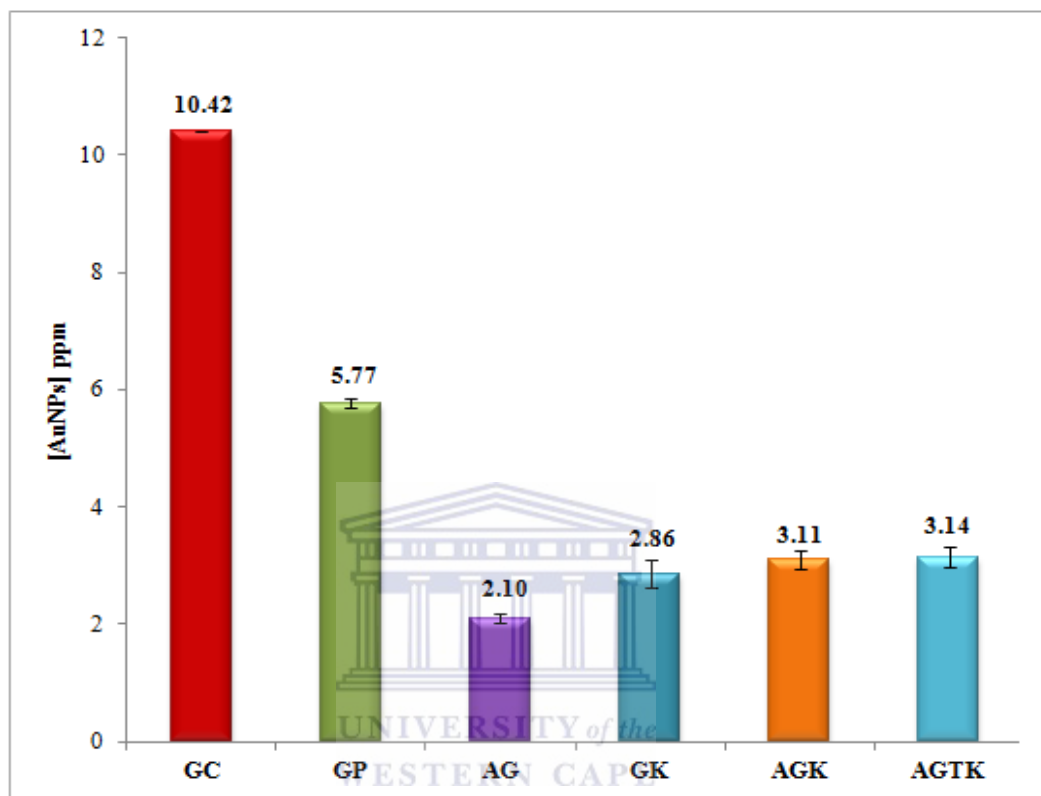


Figure 4.8: Quantification of AuNPs by ICP-OES. To determine the amount of gold present in each sample, the samples were diluted 1:10 in dH₂O. Elemental analysis was carried out by ICP-OES. GC = citrate coated AuNPs, GP = PEGylated AuNPs, AG = targeted GP, GK = AuNPs with therapeutic peptide, AGK = has both targeting and therapeutic peptides, AGTK = has PTD, targeting and therapeutic peptides.

The variations in the quantity of gold detected is due to the biomolecules attached to the surface of the AuNPs, further confirming that the targeting and the pro-apoptotic peptides were successfully conjugated to the NPs. The ICP-OES data suggested that in order to correct the variability in the concentration of the AuNPs, the following ratios had to be used per 1part of GC: 1.8 GP, 4.96 AG, 3.64 GK, 3.35 AGK and 3.32 AGTK.

4.2.4 Therapeutic potential of targeted nanotherapy

Biochemical assays were used to determine the therapeutic potential of PHB-targeted nanotherapy on the model cell line (Caco-2 cell line). The WST-1 assay was used to monitor cell viability, CM-H₂DCFDA probe to quantify ROS generation and the APOPercentage™ Apoptosis assay to determine possible apoptotic cell death induced by exposure of cells to various AuNP conjugates.

The citrated coated AuNPs (GC) and the pegylated AuNPs (GP) have neither a targeting nor a therapeutic peptide, therefore these AuNPs are not expected to be taken up by the cells or cause cell death. The GP particles have PEG as a stabilizing agent, PEG is known for its passivation properties (Roberts *et al.*, 2002; Ryan *et al.*, 2008). AG is made of GP and has a targeting peptide that recognises the PHB receptor. These AuNPs will be taken up by the cells but is not expected to be toxic due to the presence of PEG on their surface. GK have a therapeutic peptide but since they did not have a targeting peptide, these AuNPs is expected not to be taken up by cells or cause cell death. The therapeutic or pro-apoptotic peptide attached to it, shall only have an effect when internalized by the cells (Ellerby *et al.*, 1999). AGK and AGTK have both the targeting and therapeutic peptides attached to the AuNPs. These AuNPs are expected to bind to the PHB receptor on the Caco-2 cells and be internalized by the cells. Once internalized, the therapeutic peptide is expected to disrupt the mitochondrial membrane causing cytochrome c release and caspase activation that will trigger cell death by apoptosis. The only difference between the two AuNPs, is that AGTK has an additional PTD (TAT) which is expected to enhance the uptake of AGTK and increase its therapeutic efficacy compared to AGK.

4.2.4.1 Effect of AuNP conjugates on Caco-2 cell viability: WST-1 assay

To determine if the NPs exhibited cytotoxic effects on the Caco-2 cell line, the cells were exposed to increasing concentrations of various AuNP conjugates for 24 hours. Cell viability was measured using the WST-1 cell proliferation assay, a colorimetric assay used to measure metabolic activity of cells. The assay relies on the conversion of the tetrazolium salt (WST-1) through the action of mitochondrial dehydrogenase into a yellow coloured product that is measurable by spectrophotometer at 440nm. The colour change is directly proportional to the amount of mitochondrial dehydrogenase in a sample reflective of live cells.

Figure 4.9 compares the cell viability of cells treated with the various AuNPs against untreated cells. The viability of cells after exposure to AuNPs decreased, especially at high concentrations (2-8 nM) for all AuNPs used except GP. GP showed negligible response even at 8nM. Increased cytotoxicity was observed in the cells treated with AuNPs that contained the therapeutic and/ or targeting peptide in a dose dependent manner. The viability assay indicated a significant cytotoxicity in cells that were treated with AG, GK, AGK and AGTK. At the highest concentration (8 nM), the targeted AuNPs reduced the viability to less than 30% with respect to the control. No significant difference was observed in cells treated with GP at all tested concentrations.

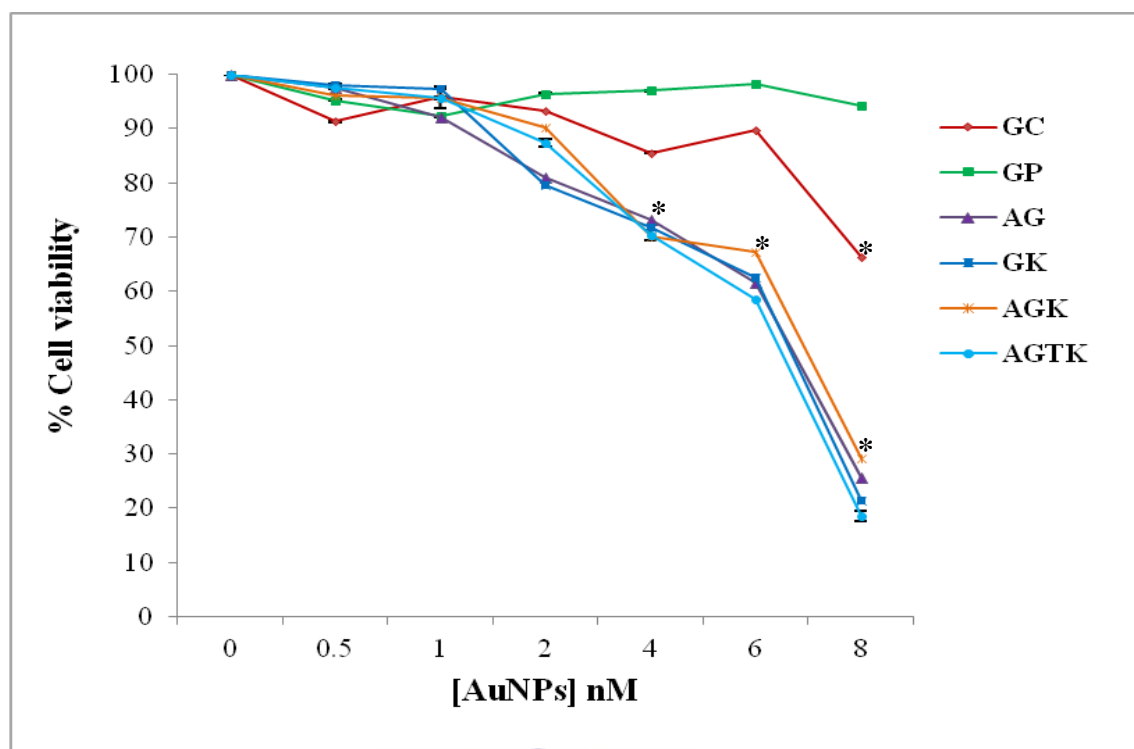


Figure 4.9: Viability and proliferation of Caco-2 cells after 24 h exposure to various AuNPs. The cells were exposed to different amounts of nanoparticles ranging from 0.5 to 8 nM. Cell viability was measured by the WST-1 proliferation assay. The result represents the mean \pm standard deviation of two independent experiments, each performed in triplicates. GC = citrate coated NPs, GP = PEGylated NPs, AG = targeted GP, GK = NPs with therapeutic peptide, AGK = has both targeting and therapeutic peptides, AGTK = has PTD, targeting and therapeutic peptides. A two-tailed, unpaired t-test was used to analyse significance. * $p < 0.05$, significant difference compared to untreated sample.

Surprisingly, the targeted-PEGylated AuNPs (AG) and the untargeted NPs with the therapeutic peptide (GK) were shown to be toxic to the Caco-2 cells. This suggests that the GK AuNPs were able to be taken up by the cells and cause cell death. AG was expected to behave in a similar manner as GP whether internalized or not since they have a protective layer (PEG) on the surface. The interference test was performed to determine whether AuNPs interferes with the WST-1 formazan reaction product by incubating 8nM AuNPs with the dye reagent. No interference was observed for all six AuNPs used (data not shown). The concentration that caused 50% (IC_{50}) cell death was determined by GraphPad[®] Prism 6 for all AuNPs, IC_{50} values are shown in Table 4.1.

IC₅₀ values for GC and GP was higher than 8 nM, 6.17 nM for AG, 6.23 nM for GK, 6.23 nM for AGK and 6.13 nM for AGTK.

Table 4.1: The IC₅₀ values of various AuNP conjugates after their exposure to Caco-2 cells.

Cell line	IC ₅₀ (nM)
GC	>8
GP	>8
AG	6.17
GK	6.23
AGK	6.23
AGTK	6.13

4.2.4.2 Cellular uptake of AuNPs by Caco-2 cells as determined by ICP-OES

To quantify AuNP uptake, elemental analysis was carried out by ICP-OES to determine the amount of the metals that were taken up by the cells. After 24 hours of treatment with 5 nM of differently functionalized AuNPs, the cells were lysed by aqua regia and analysed for gold uptake by ICP-OES as described in section 2.3.6.2a). The amount of gold detected from each sample was equivalent to the amount of AuNP taken up by the cells. Figure 4.10 shows the percentage uptake of AuNPs by cells, as a function of the initial amount applied.

The GC AuNPs were taken up more by the cells compared to the other nanoparticles which showed a very small amount of AuNPs compared to the initial amount applied (less than 10%). At 65%, the overall amount of gold taken up by the cells treated with citrate coated AuNPs (GC) was significantly higher than the cells treated with the other AuNP conjugates. This was unexpected since the ζ -potential (Figure 4.7) showed that the GC NPs are highly negatively charged. Since these NPs have a similar charge as the

lipid bilayer, the two are supposed to repel each other. This was further investigated by TEM to determine the localization of the AuNPs.

For the bio-conjugated AuNPs, AG has highest uptake at 8.01% compared to the other targeted NPs. AGK and AGTK uptake was 4.91 % and 3.83 %, respectively. GK uptake was comparable to AGK at 4.97. GK has no targeting peptide and was not expected to be taken up as much as the NPs containing targeting peptide (AG, AGK and AGTK).

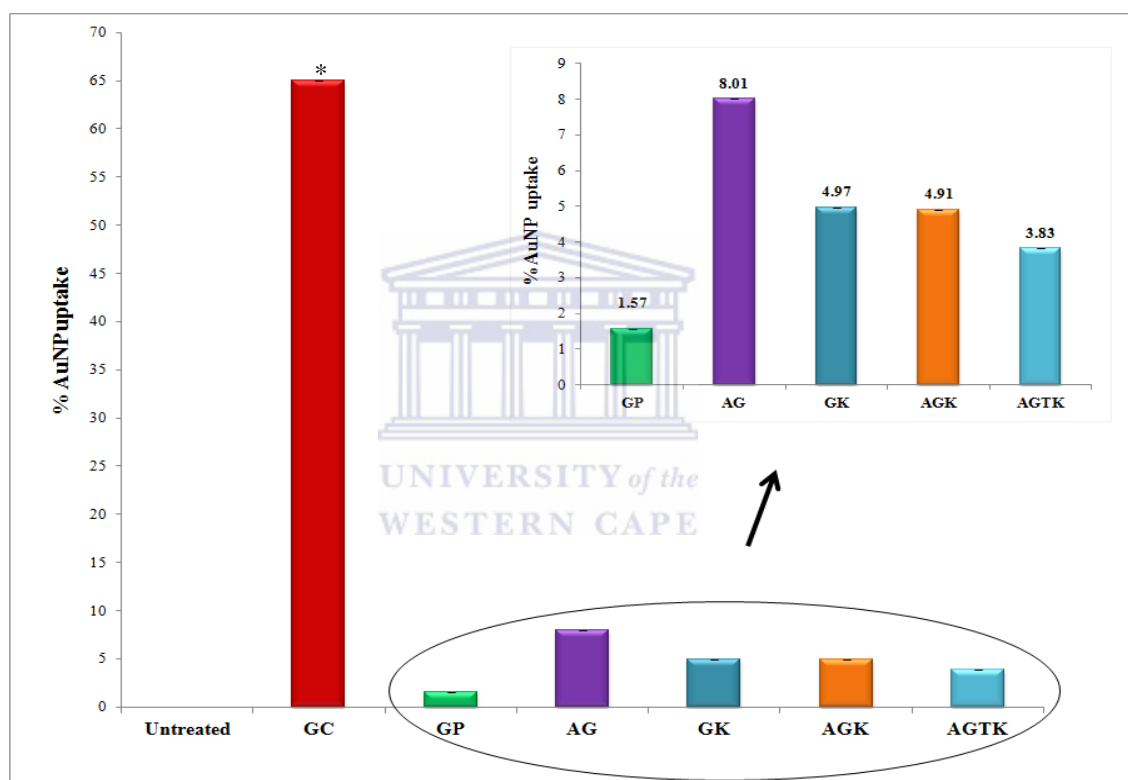


Figure 4.10: Quantification of internalized AuNPs in Caco-2 cells by ICP-OES. The cells were incubated with 5 nM of nanomaterials at 37°C for 24 hours. Cells were washed, lysed in aqua regia (3:1 hydrochloric acid: nitric acid) and analysed for gold concentration by ICP-OES. The percentage of nanoparticles taken up by the cells was determined as a function of the total amount of AuNPs applied. GC = citrate coated AuNPs, GP = PEGylated NPs, AG = targeted GP, GK = AuNPs with therapeutic peptide, AGK = has both targeting and therapeutic peptides, AGTK = has PTD, targeting and therapeutic peptides.

4.2.4.3 Intracellular localization of AuNPs by TEM

The cellular uptake and localization of nanomaterials was investigated by incubating the cells with 5 nM concentration of GC, AGK and AGTK for 24 hours. Untreated cells were used as a control. Intracellular localization of NPs was analysed by TEM. The TEM micrographs (Figure 4.11) demonstrated that the internalized GC NPs were located in the cytoplasm (red arrows) and cell membrane surfaces (green arrows) with no signs of cytotoxicity. Some AGK nanoparticles were detected in the cytoplasm and some bound on the cell surfaces. However, no AuNPs were detected in the cytoplasm or in other cellular compartments, such as nuclei or mitochondria for the cells treated with AGTK.

In addition to the intracellular localization of the AuNPs, the TEM analyses showed that cell exposure to GC did not alter the cell morphology of the cells when compared to cells treated with AGK and AGTK. Cells exposed to GC still retained the elongated shape seen in untreated cells. When compared to the untreated cells, the morphology of the cells treated with AGK and AGTK had been altered. Their nuclear shape and size were altered.

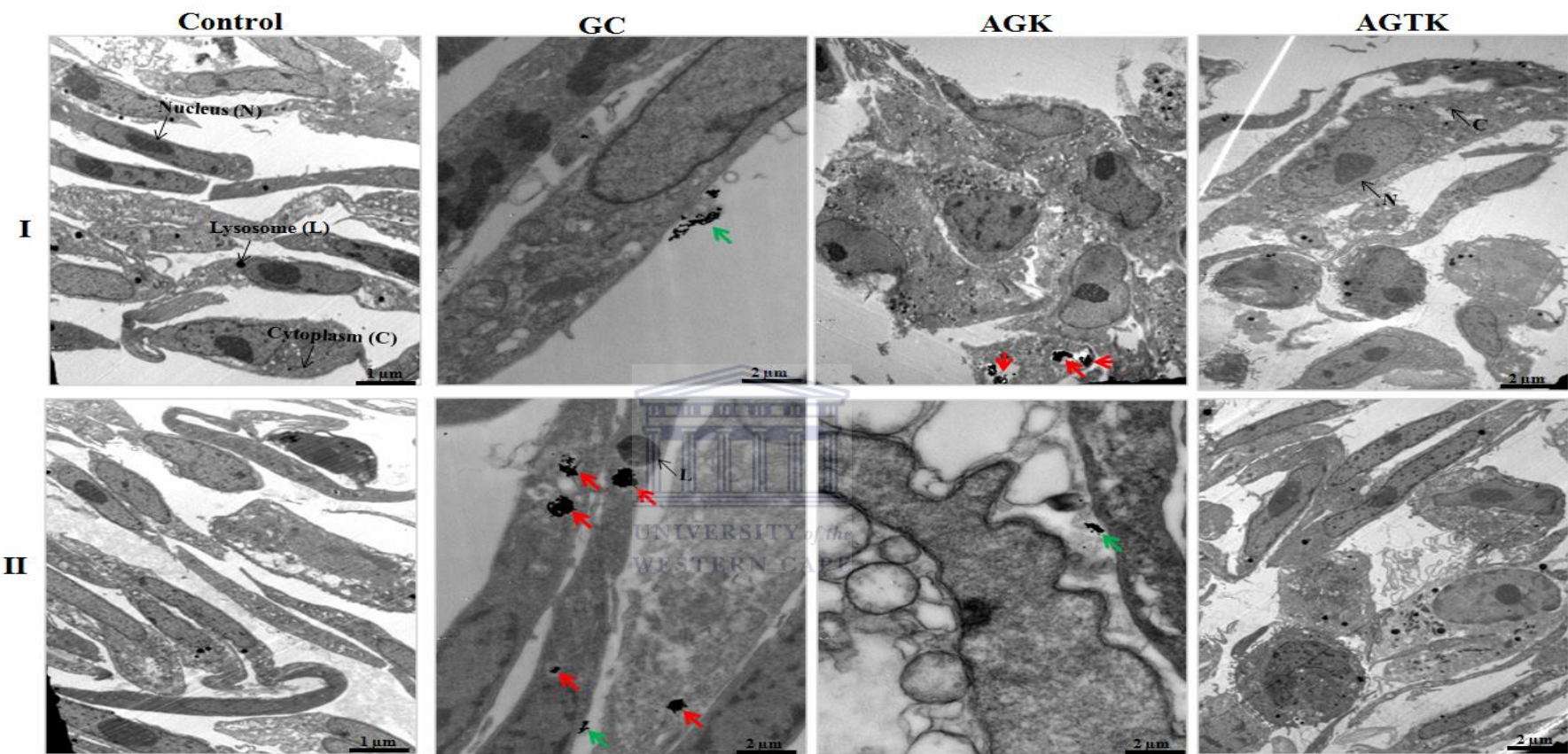


Figure 4.11: Localization of AuNPs in Caco-2 cells analysed by TEM. Cells were incubated with 5nM AuNPs for 24 hours. After exposure, cells were fixed with 4% paraformaldehyde and stored in 2.5% glutaraldehyde until further analysis. AuNP uptake was examined by TEM. The red arrows points at AuNPs localised within the cytoplasm and green arrows indicate the AuNPs on the cell surface. I and II represents micrographs treated with same NPs from different grids. GC = citrate coated AuNPs, AGK = has both targeting and therapeutic peptides, AGTK = has TAT, targeting and therapeutic peptides. N - nucleus, L – lysosome.

4.2.5 Investigation into the mode of cell death induced by AuNPs conjugates

The cytotoxicity and mode of cell death induced by various AuNP conjugates (GC, GP, GK, AG, AGK and AGTK) were further investigated by cell biology and biochemical assays.

4.2.5.1 Cellular morphological changes induced by AuNPs in Caco-2 cells

Once the AuNPs reach their target, the cell membrane is the first barrier that the AuNPs come into contact with. The interaction between the AuNPs and the cell membrane can affect intracellular biochemical events and induce toxicity that can be detected by morphological changes through light microscopy. Any disturbances in the phospholipids bilayer compromises the integrity of the cell and serve as an indication of altered cellular functions. Typical cellular features of Caco-2 cells are shown in untreated cells in Figure 4.12. Caco-2 cells grow and differentiate into monolayers characterized by elongated shape that resemble the small intestinal epithelium structurally and functionally under microscopy (Herold *et al.*, 1994). No morphological changes were observed in cells treated with GC and AG. The cell density and shape was similar to untreated cells. The same was observed in cells treated with GP (data not shown).

Cells treated with GC, AG and GK had the same cell density as the untreated control cells, while cells treated with AGK and AGTK had reduced cell density. The shape and size of cells treated with GK, AGK and AGTK was also different in comparison to the untreated cells. Cells treated with GK displayed vacuoles which were not observed in any of the other treatments. The formation of “holes” may be induced by the presence of $D(KLAKLAK)_2$ peptide on the surface of AuNPs, that could influence the interaction of

the NPs with the lipid bilayer and result in unexpected toxicity shown in Figure 4.9. Although the results for cells treated with GP is not shown, these NP had the same effect as GC and AG.

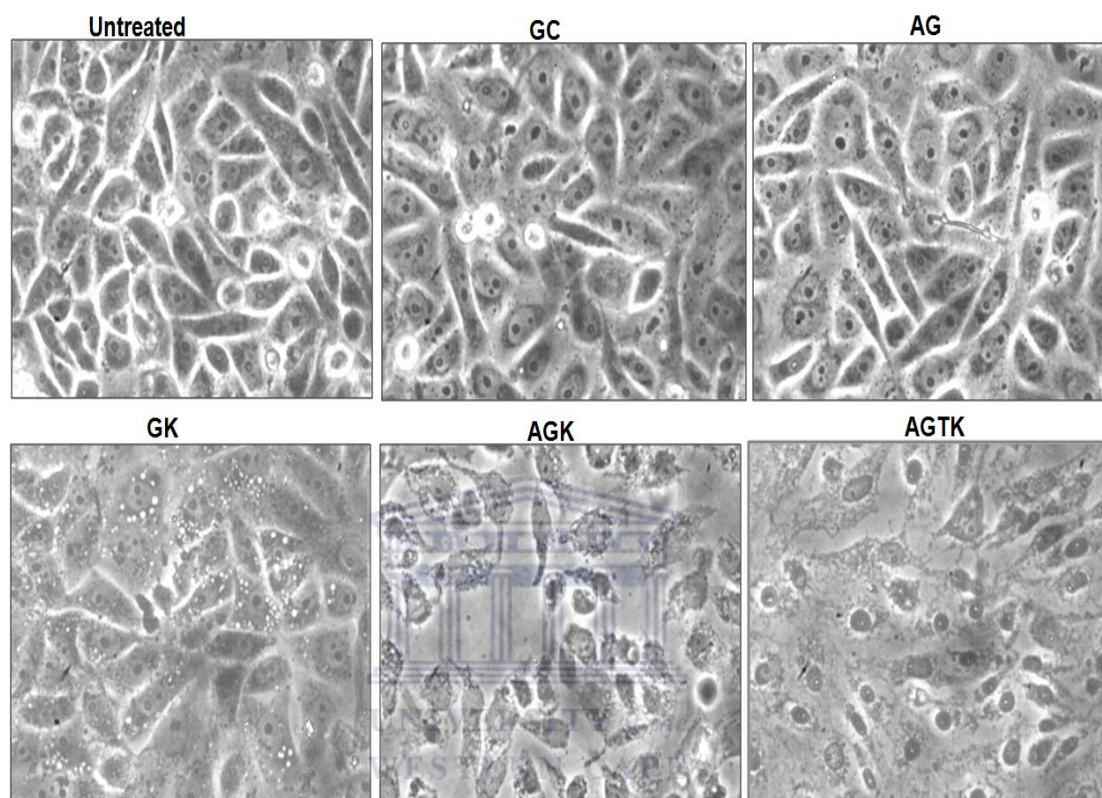


Figure 4.12: Light microscopy depicting cell morphology after the Caco-2 cells were exposed to various AuNPs for 24 hours. The cells were grown in a 12 well plate and treated with IC_{50} of the AuNP conjugates, the cellular morphology were viewed under light microscope at 20X magnification and captured by the Leica camera. GC = citrate coated AuNPs, AG = targeted GP, GK = AuNPs with therapeutic peptide, AGK = has both targeting and therapeutic peptides, AGTK = has TAT, targeting and therapeutic peptides.

4.2.5.2 Detection of intracellular oxidative stress induced by AuNP conjugates

Mitochondrial dysfunction in cells seals the fate of the cell. The effect of the AuNP conjugates on mitochondrial function and oxidative stress was assessed to determine the health status of the cells. The amount of ROS within the cells was examined to determine whether the AuNPs induce the cellular oxidative stress. The CM- H_2DCFDA

probe was used to detect and quantify the intracellular ROS produced by the cells. CM-H₂DCFDA is a nonfluorescent ROS indicator that is oxidized to 2',7'-dichlorofluorescein (DCF) in the presence of ROS. CM-H₂DCFDA is a cell permeable fluorogenic probe that can be used to assess oxidative stress in cultured cells (Wu and Yotnda, 2011). This probe detects ROS such as hydroxyl, peroxy, nitric oxide, oxide anion, peroxynitrite, hydrochlorous acid and hydroxyl radical species within the cell. When the CM-H₂DCFDA probe is taken up by the cells, the cellular esterases deacetylate the probe to a non-fluorescent compound that is later oxidized by ROS into highly fluorescent compound, DCF. The fluorescence correlates to the amount of ROS generated in the cells, and can be detected and quantified by flow cytometry.

The intracellular ROS levels were examined in Caco-2 cells treated with different AuNPs by flow cytometric analysis as described in section 2.3.6.3d). Figure 4.12 shows the level of ROS activity induced by exposing the cells to various AuNP conjugates (GC, GP, GK, AGK and AGTK). An increase in cell fluorescence was an indication of ROS production in the cells. The untreated cells and cells treated with cisplatin were used as controls. Cells treated with AGTK showed higher ROS levels compared to other AuNPs tested. Untargeted AuNPs (GP) had a negligible effect on cellular levels of ROS as indicated in Figures 4.13 when compared to untreated cells. The increased ROS levels in cells treated with cisplatin GC, GK, AGK and AGTK were statistical significant. The findings could suggest that the cytotoxicity induced by the AuNPs is somehow mediated through the induction of increased levels of oxidative stress through the effects of ROS production within the cell.

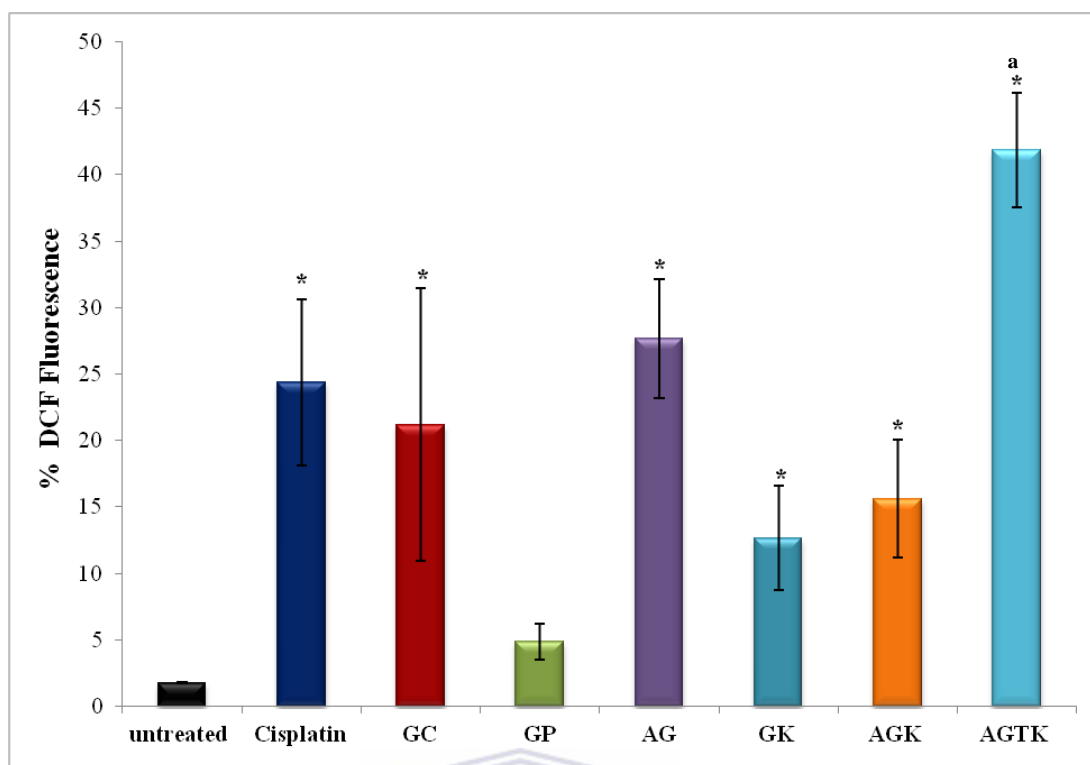


Figure 4.13: ROS activity in response to AuNPs treatment. Cells were treated with various AuNPs for 24 hours and ROS levels were assessed by incubating the cells with 10 μ M CM-H₂DCFDA at 37 °C for 30 min. The fluorescence staining was analysed with the Attune flow cytometer. For each sample 10 000 events were recorded. GC = citrate coated AuNPs, GP = PEGylated AuNPs, AG = targeted GP, GK = AuNPs with therapeutic peptide, AGK = has both targeting and therapeutic peptides, AGTK = has PTD, targeting and therapeutic peptides. A two-tailed, unpaired t-test was used to analyse significance. *p<0.05, significant difference compared to untreated sample, a = p<0.05 AGTK significantly different compared to other AuNP conjugates.

4.3 Discussion

The application of nanotechnology in medicine is looking very promising, in particular for development of effective therapies for chronic diseases; bringing about the exciting era of nanomedicine. Nanomaterials have physico-chemical properties that make them useful in therapeutics, diagnostics and drug targeting when conjugated to biomolecules (Provenzale and Silva, 2009; Lysik and Wu-Pong, 2003). Several drugs based on nanotechnology are currently undergoing clinically trials for targeted treatment of

cancer. Of interest to this study, are human trials conducted using gold nanoparticle formulations as drug delivery vehicles in photothermal therapy (Libutti *et al.*, 2010; ClinicalTrials.gov numbers; NCT00356980, NCT00436410 and, NCT00848042). The field has grown since and has potential to revolutionize medicine, advancing the treatment and diagnosis of chronic diseases. However, applications of NPs in therapeutics are limited by their possible toxicity. The unique physico-chemical properties of NPs not only increase their usefulness in biomedical applications, but their ability to interact with biological systems can also increase their cytotoxicity. It is essential that the toxicity of the NPs be tested in pre-clinical studies before they can be considered for human trials (Caruthers *et al.*, 2007).

The goal of the present chapter was to develop a PHB-targeted nanotherapy and examine the effects of targeted and untargeted AuNPs on the viability of human Caco-2 cells. This cell line was chosen because it expresses PHB as a cell surface receptor that can bind to the PHB-targeting peptide (AHP) as shown in Figure 3.13. The AuNPs were produced by reduction of HAuCl₄ adapted from Turkevich *et al* (1951). AuNPs were characterized by UV-Vis spectroscopy (Figure 4.5) and TEM analysis (Figure 4.6). A shift in the peak position of the AuNP's SPR with respect to citrate capped AuNPs was used as an indicator for successfully capping of the AuNP surfaces with the peptide molecules as shown in Figure 4.5.

The potential cytotoxicity of the AuNP conjugates and their uptake was studied using cell biology and biochemical assays in *in vitro* studies. The cytotoxicity and effect of the AuNP conjugates on cell viability was evaluated on the Caco-2 cell line using the WST-1 assay. The viability of cells treated with GP was higher than 90% at all the concentrations tested as shown in Figure 4.9. Higher concentrations (2 -8 nM) of GK

and AG unexpectedly negatively influenced the cell viability. GK does not have a targeting peptide and was therefore not expected to be taken up by cells and have toxic effects. AG has a targeting peptide and expected to be taken up by the cells but not have toxic effects. The cell death induced by GK, AG, AGK and AGTK was dose-dependent. Both AGK and AGTK have both the targeting and therapeutic peptides and when taken up and internalized by the cells, these AuNPs were expected to cause cell death. AGTK was expected to have more pronounced effect on cell viability than AGK since it has TAT that is expected to enhance its uptake and therapeutic activity. However, Table 4.1 shows no significant difference in the activity induced by AGTK compared to AG, GK and AGK. Judging from these data, both the targeted and untargeted particles (including the negative controls) had a comparable response at the same concentrations (Figure 4.9).

The amount of internalized AuNPs in Caco-2 cells was quantified and compared using ICP-OES to determine the relationship between cytotoxicity and the amount of AuNPs taken up by the cells. ICP-OES is a more sensitive and accurate method to quantify small amounts of metals in samples. It can detect differences in the gold concentrations of the order of parts per billion. Again, the internalization of AuNPs was lower for the targeted AuNP conjugates compared to GC (Figure 4.10). TEM analysis was conducted to confirm localization of the GC, AGK and AGTK in Caco-2 cells. The cells were incubated for 24 h with the mentioned AuNPs. TEM images (Figure 4.11) showed that GC internalization was higher than that of peptide-AuNP conjugates. GC NPs were localized in the cytoplasm but also on the cell membrane. Lower numbers of AuNPs were observed in cells treated with AGK and no AuNPs were detected in cells treated with AGTK. Conjugating targeting peptides to the NPs were expected to improve the ability of the AuNPs to target and enter into cells expressing PHB. This is expected to

allow higher concentrations of therapeutic particles to accumulate in cells expressing PHB and enhance cytotoxicity within these cells. This may explain why so few particles were detected in cells treated with AGK and AGTK. Cells taking up these AuNPs (i.e. AGK and AGTK) are expected to die, as such the contents in dead cells might not be recoverable.

The TEM data confirmed the ICP-OES results, by showing that GC particles were taken up more readily than AGK and AGTK. Although the PHB-targeted nanotherapies (AGK and AGTK) proved to be toxic (Figure 4.9), the peptides were considered unsuccessful due to their lack of selectivity when compared to the other AuNP conjugates. Their activity was hardly convincing because their biological response in Caco-2 cells was comparable to GK and AG. Certain parameters in the design of the AuNPs were suspected to influence the AuNP uptake and their cellular toxicity, such as the inability of the $D(KLAKLAK)_2$ to detach from the NPs once internalized. These parameters were changed in the design of the modified PHB-targeted nanotherapy as described in the next chapter.

Chapter 5: Conjugation of modified D(KLAKLAK) to AuNPs for development of the ideal PHB-targeted nanotherapy

5.1 Introduction

The PHB-targeted nanotherapy developed in Chapter 4 did not perform to expectations, although it showed some desirable traits (e.g. toxicity towards the model cell line, Figures 4.9) the response was questionable as it was similar to the negative controls. The drawbacks were addressed by changing the design of the AuNPs in order to improve its specificity and sensitivity as discussed below.

Drug specificity and sensitivity is crucial in development of treatment for chronic diseases, and yet proves to be a major challenge that delays the progress in developing disease specific therapies. Available drugs are either wrong for the specified disease, used at a very low dose to effectively reverse the condition or highly toxic to unaffected tissues to give it enough time to completely cure the affected areas. Although the drugs have beneficial health effects, their side effects outweigh their usefulness (William, 2010). These drawbacks can be easily avoided through the use of targeted nanotherapy which is not without challenges, discussed in Chapter 4.

Development of nanotherapy with precise biological activities in target cells has potential in treatment of chronic diseases. The strategy of using bifunctional AuNPs could increase the specificity and binding capacity of the therapy and confer the therapeutic effect only on the target cells. The success of the described targeted therapy could facilitate the development of precision medicine, diagnostics, that can

differentiate distinct cellular states and target specified cell types and spare the surrounding cells.

5.2 Results

5.2.1 Analysis of TAT-D(KLAKLAK)₂ biological activity on cancer cells

The pro-apoptotic D(KLAKLAK)₂-DEVD-SH peptide was obtained from Dr Maya Makatini (Advanced Materials Division, Mintek). The synthesis was done via N-fluorenyl-9-methoxycarbonyl (Fmoc) standard solid phase peptide synthesis using D-amino acids. Caspase 3 cleavage site (DEVD) was incorporated between the thiol group and the therapeutic peptide to allow separation of the pro-apoptotic peptide from the AuNPs once internalized by the cells.

To test the antiproliferative activity of the redesigned peptide [D(KLAKLAK)₂-DEVD-SH] *in vitro*, this pro-apoptotic peptide was synthesized with a PTD (TAT) on the N-terminus of the peptide to facilitate entry into cells. The activity of TAT-D(KLAKLAK)₂-DEVD-SH was tested on a panel of cancer cell lines which included: Caco-2, HT-29 and MCF-7. The cell lines were treated with increasing concentrations (0-250 µg/ml) of the fusion peptide for 24 hours. The viability of the cells was investigated using the WST-1 assay. A dose response activity was observed in all 3 cancer cell lines as shown in Figure 5.1. The peptide was significantly toxic to all 3 cell lines at all doses tested. At concentrations of 100- 250 µg/ml, the peptide had killed more than 70% of the cells.

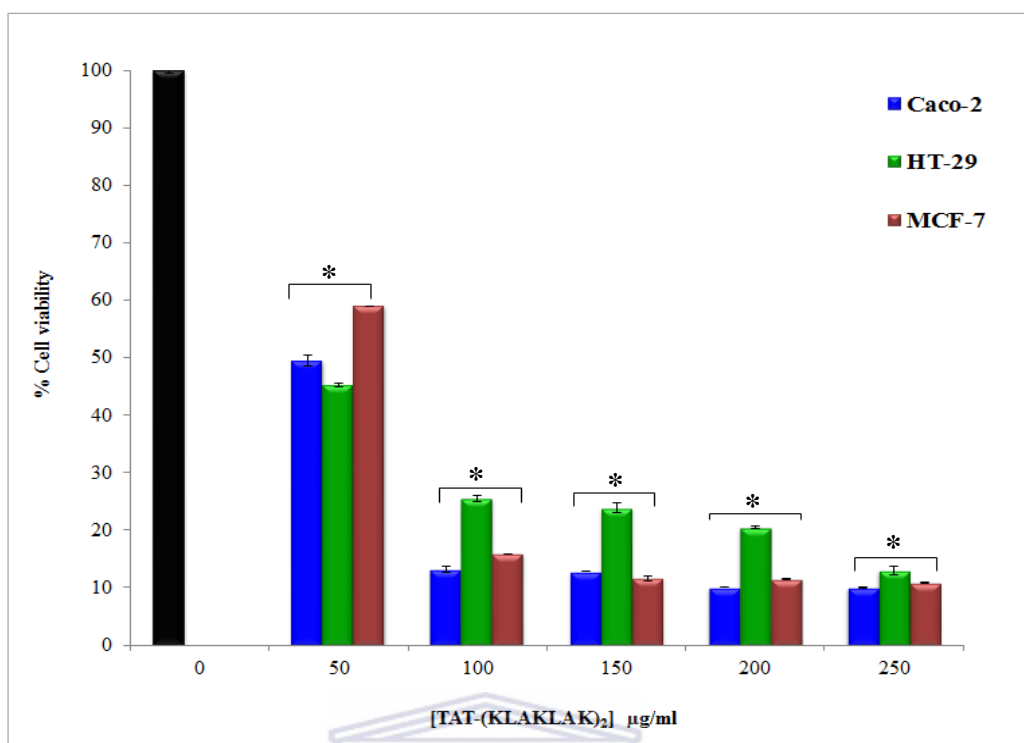


Figure 5.1: Anti-proliferative activity of TAT-_D(KLAKLAK)₂-DEVD-SH on colon and breast cancer cells. The cells were treated with increasing concentrations of TAT-_D(KLAKLAK)₂-DEVD-SH and cell viability was assessed using the WST-1 assay. Data is presented as mean ±SEM estimated using one way ANOVA test and Student Ttest. *P<0.05 indicates statistical significance when compared to untreated.

The activity of synthetic TAT-_D(KLAKLAK)₂-DEVD-SH was high at the very low concentration as shown in Figure 5.1. The highest potency of TAT-_D(KLAKLAK)₂-DEVD-SH was observed in Caco-2 cells (30.8 µg/ml) followed by MCF-7 (37.1 µg/ml) cells then HT-29 cells (41.7 µg/ml) as shown in Table 5.1.

Table 5.1: IC₅₀ values for TAT-_D(KLAKLAK)₂ on cancer cell lines.

Cell line	IC ₅₀ (µg/ml)
Caco-2	30.8
HT-29	41.7
MCF-7	37.1

The major problem concerning the use PTDs for delivery is their lack of selectivity to target a specific cell type. Figure 5.1 shows that the TAT-_D(KLAKLAK)₂-DEVD-SH peptide was toxic to the colon (HT 29 and Caco-2) and breast (MCF-7) cancer cell lines. Although, the capacity of PTDs to deliver a bioactive molecule to cells has opened avenues for intracellular targeting, specificity is required for *in vivo* targeting. This can be achieved by using targeting peptides such as AHP that home to specific cell receptors. In this study, a PHB-targeted nanotherapy was developed by replacing TAT with AHP targeting peptide to increase the selectivity of the therapeutic peptide as described in section 5.2.2.

5.2.2 Development and analysis of anti-proliferative activity of the AuNP-conjugates

5.2.2.1 Design of the AuNP-conjugates

The targeting (AHP) and pro-apoptotic [_D(KLAKLAK)₂-DEVD-SH] peptides were synthesized via Fmoc as described in 5.2.1. AuNP conjugates were synthesized and functionalized for biological application by Dr Frankline Keter (Advanced Materials Division, Mintek) following the methodology described in section 4.2.2. The design together with the acronyms used for the AuNP conjugates is illustrated in Figure 5.2. A in the acronyms signifies the targeting peptide, G –gold nanoparticles, D –DEVD a caspase 3 cleavage site, N- non-targeting peptide (scrambled version of A), K- therapeutic or pro-apoptotic peptide and S- scrambled peptide with no known biological activity.

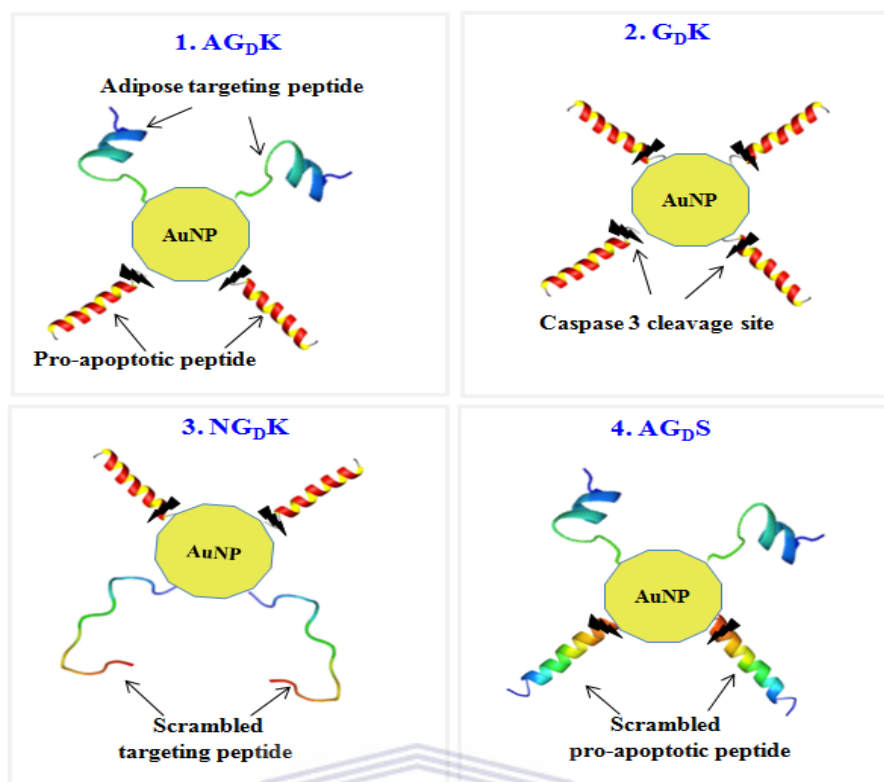


Figure 5.2: Schematic diagram of the AuNP design. AG_DK = AuNPs with targeting and therapeutic peptides (PHB-targeted nanotherapy), G_DK = untargeted AuNPs with therapeutic peptide, NG_DK = AuNPs with scrambled targeting and therapeutic peptides, AG_DS = targeted AuNPs with scrambled peptide.

AG_DK is the experimental PHB-targeted nanotherapy, containing both the PHB targeting and the pro-apoptotic peptides. Once taken up by the cells that express PHB, the pro-apoptotic peptide [D(KLAKLAK)₂-DEVD-SH] will disrupt the mitochondrial membrane resulting in cleavage of D(KLAKLAK)₂ by caspase 3 and induce cell death by apoptosis. AG_DK is the only AuNP expected to kill the cells, the other AuNPs (GC, G_DK, NG_DK, AG and AG_DS) were used as a negative controls. GC has neither the targeting nor therapeutic peptide, as such the AuNPs were not expected to be taken up by the cells or affect their cell viability. The AG and AG_DS have a targeting peptide and when taken up by the cells are not expected to have any toxicity towards the cells since it does not have a pro-apoptotic peptide. G_DK and NG_DK AuNPs are also not expected

to be toxic since they did not have the targeting peptide and are therefore not expected to be taken up by the cells.

5.2.2.2 Characterization of AuNPs and conjugates

The physico-chemical properties of the AuNP conjugates were characterized as in Chapter 4 using UV-Vis, TEM and ζ -potential. The optical properties of the AuNPs after attaching the biomolecules were compared to the citrate coated AuNPs (GC). A red shift in the maximum absorption peak of GC (523 nm) was observed in the AuNPs that contained the bio-active molecules (Table 5.2). The shift in the absorption spectra signifies a modification of the surface of the AuNPs.

Table 5.2: AuNP optical properties.

AuNPs and conjugates	λ_{\max} (nm)	Absorbance at λ_{\max}
GC	523	0.9
AG	523	1.0
AG _D S	526	1.2
G _D K	528	1.1
NG _D K	524	0.9
AG _D K	524	0.8

TEM analysis was conducted to determine the size distribution and shape of the AuNP conjugates. All the AuNPs still retained the average size of 14 nm. The TEM micrographs in Figure 5.3 show that the nanoparticles were mostly spherical in shape with few irregular or triangular shaped NPs. They were all mono dispersed with no sign of aggregation or clumping.

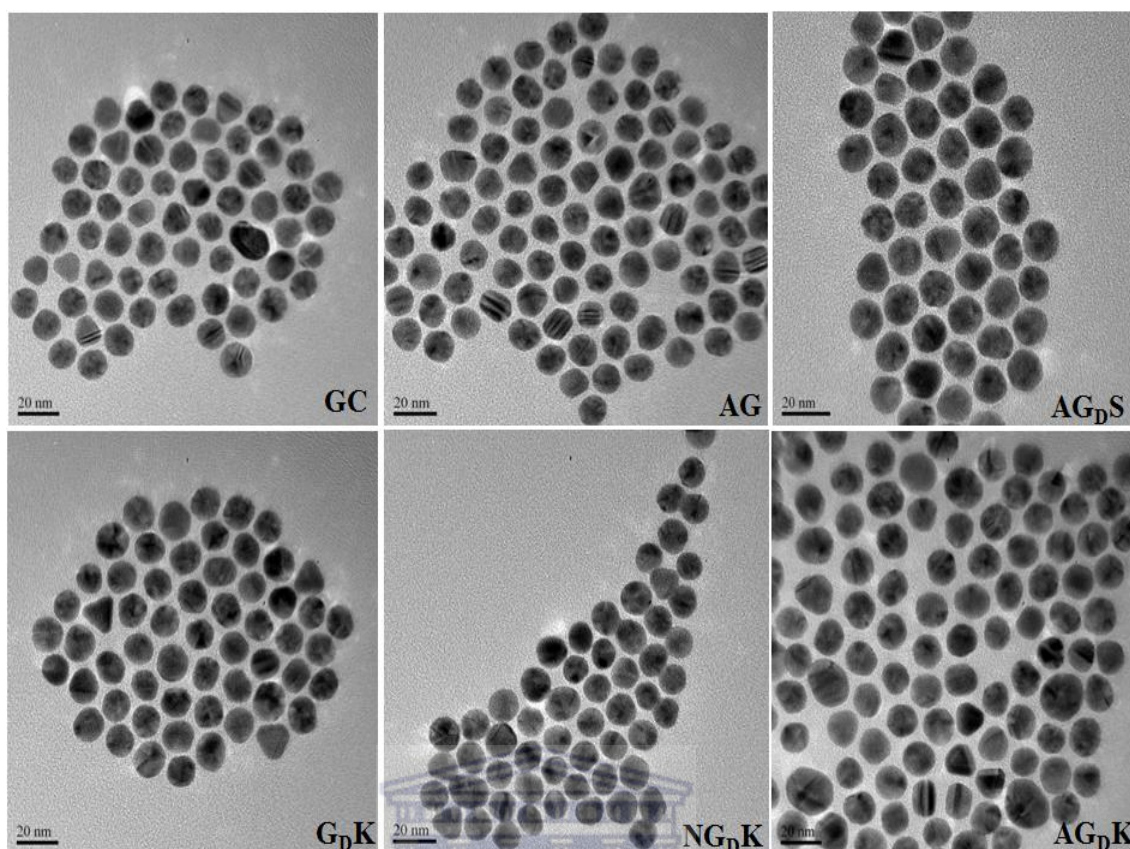


Figure 5.3: Representative TEM micrographs of the AuNP conjugates. GC = citrate coated AuNPs, AG = targeted PEGylated AuNPs, AG_DS = targeted AuNPs with scrambled peptide, G_DK = untargeted AuNPs with therapeutic peptide, NG_DK = AuNPs with scrambled targeting and therapeutic peptides, AG_DK = AuNPs with targeting and therapeutic peptides (PHB-targeted nanotherapy). Scale bars in the micrographs are used to represent magnification of AuNPs.

The surface charge of the AuNP conjugates was measured using ζ -potential to determine the electrokinetic potential of the colloidal NPs. The variation in ζ -potential among the AuNPs samples is shown in Figure 5.4. GC had lowest value of -35.9 mV. The values increased after bio-conjugation of targeting and therapeutic peptides. Of all the synthesized AuNPs, NG_DK had the highest ζ -potential at -3.7 mV followed by AG (-5.8 mV), GK (-12.7 mV), AG_DK (-13.2mV) and AG_DS (-15.9 mV). The changes in the charge are attributable to molecules attached to the AuNP surface and indicate modification of the AuNP surfaces. This is a physical property which is exhibited by any particle in a suspension which can be used to predict how these AuNPs are going to

behave when used in biological system. AuNPs with a large negative (AG_{DS}) or positive (NG_{DK}) ζ -potential values will repel each other and there will be no aggregation of the NPs. AuNPs with small ζ -potential will easily flocculate since the force between them is not strong enough to cause repulsion.

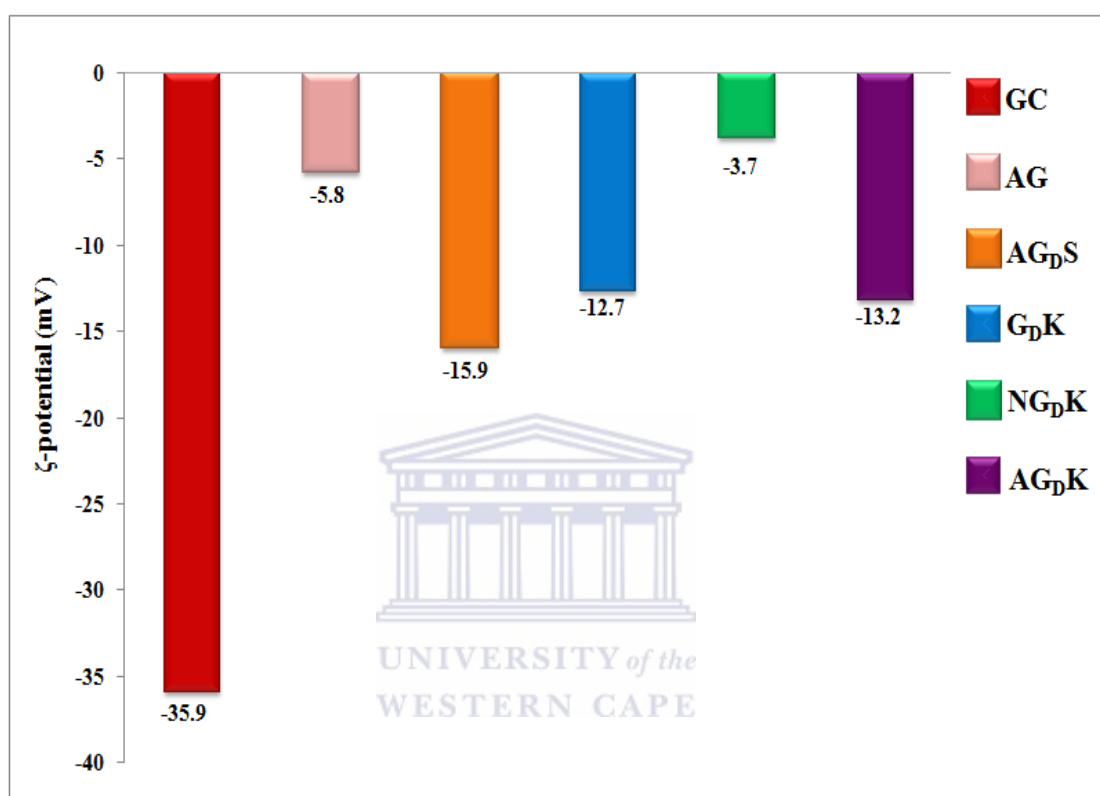


Figure 5.4: Zeta potential of the AuNP conjugates determined using Malvern Zetasizer. GC = citrate coated AuNPs, AG = targeted PEGylated AuNPs, AG_{DS} = targeted AuNPs with scrambled peptide, G_{DK} = untargeted AuNPs with therapeutic peptide, NG_{DK} = AuNPs with scrambled targeting and therapeutic peptides, AG_{DK} = AuNPs with targeting and therapeutic peptides (PHB-targeted nanotherapy).

5.2.2.3 Nanoparticle quantification by ICP-OES

The concentrations of the AuNP samples were first determined using UV-Vis data, the stock concentration for all was 20 nM. ICP-OES was used to quantify the amount of Au metal from equal amount of the AuNPs (as described in section 2.3.5.3. The highest

amount of Au metal as shown in Figure 5.5 was detected on citrate coated AuNPs (GC) at 10.76 ppm. The bio- functionalized AuNP concentration of Au atoms was around 2 ppm in all the other AuNPs, the difference among the five AuNPs (AG, AG_DS, G_DK, NG_DK and AG_DK) was negligible.

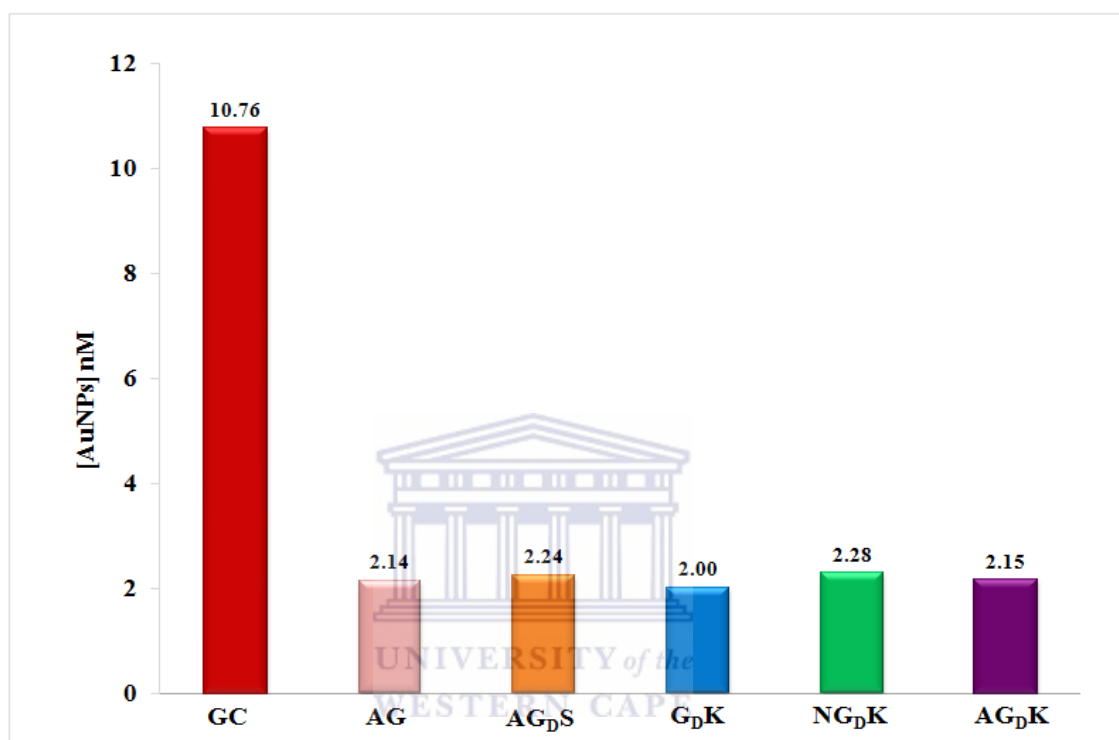


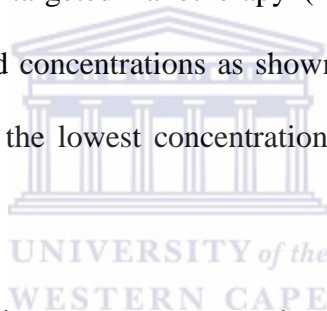
Figure 5.5: Quantification of AuNP conjugates by ICP-OES. To determine the amount of gold present in each sample, the samples were diluted 1:10 in dH₂O. Elemental analysis was carried out by ICP-OES. GC = citrate coated AuNPs, AG = targeted PEGylated AuNPs, AG_DS = targeted AuNPs with scrambled peptide, G_DK = untargeted AuNPs with therapeutic peptide, NG_DK = AuNPs with scrambled targeting and therapeutic peptides, AG_DK = AuNPs with targeting and therapeutic peptides (PHB-targeted nanotherapy).

5.2.2.4 Therapeutic activity of the nanotherapy in cancer cells using the WST-1 assay

The toxicity of the AuNP conjugates was screened against three different cancer cell lines: two colon cancer cell lines (Caco-2 and HT-29), and a breast cancer cell line

(MCF-7). Of the three cell lines, Caco-2 was shown to express PHB on the cell surface, while MCF-7 express PHB within the cell and HT-29 does not express PHB as shown in Figure 3.13.

The activity of AG, AG_DS, G_DK as shown in Figure 5.6 was negligible on the Caco-2 cell line, at the highest dosage of 8 nM, more than 90 % of the cells were still viable. The NG_DK was not toxic from 0.5 to 4 nM, however a significant decrease in cell viability was unexpectedly observed at 6 and 8 nM. At 8 nM, the NG_DK had killed over 90% of the cells. This is unexpected result since NG_DK was conjugated with a scrambled version of the targeting peptide and should therefore not be taken up by PHB expressing cells. The PHB-targeted nanotherapy (AG_DK) was highly toxic to PHB expressing cells at all tested concentrations as shown in Figures 5.6A. AG_DK showed significant toxicity even at the lowest concentration (0.5 nM) when compared to the other AuNP conjugates.



The effect of the AuNP-conjugates was compared among the MCF-7 breast cancer and HT-29 colon cancer cell lines to determine the specificity of the AuNP toxicity. The MCF-7 cells express the PHB receptor as a cytosolic protein and HT-29 cells does not express the protein at all. The cells were exposed to various increasing concentrations of the AuNP conjugates for 24 hours. The cell viability was determined as before, using the WST-1 assay. None of the AuNPs (AG_DS, AG, G_DK, NG_DK and AG_DK), were expected to have toxic effects on the MCF-7 and HT-29 cells. AG_DK in particular should not be toxic to MCF-7 and HT-29 cells since they do not express PHB on the surface. Figure 5.6(B and C) shows that AG_DS, AG, G_DK and AG_DK were not toxic to MCF-7 and HT-29 cells. However, as was the case for Caco-2 cells, MCF-7 and HT-29 cells were susceptible to NG_DK at concentrations of 4-8 nM.

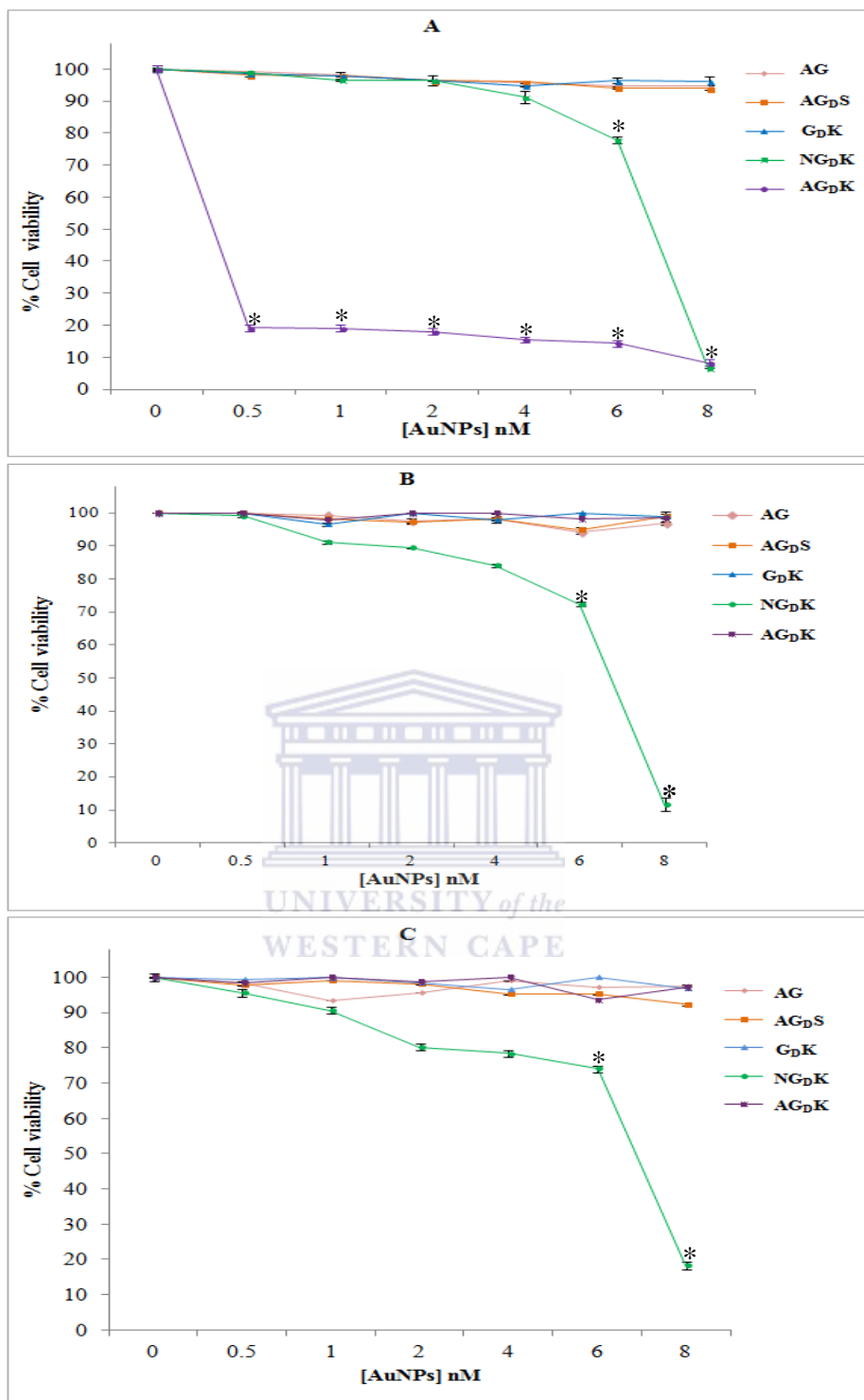


Figure 5.6: Effect of targeted and untargeted NP conjugates on Caco-2 cells. Toxicity in Caco-2 (A), HT 29 (B) and MCF-7 (C) cells was investigated by WST-1 assay after 24 hour treatment with AuNPs. AG = targeted PEGylated AuNPs, AG_DS = targeted AuNPs with scrambled peptide, G_DK = untargeted AuNPs with therapeutic peptide, NG_DK = AuNPs with scrambled targeting and therapeutic peptides, AG_DK = AuNPs with targeting and therapeutic peptides (PHB-targeted nanotherapy). A two-tailed, unpaired t-test was used to analyse significance. *p<0.05, difference statistically significant when compared to untreated samples.

Figure 5.7 shows the results for cells treated with 8 nM of various AuNP conjugates for Caco-2, MCF-7 and HT-29 cells in a bar graph. The data was extrapolated from Figure 5.6A-C and clearly demonstrates the selective toxicity of AG_DK to Caco-2 cells.

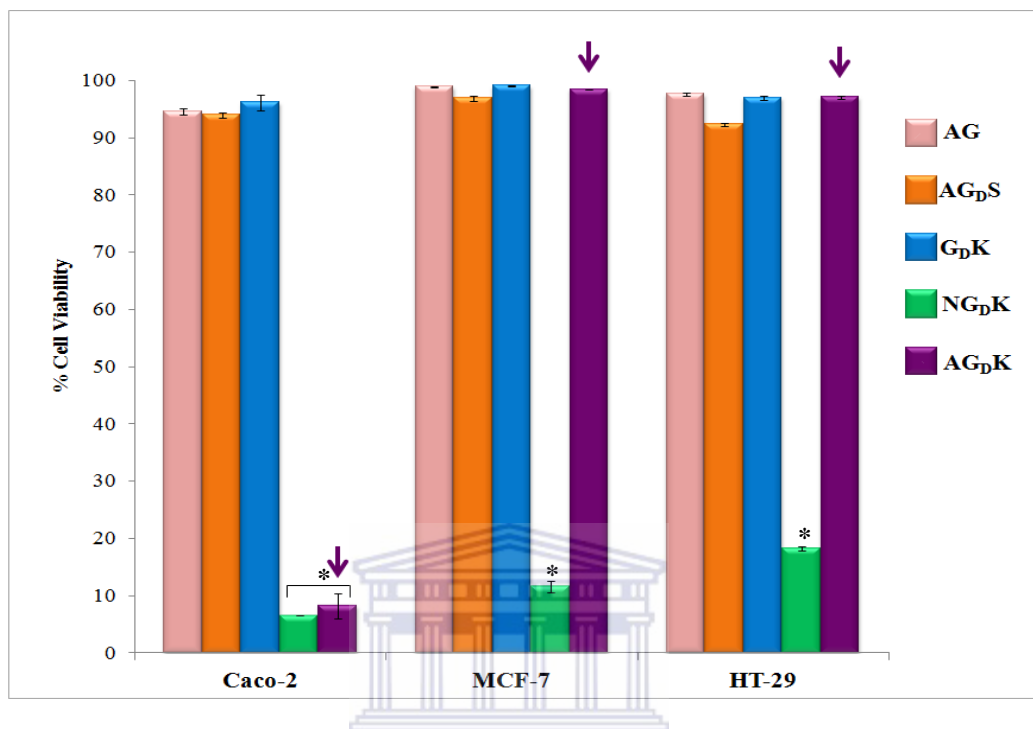


Figure 5.7: Selectivity of AG_DK compared with other AuNP conjugates on Caco-2, MCF-7 and HT-29 cells treated with 8 nM AuNP conjugates. AG = targeted PEGylated AuNPs, AG_DS = targeted AuNPs with scrambled peptide, G_DK = untargeted AuNPs with therapeutic peptide, NG_DK = AuNPs with scrambled targeting and therapeutic peptides, AG_DK = AuNPs with targeting and therapeutic peptides. Arrow points at cells treated with AG_DK and their effect on the three cell lines. A two-tailed, unpaired t-test was used to analyse significance. *p<0.05

The IC₅₀ concentrations (Table 5.3) for AG_DK and NG_DK in Caco-2 cells were determined to be 0.3 nM and 7.5 nM, respectively.

Table 5.3: IC₅₀ of AuNP conjugates on Caco-2 cell line.

AuNP conjugates	IC ₅₀ (nM)
AG _D K	0.3
NG _D K	7.5
AG	>8
G _D K	>8
AG _D S	>8

5.2.2.5 Cellular uptake of AuNPs by cancer cells as determined by ICP-OES

Uptake of the AuNPs by Caco-2, HT-29 and MCF-7 cancer cell lines was quantified by ICP-OES to determine the concentration of the metals that was taken up by the cells as described in section 2.3.6.2a). Figure 5.8 shows the percentage of gold recovered from the cells as function of the total content of AuNPs the cells were exposed to. For all three cell lines, the amount of gold was significantly higher in cells treated with GC compared to the other AuNP conjugates.

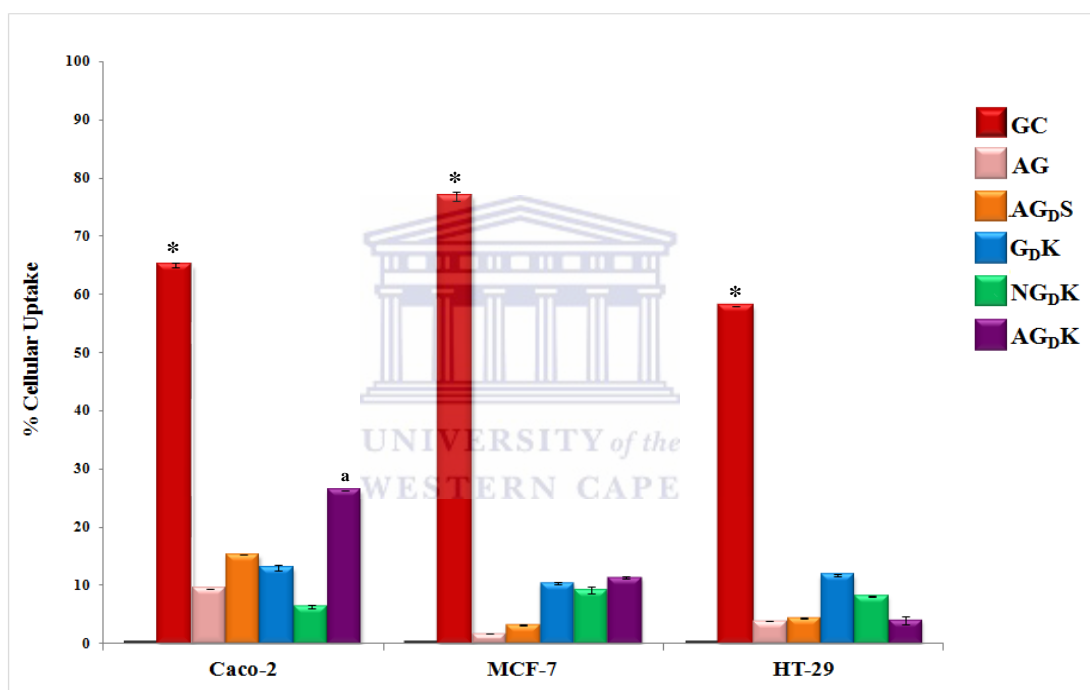


Figure 5.8: Quantification of internalized AuNPs in cancer cell lines by ICP-OES. The cells (were incubated with various nanomaterials at 37°C for 24 hours. Cells were washed, lysed in aqua regia and analysed for gold content by ICP-OES. The percentage of nanoparticles taken up by the cells was determined as a function of the total amount of AuNPs applied. GC = citrate coated AuNPs, AG = targeted PEGylated AuNPs, AG_DS = targeted AuNPs with scrambled peptide, G_DK = untargeted AuNPs with therapeutic peptide, NG_DK = AuNPs with scrambled targeting and therapeutic peptides, AG_DK = AuNPs with targeting and therapeutic peptides (PHB-targeted nanotherapy). A two-tailed, unpaired t-test was used to analyse significance. *p<0.05, significant difference compared to untreated sample, a = p<0.05 AG_DK significantly different compared to other AuNP conjugates in MCF-7 and HT-29.

The average amount of gold recovered from cells treated with GC was 65% for Caco-2, 76.9% for MCF-7 and 58% for HT-29 cells. For treatments with AuNPs with the

targeting peptide (AG, AG_DS and AG_DK), the gold content in Caco-2 cells was significantly higher compared to HT-29 and MCF-7 cells that lack the PHB receptor on the surface of the cell. The amount of gold detected in Caco-2 cells treated with targeted AuNPs (AG, AG_DS and AG_DK) was significantly higher than the cells exposed to AuNPs without the targeting peptide (G_DK and NG_DK). The amount of gold recovered in cells treated with G_DK and NG_DK were comparable in all the cell lines.

5.2.2.6 Intracellular localization of AuNPs by TEM

TEM analysis was used to determine cellular localization of the GC, AG, AG_DS, G_DK, NG_DK and AG_DK in Caco-2 cells. The cells were treated with IC₅₀ concentrations for 24 hours, TEM was used to examine the intracellular distribution of the six AuNPs after fixation. Representative TEM micrographs of Caco-2 cells treated with the different AuNPs are shown in Figure 5.9. Clusters of AuNPs in cells treated with GC, AG, AG_DS, NG_DK and AG_DK were detected mostly in the cytoplasm. No particles were found on the cell surface or inside the cells exposed to G_DK. The cells subjected to GC, AG, AG_DS and G_DK retained the typical elongated morphology of Caco-2 cells with no signs of cytotoxicity as compared to cells exposed to NG_DK and AG_DK. The cells treated with AG_DK show a circular nucleus with distorted cellular features and shape, indicating cellular toxicity.

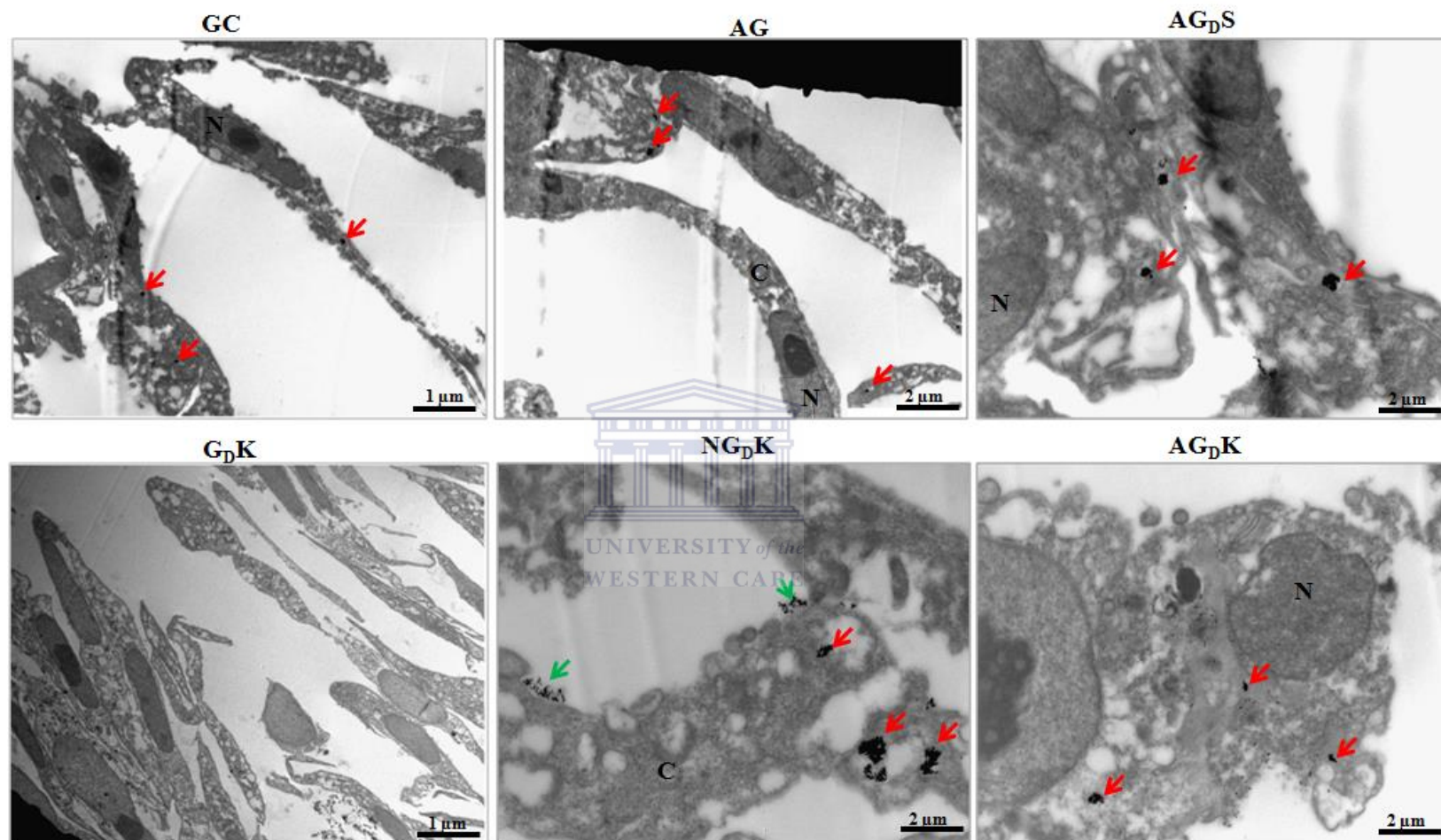


Figure 5.9: Localization of AuNPs in Caco-2 cells by TEM. Cells were incubated with various AuNPs at IC₅₀ concentration for 24 hours. After exposure, cells were fixed with 4% paraformaldehyde and stored in 2.5% glutaraldehyde until further analysis. AuNP uptake was examined by TEM. The red arrows points at NPs localised within the cytoplasm and green arrows indicate the NPs on the cell surface. N - Nucleus, C - Cytoplasm. GC = citrate coated AuNPs, AG = targeted PEGylated AuNPs, AG_DS = targeted AuNPs with scrambled peptide, G_DK = untargeted AuNPs with therapeutic peptide, NG_DK = AuNPs with scrambled targeting and therapeutic peptides, AG_DK = AuNPs with targeting and therapeutic peptides (PHB-targeted nanotherapy).

5.2.3 Cell death analysis: investigation of possible apoptotic cell death

To assess the mode of cell death following exposure of cells to AuNP-conjugates, several apoptotic cell death parameters were studied. The most commonly used markers of apoptosis such as phosphatidyl serine (PS) externalization at the cell surface, caspase (3 and 9) activation and oxidative stress were investigated. PS exposure and ROS induction in the Caco-2 cell line was determined by flow cytometry. Caspase activation was studied by both flow cytometry and Western blot analyses.

5.2.3.1 Effect of AuNPs on cell morphology

The first and most readily noticeable effect following exposure of cells to toxic substances is the alteration of cellular features such as shape and size. The cell membrane has physical features designed to modulate cell signalling, maintain the integrity and stability of the internal environment. The surface charge and size of nanomaterials are thought to play a role in the cellular membrane disruption. Interaction of NPs and the cell through membrane protein, may induce the changes that can be used to assess the cell integrity (Arvizo *et al.*, 2010).

The three cancer cell lines used in this study differentiate into monolayers in cell culture. After treatment with the 0.3 nM AG_DK, 7.5 nM NG_DK and 50 μM Ceramide (a positive control) distinct morphological changes (such as cell shrinkage, rounding, membrane blebbing and cell detachment) were observed under the light microscope as shown in Figure 5.10 indicating unhealthy cells. The effect of AG_DK was only seen in the Caco-2 cells and not in HT-29 or MCF-7 cells. NG_DK and Ceramide were toxic to all three cell lines. Ceramide is a known apoptosis inducer and used as a positive control (Park *et al.*, 2011; Siskind, 2005).

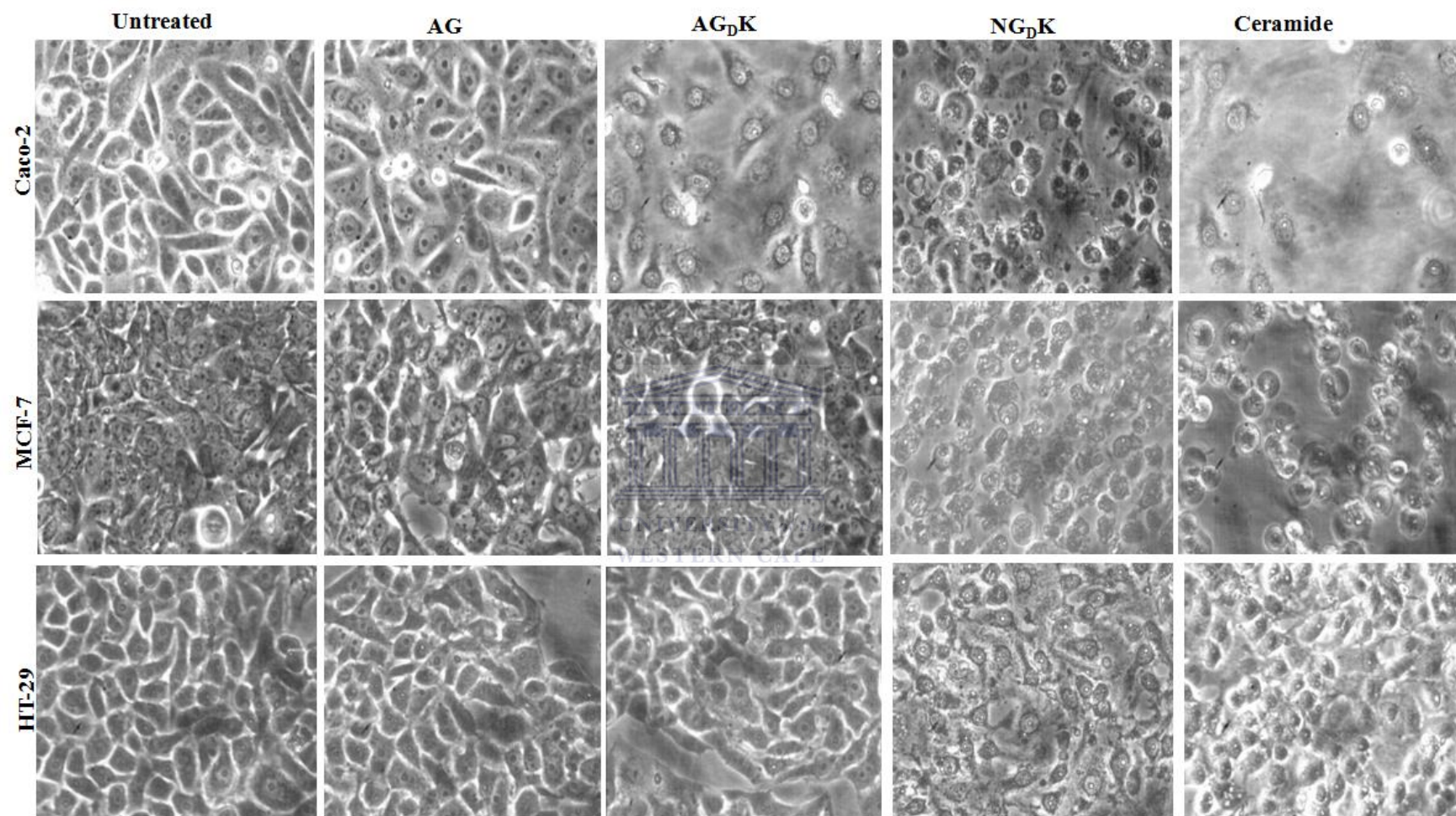


Figure 5.10: Light microscopy depicting cell morphological of Caco-2, MCF-7 and HT-29 cells after exposure to various AuNPs for 24 hours. The cells were grown in a 12 well plate and treated with IC₅₀ of the AuNPs, the cellular morphology were observed under light microscope and captured by the Leica camera. AG = targeted PEGylated AuNPs, NG_DK = AuNPs with scrambled targeting and therapeutic peptides, AG_DK = AuNPs with targeting and therapeutic peptides (PHB-targeted nanotherapy).

Cells exposed to AG did not show any sign of distress, their cellular features appeared normal. As shown in Figure 5.10, no morphological changes were observed on cells treated with AG, the cells were comparable to untreated cells in all cell lines. Cells treated with AG_DS and G_DK was similarly unaffected (data not shown). Cells treated with AG_DK and NG_DK appeared to be clustered with a few cellular extensions, the cells detached from each other as compared to control cells.

5.2.3.2 Analysis of apoptotic effects induced by AuNP conjugates in Caco-2 cells

The _D(KLAKLAK)₂ peptide has pro-apoptotic activity and has been shown to induce cell death through apoptosis when internalized by cells (Ellerby *et al.*, 1999; Kwon *et al.*, 2008). The APOPercentageTM apoptosis assay was used to confirm that the _D(KLAKLAK)₂-DEVD-SH peptide still retained its apoptotic ability after conjugation to AuNPs following the protocol described in section 2.3.6.3 a). The APOPercentageTM assay employs the disodium salt of 3,4,5,6,-tetrachloro-2',4',5',7'-tetraiodofluorescein to stain cells that are undergoing apoptosis, purple-red. The APOPercentageTM dye can only be taken up by apoptotic cells that are undergoing the membrane flip-flop and translocation of the PS to the outer leaflet. Apoptosis was quantified by measuring the dye incorporated in apoptotic cells using Accuri flow cytometer, following the protocol that was developed by Meyer *et al.*, (2008).

Caco-2 cells were exposed to various AuNP conjugates at IC₅₀ concentrations for 24 hours and stained with APOPercentageTM dye as described in section 2.3.6.3 a). After 24 hours of treatment, negligible numbers of apoptotic cells were observed in cells treated with AG, AG_DS and G_DK as shown in Figure 5.11. The number of apoptotic cells in those treatments was not significantly different when compared to untreated cells. Cells treated with 50 μM of cisplatin were used as a positive control. Cisplatin is

a known apoptosis inducer (Okamura *et al.*, 2004). Only two of the AuNPs (AG_DK and NG_DK) were able to induce significant levels of apoptosis in Caco-2 cells as shown in Figure 5.11. The levels of apoptosis in cells treated with AG, AG_DS and G_DK was not significantly higher than the untreated controls.

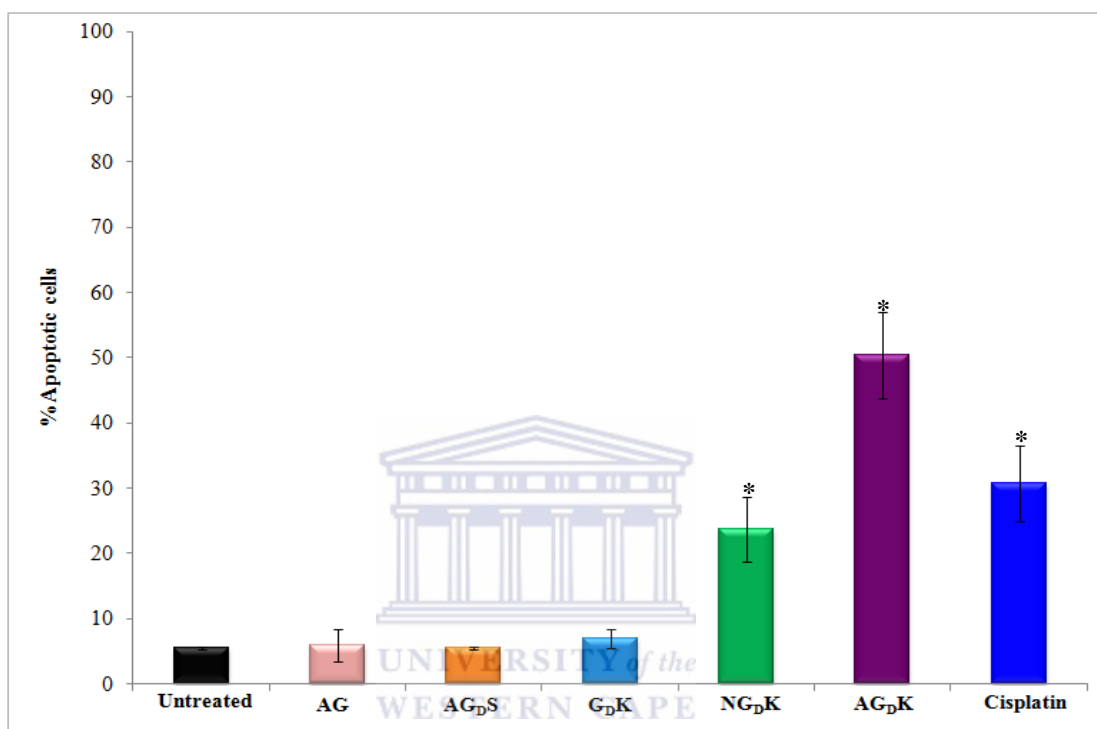
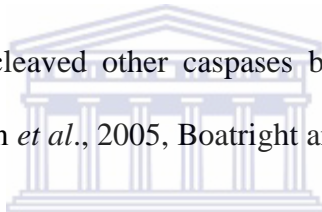


Figure 5.11: Analysis of apoptotic cells by APOPercentage™ staining. Caco-2 cells were treated with various AuNPs using their IC₅₀ for 24 hours. Apoptotic cells were analysed by Accuri flow cytometer. Results shown as the average of replicate samples. AG = targeted PEGylated AuNPs, AG_DS = targeted AuNPs with scrambled peptide, G_DK = untargeted AuNPs with therapeutic peptide, NG_DK = AuNPs with scrambled targeting and therapeutic peptides, AG_DK = AuNPs with targeting and therapeutic peptides (PHB-targeted nanotherapy). A two-tailed, unpaired t-test was used to analyse significance. *p<0.05, significant difference compared to untreated sample and other AuNP conjugates.

Cells treated with the AG_DK showed significantly higher number of apoptotic cells (50%) when compared to the untreated and positive controls. Only 24% of the cells treated with 7.5 nM of NG_DK were apoptotic and 31% for those treated with 50 μM Cisplatin.

5.2.3.3 Analysis of caspase activity

$\text{D}(\text{KLAKLAK})_2$ has been shown to induce apoptotic cell death via caspase activation (Ellerby *et al.*, 1999; Kwon *et al.*, 2008). Activation of caspase 3 and 9 in Caco-2 cells induced by AuNP exposure was investigated in order to confirm the role of $\text{D}(\text{KLAKLAK})_2$ in the induction of apoptosis. Both caspase 9 and 3 are important apoptosis-associated proteins involved in the early and late stage apoptotic pathway, respectively as reviewed by Fan *et al.*, (2005). The initiator caspase 9 is involved in the formation of the apoptosome complex responsible for caspase 3 activation. Caspase 3 is a key effector caspase that executes cell death in apoptotic cells. Activation of caspase 3 is responsible for most apoptosis hallmarks and seals the fate of the cell. Once the proenzyme is proteolytically cleaved other caspases become activated resulting in cell death through apoptosis (Fan *et al.*, 2005, Boatright and Salvesen, 2003).



WESTERN CAPE

a) Analysis of caspase 3 activation by Western blot

Ten microgram of protein sample obtained from the total protein fraction of cells treated with various AuNP-conjugates at their IC_{50} was analysed by western blot assay. Representative immunoblot of caspase 3 activity in Caco-2 cells after 24 hours of treatment with various AuNP conjugates is shown in Figure 5.12A. The caspase 3 antibody used in Figure 5.12A recognises the 32 kDa proenzyme and the cleaved subunits at 20, 17 and 11 kDa. Pro-caspase 3 was absent in the positive control (Cisplatin treated cells) and cells treated with $\text{AG}_{\text{D}}\text{K}$. This suggests that the pro-caspase 3 was activated and cleaved. Pro-caspase 3 was present in cells treated with GC, AG, $\text{AG}_{\text{D}}\text{S}$, $\text{G}_{\text{D}}\text{K}$ and $\text{NG}_{\text{D}}\text{K}$. The cleaved products of pro-caspase 3 were only detected in cells treated with $\text{NG}_{\text{D}}\text{K}$, suggesting that pro-caspase 3 was activated in these cells but not to the same extent as in $\text{AG}_{\text{D}}\text{K}$ and Cisplatin treated cells. This corroborates the

APOPercentage data shown in Figure 5.11. Figure 5.12B shows samples immunoblotted with the Actin antibody demonstrating equal protein loading.

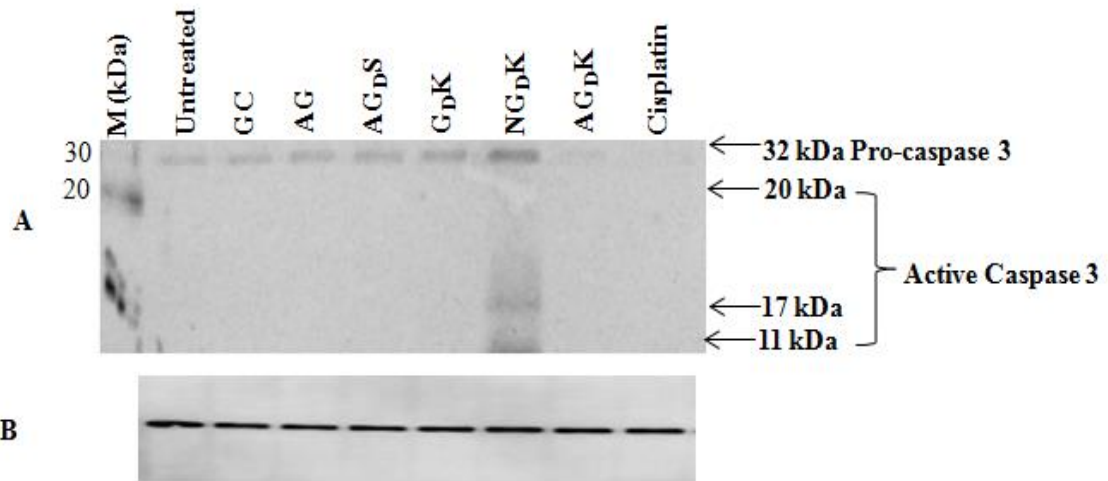


Figure 5.12: Western blot analysis of Caspase activation in Caco-2 cells. Cells were treated with AuNP conjugates for 24 hours. Protein expression was determined by western blotting using specific antibodies. A – Caspase 3 western blot and B - Actin western blot was used as a loading control. GC = citrate coated AuNPs, AG = targeted PEGylated AuNPs, AG_DS = targeted AuNPs with scrambled peptide, G_DK = untargeted AuNPs with therapeutic peptide, NG_DK = AuNPs with scrambled targeting and therapeutic peptides, AG_DK = AuNPs with targeting and therapeutic peptides (PHB-targeted nanotherapy).

b) Analysis of Caspase 9 activation by flow cytometry

In the mitochondrial mediated apoptosis pathway, caspase 9 is known to activate effector caspases (3/6 and 7) resulting in cell death via apoptosis (Fan *et al.*, 2005). A fluorogenic caspase 9 (Caspalux[®] 9-M₁D₂) substrate was used to detect caspase 9 activation in cells treated with AG, AG_DS, G_DK, NG_DK (7.5 nM) and AG_DK (0.3 nM). Caspalux[®] 9-M₁D₂ substrate is an enzymatic assay that is used to measure enzyme (caspase 9) activity, the substrate is composed of two identical fluorescent monomers that are covalently linked together by a caspase 9 cleavage site (LEHD peptide). The LEDH peptide dimerizes the two fluorescent probes forming a loop structure which keep the two probes at close proximity and quench their fluorescence. The substrate can

passively diffuse across all membranes of intact cells. Once inside the cell, the LEDH linker will be cleaved by the active caspase 9 and releases the fluorescent probes. The probes generate a fluorescent signal within the cells that can be used to measure intracellular protease activities in live cells. The fluorescence can be quantified by either fluorescence microscopy or flow cytometry.

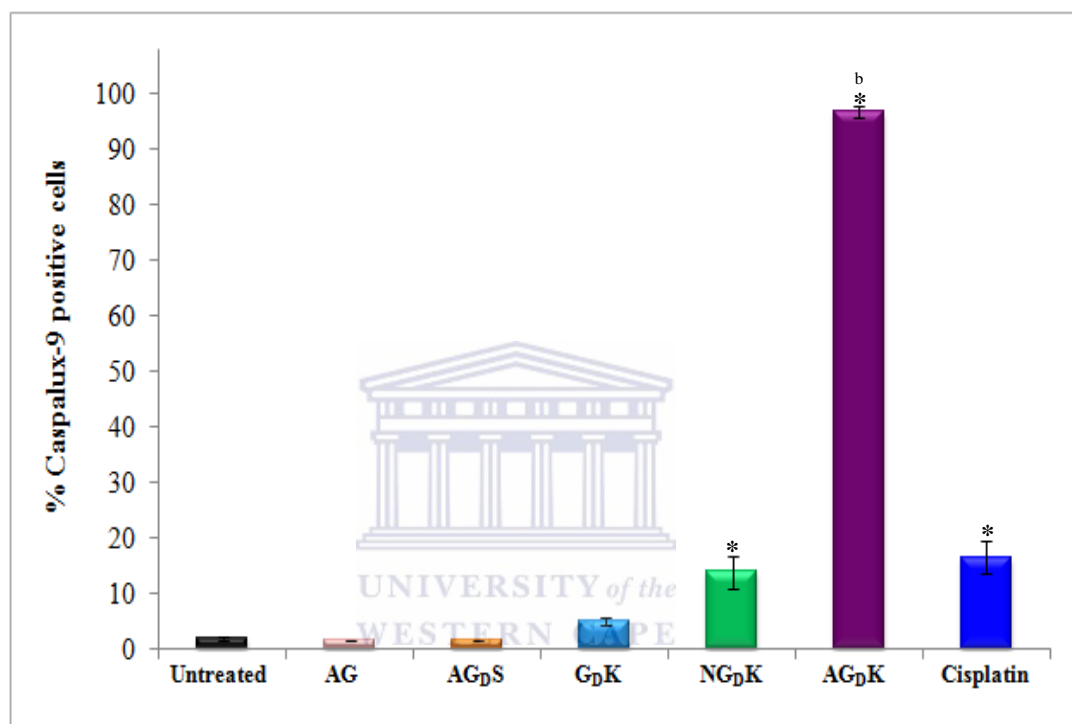


Figure 5.13: Evaluation of caspase 9 activity by flow cytometry in Caco-2 cells exposed to various AuNP conjugates. AG = targeted PEGylated AuNPs, AGpS = targeted AuNPs with scrambled peptide, GpK = untargeted AuNPs with therapeutic peptide, NGpK = AuNPs with scrambled targeting and therapeutic peptides, AGpK = AuNPs with targeting and therapeutic peptides (PHB-targeted nanotherapy). A two-tailed, unpaired t-test was used to analyse significance. * $p < 0.05$, significant difference compared to untreated sample, b = $p < 0.05$ AGpK significantly different compared to NGpK.

Caco-2 cells were exposed to various AuNP conjugates at IC_{50} concentrations for 24 hours. Post treatment, caspase 9 activity was evaluated by subjecting the cells to CaspaLux[®] 9-M₁D₂ fluorogenic substrate as described in section 2.3.6.3 c). The experiment was performed once in triplicate. Intracellular levels of caspase 9 or caspase 9 activity was significantly increased in cells treated with PHB-targeted nanotherapy

(AG_DK) when compared to cells treated with the control AuNPs (AG, AG_DS, G_DK, NG_DK) and the cisplatin as a positive control. As shown in Figure 5.13, the CaspaLux[®] 9-positive cells were significantly higher for AG_DK (97%) treated cells in relation to the negative and positive controls. The data suggests that caspase 9 activation does occur and the cell death is mediated through the intrinsic apoptosis pathway.

5.2.3.2 Detection of intracellular oxidative stress induced by AuNPs: ROS activity

CM-H₂DCFDA was used to monitor generation of ROS in Caco-2 cells after treatment with the various AuNPs with IC₅₀ concentration at 6, 12 and 24 hours as described in section 4.2.5.2. The amount of reactive oxygen intermediates in intact cells was quantified by flow cytometry as described in section 2.3.6.3 d).

The intracellular ROS levels induced by exposing the cells to various AuNP conjugates for 6 to 24 hours are shown in Figure 5.14. The untreated cells and cells treated with either 50 μM cisplatin or H₂O₂ were included as controls. Increased intracellular ROS levels were observed in cells treated with the positive control (H₂O₂) at all time points. Only cells treated with AG_DK and NG_DK undergo oxidative stress. There is a time dependent increase in the number of cells undergoing oxidative stress for both AG_DK and NG_DK. Cells treated with AG_DK undergo oxidative stress from 6 hours while NG_DK induce oxidative stress only from 12 hours. AG_DK and H₂O₂ had significantly higher amount of ROS (13 and 28%, respectively) compared to the other groups. Cells treated with GC, AG, AG, AG_DS and G_DK showed no significant difference in ROS levels when compared to untreated cells at 6-24 hours.

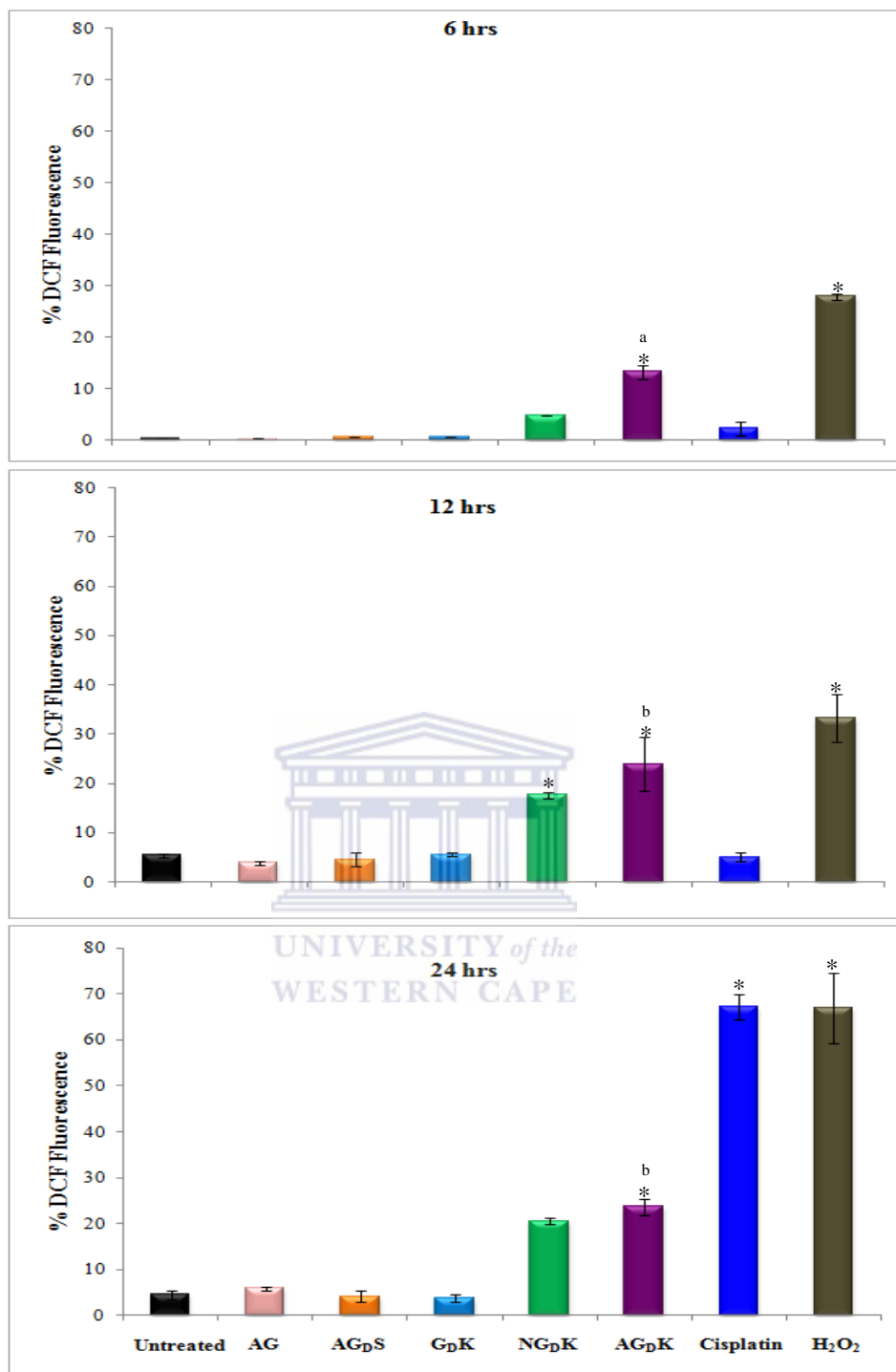


Figure 5.14: ROS levels in Caco-2 cells in response to AuNPs treatment. Cells were treated with various AuNP conjugates for 24 hours and the ROS levels were determined using the CM H₂DCFDA probe. Cell fluorescence was analysed with the Accuri flow cytometer. AG = targeted PEGylated AuNPs, AG_DS = targeted AuNPs with scrambled peptide, G_DK = untargeted AuNPs with therapeutic peptide, NG_DK = AuNPs with scrambled targeting and therapeutic peptides, AG_DK = AuNPs with targeting and therapeutic peptides (PHB-targeted nanotherapy). A two-tailed, unpaired t-test was used to analyse significance. *p<0.05, significant difference compared to untreated sample, a = p<0.05 AG_DK significantly different compared to other AuNP conjugates, b = p<0.05 AG_DK significantly different compared to NG_DK.

5.3 Discussion

Targeted nanotherapy offers hope for the treatment of chronic diseases by developing drugs that specifically inhibit the actions of molecular targets known to promote the growth of pathological tissues. Preclinical and human trials conducted using such therapies provides a concrete evidence of the therapeutic potential of regimens that might be capable of treating debilitating diseases such as cancer (Kumar *et al.*, 2014; Libutti *et al.*, 2009) and obesity (Hossen *et al.*, 2010).

A PHB-targeted nanotherapy that showed specificity and increased efficacy in target cells was developed in this study. The $D(KLAKLAK)_2$ peptide is not capable of entering cells on its own and can therefore not affect cell viability. Incorporating the PHB homing peptide on the nanotherapy has increased its specificity and efficacy as determined by WST-1 assay *in vitro* in three cancer cell lines, refer to Figures 5.6 (A-C). Exposing the three cell lines to increasing dosage of the AuNP conjugates showed that AG_{DK} triggered cell death only on PHB-expressing cell line (Caco-2 cells), and not the other two cell lines and confirmed the specificity of the targeted nanotherapy (Figure 5.7). The negative controls (G_{DK} , AG and AG_{DS}) did not deter the cell viability even at the highest dosage used. Surprisingly NG_{DK} , a negative control with scrambled targeting peptide sequence showed toxicity on all cell lines at the higher doses. The mechanism on how this NPs (NG_{DK}) are taken up by the cells is under investigation.

The targeting (AHP) peptide significantly enhanced the AG_{DK} specificity, resulting in increased cytotoxicity on the cell line that overexpress the target receptor (PHB) *in vitro* and significantly improved the sensitivity of the therapeutic peptide leading to reduced IC_{50} compared to the other AuNPs as shown in Table 5.3. AG_{DK} killed 50% of the cells at only 0.3 nM compared to 7.5 nM for NG_{DK} . The target selectivity was increased

resulting in enhancement of therapeutic index of the potential anti-obesity therapy. Thus, this demonstrates that nanotechnology drug-delivery systems coupled to targeting moieties could be able to overcome the non-specificity and bystander effects of currently available therapies by targeting disease-specific markers.

Results from cytological images in Figure 5.10 clearly exhibited cellular changes consistent with the typical hallmarks of apoptotic demise 24 hours post-treatment for cells treated with AG_DK, NG_DK and Cisplatin. This result was subsequently confirmed using biochemical assays, where activation of caspases (3 and 9) and externalization of PS was investigated. AG_DK was capable of altering key biochemical events leading to apoptotic cell death within 24 hours post-treatment. The _D(KLAKLAK)₂-DEVD-SH peptide attached to AuNPs induced cell death when internalized with the help of AHP peptide and caused cell death by apoptosis. APOPercentage data in Figure 5.11 observed a remarkably high percentage of apoptotic cells at the low concentration of 0.3 nM for AG_DK compared to the negative and positive controls. The pro-apoptotic effects of the targeted nanotherapy was further confirmed by activation of caspase 3 (Figure 5.12) and 9 (Figure 5.13), which was higher for cells treated by AG_DK followed by NG_DK. These data correlated strongly with the APOPercentage data. Results from *in vitro* studies showed that targeted nanotherapy had a more pronounced cytotoxic effect than the other AuNP-conjugates which had negligible impact on cellular function at a very high dosage. These results indicate that neither targeting peptide nor the therapeutic peptide have effect on cell viability on their own and are incapable of inducing cell death unless the therapeutic peptide is taken up by the cells. These data confirmed that _D(KLAKLAK)₂-DEVD-SH was responsible for the death of PHB expressing cells in response to AG_DK and NG_DK treatment.

The AuNPs used as drug delivery agents in this study improved the efficacy and toxicity of the PHB-targeted nanotherapy. Modifying the AuNP surface by chemical conjugation of bio-active molecules influenced the interaction of the AuNPs with cells, and their effects by increasing the cellular uptake and activity of the nanotherapy. Similar effects have been reported on the use of AuNPs as delivery vehicles for gene therapy (Huo *et al.*, 2014) and anticancer therapies (Kumar *et al.*, 2012; Chen *et al.*, 2014; Xiao *et al.*, 2012). The NP-based delivery systems have been extensively studied in cancer preclinical studies, the multimodal systems are effective in selective targeting of diseased cells and tissues through the use of antibodies (Karmani *et al.*, 2014), aptamers (Xiao *et al.*, 2012) and targeting ligands (Chen *et al.*, 2014). The targeted nanotherapeutics has progressed successful to human trials, with a lot of drug candidates still in the pipeline. The recently evaluated human clinical trials for targeted nanotherapies provide evidence that these systems can provide improved and better treatment strategies (ClinicalTrials.gov numbers; NCT00356980, NCT00436410 and, NCT00848042).

The versatility of AuNPs as drug carriers was reported by Chen and colleagues, where multifunctional NPs were constructed for theranostic purposes. The AuNPs were targeted at folate expressing cancer cells and induced cell death through apoptosis, while the events were imaged in real-time (Chen *et al.*, 2014). These studies further extend that the overall concept could be useful in treatment of chronic diseases. The ability to target theranostic agents to diseased tissues provides a viable approach to reduce off-target effects and increase the drug efficacy even at a very low dosage (Cho *et al.*, 2008; Ruoslahti *et al.*, 2010). Targeting the underlying pathophysiology of the disease through disease-specific markers can discriminate between healthy and diseased cells and eradicate the cells without any harm to normal cells (Ruoslahti *et al.*, 2010).

The test nanotherapy understudy can serve as an alternative treatment for obesity, the effect of the targeted therapy will be studied in a rat model of obesity to help understand the interactions between targeted AuNPs and biological systems. The AuNPs proved to be effective drug delivery systems and are biocompatible, when targeted to specific cells can deliver and release a therapeutic payload at the target site. The *in vitro* data showed that AG_DK was more efficacious (IC₅₀ = 0.3 nM) than NG_DK (IC₅₀ = 7.5 nM). The study demonstrated PHB-targeting through AHP in Caco-2 cells, and that using the targeting peptide it is possible to safely deliver AHP-cargo to target cells. The cells that express PHB (Caco-2) were killed by the targeted nanotherapy AG_DK.

The cells served as a model cell line for ECs in the WAT of obese subjects and indicated that the ECs can be targeted by this therapy. Targeting the ECs with AG_DK can result in cell death, increases lipolysis in the adipocytes and starve the cells to death. In a study done by Thovhogi *et al.*, a similar strategy was tested and this study shows the targeted biodistribution of QDs and AuNPs conjugated to AHP peptide in diet-induced obese rats. The targeted NPs were administered for 24 hours, uptake of the NPs in various tissues was studied through ICP OES (Thovhogi *et al.*, 2013; Thovhogi *et al.*, 2015). Localization of the QDs was studied by *in vivo* imaging. The techniques indicated that the AHP-targeted NPs were localized selectively in the WATs (Thovhogi *et al.*, 2013). Similar findings were published on the selectivity and specificity of AHP to target PHB on obese mice (Kolonin *et al.*, 2004; Hossen *et al.*, 2012). This suggests that the therapy can be safely delivered intracellularly to trigger cytotoxic effects, and can be more potent than the current therapies.

Chapter 6: General Discussion, concluding remarks and future perspectives.

6.1 General Discussion

Pharmacotherapy is used as an adjunct in obesity management. Although the drugs used in the management of obesity are effective in reducing body weight for the period in use, they are limited by nonspecificity and off-target side effects (Bray, 2000; Hainer *et al.*, 2008). Nonspecific distribution through the body results in insufficient drug dosage reaching the desired tissue, toxicity towards both normal and diseased cells has resulted in withdrawal of useful anti-obesity drugs such as sibutramine. Currently, orlistat is the only drug that can be used on a long term basis to manage obesity (William, 2010). The greatest challenge faced by anti-obesity drugs after lack of drug specificity, is the maintenance of weight loss. Clearly research into less toxic, more potent therapies is required. Ideally, an effective treatment for obesity should be able to reach the affected or diseased tissues and cells with minimal toxicity to healthy cells, escape biodegradation while retaining their activity in the blood circulation and be able to confer the ability to selectively kill only the target cells.

Lack of drug specificity and sensitivity reduces the drug's therapeutic index. In an attempt to avoid detrimental effects to healthy tissue, the drug dosage and frequency of conventional therapies are often reduced (Breunig *et al.*, 2008). Nanotechnology-based delivery systems coupled with targeted therapy has the potential to address these issues. Nanomaterials have a large surface area which increases their capacity to carry drugs or biomolecules. These features can be exploited for bio-medical applications by attaching

bio-active molecules for either diagnostic and/or therapeutic purposes. The use of nanotechnology to deliver therapeutics to target tissues and cells has been the highlight of nanomedicine (Kumar *et al.*, 2014; Libutti *et al.*, 2009). Through targeted therapy alone, the major issues associated with current anti-obesity therapies could be resolved (Cho *et al.*, 2008; Ruoslahti *et al.*, 2010). Targeted therapy has shown improvements in cancer patients' survival rate, quality of life and reduced bystander cytotoxicity (Ruoslahti *et al.*, 2010). The objective with targeted therapy is to increase the specificity and sensitivity of the therapy to selected cells, without causing harm to surrounding healthy tissues (Cho *et al.*, 2008; Ruoslahti *et al.*, 2010). These qualities can be magnified through nanotechnology. Nanomaterials offer the potential to be effective drug carrier systems without compromising the drug's activity (Conti *et al.*, 2006; Sinha *et al.*, 2006).

Nanotechnology-based targeted therapies that are tissue-specific and have potential to be non geno- and cytotoxic to healthy cells can be used as an alternative to the current management strategies to help combat obesity. In this study, biological active molecules (peptides) were attached to 14 nm AuNPs to develop a receptor targeted nanotherapy that can improve drug transportation and drug efficacy by targeting the PHB cell receptor, which is only expressed by the target cells. A number of challenges were encountered in the process of developing this nanotherapy, the first two attempts described in Chapter 4 were unsuccessful. The first attempt involved the conjugation of recombinant proteins (the expression of these proteins was described in Chapter 3) to 5 nm AuNP-GSH-NTA as discussed in section 4.2.1.1. The AuNP-GSH-NTA aggregated when the recombinant proteins were conjugated to it and this could be attributed to NP instability caused by the ratios of materials used to stabilize the AuNP.

In the second attempt AuNPs were successfully synthesized and functionalized for biological application by attaching targeting (AHP) and therapeutic [$D(KLAKLAK)_2$ -SH] peptides as described in section 4.2.2.1. The AuNPs unfortunately showed that the PHB-targeted nanotherapy (AGK and AGTK) had similar effects as the negative controls (AG and GK) when used to investigate their toxicity *in vitro*, as shown in Figure 4.9. Certain parameters were changed to develop more potent targeted nanotherapy as described in Chapter 5, the major change was the addition of the caspase 3 (DEVD) cleavage site into $D(KLAKLAK)_2$ -SH peptide. The receptor targeted nanotherapy (AG_DK) showed selective targeting and cell specificity demonstrated in colon and breast cancer cell lines as shown in Figure 5.6 (A-C). The extent of cellular uptake or internalization of targeted nanoparticles was dependent on the surface characteristics of the AuNPs, the targeted nanotherapy selectively targeted the cells that expressed PHB on the cell surface and proved its potential as an anti-obesity treatment.

Targeting enhanced the efficacy of the PHB-targeted nanotherapy and restricted the toxicity of the treatment to specified target cells under *in vitro* conditions. With an IC₅₀ of 0.3 nM the targeted test nanotherapy (AG_DK) was 25X more potent than the untargeted AuNPs (NG_DK) which had IC₅₀ of 7.5 nM (Table 5.3). The cell viability of PHB expressing cells were significantly reduced at all concentrations, compared to the negative controls. Biochemical analysis was used to examine whether the morphological changes the cells displayed when exposed to the AG_DK were the results of apoptotic cell death. Figures 5.10 - 5.13 show that the majority of the cells died through apoptosis. The data confirmed that the activity of the pro-apoptotic peptide [$D(KLAKLAK)_2$] was retained after it was conjugated to the AuNPs. These results indicate that AuNPs are well suited as delivery agents of therapeutic materials to treat

obesity due to their tunable cellular uptake and low toxicity. The study confirms and extends the tremendous potential of targeted therapy using AuNPs as drug delivery agents. NP-mediated drug delivery system in cancer are extensively studied, examples of established gold nanoparticle-based formulations in clinical trials include Aurimmune (ClinicalTrials.gov numbers, NCT00356980 and NCT00436410) and Aurolase (ClinicalTrials.gov number, NCT00848042).

Caco-2 as a model cell line simulates more closely the vascular ECs in WATs of obese subjects, as the cells express the PHB receptor that is overexpressed in obese WAT vasculature. These cells were used to investigate the effects of PHB-targeted nanotherapy (AG_DK), the therapy successfully caused cell death. The effect was only observed in target (Caco-2) cells, sparing HT-29 and MCF-7 cells. This strongly indicated the specificity of the nanotherapy, and a similar response can be expected in PHB expressing ECs. Cutting off the blood supply to the WATs (anti-angiogenesis) by killing the ECs in the WAT vasculature through the use of AG_DK can reduce nutrient and oxygen supply to the adipocytes resulting in the reduction of the total body weight and obesity reversal. This work proves that PHB-targeted nanotherapy can be a feasible strategy for treatment of obesity by targeting the cells that are responsible for development of obesity through its vasculature.

AG_DK was able to target and induce apoptotic cell death in cells expressing PHB (Caco-2), which can be translated to the targeting of ECs in WAT. This indicates that effective and selective biologic effects can be achieved through PHB targeting, and that the receptor-mediated cell death proved to be an attractive strategy for obesity reversal. The efficient delivery of drugs into PHB-positive cells forms the basis for the concept of targeted therapy in obesity. The data generated in this study demonstrated that AG_DK

can be used to inhibit of angiogenesis in the WAT vasculature of obese subjects and cause weight loss.

6.2 Concluding remarks and future perspectives

The study demonstrated the potential utility of targeted nanotherapy, its efficacy and sensitivity *in vitro* and therefore provides the proof of principle for antiangiogenic therapy for obesity. Through the use of cell culture model system, the study proved that a targeted nanotherapy is feasible for obesity treatment by exploring PHB-targeted nanotherapy. Future perspectives include investigation of possible anti-obesity effects of the targeted vascular nanotherapy in diet induced obesity rat models. Avenues to be explored are not limited to the effect of targeted nanotherapy on body weight (BW), effect of discontinuation of nanotherapy on BW while continuing on the high fat (HF) diet or change to low fat diet.

To corroborate the *in vitro* toxicity of the PHB-targeted nanotherapy described in Chapter 5, *in vivo* investigations are necessary and can better clarify the mechanisms governing the AuNPs toxicity. Animal models of obesity are excellent models for toxicology and genetic studies of human obesity, and has many advantages, for example the induction of obesity only takes weeks to perform, and the animals have a high (~80%) gene homology to human (Fenton and Carr, 1951). The diet-induced animal models of obesity were established over six decades ago (Fenton and Carr, 1951; Mickelsen *et al.*, 1955), and has since been approved as acceptable models to study human obesity and its related diseases (Buettner *et al.*, 2006).

Animal models have a complex physiologic system and represent a much better model system when compared to *in vitro* cell cultures and can provide meaningful information

about the body's response to targeted nanotherapy. The *in vivo* toxicity is determined by many parameters including the drug dosage, route of administration, metabolism, excretion and immune response (Zhang *et al.*, 2010). The size similarity between NPs and cellular components raises concerns with regard to *in-vivo* use of NPs, as their size and charge allows for easy cell penetration and protein interaction and thus modulate their functions (Leroueil *et al.*, 2007; Verma *et al.*, 2008; Fischer and Chan, 2007). The interaction between NPs and the biological components such as proteins, lipids and cells, could lead to unique biodistribution, metabolism, clearance, and immune response (Fischer and Chan, 2007; Wu *et al.*, 2013).

The PHB-targeted nanotherapy under study can be a plausible therapeutic approach for obesity treatment. Several studies have shown that AHP targeted cargoes can be selectively delivered to PHB-expressing ECs in WATs of obese mice (Hossen *et al.*, 2012; Kolonin *et al.*, 2004) and rats (Thovhogi *et al.*, 2015). The data presented in Chapter 5 suggests that AG_DK can be targeted to the ECs of WAT of obese subjects and induce cell death by apoptosis. Cutting off the blood supply to the WAT can result in tissue weight loss that can be translated into obesity reversal. The WAT growth is angiogenic dependent and by targeting the cells that promote angiogenesis and inhibiting their growth, the physiological processes in the affected tissue can be restored (Cao, 2010). Moreover, eliminating the cells that express PHB could lead to sustainable weight loss and reversal of obesity-induced diseases. Thus, targeted vascular nanotherapy could potentially provide a better strategy that might be superior to many of the current obesity therapies.

The ability to target therapeutic agents to pathological cells offers a viable approach for the treatment of obesity, the therapy can reduce off-target effects, improves drug

sensitivity and efficacy. The targeted nanotherapy under study presents a lot of exciting promises as a potential and an alternative strategy for treatment of obesity. The nano-based therapy (AG_DK) has showed pronounced efficacy in Caco-2 cells, the therapy's selectivity was demonstrated by their lack of toxicity on cells that does not express cell surface PHB. Figure 5.6 showed the importance of channelling toxicity of the treatment to diseased cells, targeting increased the therapy's biocompatibility and activity and this can help prevent adverse immune response when used *in vivo*.

The PHB-targeted nanotherapy showed pronounced effects on the Caco-2 cells. Since Caco-2 cells originate from colon cancer patient, PHB targeting might also be able to help in the treatment of colon cancer. Expression of PHB in colon cancer patients need to be investigated, the protein has been shown to be upregulated in tissue samples of colon cancer patients (Chen *et al.*, 2010; O'Dwyer *et al.*, 2011). There is no information published about PHB's expression in the tissue's vasculature, it could be interesting to use the same strategy in colon cancer. However, the current strategy can be used to kill the colon cancer cells directly. The strategy requires further investigation to determine the effect of the PHB-targeted therapy in animal models of colon cancer. Surprisingly colon cancer is common in obese subjects (Kimura *et al.*, 2014; Neumann *et al.*, 2015), this therapy may therefore be used as a dual targeting in this case.

References

- Afridi, A.K., Khan, A., 2004. Prevalence and etiology of obesity - an overview. *Pakistan Journal of Nutrition*, **3**(1): 14-25
- Ahima, R.S., Flier, J.S., 2000. Adipose tissue as an endocrine organ. *Trends in Endocrinology and Metabolism*, **11**(8): 327-332
- Alkhoury, N., Gornicka, A., Berk, M.P., Thapaliya, S., Dixon, L.J., Kashyap, S., Schauer, P.R., Feldstein, A.E., 2009. Adipocyte apoptosis: a link between obesity, insulin resistance and hepatic steatosis. *The Journal of Biological Chemistry*, **285**: 3428-3438
- Arap, W., Haedicke, W., Bernasconi, M., Kain, R., Rajotte, D., Krajewski, S., Ellerby, H.M., Bredesen, D.E., Pasqualini, R., Ruoslahti, E., 2002. Targeting the prostate for destruction through a vascular address. *Proceedings of the National Academy of Science*, **99**(3): 1527-1531
- Arner, P., 2000. Obesity – a genetic disease of adipose tissue? *British Journal of Nutrition*, **83**(Supplement 1): S9-S16
- Arojo, O.O., Osungbade, K.O., 2013. Trends of obesity epidemic and its socio-cultural dimensions in Africa: implications for health systems and environmental interventions. *Emerging Issues in Medical Diagnosis and Treatment*, **7**(1)
- Artal-Sanz, M., Tavernarakis, N., 2009. Prohibitin and mitochondrial biology. *Trends in Endocrinology and Metabolism*, **8**: 394-401
- Arvizo, R.R., Miranda, O.R., Thompson, M.A., Pabelick, C.M., Bhattacharya, R., Robertson, J.D., Rotello, V.M., Prakash, Y.S., Mukherjee, P., 2010. Effect of nanoparticles surface charge at the plasma membrane and beyond. *Nano letters*, **10**: 2543-2548
- Arvizo, R.R., Rana, S., Miranda, O.R., Bhattacharya, R., Rotello, V.M., Mukherjee, P., 2011. Mechanism of anti-angiogenic property of gold nanoparticles: role of nanoparticle size and surface charge. *Nanomedicine*, **7**(5): 580-587
- Asoh, S., Ohta, S., 2008. PTD-mediated delivery of anti-cell death proteins/peptides and therapeutic enzymes. *Advanced Drug Delivery Reviews*, **60**: 499-516
- Barnhart, K.F., Christianson, D.R., Hanley, P.W., Driessen, W.H., Bernacky, B.J., Baze, W.B., Wen, S., Tian, M., Ma, J., Kolonin, M.G., Saha, P.K., Do, K.A., Hulvat, J.F., Gelovani, J.G., Chan, L., Arap, W., Pasqualini, R., 2011. A Peptidomimetic targeting white fat causes weight loss and improved insulin resistance in obese monkeys. *Science Translational Medicine*, **3**: 108-112
- Bays, H.E., 2004. Current and investigational antiobesity agents and obesity therapeutic treatment targets. *Obesity Research*, **12**: 1197-1211

- Bell, L.N., Cai, L., Johnstone, B.H., Traktuev, D.O., March, K.L., Considine, R.V., 2008. A central role for hepatocyte growth factor in adipose tissue angiogenesis. *American Journal of Physiology, Endocrinology and Metabolism*, **294**: E336-E344
- Bhattacharya, R., Patra, C.R., Earl, A., Wang, S., Katarya, A., Lu, L., Kizhakkedathu, J.N., Yaszemski, M.J., Greipp, P.R., Mukhopadhyay, D., Mukherjee, P., 2007. Attaching folic acid on gold nanoparticles using noncovalent interaction via different polyethylene glycol backbones and targeting of cancer cells. *Nanomedicine: Nanotechnology, Biology, and Medicine*, **3**: 224-238
- Bhattacharyya, S., Kudgus, R.A., Bhattacharya, R., Mukherjee, P., 2010. Inorganic nanoparticles in cancer therapy. *Pharmaceutical Research*, **28**(2): 237-259
- Boatright, K.M., Salvesen, G.S., 2003. Mechanisms of caspase activation. *Current Opinion in Cell Biology*, **15**: 725-731
- Bradford, M.M., 1976. A rapid and sensitive method for the quantitation of microgram quantities of protein utilizing the principle of protein-dye binding. *Analytical Biochemistry*, **72**: 248-254
- Bråkenhielm, E., Cao, R., Gao, B., Angelin, B., Cannon, B., Parini, P., Cao, Y., 2004. Angiogenesis inhibitor, TNP-470, prevents diet-induced and genetic obesity in mice. *Circulation Research*, **94**: 1579-1588
- Brandt, K., Langhans, W., Geary, N., Leonhardt, M., 2006. Beneficial and deleterious effects of hydroxycitrate in rats fed a high-fructose diet. *Nutrition*, **22**(9): 905-912
- Bray, G.A., 2000. A concise review on the therapeutics of obesity. *Nutrition*, **16**(10): 953-960
- Bray, G.A., 2002. The underlying basis for obesity: relationship to cancer. *Journal of Nutrition*, **132**: 3451S-3455S
- Breunig, M., Bauer, S., Goepferich, A., 2008. Polymers and nanoparticles: Intelligent tools for intracellular targeting? *European Journal of Pharmaceutics and Biopharmaceutics*, **68**: 112-128
- Brigger, I., Dubernet, C., Couvreur, P., 2002. Nanoparticles in cancer therapy and diagnosis. *Advanced Drug Delivery Reviews*, **54**: 631-651
- Brown, C.L., Whitehouse, M.W., Tiekink, E.R., Bushell, G.R., 2008. Colloidal metallic gold is not bio-inert. *Inflammopharmacology*, **16**(3): 133-137
- Buettner, R., Parhofer, K.G., Woenckhaus, M., Wrede, C.E., Kunz-Schughart, L.A., Schölmerich, J., Bollheimer, L.C., 2006. Defining high-fat-diet rat models: metabolic and molecular effects of different fat types. *Journal of Molecular Endocrinology*, **36**(3): 485-501
- Cao, Y., 2010. Adipose tissue angiogenesis as a therapeutic target for obesity and metabolic diseases. *Nature Reviews*, **9**: 107-115

- Carl, J., Lavie, M.D., Richard, V., Milani, M.D., Hector, O., Ventura, M.D., 2009. Obesity and cardiovascular disease risk factor, paradox, and impact of weight loss. *Journal of the American College of Cardiology*, **53**: 1925-1932
- Carmeliet, P., 2005. Angiogenesis in life, disease and medicine. *Nature*, **438**: 932-936
- Carriere, F., Renou, C., Ransac, S., Lopez, V., De Caro, J., Ferrato, F., De Caro, A., Fleury, A., Sanwald-Ducray, P., Lengsfeld, H., Beglinger, C., Hadvary P., Verger, R., Laugier, R., 2001. Inhibition of gastrointestinal lipolysis by orlistat during test meals in healthy volunteers. *American Journal of Physiology, Gastrointestinal and Liver Physiology*, **281**: G16-G28
- Caruthers, S.D., Wickline, S.A., Lanza, G.M., 2007. Nanotechnological applications in medicine. *Current Opinion in Biotechnology*, **18**: 26-30
- Chen, D., Garg, A., 1999. Monogenic disorders of obesity and body fat distribution. *Journal of Lipid Research*, **40**(10): 1735-1746
- Chen, F., Lu, X., Yang, X., Xu, Z., Pan, J., Huang, Y., Lin, H., Chi, P., 2010. Identification of prohibitin as a potential biomarker for colorectal carcinoma based on proteomics technology. *International Journal of Oncology*, **37**(2): 355-365
- Chen, W.H., Luo, G.F., Xu, X.D., Jia, H.Z., Lei, Q., Han, K., Zhang, X.Z., 2014. Cancer-targeted functional gold nanoparticles for apoptosis induction and real-time imaging based on FRET. *Nanoscale*, **6**(16): 9531-9535
- Cheung, B.M.Y., Cheung, T.T., Samaranayake, N.R., 2013. Safety of antiobesity drugs. *Therapeutic Advances in Drug Safety*, **4**(4): 171-181
- Cho, K., Wang, X., Nie, S., Chen, Z.G., Shin, D.M., 2008. Therapeutic nanoparticles for drug delivery in cancer. *Clinical Cancer Research*, **14**(5): 1310-1316
- Cho, W.S., Cho, M., Jeong, J., Choi, M., Cho, H.Y., Han, B.S., Kim, S.H., Kim, H.O., Lim, Y.T., Chung, B.H., Jeong, J., 2009. Acute toxicity and pharmacokinetics of 13 nm-sized PEG-coated gold nanoparticles. *Toxicology and Applied Pharmacology*, **236**(1): 16-24
- Christiaens, V., Lijnen, H.R., 2010. Angiogenesis and development of adipose tissue. *Molecular and Cellular Endocrinology*, **318**: 2-9
- Cinti, S., 2005. The adipose organ. *Prostaglandins, Leukotrienes and Essential Fatty Acids*, **73**: 9-15
- Cinti, S., Mitchell, G., Barbatelli, G., Murano, I., Ceresi, E., Faloia, E., Wang, S., Fortier, M., Greenberg, A.S., Obin, M.S., 2005. Adipocyte death defines macrophage localization and function in adipose tissue of obese mice and humans. *Journal Lipid Research*, **46**: 2347-2355

ClinicalTrials.gov number, NCT00356980 TNF-bound colloidal gold in treating patients with advanced solid tumours

ClinicalTrials.gov number, NCT00436410 Tumor necrosis factor in patients undergoing surgery for primary cancer or metastatic cancer

ClinicalTrials.gov number, NCT00848042. Pilot study of AuroLase(tm) therapy in refractory and/or recurrent tumours of the head and neck

Clogston, J.D., Patri, A.K., 2011. Zeta potential measurement. *Methods in Molecular Biology*, **697**: 63-70

Coffey, C.S., Steiner, D., Baker, B.A., Allison, D.B., 2004. A randomized double-blind placebo-controlled clinical trial of a product containing ephedrine, caffeine, and other ingredients from herbal sources for treatment of overweight and obesity in the absence of lifestyle treatment. *International Journal of Obesity and Related Metabolic Disorders*, **28**(11): 1411-1419

Cohen, B., Barkan, D., Levy, Y., Goldberg, I., Fridman, E., Kopolovic, J., Rubinstein, M., 2001. Leptin Induces Angiopoietin-2 Expression in Adipose Tissues. *The Journal of Biological Chemistry*, **276**(11): 7697-7700

Colville-Nash, P.R., Scott, D.L., 1992. Angiogenesis and rheumatoid arthritis: pathogenic and therapeutic implications. *Annals of Rheumatic Disease*, **51**(7): 919-925

Console, S., Marty, C., Garcí'a-Echeverri', C., Schwendener, R., Ballmer-Hofer, K., 2003. Antennapedia and HIV transactivator of transcription (TAT) "Protein Transduction Domains" promote endocytosis of high molecular weight cargo upon binding to cell surface glycosaminoglycans. *The journal of biological chemistry*, **278**(37): 35109-35114

Conti, M., Tazzari, V., Baccini, C., Pertici, G., Serino, L.P., De Giorgi, U., 2006. Anticancer drug delivery with nanoparticles. *In vivo*, **20**(6A): 697-702

Cunningham, A., 2014. How Nanomaterials Are Affecting the Food Industry. . <http://www.strategicbusinessinsights.com/about/featured/2014/2014-03-nanomaterials-food.shtml#.VFErzVfPuqE>. Accessed April 2014

Derakhshan, M., 2007. Apoptosis at a glance: death or life? *Pakistan Journal of Medical Sciences*, **23**(6): 979-982

Donaldson, K., Stone, V., Tran, C.L., Kreyling, W., Borm, P.J.A., 2004. Nanotoxicology. *Occupational and Environmental Medicine*, **61**: 727-728

Dubnov, G., Brzezinski, A., Berry, E.M., 2003. Weight control and the management of obesity after menopause: the role of physical activity. *Maturitas*, **44**(2): 89-101

Eckel, R.H., Kahn, S.E., Ferrannini, E., Goldfine, A.B., Nathan, D.M., Schwartz, M.W., Smith, R.J., Smith, S.R., 2011. Obesity and Type 2 Diabetes: What can be

unified and what needs to be individualized? *Journal of Clinical Endocrinology and Metabolism*, **96**: 1654-1663

El-Andaloussi, S., Järver, P., Johansson, H.J., Langel, U., 2007. Cargo-dependent cytotoxicity and delivery efficacy of cell-penetrating peptides: a comparative study. *The Biochemical Journal*, **407**(2): 285-292

Eliceiri, B.P., Cheresh, D.A., 2001. Adhesion events in angiogenesis. *Current Opinion in Cell Biology*, **13**: 563-568

Ellerby, H.M., Arap, W., Ellerby, L.M., Kain, R., Andrusiak, R., Rio, G.D., Krajewski, S., Lombardo, C.R., Rao, R., Ruoslahti, E., Bredesen, D.E., Pasqualini, R., 1999. Anti-cancer activity of targeted pro-apoptotic peptides. *Nature Medicine*, **5**(9): 1032-1038

Fan, T.J., Han, L.H., Cong, R.S., Liang, J., 2005. Caspase family proteases and apoptosis. *Acta Biochimica et Biophysica Sinica*, **37**(11): 719-727

Fantin, V.R., Berardi, M.J., Babbe, H., Michelman, M.V., Manning, C.M., Leder, P., 2005. A bifunctional targeted peptide that blocks HER-2 tyrosine kinase and disables mitochondrial function in HER-2-positive carcinoma cells. *Cancer Research*, **65**(15): 6891-6900

Fei, H., Okano, H.J., Li, C., Lee, G., Zhao, C., Darnell, R., Friedman J.M., 1997. Anatomic localization of alternatively spliced leptin receptors (Ob-R) in mouse brain and other tissues. *Proceedings of the National Academy of Sciences*, **94**: 7001-7005

Fenton, P.F., Carr, C.J., 1951. The nutrition of the mouse: XI. Response of four strains to diets differing in fat Content. *Journal of Nutrition*, **45**(2): 225-233

Fischer, H.C., Chan W.C.W., 2007. Nanotoxicity: the growing need for *in vivo* study. *Current Opinion in Biotechnology*, **18**: 565-571

Frankel, A.D., Pabo, C.O., 1988. Cellular uptake of the tat protein from human immunodeficiency virus. *Cell*, **55**(6): 1189-1193

Fraser, T.N., 1945. Gold treatment in rheumatoid arthritis. *Annals of the Rheumatic Diseases*, **4**(4): 71-75

Freese, C., Uboldi, C., Gibson, M.I., Unger, R.E., Weksler, B.B., Romero, I.A., Couraud, P.O., Kirkpatrick, C.J., 2012. Uptake and cytotoxicity of citrate-coated gold nanospheres: Comparative studies on human endothelial and epithelial cells. *Particle and Fibre Toxicology*, **9**(23): 1-11

Fruhbeck, G., Gomez-Ambrosi, J., Muruzabal, F.J., Burrell, M.A., 2001. The adipocyte: a model for integration of endocrine and metabolic signaling in energy metabolism regulation. *American Journal of Physiology Endocrinology and Metabolism*, **280**(6): E827-E847

Galic, S., Oakhill, J.S., Steinberg, G.R., 2009. Adipose tissue as an endocrine organ. *Molecular and Cellular Endocrinology*, **316**(2): 129-139

- Gamble, S.C., Odontiadis, M., Waxman, J., Westbrook, J.A., Dunn, M.J., Wait, R., Lam, E.W., Bevan, C.L., 2004. Androgens target prohibitin to regulate proliferation of prostate cancer cells. *Oncogene*, **23**: 2996-3004
- Ghosh, S.K., Nath, S., Kundu, S., Esumi, K., Pal, T., 2004. Solvent and ligand effects on the localized surface plasmon resonance of gold colloids. *Journal of Physical Chemistry B*, **108**(37): 13963-13971
- Gibson, M.I., Danial, M., Klok, H.A., 2011. Sequentially modified, polymer-stabilized gold nanoparticle libraries: convergent synthesis and aggregation behavior. *ACS Combinatorial Science*, **13**(3): 286-297
- Goossens, G.H., 2008. The role of adipose tissue dysfunction in the pathogenesis of obesity-related insulin resistance. *Physiology and Behavior*, **94**: 206-218
- Green, I., Christison, R., Voyce, C.J., Bundell, K.R., Lindsay, M.A., 2003. Protein transduction domains: are they delivering? *TRENDS in Pharmacological Sciences*, **24** (5): 213-215
- Greenberg, A.S., Obin, M.S., 2006. Obesity and the role of adipose tissue in inflammation and metabolism. *American Journal of Clinical Nutrition*, **83**(2): 461S-465S
- Griffioen, A.W., Molema, G., 2000. Angiogenesis: potentials for pharmacologic intervention in the treatment of cancer, cardiovascular diseases, and chronic inflammation. *Pharmacological Reviews*, **52** (2): 237-267
- Gullicksen, P.S., Della-Fera, M.A., Baile, C.A., 2003. Leptin-induced adipose apoptosis: Implications for body weight regulation. *Apoptosis*, **8**: 327-335
- Guo, Y., Cordes, K.R., Farese Jr, R.V., Walther, T.C., 2009. Lipid droplets at a glance. *Journal of Cell Science*, **122**: 749-752
- Gupta, K., Zhang, J., 2005. Angiogenesis: a curse or cure? *Postgraduate Medical Journal*, **81**: 236-242
- Guri, A.M., Hontecillas, R., Bassaganya-Riera, J., 2006. Peroxisome proliferator-activated receptors: Bridging metabolic syndrome with molecular nutrition. *Clinical Nutrition*, **25**(6): 871-885
- Hainer, V., Toplak, H., Mitrakou, A., 2008. Treatment modalities of obesity. *Diabetes Care*, **31**(Supplement 2): S269-S277
- Haiss, W., Thanh, N.T.K., Aveyard, J., Fernig, D.G., 2007. Determination of size and concentration of gold nanoparticles from UV-Vis Spectra. *Analytical Chemistry*, **79**(11): 4215-4221
- Hajer, G.R., van Haefen, T.W., Visseren, F.L.J., 2008. Adipose tissue dysfunction in obesity, diabetes, and vascular diseases. *European Heart Journal*, **29**: 2959-2971

- Hauner, H., 2001. Current Pharmacological approaches to treating obesity. *International Journal of Obesity*, **25** (Supplement 1): S102-S106
- Hauner, H., 2004. The new concept of adipose tissue function. *Physiology and Behavior*, **83**: 653-658
- Hausman, D.B., DiGirolamo, M., Bartness, T.J., Hausman, G.J., Martin, R.J., 2001. The biology of white adipocyte proliferation. *Obesity reviews*, **2**: 239-254
- Hausman, G.J., Richardson, R.L., 2004. Adipose tissue angiogenesis. *Journal of Animal Science*, **82**: 925-934
- Hegyí, K., Fülöp, K.A., Kovács, K.J., Falus, A., Tóth, S., 2004. High leptin level is accompanied with decreased long leptin receptor transcript in histamine deficient transgenic mice. *Immunology Letters*, **92**(1-2): 193-197
- Heitz, F., Morris, M.C., Divita, G., 2009. Twenty years of cell-penetrating peptides: from molecular mechanisms to therapeutics. *British Journal of Pharmacology*, **157**: 195-206
- Herce, H.D., Garcia, A.E., 2007. Cell penetrating peptides: how do they do it? *Journal of Biological Physics*, **33**: 345-356
- Hernandez, T.L., Kittelson, J.M., Law, C.K., Ketch, L.L., Stob, N.R., Lindstrom, R.C., Scherzinger, A., Stamm, E.R., Eckel, R.H., 2011. Fat redistribution following suction lipectomy: defense of body fat and patterns of restoration. *Obesity (Silver Spring)*, **19**(7): 1388-1395
- Herold, G., Rogler, G., Rogler, D., Stange, E.F., 1994. Morphology of CaCo-2 cells varies in different cell batches. *In Vitro Cellular and Developmental Biology*, **30A**(5): 289-291
- Hill, J.O., Peters, J.C., 1998. Environmental contributions to the obesity epidemic. *Science*, **280**(5368): 1371-1374
- Hollander, P.A., Elbein, S.C., Hirsch, I.B., Kelly, B., McGill, J., Taylor, T., 1998. Role of orlistat in the treatment of obese patient with type 2 diabetes; a 1-year randomized double-blind study. *Diabetes Care*, **21**(8): 1288-1294
- Hossen, N., Kajimoto, K., Akita, H., Hyodo, M., Ishitsuka, T., Harashima, H., 2010. Ligand-based targeted delivery of a peptide modified nanocarrier to endothelial cells in adipose tissue. *Journal of Controlled Release*, **147**: 261-268
- Hossen, N., Kajimoto, K., Akita, H., Hyodo, M., Harashima, H., 2012. Vascular-targeted nanotherapy for obesity: Unexpected passive targeting mechanism to obese fat for the enhancement of active drug delivery. *Journal of Controlled Release*, **163**: 101-110

- Huo, S., Jin, S., Ma, X., Xue, X., Yang, K., Kumar, A., Wang, P.C., Zhang, J., Hu, Z., Liang, X.J., 2014. Ultrasmall gold nanoparticles as carriers for nucleus-based gene therapy due to size-dependent nuclear entry. *ACS Nano*, **8**(6): 5852–5862
- Ingber, D., Fujita, T., Kishimoto, S., Sudo, K., Kanamaru, T., Brem, H., Folkman, J., 1990. Synthetic analogues of fumagillin that inhibit angiogenesis and suppress tumour growth. *Nature*, **348**(6301): 555-557
- Javadpour, M.M., Juban, M.M., Lo, W.C., Bishop, S.M., Alberty, J.B., Cowell, S.M., Becker, C.L., McLaughlin, M.L., 1996. De novo antimicrobial peptides with low mammalian cell toxicity. *Journal of Medicinal Chemistry*, **39**: 3107–3113
- Kang, T., Lu, W., Xu, W., Anderson, L., Bacanamwo, M., Thompson, W., Chen, Y.E., Liu, D., 2013. MicroRNA-27 (miR-27) targets prohibitin and impairs adipocyte differentiation and mitochondrial function in human adipose-derived stem cells. *The Journal of Biological Chemistry*, **288**(48): 34394-34402
- Karmani, L., Bouchat, V., Bouzin, C., Levêque, P., Labar, D., Bol, A., Deumer, G., Marega, R., Bonifazi, D., Haufroid, V., Michiels, C., Grégoire, V., Feron, O., Lucas, S., Vander Borgh T., Gallez, B., 2014. ⁸⁹Zr-labeled anti-endoglin antibody-targeted gold nanoparticles for imaging cancer: implications for future cancer therapy. *Nanomedicine*, **9**(13): 1923-1937
- Kelly, Y., Kim, M.A., 2007. Nanotechnology platforms and physiological challenges for cancer therapeutics. *Nanomedicine: Nanotechnology, Biology and Medicine*, **3**: 103-110
- Kennedy, A.J., Ellacott, K.L., King, V.L., Hasty, A.H., 2010. Mouse models of the metabolic syndrome. *Disease Models and Mechanisms*, **3**(3-4): 156-166
- Kiechle, F.L., Zhang, X., 2002. Apoptosis: biochemical aspects and clinical implications. *Clinica Chimica Acta*, **326**: 27-45
- Kim, D., Jeong, Y.Y, Jon, S., 2010. A drug-loaded aptamer-gold nanoparticle bioconjugate for combined CT imaging and therapy of prostate cancer. *ACS Nano*, **4**: 3689-3696
- Kim, G.J., Nie, S., 2005. Targeted cancer nanotherapy. *Materials today* **8**(8 Supplement 1): 28-33
- Kim, Y.M., An, J.J., Jin, Y.J., Rhee, Y., Cha, B.S., Lee, H.C., Lim, S.K., 2007. Assessment of the anti-obesity effects of the TNP-470 analog, CKD-732. *Journal of Molecular Endocrinology*, **38**(4): 455-465
- Kimling, J., Maier, M., Okenve, B., Kotaidis, V., Ballot, H., Plech, A., 2006. Turkevich method for gold nanoparticle synthesis revisited. *Journal of Physical Chemistry B*, **110** (32): 15700-15707
- Kimura, Y., Matsumoto, H., Oosawa, M., Fujita, M., Tarumi, K., Kamada, T., Shiotani, A., Haruma, K., 2014. Relationship between visceral fat and development of colorectal

neoplasms using computed tomographic colonography and adipocytokine levels. *The Japanese Journal of gastro-enterology*, **111**(11): 2121-2130

Kingsley, J.D., Dou, H., Morehead, J., Rabinow, B., Gendelman, H.E., Destache, C.J., 2006. Nanotechnology: A Focus on nanoparticles as a drug delivery system. *Journal of Neuroimmune Pharmacology*, **1**(3): 340-350

Koerner, A., Kratzsch, J., Kiess, W., 2005. Adipocytokines: leptin - the classical, resistin - the controversial, adiponectin - the promising, and more to come. *Best Practice and Research Clinical Endocrinology and Metabolism*, **19**(4): 525-546

Kolonin, M.G., Saha, P.K., Chan, L., Pasqualini, R., Arap, W., 2004. Reversal of obesity by targeted ablation of adipose tissue. *Nature Medicine*, **10**: 625-632

Krug, A.W., Ehrhart-Bornstein, M., 2005. Newly discovered endocrine functions of white adipose tissue: possible relevance in obesity-related diseases. *Cellular and Molecular Life Sciences*, **62**: 1359-1362

Kumar, A., Ma, H., Zhang, X., Huang, K., Jin, S., Liu, J., Wei, T., Cao, W., Zou, G., Liang, X.J., 2012. Gold nanoparticles functionalized with therapeutic and targeted peptides for cancer treatment. *Biomaterials*, **33**(4): 1180-1189

Kutuk, O., Basaga, H., 2006. Bcl-2 protein family: Implications in vascular apoptosis and atherosclerosis. *Apoptosis*, **11**: 1661-1675

Kwon, M.K., Nam, J.O., Park, R.W., Lee, B.H., Park, J.Y., Byun, Y.R., Kim, S.Y., Kwon, I.C., Kim, I.S., 2008. Antitumour effect of a transducible fusogenic peptide releasing multiple proapoptotic peptides by caspase-3. *Molecular Cancer Therapeutics*, **7**(6): 1514-1522

Kyle, S., Aggeli, A., Ingham, E., McPherson, M.J., 2009. Production of self-assembling biomaterials for tissue engineering. *Trends in Biotechnology*, **27**: 423-433

Langin, D., 2006. Adipose tissue lipolysis as a metabolic pathway to define pharmacological strategies against obesity and the metabolic syndrome. *Pharmacological Research*, **53**(6): 482-491

Lau, D.C.W., Dhillon, B., Yan, H., Szmitko, P.E., Verma, S., 2005. Adipokines: Molecular links between obesity and atherosclerosis. *American Journal of Heart and Circulatory Physiology*, **288**: H2031-H2041

Lee, M., Aronne, L.J., 2007. Weight management for type 2 Diabetes Mellitus: global cardiovascular risk reduction. *The American Journal of Cardiology*, **99**(4 Supplement 1): 68-79

Leifert, J.A., Harkins, S., Whitton, J.L., 2002. Full-length proteins attached to the HIV tat protein transduction domain are neither transduced between cells, nor exhibit enhanced immunogenicity. *Gene Therapy*, **9**: 1422-1428

Lenaerts, K., Bouwman, F.G., Lamers, W.H., Renes, J., Mariman, E.C., 2007. Comparative proteomic analysis of cell lines and scrapings of the human intestinal epithelium. *BMC Genomics*, **8**: 91

Leroy, P., Tournassat, C., Bizi, M., 2011. Influence of surface conductivity on the apparent zeta potential of TiO₂ nanoparticles. *Journal of Colloid and Interface Science*, **356**(2): 442-453

Li, N., Sioutas, C., Cho, A., Schmitz, D., Misra, C., Sempf, J., Wang, M., Oberley, T., Froines, J., Nel, A., 2003. Ultrafine particulate pollutants induce oxidative stress and mitochondrial damage. *Environmental Health Perspectives*, **111**: 455-460

Libutti, S.K., Paciotti, G.F., Byrnes, A.A., Alexander, H.R. Jr, Gannon, W.E., Walker, M., Seidel, G.D., Yuldasheva, N., Tamarkin, L., 2010. Phase I and pharmacokinetic studies of CYT-6091, a novel PEGylated colloidal gold-rhTNF nanomedicine. *Clinical Cancer Research*, **16**(24): 6139-6149

Libutti, S.K., Paciotti, G.F., Myer, L., Haynes, R., Gannon, W., Walker, M., Seidel, G., Byrnes, A., Yuldasheva, N., Tamarkin, L., 2009. Results of a completed phase I clinical trial of CYT-6091: a pegylated colloidal gold-TNF. *Nanomedicine*, **27**: 3586

Liekens, S., De Clercq, E., Neyts, J., 2001. Angiogenesis: regulators and clinical applications. *Biochemical Pharmacology*, **61**: 253-270

Lijnen, H.R., 2008. Angiogenesis and obesity. *Cardiovascular Research*, **78**: 286-293

Lindgren, M., Hällbrink, M., Prochiantz, A., Langel, Ü., 2000. Cell-penetrating peptides. *Trends in Pharmacological Sciences*, **21**(3): 99-103

Liu, Y., Franzen, S., 2008. Factors determining the efficacy of nuclear delivery of antisense oligonucleotides by gold nanoparticles. *Bioconjugate Chemistry*, **19**(5): 1009-1016

Lysik, M.A., Wu-Pong, S., 2003. Innovations in oligonucleotide drug delivery. *Journal of Pharmaceutical Sciences*, **92**(8): 1559-1573

Mallat, Z., Tedgui, A., 2000. Apoptosis in the vasculature: mechanisms and functional importance. *British Journal of Pharmacology*, **130**: 947-962

Martinac, K., Metelko, Ž., 2006. Nanotechnology and diabetes. *Diabetologia Croatica*, **34**(4): 105-110

Mauer, M.M., Harris, R.B., Bartness, T.J., 2001. The regulation of total body fat: lessons learned from lipectomy studies. *Neuroscience and Biobehavioral Reviews*, **25**(1): 15-28

McConkey, D.J., 1998. Biochemical determinants of apoptosis and necrosis. *Toxicology Letters*, **99**: 157-168

- Merkwirth, C., Langer, T., 2009. Prohibitin function within mitochondria: essential roles for cell proliferation and cristae morphogenesis. *Biochimica et Biophysica Acta* **1793**(1): 27-32
- Meyer, M., Essack, M., Kanyanda, S., Rees, J., 2008. A low-cost flow cytometric assay for the detection and quantification of apoptosis using an anionic halogenated fluorescein dye. *Biotechniques*, **45**(3): 317-320
- Mickelsen, O., Takahashi, S., Craig, C., 1955. Experimental obesity I. Production of obesity in rats by feeding high-fat diets. *Journal of Nutrition*, **57**(4): 541-554
- Mishra, S., Murphy, L.C., Nyomba, B.L.G., Murphy, L.J., 2005. Prohibitin: a potential target for new therapeutics. *TRENDS in Molecular Medicine*, **11**(4): 192-197
- Mitchell, K.S., Mazzeo, S.E., Aggen, S.H., Maes, H.H., Kendler, K.S., Neale, M.C., Bulik, C.M., 2007. Characteristics of monozygotic male and female twins discordant for overweight: A descriptive study. *Eating Behaviours*, **9**(3): 366-369
- Moghimi, S.M., Hunter, A.C., Murray, J.C., 2005. Nanomedicine: current status and future prospects. *The Federation of American Societies for Experimental Biology Journal*, **19**: 311-330
- Montague, M.C., 2003. The physiology of obesity. *The Association of Black Nursing Faculty Journal*, **3**: 56-60
- Murphy, C.J., Gole, A.M., Stone, J.W., Sisco, P.N., Alkilany, A.M., Goldsmith, E.C., Baxter, S.C., 2008. Gold nanoparticles in biology: beyond toxicity to cellular imaging. *Accounts of Chemical Research*, **41**(12): 1721-1730
- Naggert, J., Harris, T., North, M., 1997. The genetics of obesity. *Current Opinion in Genetics and Development*, **7**: 398-404
- Narkiewicz, K., 2006. Obesity and hypertension-the issue is more complex than we thought. *Nephrology Dialysis Transplantation*, **21**: 264-267
- Nel, A., Xia, T., Mädler, L., Li, N., 2006. Toxic potential of materials at the nanolevel. *Science*, **311**: 622-627
- Nel, A.E., Madler, L., Velegol, D., Xia, T., Hoek, E.M.V., Somasundaran, P., Klaessig, F., Castranova, V., Thompson, M., 2009. Understanding biophysico-chemical interactions at the nano-bio interface. *Nature Materials*, **8**: 543-557
- Nelson-Dooley, C., Della-Fera, M.A., Hamrick, M., Baile, C.A., 2005. Novel treatments for obesity and osteoporosis: targeting apoptotic pathways in adipocytes. *Current Medicinal Chemistry*, **12**: 2215-2225
- Neumann, K., Mahmud, S.M., McKay, A., Park, J., Metcalfe, J., Hochman, D.J., 2015. Is obesity associated with advanced stage or grade of colon cancer? *Canadian Journal of Surgery*, **58**(1)

- Nishida, N., Yano, H., Nishida, T., Kamura, T., Kojiro, M., 2006. Angiogenesis in cancer. *Vascular Health and Risk Management*, **2**(3): 213-219
- Oberdorster, G., Maynard, A., Donaldson, K., Castranova, V., Fitzpatrick, J., Ausman, K., Carter, J., Karn, B., Kreyling, W., Lai, D., Olin, S., Monteiro-Riviere, N., Warheit, D., Yang, H., ILSI Research Foundation/Risk Science Institute Nanomaterial Toxicity Screening Working Group, 2005. Principles for characterizing the potential human health effects from exposure to nanomaterials: elements of a screening strategy. *Particle and Fibre Toxicology*, **2**: 8
- O'Dwyer, D., Ralton, L.D., O'Shea, A., Murray, G.I., 2011. The proteomics of colorectal cancer: identification of a protein signature associated with prognosis. *PLoS One*, **6**(11): e27718
- Ofei, F., 2005. Obesity- a preventable disease. *Ghana Medical Journal*, **39**(3): 98-101
- Okaji, Y., Tsuno, N.H., Saito, S., Yoneyama, S., Tanaka, M., Nagawa, H., Takahashi, K., 2006. Vaccines targeting tumour angiogenesis--a novel strategy for cancer immunotherapy. *European Journal of Surgical Oncology*, **32**: 363-370
- Okamura, M., Hashimoto, K., Shimada, J., Sakagami, H., 2004. Apoptosis-inducing activity of cisplatin (CDDP) against human hepatoma and oral squamous cell carcinoma cell lines. *Anticancer Research*, **24**(2B): 655-661
- O'Rahilly, S., Farooqi, I.S., Yeo, G.S.H., Challis, B.G., 2003. Human obesity-lessons from monogenic disorders. *Endocrinology*, **144**: 3757-3764.
- O'Reilly, M.S., Holmgren, L., Shing, Y., Chen, C., Rosenthal, R.A., Moses, M., Lane, W.S., Cao, Y., Sage, E.H., Folkman, J., 1994. Angiostatin: a novel angiogenesis inhibitor that mediates the suppression of metastases by a Lewis lung carcinoma. *Cell*, **79**(2): 315-328
- Otero, M., Lago, R., Lago, F., Casanueva, F.F., Dieguez, C., Gomez-Reino, J.J., Gualillo, O., 2005. Leptin, from fat to inflammation: old questions and new insights. *Federation of the Societies of Biochemistry and Molecular Biology Letters*, **579**(2): 295-301
- Pal, D., Nayak, A.K., 2010. Nanotechnology for targeted delivery in cancer therapeutics. *International Journal of Pharmaceutical Sciences Review and Research*, **1**(1): 1-7
- Palm-Apergi, C., Lönn, P., Dowdy, S.F., 2012. Do cell-penetrating peptides actually "penetrate" cellular membranes? *Molecular Therapy*, **20**(4): 69-697
- Pandya, N.M., Dhalla, N.S., Santani, D.D., 2006. Angiogenesis - a new target for future therapy. *Vascular Pharmacology*, **44**: 265-274
- Park, J.Y., Kim, M.J., Kim, Y.K., Woo, J.S., 2011. Ceramide induces apoptosis via caspase-dependent and caspase-independent pathways in mesenchymal stem cells derived from human adipose tissue. *Archives of Toxicology*, **85**(9): 1057-1065

- Philip, D., 2008. Synthesis and spectroscopic characterization of gold nanoparticles. *Spectrochimica Acta. Part A, Molecular and Biomolecular Spectroscopy*, **71**(1): 80-85
- Pinto, M., Robine-Leon, S., Appay, M.D., Kedinger, M., Triadou, N., Dussaulx, E., Lacroix, B., Simon-Assman, P., Haffen, K., Fogh, J., Zweibaum, A., 1983. Enterocyte-like differentiation and polarization of the human colon carcinoma cell line Caco-2 in culture. *Biology of the Cell*, **47**: 323-330
- Pompa, P.P., Vecchio, G., Galeone, A., Brunetti, V., Sabella, S., Maiorano, G., Falqui, A., Bertoni, G., Cingolani, R., 2011. *In Vivo* toxicity assessment of gold nanoparticles in *Drosophila melanogaster*. *Nano Research*, **4**(4): 405-413
- Praetorius, N.P., Mandal, T.K., 2007. Engineered nanoparticles in cancer therapy. *Recent Patents on Drug Delivery and Formulation*, **1**: 37-51
- Prins, J.B., Niesler, C.U., Winterford, C.M., Bright, N.A., Siddle, K., O'Rahilly, S., Walker, N.I., Cameron, D.P., 1997. Tumor necrosis factor- α induces apoptosis of human adipose cells. *Diabetes*, **46**: 1939-1944
- Prins, J.B., Walker, N.I., Winterford, C.M., Cameron, D.P., 1994. Human adipocytes apoptosis occurs in malignancy. *Biochemical and Biophysical Research Communications*, **205**(1): 625-630
- Provenzale, J.M., Silva, G.A., 2009. Uses of nanoparticles for central nervous system imaging and therapy. *American Journal of Neuroradiology*, **30**: 1293-1301
- Puoane, T., Steyn, K., Bradshaw, D., Laubscher, R., Fourie, J., Lambert, V., Mbananga, N., 2002. Obesity in South Africa: The South African demographic and health survey. *Obesity Research*, **10**(10): 1038-1048
- Qian, H., Azain, M.J., Compton, M.M., Hartzell, D.L., Hausman, G.J., Baile, C.A., 1998. Brain administration of leptin causes deletion of adipocytes by apoptosis. *Endocrinology*, **139**: 791-794
- Racette, S.B., Deusinger, S.S., Deusinger, R.H., 2003. Obesity: overview of prevalence, etiology, and treatment. *Physical Therapy*, **83**(3): 276-288
- Rau, R., Rheumatol, C., 2005. Have traditional DMARDs had their day? Effectiveness of parenteral gold compared to biologic agents. *Clinical Rheumatology*, **24** (3): 189-202
- Renzaho, A.M., 2004. Fat, rich and beautiful: changing socio-cultural paradigms associated with obesity risk, nutritional status and refugee children from sub-Saharan Africa. *Health and Place*, **10**(1): 105-113
- Roberts, M.J., Bentley, M.D., Harris, J.M., 2002. Chemistry for peptide and protein PEGylation. *Advanced Drug Delivery Reviews*, **54**(4): 459-476
- Ronti, T., Lupattelli, G., Mannarino, E., 2006. The endocrine function of adipose tissue: an update. *Clinical Endocrinology*, **64**: 355-365

Royal Society, 2004. Nanoscience and nanotechnologies: opportunities and uncertainties. www.nanotec.org.uk/finalReport.htm. Accessed 5 April 2013

Ruoslahti, E., 2000. Targeting tumor vasculature with homing peptides from phage display. *Seminars in Cancer Biology*, **10**: 435-442

Ruoslahti, E., Bhatia, S.N., Sailor, M.J., 2010. Targeting of drugs and nanoparticles to tumours. *Journal Cell Biology*, **188**(6): 759-768

Rupnick, M.A., Panigrahy, D., Zhang, C.Y., Dallabrida, S.M., Lowell, B.B., Langer, R., Folkman, M.J., 2002. Adipose tissue mass can be regulated through the vasculature. *Proceedings of the National Academy of Science*, **99**: 10730-10735

Ryan, S.M., Mantovani, G., Wang, X., Haddleton, D.M., Brayden, D.J., 2008. Advances in PEGylation of important biotech molecules: delivery aspects. *Expert Opinion on Drug Delivery*, **5**(4): 371-383

Sabella, S., Brunetti, V., Vecchio, G., Galeone, A., Maiorano, G., Cingolani, R., Pompa, P.P., 2011. Toxicity of citrate-capped AuNPs: an *in vitro* and *in vivo* assessment. *Journal of Nanoparticle Research*, **13**: 6821-6835

Sandoval, C.M., Salzameda, B., Reyes, K., Williams, T., Hohman, V.S., Plesniak, L.A., 2007. Anti-obesity and anti-tumour pro-apoptotic peptides are sufficient to cause release of cytochrome c from vesicle. *Federation of European Biochemical Societies Letters*, **581**: 5464-5468

Sebbage, V., 2009. Cell-penetrating peptides and their therapeutic applications. *Bioscience Horizons*, **2**(1): 64-72

Sengenès, C., Miranville, A., Lolmède, K., Curat, C.A., Bouloumié, A., 2007. The role of endothelial cells in inflamed adipose tissue. *Journal of Internal Medicine*, **262**: 415-421

Sengupta, S., Eavarone, D., Capila, I., Zhao, G., Watson, N., Kiziltepe, T., Sasisekharan, R., 2005. Temporal targeting of tumour cells and neovasculature with a nanoscale delivery system. *Nature*, **436**: 568-572

Sengupta, S., Sasisekharan, R., 2007. Exploiting nanotechnology to target cancer. *British Journal of Cancer*, **96**(9): 1315-1319

Service, R.F., 2004. Nanotoxicology: nanotechnology grows up. *Science*, **304**: 1732-1734

Sethi, J.K., Vidal-Puig, A.J., 2007. Adipose tissue function and plasticity orchestrate nutritional adaptation. *Journal of Lipid Research*, **48**: 1253-1262

Shore, G.C., 2009. Apoptosis: it's BAK to VDAC. *The European Molecular Biology Organization Reports*, **10**(12): 1311-1313

- Shoshan-Barmatz, V., Keinan, N., Abu-Hamad, S., Tyomkin, D., Aram, L., 2010. Apoptosis is regulated by the VDAC1 N-terminal region and by VDAC oligomerization: release of cytochrome c, AIF and Smac/Diablo. *Biochimica et Biophysica Acta*, **1797**(6-7): 1281-1291
- Sinha, R., Kim, G.J., Nie, S., Shin, D.M., 2006. Nanotechnology in cancer therapeutics: Bioconjugated nanoparticles for drug delivery. *Molecular Cancer Therapeutics*, **5**: 1909-1917
- Siskind, L.J., 2005. Mitochondrial ceramide and the induction of apoptosis. *Journal of Bioenergetics and Biomembranes*, **37**(3): 143-153
- Sorensen, T.I.A., Echwald, S.M., 2001. Identifying single genes involved in polygenic inheritance is not easy. *British Medical Journal*, **322**: 630-631
- Sorisky, A., Magun, R., Gagnon, A.M., 2000. Adipose cell apoptosis: death in the energy depot. *International Journal of Obesity*, **24** (Supplement 4): S3-S7
- Sperling, R.A., Gil, P., Zhang, F., Zanella, M., Parak, W.J., 2008. Biological applications of gold nanoparticles. *Chemical Society Reviews*, **37**: 1896-1908
- Sternby, B., Hartmann, D., Borgstrom, B., Nilsson, A., 2002. Degree of in vivo inhibition on human gastric and pancreatic lipases by orlistat (tetrahydrolipstatin, THL) in the stomach and small intestine. *Clinical Nutrition*, **21**(5): 395-402
- Sun, L., Liu, D., Wang, Z., 2008. Functional gold nanoparticle-peptide complexes as cell-targeting agents. *Langmuir*, **24**(18): 10293-10297
- Tam, J., Duda, D.G., Perentes, J.Y., Quadri, R.S., Fukumura, D., Jain, R.K., 2009. Blockade of VEGFR2 and not VEGFR1 can limit diet-induced fat tissue expansion: role of local versus bone marrow-derived endothelial cells. *PloS ONE*, **4**(3): e4974
- Tassi, E., Wellstein, A., 2006. Tumour angiogenesis: Initiation and targeting-therapeutic targeting of an FGF-Binding protein, an angiogenic switch molecule, and indicator of early stages of gastrointestinal adenocarcinomas. *Cancer Research and Treatment*, **38**(4): 189-197
- Taute, F., Onani, M., Madiehe, A., Meyer, M., 2014. Aqueous soluble gold nanoparticles synthesis using polyethyleneimine and reduced glutathione. *International Journal of Materials Research*, **10**: 1025-1039
- Thakor, A.S., Jokerst, J., Zavaleta, C., Massoud, T.F., Gambhir, S.S., 2011. Gold nanoparticles: A revival in precious metal administration to patients. *Nano Letters*, **11**(10): 4029-4036
- The Endocrine Society, 2005. White adipose tissue, inert no more! *Endocrinology*, **146**(5): 2154-2156

- Thovhogi, N., Meyer, M., Madiehe, A.M, 2013. Development of nanotechnology-based drug delivery and imaging system to the white adipose tissue vasculature using Wistar rat model. PhD thesis submitted to the University of the Western Cape
- Thovhogi, N., Sibuyi, N., Martin, O., Meyer, M., Madiehe, A., 2015. Targeted delivery of peptide-functionalized gold nanoparticles to white adipose tissues of obese rats. *Journal of Nanoparticle Research*, **17**: 112
- Trayhurn, P., 2007. Adipocyte biology. *Obesity reviews*, **8** (Supplement 1): 41-44
- Trehin, R., Merkle, H.P., 2004. Chances and pitfalls of cell penetrating peptides for cellular drug delivery. *European Journal of Pharmaceutics and Biopharmaceutics*, **58**: 209-223
- Turkevich, J., Stevenson, P.C., Hillier, J., 1951. A study of the nucleation and growth processes in the synthesis of colloidal gold. *Discuss Faraday Society*, **11**: 55-75
- Ucuzian, A.A., Greisler, H.P., 2007. *In vitro* models of angiogenesis. *World Journal of Surgery*, **31**: 654-663
- Van der Merwe, M.T., Pepper, M.S., 2006. Obesity in South Africa. *Obesity Review*, **7**(4): 315-322
- Vázquez-Vela, M.E.F., Torres, N., Tovar, A.R., 2008. White adipose tissue as endocrine organ and its role in obesity. *Archives of Medical Research*, **39**(8): 715-728
- Verma, A., Uzun, O., Hu, Y.H., Hu, Y., Han, H.S., Watson, N., Chen, S.L., Irvine, D.J., Stellacci, F., 2008. Surface-structure-regulated cell-membrane penetration by monolayer-protected nanoparticles. *Nature Materials*, **7**(7): 588-595
- Veronese, F.M., Pasut, G., 2005. PEGylation, successful approach to drug delivery. *Drug Discovery Today*, **10**(21): 1451-1488
- Vivès, E., Schmidt, J., Pèlegri, A., 2008. Cell-penetrating and cell-targeting peptides in drug delivery. *Biochimica et Biophysica Acta*, **1786**: 126-138
- Warne, J.P., 2003. Tumour necrosis factor α : a key regulator of adipose tissue mass. *Journal of Endocrinology*, **177**: 351-355
- WHO, 2010. WHO global infobase, Data for saving lives. International comparisons. Accessed 4 August 2012. <https://apps.who.int/infobase/Comparisons.aspx>
- Williams, G., 2010. Withdrawal of sibutramine in Europe. *British Medical Journal*, **340**: 377
- Wu, D., Yotnda, P., 2011. Production and detection of reactive oxygen species (ROS) in cancers. *Journal of visualized experiments*, **57**: 3357

Wu, Y.L., Putcha, N., Ng, K.W., Leong, D.T., Lim, C.T., Loo, S.C.J., Chen, X., 2013. Biophysical responses upon the interaction of nanomaterials with cellular interfaces. *Accounts of Chemical Research*, **46**(3): 782-791

Xiao, Z., Levy-Nissenbaum, E., Alexis, F., Lupták, A., Teply, B. A., Chan, J. M., Shi, J., Digga, E., Cheng, J., Langer, R., Farokhzad, O.C., 2012. Engineering of targeted nanoparticles for cancer therapy using internalizing aptamers isolated by cell-uptake selection. *ACS Nano*, **6**(1): 696-704

Yan, Y., Such, G.K., Johnston, A.P.R., Best, J.P., Caruso, F., 2012. Engineering particles for therapeutic delivery: prospects and challenges. *Acsnano*, **6**(5): 3663-3669

Yezhelyev, M.V., Gao, X., Xing, Y., Al-Hajj, A., Nie, S., O'Regan, R.M., 2006. Emerging use of nanoparticles in diagnosis and treatment of breast cancer. *Lancet Oncology*, **7**: 657-667

Zhang, X.D., Wu, H.Y., Wu, D., Wang, Y.Y., Chang, J.H., Zhai, Z.B., Meng, A.M., Liu, P.X., Zhang, L.A., Fan, F.Y., 2010. Toxicologic effects of gold nanoparticles in vivo by different administration routes. *International Journal of Nanomedicine*, **5**: 771-781

Zhang, Y., Proenca, R., Maffei, M., Barone, M., Leopold, L., Friedman, J.M., 1994. Positional cloning of the mouse obese gene and its human homologue. *Nature*, **372**(6505): 425-432

Zieba, D.A., Amstalden, M., Williams, G.L., 2005. Regulatory roles of leptin in reproduction and metabolism: A comparative review. *Domestic Animal Endocrinology*, **29**(1): 166-185

Ziegler, A., Seelig, J., 2004. Interaction of the protein transduction domain of HIV-1 TAT with heparin sulfate: binding mechanism and thermodynamic parameters. *Biophysical Journal*, **86**: 254-263

